National Library of Canada

Acquisitions and Bibliographic Services Branch

395 Wellington Street
Ottawa, Ontario
K1A 0N4

Bibliothèque nationale du Canada

Direction des acquisitions et des services bibliographiques

395, rue Wellington
Ottawa (Ontario)
K1A 0N4

Your file Votre référence

Our file Notre référence

NOTICE

The quality of this microform is heavily dependent upon the quality of the original thesis submitted for microfilming. Every effort has been made to ensure the highest quality of reproduction possible.

If pages are missing, contact the university which granted the degree.

Some pages may have indistinct print especially if the original pages were typed with a poor typewriter ribbon or if the university sent us an inferior photocopy.

AVIS

La qualité de cette microforme dépend grandement de la qualité de la thèse soumise au microfilmage. Nous avons tout fait pour assurer une qualité supérieure de reproduction.

S'il manque des pages, veuillez communiquer avec l'université qui a conféré le grade.

La qualité d'impression de certaines pages peut laisser à désirer, surtout si les pages originales ont été dactylographiées à l'aide d'un ruban usé ou si l'université nous a fait parvenir une photocopie de qualité inférieure.

Canada

Grid Turbulence in Compressible Flow

by

Philip J. Zwart

A thesis presented to the
School of Graduate Studies and Research
in partial fulfillment of the
requirement for the degree of

MASTER of APPLIED SCIENCE
in
MECHANICAL ENGINEERING

Ottawa-Carleton Institute for Mechanical and Aerospace Engineering
Department of Mechanical Engineering
University of Ottawa
Ottawa, Ontario, Canada
December, 1995

ISBN 0-612-11617-4

UNIVERSITÉ D'OTTAWA
UNIVERSITY OF OTTAWA

Abstract

The flow downstream of a grid in a wind tunnel is of considerable interest for two reasons. Theoretically, it represents a good approximation to the idealized concept of homogeneous and isotropic turbulence, and therefore provides a benchmark to evaluate various analytical theories of turbulence. On the practical side, grids and screens are used extensively in the management of turbulence in a variety of applications. Experimental studies of grid turbulence are numerous in incompressible flow, but far scarcer in compressible flow.

The present study considers the characteristics of grid turbulence over a range of Mach numbers, M, ranging from the essentially incompressible ($M = 0.16$), through the moderate subsonic ($0.16 < M < 0.7$) and high subsonic ($0.7 < M < 1.0$), to the supersonic ($M = 1.55$). The experiments comprise flow visualization, performed with the shadowgraph method, and mean and fluctuating velocity measurements, made with a laser-Doppler velocimeter. Characteristics of the flow near the grid were visualized in a demonstration nozzle using the schlieren technique.

In the moderate subsonic regime, flow visualization indicated that the flow near the grid underwent major changes as M increased. The turbulence intensity and decay characteristics were also found to be influenced, which was attributed to the changes in the flow near the grid. In the high subsonic regime, an unsteady quasi-

normal shock was present in the test section. This induced relatively large velocity fluctuations and anisotropic turbulence. In the supersonic regime, stationary oblique shocks generated by the grid were present throughout the test section, which interfered with the turbulence and introduced errors in the measurement technique.

Acknowledgements

I would like to express my gratitude to Professor S. Tavoularis, who suggested the topic and offered guidance, encouragement, and advice through many discussions. His patience and friendship are greatly appreciated. I am also very thankful to Professor R. Budwig, of the University of Idaho, who worked on the project in its initial phase during a sabbatical at the University of Ottawa, and has maintained long-distance interest and assistance since then.

I would also like to thank the staff of the High Speed Aerodynamics Laboratory for their involvement. The project would not have been possible without the encouragement and assistance of Dr. V. D. Nguyen, the support of Drs. L. Chan and B. H. K. Lee, and the help of Mr. S. Pynn, Miss C. Lord, and others in the Wind Tunnel Operating Group. Discussions with Dr. Lee about quasi-normal shocks were particularly helpful.

I am also grateful to the Mechanical Engineering machine shop staff at the University of Ottawa, in particular to Mr. M. Makasare, for their help with designing and constructing the test section for the demonstration nozzle.

The financial support of the Natural Sciences and Engineering Research Council of Canada is gratefully acknowledged.

Appreciation is also due to colleagues Sebastien Marineau-Mes, Sadok Guellouz, and many others, for interesting conversations both related and unrelated to this thesis. Their friendships made my time here enjoyable. I am also thankful for the support of family and friends, as well as the special friendship of Evelyn Fintelman. Finally, I would like to thank God, who has allowed me the privilege of studying a small piece of his creation, in which His glory shines.

Contents

Abstract ii

Acknowledgements iv

Nomenclature xvi

1 Introduction 1

1.1 Motivation 1

1.2 Objectives 3

1.3 Organization of the Thesis 3

2 Literature Review 5

2.1 Incompressible Flow 5

2.1.1 Analytical Studies of Isotropic Turbulence 6

2.1.2 Experimental Studies of Decaying Turbulence 8

2.2 Compressible Flow 13

2.2.1 Analytical Studies 14

2.2.2 Numerical Studies 16

2.2.3 Experimental Studies 18

2.3 Previous Measurements at the Facility Used in the Present Study . . 21

2.4 Summary 21

2.4.1 High Reynolds Number Flow 22
2.4.2 Compressible Flow 22
2.4.3 Compressible Turbulence 23

3 Experimental Techniques **24**
3.1 Facility 24
3.1.1 Wind Tunnels 24
3.1.2 Turbulence Generators 26
3.1.3 Flow Visualization 28
3.2 Instrumentation 29
3.2.1 Pressure and Temperature Measurements 29
3.2.2 Laser Doppler Velocimetry Equipment 29
3.3 Data Acquisition and Processing 32
3.4 Error Sources and Estimating Procedures 33
3.4.1 Wind Tunnel Characteristics 33
3.4.2 Particle Dynamics 34
3.4.3 LDV System 37

4 Measurements **40**
4.1 Wind Tunnel Operating Characteristics 40
4.2 Experimental Conditions 43
4.2.1 Wind Tunnel 43
4.2.2 Demonstration Nozzle 43
4.3 Presentation of Results 46
4.3.1 Moderate Subsonic Regime 47
4.3.2 High Subsonic Regime 49
4.3.3 Supersonic Regime 49

5 Analysis 51

5.1 Turbulence Intensities 51

5.2 Moderate Subsonic Regime 52

5.2.1 Background Turbulence Intensity 54

5.2.2 Flow Uniformity and Homogeneity 54

5.2.3 Turbulence Gaussianity 55

5.2.4 Turbulence Isotropy 56

5.2.5 Mean Velocity Profiles 57

5.2.6 The Decay Law 58

5.2.7 Some Turbulence Parameters 61

5.2.8 Applicability to Computational Turbulence Studies 66

5.2.9 Flow near the Grid 66

5.3 High Subsonic Regime 67

5.3.1 Qualitative Analysis 67

5.3.2 Quantitative Analysis 68

5.4 Supersonic Regime 69

5.4.1 Qualitative Analysis 69

5.4.2 Quantitative Analysis 70

5.4.3 Flow near the Grid 71

5.4.4 Towards Generating Compressible Isotropic Turbulence 72

5.5 Measurement Error and Uncertainty 73

5.5.1 Wind Tunnel Operation 74

5.5.2 Particle Dynamics 75

5.5.3 LDV System 77

5.5.4 Estimate of Uncertainty in Measured Turbulence Intensity . . 78

6 Conclusions and Recommendations 80

6.1 Conclusions 80
6.2 Recommendations for Further Research 82

Bibliography 84

Plates 91

Figures 109

A Further Tests of the Flow Homogeneity and Isotropy 144

A.1 Estimates of the Neglected Terms in the Streamwise Reynolds Stress Equation 144
A.2 Estimate of the Number of Eddy Turnovers 146

B LDV Equipment: Some Practical Considerations 148

B.1 Hardware 148
B.1.1 Description 148
B.1.2 Changing the System Order 153
B.1.3 Beam Polarization 155
B.1.4 Sign Convention 155
B.2 The FLOware Software 156
B.2.1 Setup 156
B.2.2 Acquire 158

C Computer Program Used for Data Processing 160

D Detailed Measurement Data 179

List of Plates

1	Photographs of the Wind Tunnel Facility	92
2	Photographs of the Demonstration Nozzle.	93
3	Photograph of the Perforated Plates	94
4	Photographs of the Wind Tunnel with the Flow Visualization System.	95
5	Shadowgraphs of the Quasi-Normal Shock, $A_{dt}/A = 0.94$	96
6	Shadowgraphs of the Quasi-Normal Shock, $A_{dt}/A = 0.98$	97
7	Shadowgraph Images with the Unmodified MHP	98
8	Shadowgraph Images with the Modified MHP	99
9	Shadowgraph Images with the LHP	100
10	Schlieren Images in the Demonstration Nozzle with Round Rods (1) .	101
11	Schlieren Images in the Demonstration Nozzle with Square Rods I (1)	102
12	Schlieren Images in the Demonstration Nozzle with Square Rods II (1)	103
13	Schlieren Images in the Demonstration Nozzle with Diamond Rods (1)	104
14	Schlieren Images in the Demonstration Nozzle with Round Rods (2) .	105
15	Schlieren Images in the Demonstration Nozzle with Square Rods I (2)	106
16	Schlieren Images in the Demonstration Nozzle with Square Rods II (2)	107
17	Schlieren Images in the Demonstration Nozzle with Diamond Rods (2)	108

List of Figures

1 Schematic of the Wind Tunnel Facility 110
2 Schematic of a Perforated Plate 111
3 Schematic of the Flow Visualization System. 111
4 Locations of the Wind Tunnel Measuring Stations 112
5 Distribution of Particle Sizes in Polyethylene Glycol Aerosol 112
6 Typical Wind Tunnel Characteristics in the Moderate Subsonic Regime 113
7 Typical Wind Tunnel Characteristics to the High Subsonic Regime . 114
8 Typical Wind Tunnel Characteristics to the Supersonic Regime . . . 115
9 Background Turbulence Intensities, $M = 0.69$ 116
10 Transverse Mean Velocity Profiles, y-Traverse 117
11 Transverse Mean Velocity Profiles, z-Traverse 117
12 Streamwise Velocity Variances, y-traverse 118
13 Streamwise Velocity Variances, z-traverse 118
14 Mean Velocity Profiles for $M = 0.16$ 119
15 Mean Velocity Profiles for $0.24 \leq M \leq 0.58$ 119
16 Mean Velocity Profiles for $M = 0.52$ 120
17 Mean Velocity Profiles for $0.64 \leq M \leq 0.68$ 120
18 Mean Velocity Profiles for Anomalous Cases, $M = 0.66$ 121
19 Streamwise Velocity Variances Profiles for $M = 0.16$ 122
20 Streamwise Velocity Variances Profiles for $0.24 \leq M \leq 0.58$ 122

21 Streamwise Velocity Variance Profiles for $M = 0.52$ 123
22 Streamwise Velocity Variance Profiles for $0.64 \leq M \leq 0.68$ 123
23 Streamwise Velocity Variance Profiles for Anomalous Cases, $M = 0.66$ 124
24 Skewness Factors for $M = 0.16$ 125
25 Skewness Factors for $0.24 \leq M \leq 0.58$ 125
26 Skewness Factors for $M = 0.52$ 126
27 Skewness Factors for $0.64 \leq M \leq 0.68$ 126
28 Skewness Factors for Anomalous Cases, $M = 0.66$ 127
29 Turbulent Shear Stress Correlation Coefficients in the Moderate Subsonic Regime 127
30 Mean Velocity Profiles in the High Subsonic Regime. 128
31 Velocity Variances in the High Subsonic Regime. 128
32 Skewness Factors in the High Subsonic Regime. 129
33 Mean Velocity Profiles in the Supersonic Regime, MHP. 130
34 Mean Velocity Profiles in the Supersonic Regime, LHP. 130
35 Streamwise Velocity Variance Profiles in the Supersonic Regime, MHP. 131
36 Streamwise Velocity Variance Profiles in the Supersonic Regime, LHP. 131
37 Skewness Factors in the Supersonic Regime, MHP. 132
38 Skewness Factors in the Supersonic Regime, LHP. 132
39 Turbulence Intensities at $x/m = 58.5$. 133
40 A typical velocity histogram 134
41 Typical Mean Velocities in the Moderate Subsonic Regime 135
42 Typical Streamwise Velocity Variance Profiles in the Moderate Subsonic Regime 136
43 Two Potential Decay Laws for MS8b 137
44 Decay Exponents in the Moderate Subsonic Regime 138
45 Effective Origins in the Moderate Subsonic Regime 138

46 Dissipation Rates in the Moderate Subsonic Regime 139
47 Integral Length Scales in the Moderate Subsonic Regime 139
48 Taylor Microscales in the Moderate Subsonic Regime 140
49 Kolmogoroff Microscales in the Moderate Subsonic Regime 140
50 Turbulence Reynolds Numbers in the Moderate Subsonic Regime . . 141
51 Mean Velocity Profile Across a Wave 142
52 Velocity Variance Profile Across a Wave 142
53 Decay Exponents in all Regimes 143

List of Tables

3.1 Turbulence Generator Dimensions 26

3.2 Attributes of Demonstration Nozzle Grids 28

3.3 Characteristics of Lenses Used in the Experiments 31

4.1 Wind Tunnel Settings Used in Experiments 44

4.2 LDV Settings Used in Experiments 45

4.3 Demonstration Nozzle Settings for the Subsonic Regime 46

5.1 Mean Velocities, Turbulence Intensities, and Grid Reynolds Numbers 53

5.2 Sensitivity of n to Sample Rejection Criterion 59

5.3 Decay Law Parameters for the Moderate Subsonic Regime 62

5.4 Turbulence Parameters in the Moderate Subsonic Regime 65

5.5 Streamwise Turbulence Intensities in the Supersonic Regime 71

5.6 Estimated Error Due to Particle Inertia 76

5.7 Estimated Error Due to Volume-Averaging 78

A.1 Estimates of the Neglected Terms in the Streamwise Reynolds Stress Equation at $M = 0.16$ 145

A.2 Estimates of the Streamwise Production Term in the Moderate Subsonic Regime 146

B.1 Velocity Ranges with the Green Beam 151

B.2 Velocity Ranges with the Blue Beam 151

B.3 Probe Volume Data for the Green Beam 157
B.4 Probe Volume Data for the Blue Beam 158

Nomenclature

Alphanumerical variables

A	test section area
A_{dt}	diffuser throat area
B	decay coefficient
c	local speed of sound
d'	fluctuating dilatation
d_p	aerodynamic diameter of particle
E	three-dimensional spectrum
F	flatness factor
h	wind tunnel width and height
k	turbulence kinetic energy per unit mass
L_f	streamwise integral length scale
m	effective mesh size
M	Mach number
M_t	turbulence Mach number
M_{1d}	Mach number predicted from one-dimensional isentropic flow theory
n	decay coefficient

N_{to}	number of eddy turnovers
p'	fluctuating pressure
P	static pressure
P_t	total pressure
R_m	grid Reynolds number
R_x	Reynolds number used for boundary layer growth calculations
R_λ	turbulence Reynolds number
S	skewness factor
t	time coordinate
T_L	Lagrangian integral time scale
u'	streamwise rms velocity (engineering notation)
u_i	rms velocity in x_i-direction (tensor notation)
u'_p	streamwise rms velocity of particle
u'_r	streamwise rms velocity resolved by LDV system
U	mean velocity in x-direction (engineering notation)
U_{cl}	mean velocity in x-direction at tunnel centreline
U_m	mean velocity averaged over all measurement locations
U_p	mean particle velocity
v'	fluctuating velocity in y-direction (engineering notation)
w'	fluctuating velocity in z-direction (engineering notation)
x	streamwise space coordinate (engineering notation)
x_i	space coordinate (tensor notation)
x_o	effective origin in decay law
Δx_t	streamwise distance between traverse positions
y, z	transverse space coordinates (engineering notation)

Greek variables

ϵ	dissipation rate
ϵ_d	dilatational dissipation rate
ϵ_s	solenoidal dissipation rate
η	Kolmogoroff microscale
κ	wave number
λ	Taylor microscale
μ	dynamic viscosity
ν	kinematic viscosity
ρ	density
ρ_p	particle density
ρ_{uv}	shear stress correlation coefficient
σ_1	probe volume length
σ_2	probe volume width
σ_3	probe volume height
τ	time constant of particle
τ_e	dissipation time scale
τ_c	convection time scale
ω	frequency
ω_i'	fluctuating vorticity in x_i-direction (tensor notation)
ω_E	Eulerian frequency
ω_L	Lagrangian frequency

Subscripts

0	measurement station 0 (in settling chamber)
1	measurement station 1 (upstream of measurement window)
2	measurement station 2 (downstream of measurement window)

Other

$(\overline{})$	time-average

Chapter 1

Introduction

1.1 Motivation

Turbulence is a state of irregular fluid motion "in which the various quantities show a random variation with time and space coordinates, so that statistically distinct average values can be discerned" (Hinze, 1975). It occurs when the Reynolds number, which characterizes the strength of inertial forces relative to viscous forces, exceeds a certain critical value. Present in most flows of industrial significance, it is important to understand and predict; its complexity, however, defies simple mathematical analysis.

Because turbulence in its general form is so complex, it is desirable to study simplified cases which are easier to analyze. The simplest possible type of turbulence is one which is homogeneous and isotropic. Such a turbulence must also be degenerate, for the kinetic energy of the turbulence dissipates into thermal energy, and there is no mechanism by which new turbulence can be produced. Even with these simplifications, however, the equations describing the turbulence cannot be solved without further assumptions.

For this reason, analysis of turbulence relies heavily upon experimental studies of its structure and statistical properties. The particular simplified case of homogeneous isotropic turbulence can be experimentally approximated by grid turbulence — the turbulence produced downstream of a grid or related geometry in a duct or wind tunnel (Corrsin, 1963). Many studies of grid turbulence in incompressible flow have been performed (e.g. Comte-Bellot and Corrsin, 1966).

In the past few years, interest in compressible turbulence has intensified. The state of research in this field has been reviewed by Lele (1994). The analysis of compressible turbulence is more complex than of incompressible turbulence, because density can also fluctuate. In homogeneous isotropic compressible turbulence, the incompressible dissipation rate is augmented by the so-called dilatational dissipation rate and the pressure-dilatation correlation (Zeman, 1990; Sarkar et al, 1991). Closure models for these extra terms rely on data from Direct Numerical Simulations, largely because there are no experimental measurements of compressible isotropic turbulence.

There are a number of grid turbulence studies in which mean compressibility is significant but turbulence compressibility is not. These studies generally had shock-turbulence interactions as their focus. Most used shock-tube flow, while some involved continuous flow wind tunnels. None had as its primary focus the decay of grid turbulence. The paucity of experimental data on grid turbulence in compressible flow forms the motivation for the present research, and leads to the objectives outlined in the following section.

1.2 Objectives

The primary objective of the present study is to determine how the homogeneity, isotropy, and decay characteristics of grid turbulence are affected by compressibility in the mean flow. The range of Mach numbers considered varies from the incompressible regime, through the moderate and high subsonic regimes, and into the supersonic regime.

A secondary objective is to identify practical barriers to the experimental realization of compressible isotropic turbulence. The turbulence intensities and Mach numbers considered in the present work are insufficient for the turbulence itself to be considered compressible, so the dilatational dissipation rate and the pressure-dilatation correlation are beyond the scope of the study. However, by identifying the phenomena which arise as the Mach number increases, progress towards this end will be made.

It is proposed to perform the study using both flow visualization and laser-Doppler velocimetry; the former to obtain a qualitative understanding of compressibility effects, and the latter to obtain quantitative measurements of the mean and fluctuating velocity fields.

1.3 Organization of the Thesis

The thesis is divided into six chapters. The current chapter contains introductory material. Chapter 2 reviews relevant literature to provide the theoretical underpinnings of the study and an up-to-date summary of the state of related research. Chapter 3 discusses the experimental methodology, including the facility, instrumentation, data

processing techniques, and methods for estimating error. The actual measurements, including the operating characteristics of the wind tunnel, are presented in Chapter 4, and are discussed further in Chapter 5. Finally, in Chapter 6, some conclusions are drawn and recommendations for further study are proposed.

Chapter 2

Literature Review

In this chapter, the literature and theory related to the thesis are reviewed. The review begins with analytical and experimental studies dealing with homogeneous isotropic turbulence in incompressible flow, and then considers analytical, numerical, and experimental investigations of compressibility effects on turbulence. Subsequently, studies which have been performed in the same facility as the present experiments are mentioned. The review finishes with a summary of the literature most directly related to this thesis.

2.1 Incompressible Flow

General introductions to turbulence can be found in the textbooks by Hinze (1975) and Tennekes and Lumley (1972). Although the sources emphasize incompressible flow, they also include some discussion of compressibility effects. They consider both effects of turbulence and some particular fundamental flows: isotropic turbulence, shear flows, jets, mixing layers, and wall-bounded flows.

2.1.1 Analytical Studies of Isotropic Turbulence

The simplest turbulent flow, discussed in detail in the third chapter of Hinze (1975), is homogeneous isotropic turbulence. By *homogeneity* it is meant that the statistical properties of the turbulence are invariant under arbitrary translations of the coordinate system. By *isotropy* it is meant that the statistical properties of the turbulence are invariant under arbitrary rotations and reflections of the coordinate system. Isotropy is a more severe restriction than homogeneity, and in fact an isotropic turbulence must also be homogeneous.

In turbulent flow, the velocity field is commonly decomposed into mean and fluctuating components. The kinetic energy of the velocity fluctuations, or *turbulence kinetic energy*, is defined using Cartesian tensor notation as

$$k = \frac{1}{2}\overline{u_i u_i}, \tag{2.1}$$

where u_i is the fluctuating velocity. In homogeneous isotropic turbulence, the rate of change of turbulence kinetic energy is given by

$$\frac{\partial k}{\partial t} = -\epsilon, \tag{2.2}$$

where ϵ is always a sink term, and is therefore called the *dissipation rate*. In homogeneous turbulence, it takes the following form:

$$\epsilon = \nu\overline{\frac{\partial u_i}{\partial x_j}\frac{\partial u_i}{\partial x_j}}. \tag{2.3}$$

For isotropic turbulence, von Kàrmàn and Howarth (1937) showed that the dissipation rate can be written in terms of a single length scale called the *Taylor microscale*, λ:

$$\epsilon = 10\nu\frac{k^2}{\lambda^2}. \tag{2.4}$$

The Taylor microscale is related to the two-point correlation coefficient of the velocity fluctuations.

From these equations it is evident that homogeneous isotropic turbulence must decay — there are no mechanisms by which new turbulence might be produced. The decay process can be divided into three phases. In the initial period, viscous forces act only on the energy-containing eddies, and the largest eddies have a permanent character. In the final period, viscous forces dominate inertial effects for all eddy sizes. These two periods are separated by a transitional period. In this thesis, attention is restricted to the initial period of decay.

The decay rate in the initial period has traditionally been expressed using a power law, as follows:

$$k = b(t - t_0)^{-n}, \tag{2.5}$$

where b is a coefficient, t_0 is the time at which the turbulence was created with infinite energy, and n is the decay exponent. Analytical studies have yielded a number of estimates for n, many of which are based on self-preserving assumptions for the turbulence spectrum. By assuming self-preservation at all scales, Batchelor (1948) found a decay exponent of unity. Others have made partially self-preserving hypotheses; for instance, assuming self-preservation for the power spectrum at wave numbers larger than that corresponding to the integral length scale, and time-independence for the power spectrum of the largest (permanent) eddies. Under these conditions, and further assuming that the energy of the largest eddies varies with the fourth power of the wave number, one obtains a decay exponent of 10/7 (Kolmogorov, 1941; Comte-Bellot and Corrsin, 1966). Saffman (1967a) has argued that the energy of the largest eddies varies rather with the square of the wave number, yielding a decay exponent of 6/5 (Saffman, 1967b). George (1992) concluded that the decay exponent depends upon the initial conditions except in the limit of infinite Reynolds number, where a universal decay exponent of unity results.

2.1.2 Experimental Studies of Decaying Turbulence

Experimental studies of decaying turbulence typically involve the study of flow behind a screen in a duct or wind tunnel. Here the term *screen* is used in a general sense, independently of geometry and fabrication process. In the first part of this section, some general characteristics of flow behind screens is considered; subsequently, literature dealing specifically with the use of screens to generate homogeneous isotropic turbulence is reviewed.

Flow through Screens

Flow through screens has been the focus of many investigations, owing to their many practical uses. In a review article, Laws and Livesey (1978) considered the most common applications: improving flow uniformity, obtaining a prescribed mean velocity profile, changing flow direction, obtaining a prescribed pressure drop, reducing turbulence intensity, and increasing turbulence intensity.

Screens can incorporate different geometries. Some of the more common ones are: grids, wire gauzes, perforated plates, and honeycombs. *Grids* involve an array of periodically-spaced rod elements. The *mesh size* is defined as the grid pitch, or the separation distance between the rods. The rods usually have a circular (*round-rod*) or square (*square-rod*) cross-sectional shape. A *parallel rod* grid has rods oriented only in one direction, whereas a *square mesh* grid has rods oriented in both transverse directions. To simplify construction, a square-mesh grid often has the rods oriented in the horizontal direction slightly offset from those oriented in the vertical direction, which is referred to as a *biplane* grid.

Wire gauzes also incorporate a square-mesh design, but have a woven construc-

tion. *Perforated plates* have circular holes drilled, punched, or machined into a blank according to some periodical pattern. *Honeycombs*, like perforated plates, have circular passages, but are usually substantially thicker and their passages are separated by thin walls.

An important attribute of any screen is its *solidity*, defined as the ratio of the projected solid area to the total area.

The characteristics of flow through screens was considered by Baines and Peterson (1951). At low Reynolds numbers, the flow remains attached to the screen elements, and the drag is due entirely to viscous shear. At the *critical Reynolds number*, the flow separates, leading to a high form drag, an increased pressure loss coefficient, and greatly increased turbulence generation. The new turbulence is produced as wakes from neighbouring elements mix, causing the large scale coherent structures to lose their identities. However, the turbulence generation process is most effective for a limited range of grid solidities. At high grid solidities, typically above 50%, individual jets may become unstable — some coalescing and others diverging — leading to large transverse inhomogeneities.

A number of investigations of flow through screens have dealt with an appropriate functional form for the pressure loss coefficient of the screen, usually in terms of a geometry-specific coefficient and the Reynolds number (e.g. Baines and Peterson, 1951; Annand, 1953; Pinker and Herbert, 1967). Pinker and Herbert (1967) also considered the effect of the Mach number on the pressure loss coefficient of wire gauzes, and tabulated the upstream Mach number for which the flow becomes choked in the gauze as a function of the gauze solidity. The results agreed closely with isentropic flow theory provided that an "effective" screen solidity is used in place of the standard solidity based on orthogonal projection.

Loehrke and Nagib (1972) studied the nature of the turbulence produced downstream of various screens, including honeycombs, grids, gauzes, perforated plates, and porous foam. Each of these devices, and especially honeycombs, suppress the incoming turbulence and produce new vigourous turbulence from shear layer instabilities. They noted that perforated plates tend to generate large-scale turbulence, and are also particularly effective in smoothing out upstream inhomogeneities in the mean flow. Tan-Atichat et al (1982) expanded on this study to investigate the influence of upstream conditions, such as mean velocity and turbulence intensity and scales, on screen performance. Provided jet instability did not ensue, they found the decay rate to be relatively insensitive to upstream flow conditions.

The Decay of Grid Turbulence

Having considered the general characteristics of flow through screens, we now consider the particular application of screens to produce an approximately isotropic turbulence. This configuration was suggested by Taylor (1935) as a test case for the theory of isotropic turbulence. Historically, grids have been used to generate the turbulence, and the phrases *grid turbulence* and *grid-generated turbulence* have become so engrained in the literature that they are used even when the turbulence is generated by other screen geometries.

Corrsin (1963) provided an overview of factors to be considered in the experimental realization of homogeneous isotropic turbulence. He noted that a developing region of about 40 mesh lengths is required before the turbulence becomes reasonably homogeneous, and even then it is only approximately so. One reason for the deviation is that the duct walls restrict the scales of the turbulence, while a truly homogeneous turbulence occupies infinite space. This restriction is minor if the duct dimensions

are large compared with the turbulence scales of interest, and if the flow in the fluid core is not significantly influenced by boundary layer effects. A second source of grid turbulence inhomogeneneity is streamwise energy decay and length scale increase; this streamwise inhomogeneity can be neglected if the turbulence scales change sufficiently slowly.

Corrsin also considered the isotropy of grid turbulence. One convenient test for isotropy involves a comparison of the root-mean-square of the streamwise and transverse fluctuations, u' and v'. In isotropic turbulence these must be equal, although Schedvin et al (1974) pointed out that the test is heavily weighted toward the energy-containing scales. In grid turbulence, u' usually exceeds v' by a factor of about 1.15. Hence the turbulence is more accurately described as *axisymmetric* (having statistical properties which are invariant under arbitrary rotations and reflections of the transverse coordinate axes) than isotropic. Uberoi and Wallis (1966) attempted to improve the degree of isotropy by using an axial contraction, finding that u' and v' tended to equalize in the contraction but return to an anisotropic state further downstream. In contrast, Comte-Bellot and Corrsin (1966) observed the isotropy to improve in the contraction with no tendency to deteriorate downstream.

It is convenient to express the decay of grid turbulence in a form somewhat different than that of Eq. (2.5). The independent variable is transformed from time to the distance from the grid, separate decay laws are written for the streamwise and transverse velocity variances, the equation is non-dimensionalized by relevant scales, and engineering notation is used. The resulting decay law for the streamwise velocity variance is

$$\frac{u'^2}{U^2} = B\left(\frac{x - x_0}{m}\right)^{-n}. \tag{2.6}$$

where U is the mean streamwise velocity, u' is the streamwise rms velocity fluctuation, B is the decay coefficient, m is the grid mesh size, x is the distance from the grid, x_0

is the effective origin, and n is the decay exponent.

Simmons and Salter (1934) were among the first to study grid turbulence. Early studies of the decay law were performed by Batchelor and Townsend (1948), who assumed a linear decay law, and Baines and Peterson (1951), who assumed $n = 10/7$. The most extensive, and most widely quoted, grid turbulence experiments are those of Comte-Bellot and Corrsin (1966), who considered a variety of grid geometries and who calculated (using the least square method), rather than assumed, values for n. Using data over the range $30 < x/m < 350$, n was measured to be between 1.15 and 1.4, depending on the grid geometry and the grid Reynolds number,

$$R_m = \frac{Um}{\nu}. \tag{2.7}$$

The exponent was also slightly larger for u' than for v', reflecting the tendency of the flow to become isotropic. Passing the turbulence through a slight contraction improved the equality not only of u' and v' but also of their decay exponents.

Mohamed and LaRue (1990) considered previous data and performed new experiments with round-rod biplane grids to argue for a universally self-similar turbulence spectrum, independent of initial conditions, with $n \approx 1.3$. In the process, they proposed an "objective" technique of obtaining x_0, based on the assumption that the empirical constants should be independent of the position of the first point of measurement. They then reviewed previous measurements to determine the effect of flow parameters on the decay law. They concluded that n is independent of Reynolds number and grid solidity, but the decay coefficient increases with solidity and decreases with Reynolds number.

Most studies of grid turbulence involved relatively low speeds, with typical turbulence Reynolds numbers,

$$R_\lambda = \frac{u'\lambda}{\nu}, \tag{2.8}$$

of 50 or lower. Kistler and Vrebalovich (1966) performed experiments in which R_m ranged from 1.2×10^5 to 2.4×10^6, and R_λ was approximately 600. They found the decay rate to be well-represented by a linear law. Other high Reynolds number measurements, performed by Schedvin et al (1974), suggested a trend toward isotropy as R_m was increased, but the range of x/m was too small to determine n.

Other types of turbulence generators have also been used. In a study designed to investigate the role of the momentum loss at the grid in the ensuing turbulence structure, Gad-el-Hak and Corrsin (1974), and later Tassa and Kamotani (1975), devised active grid systems featuring jets through which momentum could be injected into the flow, both with and against the flow. Each jet had its own nozzle, allowing good control over the resulting flow characteristics and ensuring reasonable homogeneity. The decay exponent was found to decrease with injection rate, and no peculiar behaviour was observed when the net force exerted on the grid flow was zero. Another novel turbulence generator was that of Ling and Wan (1972), who used a mechanically agitated grid, featuring counter-rotating bars, in a water tunnel. They found n to decrease from 2.0 to 1.35 as R_m increased from 6000 to 34 000.

2.2 Compressible Flow

In compressible flow, the density field cannot be assumed constant, leading to many phenomena and complexities which have no counterparts in incompressible flow. Several texts, such as the one by John (1984), have discussed general compressibility effects with an emphasis on isentropic flow. An overview of the current state of research into compressibility effects on turbulence, including both homogeneous and simple inhomogeneous flows, was provided by Lele (1994).

In the remainder of this section, various analytical, numerical, and experimental studies of turbulence in compressible flow are reviewed. Two classes of flow are emphasized: decaying isotropic turbulence and shock-turbulence interactions.

2.2.1 Analytical Studies

In incompressible turbulence, the flow variables are decomposed into mean and fluctuating components, with the mean component obtained by simple time-averaging. In compressible turbulence, where the density field fluctuates, more decomposition options exist. Favre (1967) compared conventional time-averaging with density-weighted averaging, and concluded that density-weighted averaging leads to simpler equations with clearer physical interpretations. The turbulence fluctuations themselves were decomposed by Kovasznay (1953) into vorticity, sound, and entropy modes. The vorticity mode is described by the same equations as vorticity in a viscous incompressible flow. Compressibility appears in the sound mode, which obeys a wave-type equation, and the entropy mode, which satisfies a diffusion equation. To first order, the vorticity mode is independent, while the sound and entropy modes are weakly connected. Second order interactions were considered by Chu and Kovasznay (1958).

Turbulence mechanisms in compressible boundary layers were studied by Morkovin (1961). He observed that although compressibility effects can be expected in the presence of large velocity gradients and rapid density changes, such as in shock-turbulence interactions or boundary layers with large pressure gradients, the mechanisms of turbulence are largely independent of M for $M < 5$. This observation, now commonly referred to as Morkovin's hypothesis, is equivalent to assuming that the rms density fluctuation is small compared with the mean density (Bradshaw, 1977). Sarkar et al (1991) suggested that a more natural gauge of compressibility effects on turbulence

is the turbulence Mach number, defined as

$$M_t = \frac{(2k)^{1/2}}{c}, \tag{2.9}$$

where c is the local speed of sound.

Analytical studies have also shed insight into the decay of compressible isotropic turbulence. Moyal (1953) found that compressibility enhances the dissipation rate, and derived the form of the additional terms in the Fourier domain. The dissipation of turbulence kinetic energy can also be obtained from the Reynolds stress transport equation (Zeman, 1990; Sarkar et al, 1991), as follows:

$$\overline{\rho}\frac{\partial k}{\partial t} = -\epsilon_s - \epsilon_d + \overline{p'd'}. \tag{2.10}$$

In this equation,

$$\overline{\rho}\epsilon_s = \mu\overline{\omega_i'\omega_i'}, \tag{2.11}$$

where ω_i' is the fluctuating vorticity vector. Eq. (2.11) is equivalent to Eq. (2.3), and ϵ_s is therefore called the *solenoidal* or *incompressible* dissipation rate. ϵ_d is calculated from

$$\overline{\rho}\epsilon_d = \mu\overline{d'd'}, \tag{2.12}$$

where d' is the fluctuating dilatation, finite only in compressible turbulence:

$$d' = \frac{\partial \overline{u}_i}{\partial x_i}. \tag{2.13}$$

ϵ_d is consequently called the *dilatational* or *compressible* dissipation rate. Both ϵ_s and ϵ_d are positive. The third term in Eq. (2.10), $\overline{p'd'}$, is called the pressure-dilatation term, and although it in principle can take either sign, it is usually dissipative. Hence compressibility serves to increase the dissipation rate.

A second class of flows of relevance to this thesis involves the interaction between shocks and turbulence. Ribner (1953) studied this problem analytically, considering

the convection of an inclined plane sinusoidal shear wave, which may be interpreted as a single component of the turbulence spectrum, through a normal shock. He found that the shock alters the inclination and increases the amplitude of the shear wave. A physical explanation for the anisotropic turbulence amplification was offered by Lele et al (1992), who pointed out that eddies passing through a shock are compressed in the direction normal to the shock wave, leading to an increase in mean square vorticity and turbulence kinetic energy.

2.2.2 Numerical Studies

In numerical studies, the equations representing conservation of mass, momentum, and energy, together with appropriate constitutive equations, are solved for particular flows. When the full set of equations is solved without any turbulence modelling, this procedure is called Direct Numerical Simulation (DNS). In principle DNS can be used to solve any type of flow; in practice it is limited to the simplest flows because of computational restrictions. Other numerical approaches make various assumptions to simplify the governing equations.

Isotropic Turbulence

A number of DNS studies have been performed to understand the properties of compressible isotropic turbulence. Kida and Orszag (1991) observed an exponential decay law for decaying compressible turbulence, as in incompressible flow. Using two-dimensional DNS, Passot and Pouquet (1987) found that compressibility effects become significant only when $M_t > 0.3$. They also observed "eddy shocklets" in some of their simulations, which were investigated in more detail by Lee et al (1991). The latter authors found that the shocklets have the characteristics of regular shocks, are

responsible for a major portion of ϵ_d, and become more frequent as M_t or R_λ increase. Further studies of ϵ_d were performed by Blaisdell et al (1993). They found that it depends more upon the initial conditions, in particular on how the fluctuations are partitioned, than on M_t. As R_λ increased, the sensitivity to initial conditions persisted, but was weakened.

These DNS studies have been used in conjunction with analytical theories to propose models for ϵ_d and $\overline{p'd'}$. The models of Zeman (1990, 1992), based on the eddy shocklets, and of Sarkar et al (1991), based upon an asymptotic analysis, suggest that ϵ_d varies with M_t^2. In the model of Ristorcelli (1995), ϵ_d varies with M_t^4.

The applicability of Taylor's frozen flow hypothesis in compressible flow was considered by Lee et al (1992). Because the hypothesis assumes passive advection of disturbances, they noted that it does not hold for the acoustic mode of fluctuation, which obeys a wave-type equation. Comparison of temporally-evolving and spatially-evolving compressible turbulence showed that the hypothesis breaks down as either M_t or the turbulence intensity increase.

Shock-Turbulence Interactions

A number of techniques are available to solve shock-turbulence interactions. Three common techniques are: DNS; Linear Interaction Analysis (LIA), which solves the equations derived by Ribner (1953); and Rapid Distortion Theory (RDT), which assumes that the time scale of the mean-field deformation is small relative to the turbulence time scale, so that non-linear and viscous terms may be neglected.

Using DNS and LIA, Lee et al (1993) observed that turbulence quantities, particularly the streamwise component of the Reynolds stress tensor, are amplified through the shock, leading to reduced turbulence length scales. Similar results were obtained

using DNS by Hannappel and Friedrich (1993, 1995), who also emphasized the importance of the pre-shock conditions. Anyiwo and Bushnell (1982) derived jump relations for various turbulence quantities across a shock using the linear analysis of Ribner (1953), They also identified the mechanisms responsible for the turbulence amplification (see also Zang et al, 1984), which include the direct amplification of vorticity fluctuations, interactions among the fluctuation modes, and "pumping" of turbulence by externally-driven shock oscillations.

2.2.3 Experimental Studies

Experimental Techniques in Compressible Flow

Hot-wire anemometry (HWA) is a common technique for measuring flow velocity. Kovasznay (1950) identified and analyzed three difficulties in extending its use to supersonic flow: frequency response, an alternative expression to King's law for the heat loss from the wire, and interpretation difficulties due to density and temperature fluctuations. The author concluded that, although HWA is more difficult in supersonic flow, it is still possible.

Another technique widely used for measuring flow velocities is laser Doppler velocimetry (LDV). The general principles of LDV are discussed in several monographs and essays, such as those by Durst et al (1981) and Adrian (1983). In high speed flow, particular care must be taken to ensure that the particles faithfully follow the flow (e.g. Menon and Lai, 1991; Rudoff and Bachalo, 1991; Micheli et al, 1991). Shocks pose a particular problem for LDV measurements. Because different-sized particles respond to the step velocity change at different rates, a spurious "particle turbulence" is measured. Bloomberg (1989) studied particle turbulence with monodispersed and polydispersed particles downstream of an oblique shock, observing its dependence on

particle size and distribution. Jacquin et al (1991) also considered LDV accuracy near a shock. In addition to particle inertia, they identified a second, less serious, cause of inaccuracy, related to the refraction of the incident laser beam by the shock. They went on to investigate particle inertia effects with olive oil and incense smoke particles. The former, which were smaller, yielded higher particle turbulence levels but a narrower shock width.

Measurement Results

The first known study dealing with grid turbulence in compressible flows was by Uberoi and Kovasznay (1955), who estimated the correlation function of a three-dimensional density field from shadowgraph images. One flow which they considered was the wake of a "Swiss cheese" projectile, consisting of a perforated disk travelling at Mach 1.03. The authors concluded that the flow was approximately homogeneous and isotropic at some unspecified distance behind the projectile.

Several shock tube experiments have been performed to investigate the interaction of grid turbulence with a moving shock wave. The shock, which is induced by bursting a diaphragm, diffracts through a grid, causing vortex rings to form. As these vortex rings interact with each other and dissipate, nearly homogeneous, isotropic turbulence is generated. A porous end-wall is usually used, allowing the flow to escape but the shock to reflect and interact with the turbulence field.

Among the first such shock-tube experiments are the HWA measurements of Trollier and Duffy (1985), although the manner of turbulence generation was not specified. They found that the turbulence levels were amplified by a factor which reduces with Reynolds number. Turbulence amplification was also observed by Keller and Merzkirch (1990) and Honkan and Andreopoulos (1992). The latter authors also

reported decay laws for the turbulence, with $n = 1.25$ both before and after the shock interaction, although upon scrutiny it appears that this value was assumed rather than calculated. In another experiment, Briassulis and Andreopoulos (1994) observed amplification of pressure fluctuations.

At present there are only two known experiments dealing with grid turbulence in continuous-flow wind tunnels at supersonic speeds. The first is that of Jacquin et al (1991), explained in more detail by Blin et al (1993). The authors investigated the interaction between grid turbulence and a standing normal shock wave with an upstream Mach number of 1.65. A woven screen served both as the turbulence generator and the sonic throat, but was also found to generate of compression waves. Velocity measurements were obtained with LDV. Upstream of the shock, a decay exponent of 1.3 was reported; downstream of the shock, the decay rate increased. However, no turbulence amplification through the shock was observed.

A similar, but more refined, investigation was performed by Barre et al (1995). They optimized the turbulence generator/sonic throat design by using a multi-nozzle (see p. 100 and Plate I (2) of Pankhurst and Holder, 1952), which generated a flow of $M = 3$. The compression waves generated by the multi-nozzle were of very low intensity, such that a schlieren study could not detect them $x/m = 130$. Velocity measurements were obtained with LDV for the mean flow and with HWA for the longitudinal velocity fluctuations. Turbulence amplification was found to be consistent with the predictions of LIA.

Other types of shock-turbulence interaction experiments have also been performed. For instance, Debieve and Lacharme (1986) considered the interaction between an oblique shock and turbulence generated by air injection upstream of the sonic throat. Turbulence intensities, measured with HWA, were amplified over a distance of 10 mm, before returning approximately to its upstream value. Studying the shock-turbulence

interaction in a boundary layer, Ardonceau (1984) also observed turbulence amplification, particularly for the Reynolds shear stress.

2.3 Previous Measurements at the Facility Used in the Present Study

The facility used to obtain the results presented in this thesis has been used for two related turbulence studies. The first (de Souza, 1993; de Souza et al, 1995) involved nearly homogeneous, highly-sheared turbulence in incompressible flow. The second (Budwig et al, 1995) considered grid turbulence in the incompressible ($M = 0.18$), "transonic" ($M = 0.9$; referred to in this thesis as high subsonic), and supersonic ($M = 1.6$) regimes. In the incompressible regime, a decay exponent in the range of previous incompressible studies was found. In the transonic regime, the flow was found to be anisotropic with no net turbulence decay. In the supersonic regime, weak oblique shocks were observed, resulting in oscillations in the profiles of mean and turbulence quantities. This latter study was an exploratory study and served as a springboard for the research discussed in this thesis.

2.4 Summary

In the above sections, a relatively broad range of literature has been reviewed. Some of those studies, while having some connection to this thesis, are of peripheral interest. In this section the state of research in those areas most directly related to the present work is discussed, with the goal of identifying how the work presented in the remainder of the thesis contributes to the body of knowledge.

2.4.1 High Reynolds Number Flow

Grid turbulence in low-speed incompressible flow has been studied extensively, and the experiments of Comte-Bellot and Corrsin (1966) may be regarded as the standard reference. Even in their finely-controlled experiments, a single universal decay law did not result; rather, n varied between 1.15 and 1.4. If the rest of the literature is considered, the variation is still larger.

The variability in n could be due, at least in part, to the relatively low Reynolds numbers. Schedvin et al (1972) reported earlier studies which suggest that R_λ should exceed 200 for the inertial subrange to exist, whereas in most grid turbulence studies, R_λ is less than 50. George (1992) argued that without an inertial subrange, the decay law retains a dependence on the initial conditions, and therefore varies with factors such as grid geometry and R_m. He further argued that the decay exponent should asymptotically approach unity as R_m is increased, which appears to have some experimental support. Although Mohamed and LaRue (1990) assert that n is independent of R_m, Comte-Bellot and Corrsin (1966) noticed a slight dependence and Ling and Wan (1972) reported a much stronger dependence. The only experiment in which an inertial subrange was observed is due to Kistler and Vrebalovich (1966), who observed an exponent of unity. Given the paucity of high-speed grid turbulence measurements, any additional contribution to this discussion would be valuable.

2.4.2 Compressible Flow

Experimental studies of grid turbulence in compressible subsonic flow are also scarce. They typically investigate shock-turbulence interactions in shock tubes. Only a single study was found to report a decay law in the compressible subsonic regime (Honkan and Andreopoulos, 1992), but it appears that n was assumed to be 1.25.

Experimental studies of the decay of grid turbulence in supersonic flow are also rare. In a shock-turbulence interaction study in a continuous-flow wind tunnel, Jacquin et al (1991) reported a decay exponent of 1.3 upstream of the shock, but compression waves were observed in the flow. Barre et al (1995) were able to minimize the compression waves, but did not provide details about the decay law, noting only that it was consistent with incompressible results.

From this survey, it is apparent that, although a number of studies utilizing grid turbulence in compressible flow have been performed, none have attempted to systematically study the effects of compressibility on the decay of grid turbulence. The main objective of this thesis is to contribute in this area.

2.4.3 Compressible Turbulence

For turbulence to be considered compressible, M_t must reach the appreciable levels needed for ϵ_d to become significant relative to ϵ_s. Various computations have shown that the dissipation rate of compressible isotropic turbulence is indeed augmented by compressibility effects via dilatational fluctuations. However, the Reynolds numbers for such computations is limited to approximately 1000. Although useful for developing models and theories of turbulence, such computations do not seem to represent any technologically interesting flow.

The experimental realization of nearly isotropic turbulence with significant levels of M_t is also beyond the reach of experimental work at present. It is therefore not the purpose of this thesis to study the dilatational dissipation rate or the pressure-dilatation correlation. However, it is hoped that barriers to the experimental realization of nearly isotropic compressible turbulence will be identified.

Chapter 3

Experimental Techniques

3.1 Facility

3.1.1 Wind Tunnels

The experiments were performed at two facilities. A trisonic pilot wind tunnel, located at the High Speed Aerodynamics Laboratory (HSAL) of the Institute for Aerospace Research (IAR) at the National Research Council of Canada (NRC), was used for all quantitative, and some qualitative, tests. The results were supplemented by a qualitative study of the flow near the grid using a supersonic demonstration nozzle at the University of Ottawa.

With a 127×127 mm test section, the pilot wind tunnel is a 1/12 scale model of a 1.5×1.5 m trisonic blowdown tunnel. Photographs of the facility are shown in Plate 1, and a schematic is shown in Figure 1. It is supplied with compressed air from two tanks, each having a capacity of 1420 m^3, capable of storing air at up to 2.1 MPa, and featuring thermal matrices to minimize temperature variations. The large tank

capacity permits continuous operation of the pilot tunnel for extended periods of time. The supply pipe between the tanks and the settling chamber features a shut-off valve and a hydraulic control valve, which maintains a constant pre-selected pressure in the settling chamber. The settling chamber contains a conical-shaped flow separator, to prevent separation as the air diffuses into the chamber; a series of perforated dishes and woven screens, to improve uniformity and dampen background turbulence; and a 10:1 contraction.

Housed between the contraction and the test section is an aluminum frame, to which the turbulence generator, discussed in Section 3.1.2, is bolted. The test section has constant cross-sectional dimensions of 127×127 mm and a length of 1055 mm. The floor and the ceiling of the test section features openings of length 254 mm, spanning the full width, and starting at a distance of 730 mm from the downstream end of the turbulence generator. The openings are covered with 25.4 mm-thick plexiglass windows, thereby permitting visual access to the flow for visualization and measurements.

Downstream of the test section are two joints: the contraction joint and the diffuser throat. The contraction joint permits a full range of motion of the diffuser throat, which in turn is the primary control of the test section Mach number when the tunnel is operated in the subsonic regime. Further downstream, the air passes through an adaptor, which changes the cross-sectional profile from square to circular, and is exhausted to the atmosphere. The downstream circular portion of the wind tunnel also features a telescopic section, which was used when removing or changing the grid. This procedure involved unscrewing the bolts which join the test section and settling chamber, pushing the test section downstream, dismounting the aluminum frame from its supporting dowels, and removing the grid.

The demonstration nozzle (AMRAD Model W4C) is shown in Plate 2. It has

Table 3.1: Turbulence Generator Dimensions

Plate	d (mm)	a (mm)	b (mm)	c (mm)	m (mm)	Solidity
SHP (Small-hole)	6.50	6.35	7.11	7.28	7.2	33.5%
MHP (Medium-hole)	12.70	12.70	14.29	14.57	14.5	33.2%
LHP (Large-hole)	16.27	15.82	18.46	18.32	18.4	33.0%

cross-sectional dimensions 9.8 × 6.4 mm. A test section, having plexiglass walls, a length of 45 mm, and a crude adjustable diffuser throat at its exit, could be attached to the nozzle exit.

3.1.2 Turbulence Generators

Aluminum perforated plates of thickness 4.8 mm were used to generate the turbulence in the pilot tunnel. Three plates were available from a previous study (Budwig et al, 1995), each having a solidity of about 33%. Referring to the schematic diagram shown in Figure 2, the plates have the dimensions given in Table 3.1. The variable m is an effective mesh length, determined as the average distance between a hole and its six neighbours as follows:

$$m = \frac{b + 2c}{3}. \tag{3.1}$$

The intensity of the turbulence generated by the small-hole plate was found to be too small to be measured accurately, and hence only the medium- and large-hole plates were used in the present measurements. These plates will be referred to as the MHP and LHP respectively, and are displayed in Plate 3.

For the supersonic cases, the perforated plates served not only as turbulence generators, but also as sonic nozzles, producing supersonic flow in the test section. Unlike a smooth converging-diverging nozzle, which provides an isentropic choking process, the plate is very abrupt. As a result, weak oblique shocks formed, which subsequently

reflected off the test section walls. The waves affected the LDV measurements of Budwig et al (1995) and, as will be discussed later, could be detected with the shadowgraph method (see Plates 7 to 9). As part of the present work, plate modifications were undertaken on the MHP in order to reduce the wave intensity:

1. The unmodified plate had metal blockages jutting into the flow along two opposing edges of the plate. The LHP retained this feature, as is evident in Plate 3. For the MHP, semi-circular openings were machined into the blockages.

2. Chamfers, angled at 15° and having a depth of 2.2 mm, were machined around all the holes on the downstream side of the plate.

The plates could be inserted into the aluminum frame in two orientations. In the *standard orientation*, the jagged plate edges (blocked for the unmodified plate and unblocked for the modified plate) were aligned with the $z-$axis. This orientation was used for all LDV measurements. In the *rotated orientation*, the plate was rotated by 90°, and the jagged plate edges were aligned with the $y-$axis. The rotated orientation was studied only qualitatively, using flow visualization, and only in supersonic flow.

Turbulence generators / sonic nozzles were also constructed for the demonstration nozzle. Parallel rods of different geometries, listed in Table 3.2, were clamped in between the two side walls of the test section. The rod dimension referred to in the table is the cross-sectional dimension orthogonal to the flow (e.g. diameter for a round rod). The second square rod grid had half-rods along the floor and ceiling of the test section. The rod geometries are evident in the flow visualization images shown in Plates 10 to 17.

Table 3.2: Attributes of Demonstration Nozzle Grids

Rod Geometry	Rod Dimension (mm)	Number of Rods	Solidity
Round	1.8	2	35%
Square I	1.8	2	35%
Square II	1.8	3	53%
Diamond	2.5	2	50%

3.1.3 Flow Visualization

High subsonic and supersonic flows at the measurement window in the pilot tunnel were visualized using the shadowgraph technique, which is discussed in many references (e.g. Goldstein, 1983). Photographs of the system are provided in Plate 4, and a schematic is shown in Figure 3. A slide projector was used together with a series of lenses and a pinhole to produce a collimated beam. A double-pass system was implemented, so that only a single front-surface mirror, suspended above the test section, was required. Because the light beam passed through the test section twice, the sensitivity was twice that of a comparable single-pass system, but at the expense of some blurring in the images. Because the shadowgraph technique integrates over the optical path of the light beam, only two-dimensional phenomena were captured. Three images were required to capture the entire window area.

Most images were obtained using a Nikon F-601M camera equipped with a 90 mm macro lens and Kodak TMAX-3200 film. Due to a relatively low light intensity at the screen, 0.5 second exposures were required. The negatives were developed and printed, using print exposure and development times to obtain similar background brightnesses for all prints. The three images for each set of operating conditions were pieced together after printing, and then digitized with a scanner. Some sequences were also captured with a Sony camcorder, from which individual frames were later

digitized using frame-grabbing technology.

Some tests were also performed with the schlieren technique, which required a knife edge to remove part of the light source image. However, the shadowgraph images were in general superior, apparently because the anisotropic optical characteristics of the plexiglass windows distorted the light source image. Consequently, the knife edge could not be positioned to obtain a uniform darkening of the test section image.

In the demonstration nozzle, a conventional (single-pass) schlieren system, integrated with the flow facility, was used for flow visualization. Images were obtained by filming the screen with Sony camcorder and later digitizing individual frames.

3.2 Instrumentation

3.2.1 Pressure and Temperature Measurements

During the wind tunnel runs, pressure and temperature were monitored at various stations, shown in Figure 4. Station 0 is in the settling chamber, station 1 is upstream of the measurement window, and station 2 is downstream of the window. Total pressures were monitored at stations 0 and 2 (P_{t0} and P_{t2}, respectively), static pressures at stations 1 and 2 (P_1 and P_2, respectively), and static temperature at station 0.

3.2.2 Laser Doppler Velocimetry Equipment

Flow velocity measurements were obtained using laser Doppler velocimetry (LDV) equipment, which is visible in Plate 1. Simultaneous measurement of two velocity components could be obtained using a three-beam, two-colour, dual beam system,

supplied by DANTEC. Green and blue beams, having wavelengths of 514.5 nm and 488 nm respectively, were generated in a 100 mW Argon-ion laser and transmitted to the probe head via fibre optic cables. A 40 MHz Bragg cell could be used to shift the range of measurable velocities and permit unambiguous measurement of negative velocities. The LDV equipment was operated in forward-scatter mode, with the receiving optics and photomultiplier tubes (PMTs) slightly off-axis. The Doppler frequency was extracted by the the burst-based DANTEC 55N10 Flow Velocity Analyzer, and the particle velocity calculated by the software package `FLOware`, developed by DANTEC. `FLOware` was also used to control data acquisition, using options such as validation criteria and levels, filter bandwidths, and PMT voltage levels. Some practical details of the LDV equipment and the `FLOware` software are provided in Appendix B.

The laser beams were focussed at the probe volume using a lens attached to the probe head. The fringe spacing in the probe volume was determined by the lens focal length, and therefore lenses of differing focal lengths could be used to measure different velocity ranges. The lenses which were available for the system are listed in Appendix B. Only the 160 mm and 243 mm lenses were used in the present experiments; their associated velocity ranges and probe volume data are tabulated in Table 3.3, where σ_1, σ_2, and σ_3 are defined as the probe volume length, width, and height, respectively. The 243 mm lens was a monochromat, and could therefore be used only for one-component measurements. In some two-component measurements with the 160 mm lens, the measurable velocity range was changed by rotating the probe head, and consequently the orientation of the fringes in the probe volume, by 45%. Upon processing, the resulting velocity samples were transformed to the original coordinate system.

The probe head and receiving optics were mounted to a frame, which in turn

Table 3.3: Characteristics of Lenses Used in the Experiments

	160 mm lens Green beam	160 mm lens Blue beam	243 mm lens Green beam	243 mm lens Blue beam
Velocity range 40 MHz shift (m/s)	-18.4–92.2	-17.5–87.4	-28.0–139.8	26.5–132.6
Velocity range No shift (m/s)	104.5–215.1	99.1–204.0	158.4–326.2	150.3–309.4
Velocity range -40 MHz shift (m/s)	227.4–338.0	215.7–320.6	344.8–512.6	327.1–486.2
Fringe spacing (μm)	3.074	2.916	4.660	4.420
σ_1 (mm)	0.0777	0.0737	0.1180	0.1119
σ_2 (mm)	0.0776	0.0736	0.1179	0.1118
σ_3 (mm)	1.238	1.174	2.849	2.703

was attached to a two-dimensional traverse to permit precise positioning of the probe volume in the transverse plane. The major source of imprecision in transverse positioning was leadscrew backlash, which was minimized by consistently approaching a target position from the same direction. Axial positioning for most measurements was achieved by fixing the axial position of the two-dimensional traverse using dowel pins, which could be inserted into holes at 2.54 cm intervals. A potential imprecision of 0.5 mm was associated with this method, but in practice it was less because the traverse system was consistently pushed against the dowel pin in the same direction. In some supersonic tests, the axial positioning method was altered. Shoulder bolts were screwed into the positioning holes, and the axial position of the traverse was fixed by inserting shims between the traverse and the shoulder bolts. This method permitted streamwise positioning in 1.59 mm increments, with negligible imprecision.

The flow was seeded with a polyethylene glycol aerosol generated by a TSI Model 9306 six-jet atomizer. The atomizer required a pressure of approximately 50 psi, which was supplied from a tube connected to the supply lines between the storage

tanks and the wind tunnel. The particle size distribution is shown in Figure 5. The particles were convected by dilution air through a hose with a 180°bend and into the settling chamber.

3.3 Data Acquisition and Processing

The data acquisition procedure was designed to produce statistically significant results in a reasonable period of time, such that window fogging would not pose a problem. The earliest results consisted of five separate streamwise traverses, and 3000 velocity samples at each traverse point. Most subsequent tests consisted of 15 records at each position, and 1000 samples per record. The traverse positions were visited in a random order to minimize potential error due to drift. Data at one traverse position was collected two or three times during the course of a run as a check for repeatability. When shims were used for axial positioning in the supersonic tests, the number of records per position was reduced to 10, and the order in which the traverse positions were visited in sequential order.

The raw velocity data was processed by `FLOware`, and the flow statistics were subsequently calculated with the program `LDV`, listed in Appendix C. The velocity data were weighted according to the transit time of the particle, thereby correcting the bias toward high-velocity particles (Buchhave et al, 1979). Velocity samples beyond three standard deviations of the mean, and records beyond 2.5 standard deviations, were rejected. The decay law parameters were calculated by the least-squares procedure.

3.4 Error Sources and Estimating Procedures

Error is an inevitable part of any experimental work, and its quantification is important to assess the significance of the results. Errors may either be *systematic*, for which corrections may be available, or *random*, which may be statistically quantified using ensemble-averaging to obtain an uncertainty estimate. There are three aspects of the present experiments which may lead to measurement error and uncertainty: the wind tunnel characteristics, the seed particle dynamics, and the LDV system. The remainder of this chapter considers potential sources of error in each.

3.4.1 Wind Tunnel Characteristics

Two potential sources of error resulting from fluctuations in the wind tunnel characteristics have been identified: operation of the 1.5 m tunnel and storage tank pressure changes. The former resulted in a temporary turbulence intensity spike in the pilot tunnel; consequently, samples were not collected during operation of the 1.5 m tunnel. Storage tank pressure changes might potentially affect flow conditions in more than one way. For instance, it could induce temperature fluctuations, which would in turn cause fluctuations of mean velocity. Alternatively, as the storage tank pressure changes, the pilot tunnel control valve opens or closes, which could affect flow conditions such as the background turbulence intensity and the flow angularity. However, observations did not indicate an obvious correlation between the tank pressure and the flow statistics.

3.4.2 Particle Dynamics

LDV systems do not measure the fluid velocity itself, but rather the velocity of seed particles in the flow. Hence, if the particle speed statistics do not match the flow velocity statistics, errors will occur. Two potential sources of deviation are particle inertia and particle concentration non-uniformities.

Quantitative estimates of error due to particle inertia require solution of the particle equation of motion. The general equation, presented in Durst et al (1981) and elsewhere, is rather complex, but simplifies considerably for high speed flows in which the particle density is much larger than the fluid density. Then the only relevant force acting on the particle is viscous drag, and the particle equation of motion becomes

$$\frac{dU_p}{dt} + \frac{U_p - U}{\tau} = 0, \tag{3.2}$$

where U_p is the particle velocity. The time constant τ is given by

$$\tau = \frac{d_p^2 \rho_p}{18\mu}, \tag{3.3}$$

where d_p is the aerodynamic diameter of the particle, ρ_p is the particle density (1110 kg/m^3 for polyethylene glycol), and μ is the dynamic viscosity of the fluid, which varies with M owing to its strong temperature dependency. Solution of Eq. (3.2) requires knowledge of the fluid velocity field. The particular cases of shock waves and turbulence are now considered.

Particle Dynamics Downstream of a Shock

For many purposes, a shock wave can be considered as a step change in velocity. If the fluid velocity suddenly changes from U_1 to U_2, and if the initial particle velocity

is U_1, then Eq. (3.2) has the solution,

$$\frac{U_p(t) - U_2}{U_1 - U_2} = e^{-t/\tau}. \tag{3.4}$$

Assuming the steady-state velocity to be reached after $t = 3\tau$ (corresponding to 95% of the velocity change), the shock will appear smeared over a distance of

$$\Delta x = 3\tau U. \tag{3.5}$$

Actual corrections to the velocity measurement cannot be made unless particle velocity and size are measured simultaneously, which has not been done in the present study.

Particle inertia also affects the measured turbulence statistics downstream of a shock if the seed particles are polydispersed. This is because τ varies with d_p, leading to an increase in the velocity variance. The particle-induced variance, sometimes called "particle turbulence", has been discussed by Jacquin et al (1991) and Bloomberg (1989). Again, corrections cannot be made without simultaneous measurement of particle velocity and size.

Particle Dynamics in Turbulence

For an LDV system to accurately measure turbulence intensity, the particles must follow the turbulence fluctuations; i.e., the condition $u_p' = u'$, where u_p' is the particle rms velocity, must be satisfied. The turbulence fluctuations are composed of fluctuations over a range of frequencies. Consider for a moment fluid oscillating with a single frequency ω and amplitude D, as follows:

$$U(t) = D\sin(\omega t). \tag{3.6}$$

Eq.(3.2) then has the solution,

$$U_p(t) = \frac{D\omega\tau}{1 + (\omega\tau)^2}(\omega\tau\sin(\omega t) - \cos(\omega t)) + c, \tag{3.7}$$

and the ratio u'_p/u' is

$$\frac{u'_p}{u'} = \left(\frac{1}{(1 + (\omega\tau)^2)^{1/2}} \right). \tag{3.8}$$

The particle statistics therefore match the turbulence statistics only if $(\omega\tau)^2 \ll 1$; i.e., when the relevant frequencies of the turbulence are sufficiently low and d_p is sufficiently small. It is important to note that the Lagrangian frequencies must be used, because the particles are transported by the flow.

Eq. (3.8) provides a working equation for estimating the errors in measured turbulence intensity, provided that the size distribution of the measured seed particles and the shape of the turbulence spectrum are known. Neither were measured in the present measurements, but some typical values were used to evaluate the potential significance of the errors. Typical particle sizes were obtained from the distribution shown in Figure 5. Typical frequencies must be based on the Lagrangian integral time scale, T_L, which is representative of the energy-containing range. Experimental determination of T_L is very difficult; even its usual estimate requires two-point space-time velocity correlations, which were not measured in the present flows. However, it may be crudely estimated from the Eulerian streamwise integral length scale, L_f, using the non-dimensional group $L_f/u'T_L$. Various numerical estimates for this group are: 3/2, in the limit of infinite Reynolds number (Tennekes and Lumley, 1972); 0.2 and 0.5, from the numerical computations of Huang and Leonard (1995); and 0.98, based on the experimental grid turbulence data of Shlien and Corrsin (1974). Errors in the present study were estimated assuming a value of unity, yielding the following expression for the Lagrangian frequency corresponding to the integral scale:

$$\omega_L = \frac{2\pi}{T_L} = \frac{2\pi u'}{L_f}. \tag{3.9}$$

Bias Due to Particle Concentration Non-Uniformities

The effects of particle concentration non-uniformities downstream of a point source of seed particles in LDV was discussed by Buchhave et al (1979). They noted that particle dispersion may introduce a spurious mean transverse velocity and a reduction of transverse rms velocities. In the present experiments, however, the error vanishes because the streamwise measurement locations were co-axial with the droplet injection point.

3.4.3 LDV System

Errors and uncertainties may also be present in the LDV system, where the particle velocity is evaluated. Potential sources of error include insufficient signal-to-noise ratio, volume-averaging, quantization, and statistical bias. Ambiguity broadening is not considered, because it is relevant only when the turbulence statistics are determined from a continuous signal; in the present measurements, on the other hand, burst processing was used and the flow statistics calculated by averaging the burst velocities.

The data rate for an LDV system is proportional to the signal-to-noise ratio (SNR). Primary sources of noise include shot noise, electronics noise, RF noise, and spurious heterodyne signals (Adrian, 1983). Factors affecting signal strength, discussed by Menon and Lai (1991), include: laser power, probe volume size (decreasing the size increases the signal strength), scatter mode (forward-scatter gives much stronger signals than back-scatter), and particle size (the relationship is complex, but signal strength tends to increase with d_p). The FLOware software permits specification of the minimum SNR required for a signal to be validated. The SNR threshhold suggested by the manual, and used in all measurements, is -3 dB, which is assumed to render

errors due to insufficient SNR negligible.

A second potential error source in burst-mode LDV results from volume-averaging. Because burst detectors measure only the mean velocity of each burst, they are unable to resolve particle fluctuations smaller than the streamwise probe volume dimension. The amount by which the turbulence kinetic energy is underestimated can be determined if the shape of the turbulence energy spectrum is known. In the present case, the Kàrmàn interpolation function for the three-dimensional spectrum (Hinze, 1975) was used:

$$E(\kappa) \approx \frac{1.7\epsilon^{2/3}\kappa^4}{(\kappa^2 + 0.416\kappa_m^2)^{17/6}} \tag{3.10}$$

where $\kappa_m = 2\pi/L_f$. Defining u_r' to be the fluctuating velocity resolved by the LDV system, the error in the streamwise velocity variance due to volume-averaging was calculated from

$$\frac{u_r'^2}{u'^2} = \frac{\int_0^{2\pi/\sigma_1} E(\kappa)d\kappa}{\int_0^{\infty} E(\kappa)d\kappa}. \tag{3.11}$$

Quantization of the sample velocities is another source of measurement uncertainty. The discrete velocities which may be assigned to a sample are limited in number, and distributed evenly throughout the velocity range corresponding to the FVA bandwidth. In the present measuremnts, the maximum available bandwidth (36 MHz) was necessary for all cases to ensure that the velocity histogram was not truncated. Even so, the maximum uncertainty in the sample velocities was only 0.4%, and the corresponding uncertainty in the averages was negligible.

Finally, statistical bias may be introduced when the measurements are processed (Edwards, 1987). *Velocity bias* has as its source the fact that the arrival rate of particles at the probe volume is correlated with the particle velocities, such that simple arithmetic averaging biases the calculations toward the higher velocity particles. It can be corrected by using residence-time weighting, which was applied in the present

measurements. *Filter bias* occurs when the LDV system measurement efficiency varies with the Doppler frequency, and was avoided by ensuring that the entire velocity histogram lay within the bandwidth of acceptable frequencies. *Fringe bias* occurs because processors cannot measure all speeds at all angles, and may be significant if there is a fringe crossing validation criterion. At the advice of DANTEC personnel, this criterion was turned off in the present measurements. *Gradient bias* occurs when multiple particles reside in the probe volume simultaneously and the flow has a mean velocity gradient, but was rendered negligible in the present experiments by the flow uniformity.

Chapter 4

Measurements

In this chapter, the general behaviour of the wind tunnel is discussed, and some typical plots showing the operating characteristics are presented. Then the experimental conditions at which detailed flow measurements were obtained are listed, followed by a presentation of the measurement results.

4.1 Wind Tunnel Operating Characteristics

Each wind tunnel test was categorized into one of three flow regimes, depending on the nature of the test section flow. In the *moderate subsonic* regime, the flow in the entire test section flow was subsonic, with the possible exception of some cases in which there were local supersonic pockets closely downstream of the plate holes. In the *high subsonic* regime, the flow became supersonic past the plate, but a quasi-normal shock forced the flow to turn subsonic. In the *supersonic* regime, the flow was supersonic throughout the test section. The same regimes can be observed successively during the startup of a supersonic wind tunnel (e.g. John, 1983).

Various techniques were used to determine the regime to which a particular case was assigned. The pressure measurements were used to calculate M, from P_2/P_{t2}, and the static pressure difference along the window, $P_1 - P_2$. The LDV measurements provided an independent method of estimating M, in conjunction with the temperature measurements, and also quantified the turbulence levels. Qualitative information was provided by shadowgraph flow visualization and by observing the noise generated by the wind tunnel. These tools provided the following information for each of the flow regimes:

Moderate Subsonic In this regime, P_2/P_{t2} and the LDV measurements indicated that $M < 0.7$. A typical plot of M as a function of P_{t0}, is given in Figure 6, where $A_{dt}/A = 0.90$. The plateau in M corresponds to choked-flow conditions through the diffuser throat. $P_1 - P_2$ was positive but very small, being caused by friction drag along the test section walls. The turbulence intensity was low (below 2%), the wind tunnel was quiet, and no density discontinuities were evident with the shadowgraph system.

Most tests in this regime (the exception being discussed in Section 5.2.6) were obtained with choked-flow conditions in the diffuser throat, such that M was controlled by A_{dt}/A and was insensitive to potential fluctuations in the supply pressure.

For $M > 0.43$, isentropic flow theory predicts that the flow in the plate was choked, and visualization with the demonstration nozzle indicated the presence of local supersonic pockets directly downstream of the nozzles. Shocks in these pockets forced each of the jets to turn subsonic without merging with other jets, resulting in steady, subsonic downstream flow.

High Subsonic Plots illustrating the shift from the moderate subsonic to the high

subsonic regime with $A_{dt}/A = 0.92$ are shown in Figure 7. Moderate subsonic conditions persisted for $P_{t0} < 155$ kPa; however, M did not reach a a plateau, indicating that the flow through the diffuser throat was not choked. At $P_{t0} \approx 155$ kPa, a fundamental shift in the wind tunnel behaviour occurred, with M and u'/U increasing abruptly and a large pressure rise appearing across the window. The shift in the flow quantities was accompanied by an increase in the wind tunnel noisiness, and shadowgraph analysis revealed an unsteady quasi-normal shock in the test section (see Plates 5 and 6, which will be discussed in more detail in Section 5.3). The static pressure rise associated with the shock system caused the pressure rise along the window, and its unsteadiness was responsible for u'/U being high.

The flow behaviour in this regime was very sensitive to P_{t0}, A_{dt}/A, and other downstream geometrical parameters, and was relatively unrepeatable.

Supersonic In this regime, P_2/P_{t2} and the velocity measurements indicated that $M \approx 1.55$. Plots illustrating wind tunnel behaviour to the supersonic regime with $A_{dt}/A = 0.98$ are given in Figure 8. The moderate-to-high subsonic shift occurred at $P_{t0} \approx 150$ kPa, and the shift to the supersonic regime occurred at $P_{t0} \approx 165$ kPa. In the supersonic regime, M reached a plateau and $P_1 - P_2$ became slightly negative, indicating a small static pressure rise along the window. LDV measurements of the high subsonic-to-supersonic shift were not obtained because the large velocity change was beyond the range of any single lens. The turbulence intensity was low (about 1%). Shadowgraph analysis revealed that the quasi-normal shock of the high subsonic regime was pushed downstream of the window, being replaced by steady oblique shocks which formed a shock diamond structure (see Plates 6 to 9). These shocks were responsible for the small static pressure rise along the window.

The Mach number in this regime was determined by the plate solidity. The value of P_{t0} at which the shift from the high subsonic to the supersonic regime occurred was strongly dependent upon A_{dt}/A and the contraction joint setting. In particular, increasing A_{dt} decreased the settling chamber pressure required to achieve supersonic flow throughout the test section, since the shock could be swallowed by the diffuser throat more easily (compare Plates 5 and 6).

4.2 Experimental Conditions

4.2.1 Wind Tunnel

The measurement runs chosen for quantitative processing are listed in Table 4.1, together with their associated geometry and pressure settings. Also included are the resulting Mach numbers as determined from the LDV measurements. Unless otherwise noted, all cases were performed with the modified MHP. The LDV configurations for the cases are tabulated in Table 4.2.

4.2.2 Demonstration Nozzle

The test section for the demonstration nozzle was designed to yield flow characteristics which were as qualitatively similar as possible to those in the wind tunnel, and it was therefore controlled by means similar to those used in the wind tunnel. In the subsonic regime, the primary control was the diffuser throat opening. Visualization in the subsonic regime was performed with $0.6 < A_{dt}/A < 0.95$. The resulting test section Mach numbers, based on one-dimensional isentropic flow theory, are tabulated in Table 4.3. The actual Mach number in the test section was likely slightly lower,

Table 4.1: Wind Tunnel Settings Used in Experiments

Case	M	P_{t0} (psi)	A_{dt}/A	C.J.[a]	Comments
MS1a	0.164	22	0.24	5.0	5 traverses; 1 rec./pos.
MS1b	0.162	20	0.24	5.0	
MS1c	0.162	20	0.24	5.0	z=-13 mm
MS1d	0.160	20	0.24	5.0	
MS2	0.237	20	0.36	5.0	
MS3	0.369	20	0.56	5.0	
MS4	0.462	20	0.68	5.0	
MS5a	0.517	20	0.76	5.0	
MS5b	0.517	20	0.76	5.0	
MS5c	0.525	20	0.76	5.0	
MS5d	0.525	20	0.76	5.0	
MS6	0.582	20	0.84	5.0	
MS7a	0.639	23	0.90	5.6	
MS7b	0.640	23	0.90	5.6	
MS8a	0.679	24	0.92	6.2	50.8 mm spacing
MS8b	0.683	24	0.92	6.2	
MS9a	0.673	22	0.92	5.6	
MS9b	0.656	22	0.92	5.6	
HS1	0.686	24	0.92	6.2	
HS2	0.916	23	0.94	5.6	
SP1a	1.55	24	0.98	5.6	25.4 mm spacing
SP1b	1.55	24	0.98	5.6	25.4 mm spacing
SP1c	1.58	25.5	1.00	5.6	6.35 mm spacing
SP1d	1.54	24	0.98	5.6	1.59 mm spacing
SP2a	1.55	25.5	1.00	5.6	LHP; 25.4 mm spacing
SP2b	1.55	25.5	1.00	5.6	LHP; 6.35 mm spacing
SP2c	1.55	25.5	1.00	5.6	LHP; 1.59 mm spacing

[a]Contraction joint setting.

Table 4.2: LDV Settings Used in Experiments

Case	M	1D/2D	Lens focal length (mm)	Frequency shift (MHz)	Comments
MS1a	0.164	2D	160	40	
MS1b	0.162	2D	160	40	Poor blue beam
MS1c	0.162	1D	160	40	
MS1d	0.160	1D	160	40	
MS2	0.237	1D	160	40	
MS3	0.369	1D	160	0	
MS4	0.462	1D	160	0	
MS5a	0.517	1D	243	0	
MS5b	0.517	1D	243	0	
MS5c	0.525	1D	160	0	
MS5d	0.525	1D	160	0	
MS6	0.582	1D	243	0	
MS7a	0.639	1D	243	0	
MS7b	0.640	1D	243	0	
MS8a	0.679	2D	160	0	Probe oriented at
MS8b	0.683	2D	160	0	45°to mean flow
MS9a	0.673	1D	243	0	
MS9b	0.656	1D	243	0	
HS1	0.686	1D	243	0	
HS2	0.916	1D	243	0	
SP1a	1.55	1D	243	-40	
SP1b	1.55	1D	243	-40	
SP1c	1.58	1D	243	-40	
SP1d	1.54	1D	243	-40	
SP2a	1.55	1D	243	-40	
SP2b	1.55	1D	243	-40	
SP2c	1.55	1D	243	-40	

Table 4.3: Demonstration Nozzle Settings for the Subsonic Regime

A_{dt}/A	M_{1d}
0.60	0.38
0.70	0.46
0.80	0.55
0.90	0.68
0.95	0.77

due to boundary layer growth and non-ideal flow near the diffuser throat. According to isentropic flow theory, the flow between the rods was choked all these cases.

The quasi-normal shock was not observed in the demonstration nozzle for any configuration.

In the supersonic regime, the diffuser throat was wide open, although with the diamond rods and square rods II supersonic flow was also attained at $A_{dt}/A = 0.95$. Isentropic flow theory predicts that the downstream flow had $M = 1.89$ with the round rods and square rods I, 2.27 with the square rods II, and 2.20 with the diamond rods. In reality, M was likely substantially lower, due to losses and boundary layer growth behind the grid.

4.3 Presentation of Results

Results of nearly all measurements are tabulated in Appendix D. The subset presented here, and discussed in the next chapter, corresond to tests with the empty wind tunnel, measurements in the transverse plane, and the most reliable streamwise traverses (listed in Tables 4.1 and 4.2).

4.3.1 Moderate Subsonic Regime

Background Turbulence Intensities

To estimate the background turbulence intensity, flow statistics without a plate installed were measured at $M = 0.69$. The streamwise and transverse turbulence intensities at three measuring locations, plotted in Figure 9, were approximately 1%, and were independent of P_{t0} for $120 \leq P_{t0} \leq 165$ kPa.

Measurements in the Transverse Plane

Transverse uniformity and homogeneity was evaluated using y- and z-traverses at $x/m = 58.52$ for $M = 0.16$ and $M = 0.66$. The mean velocity profiles, normalized by the centreline velocity U_{cl}, are plotted in Figures 10 and 11, respectively. The streamwise velocity variances, normalized by the square of the local mean velocity, are plotted in Figures 12 and 13. In all these plots, the distance variable is normalized by h, defined as the test section width and height.

Mean Velocity Profiles

The development of the mean velocity U, normalized by the velocity averaged over all measuring stations, U_m, is plotted for the moderate subsonic cases in Figures 14 to 18. Repeated measurements were obtained at $M = 0.16$ (Figure 14), $M = 0.52$ (Figure 16), and $M \approx 0.65$ (Figures 17 and 18). The results at other Mach numbers are plotted together in Figure 15. For reasons to be discussed in Section 5.2.6, the cases shown in Figure 18 are considered anomalous. In these plots, the distance variable x is normalized by h.

Streamwise Velocity Variance Profiles

Profiles of the streamwise velocity variance, u'^2, normalized by the square of the local mean velocity U, are presented in Figures 19 to 23. Measurements at $M = 0.52$ (Figure 21) and $M \approx 0.65$ (Figure 22), were obtained with both the 160 mm and the 243 mm lenses, which, as will be discussed later, have different measurement uncertainties. The distance variable x is normalized by the effective mesh size m. The graphs are presented in log-log coordinates; hence, the slope of the best-fit curve through the points represents the exponent n of the decay law.

Skewness Factors

The skewness factors, defined by

$$S = \frac{\overline{u^3}}{u'^3} \tag{4.1}$$

are presented in Figures 24 to 28.

Shear Stress Correlation Coefficients

Calculation of the turbulent shear stress correlation coefficient, defined by

$$\rho_{uv} = \frac{\overline{uv}}{u'v'} \tag{4.2}$$

required measurement of both the streamwise and transverse velocity components. Two-component measurements were obtained only for the first few tests, because the blue laser beam later deteriorated, such that only single-component measurements were reliable. Consequently, shear stress correlation coefficients are reported only for a few tests, at $M = 0.16$ and $M = 0.68$, and are presented in Figure 29.

4.3.2 High Subsonic Regime

The flow in the high subsonic regime was studied qualitatively using shadowgraph visualization. The shadowgraphs are shown for various geometry and pressure settings in Plates 5 and 6. Because of the complex, unsteady, and unrepeatable nature of the high subsonic flow, quantitative analysis was not considered a priority. Nevertheless, two streamwise traverses were performed, for which the mean velocity profiles are presented in Figure 30, the streamwise velocity variances in Figure 31, and the skewness factors in Figure 32.

4.3.3 Supersonic Regime

Shadowgraph images of the flow generated by the unmodified MHP, the modified MHP, and the LHP are shown in Plates 7 to 9. Images obtained with the plates in both their standard and rotated orientations are included.

The mean velocities profiles for the MHP are presented in Figure 33. Traverses were performed with streamwise traverse separation lengths, Δx_t, of 25.4 mm, 6.35 mm and 1.59 mm, which correspond to $\Delta x_t/m = 1.75$, 0.438, and 0.110, respectively. The traverses with $\Delta x_t/m = 1.75$ and 0.438 were taken on the tunnel centreline, whereas the traverse with $\Delta x_t/m = 0.110$ was obtained at $y/h = -0.035$. The latter measurement was moved off the tunnel centreline in an attempt to isolate a single wave and measure its effect on the velocity field.

The mean velocities profiles for the LHP are presented in Figure 34. The streamwise traverse separation distances were the same as with the MHP, but correspond to $\Delta x_t/m = 1.38$, 0.345, and 0.086, respectively. The traverse with $\Delta x_t/m = 0.086$ was obtained at $y/h = -0.051$ so as to obtain a clean wave crossing.

The streamwise velocity variances for the MHP and the LHP are presented in Figures 35 and 36, respectively, and the skewness factors in Figures 37 and 38.

Schlieren images of the flow near the grid, obtained using the demonstration nozzle, are shown in Plates 10 to 17. Plates 10 to 13 show images in the subsonic regime with the diffuser throat at different settings ($0.7 < A_{dt}/A < 0.95$). Plates 14 to 17 show sequences of images with $A_{dt}/A = 1$ (resulting in supersonic conditions for all rod geometries) as the supply pressure was gradually increased.

Chapter 5

Analysis

In this chapter the measurement results, which have been presented in the previous chapter, are considered in further detail. The discussion begins with the variation of turbulence intensity with Mach number over all regimes. Subsequently, the results specific to the moderate subsonic, high subsonic, and supersonic regimes are analyzed in turn. The chapter concludes with a discussion and estimation of error uncertainty.

5.1 Turbulence Intensities

A simple and useful exercise which can be performed with the measurements is to plot the turbulence intensity as a function of M. Although the term "turbulence intensity" is used in all cases, this quantity includes velocity fluctuations which may not qualify as conventional turbulence. In particular, in the high subsonic regime, the interpretation of streamwise flow oscillations due to the unsteadiness of quasi-normal shocks is uncertain.

The turbulence intensities at $x/m = 58.5$ are plotted in Figure 39 and tabulated, together with U_m and the grid Reynolds number R_m, in Table 5.1. The graph includes turbulence intensities published in the previous studies by Comte-Bellot and Corrsin (1966), Mohamed and LaRue (1990), and Kistler and Vrebalovich (1966). Comte-Bellot and Corrsin (1966) utilized biplane grids with square and round rods as well as disk grids, while the other studies used only round-rod biplane grids. The present measurements obtained with the 160 mm lens are distinguished from those obtained with the 243 mm lens, because the measurements with the two lenses have different uncertainties. Due to oscillations in the quasi-normal shock, which greatly increased the turbulence intensity, measurements in the high subsonic regime are labelled as non-stationary. The error bars were obtained from estimates discussed in Section 5.5.

In the moderate subsonic regime, at $M = 0.16$, the turbulence intensities are roughly the same as those produced by round-rod grids. For $M \leq 0.55$, the turbulence intensity is roughly constant, although a decrease for $0.16 \leq M \leq 0.25$ followed by a slight increase for $0.40 \leq M \leq 0.55$ appears to be significant. This is even more apparent when only the 160 mm results are considered. Beyond $M = 0.55$, there is a clear drop in the turbulence intensity. The variation of turbulence intensity with M may be a consequence of changes in the flow characteristics directly behind the grid, which is discussed further in Sections 5.2.9 and 5.4.3.

5.2 Moderate Subsonic Regime

In this section, the moderate subsonic cases are analyzed. Aspects of the flow which are considered include: factors affecting the degree to which the flow matches its ideal analytical counterpart, the mean velocity development, the decay law, various important turbulence parameters, and flow characteristics near the grid.

Table 5.1: Mean Velocities, Turbulence Intensities, and Grid Reynolds Numbers

Case	M	U_m (m/s)	u'/U^a (%)	R_m
MS1a	0.164	55.0	1.87	49 600
MS1b	0.162	55.7	1.84	70 200
MS1c	0.162	55.6	1.87	70 100
MS1d	0.160	55.4	1.83	68 700
MS2	0.237	81.1	1.64	99 600
MS3	0.369	126.2	1.70	142 000
MS4	0.462	156.8	1.83	160 900
MS5a	0.517	174.8	1.71	169 000
MS5b	0.517	175.3	1.75	167 700
MS5c	0.525	178.0	1.94	170 000
MS5d	0.525	177.7	1.94	171 000
MS6	0.582	194.6	1.46	193 000
MS7a	0.639	213.6	1.28	196 000
MS7b	0.640	214.5	1.26	194 000
MS8a	0.679	226.3	1.44	219 000
MS8b	0.683	227.5	1.51	219 100
MS9a	0.673	222.3	1.42	196 100
MS9b	0.656	217.2	1.29	192 600
HS1	0.686	227.4	2.93	213 000
HS2	0.916	294.3	1.96	281 300
SP1a	1.55	447.6	0.87	326 500
SP1b	1.55	448.1	0.86	321 800
SP1c	1.58	448.2	—	321 200
SP1d	1.54	448.3	—	332 800
SP2a	1.55	446.0	0.86	397 700
SP2b	1.55	445.9	—	390 300
SP2c	1.55	448.5	—	395 500

[a] $x/m = 58.5$.

5.2.1 Background Turbulence Intensity

The background turbulence intensity was about 1.0%, and the transverse fluctuations were about 25% higher than the streamwise fluctuations. The anisotropy is likely due to the settling chamber contraction, which dampened the streamwise fluctuations more than the other components. At first glance, the background turbulence intensity may seem large, particularly since the turbulence produced by the perforated plate had an intensity of the same order. However, the background turbulence is not just superimposed on the grid turbulence. Instead, the plate modifies it by dampening its intensity and by breaking the large-scale, low-frequency content into smaller eddies which are less permanent. Consequently, the background turbulence is not considered to be a significant factor.

5.2.2 Flow Uniformity and Homogeneity

In studies of decaying turbulence, it is desirable to have a uniform mean velocity and homogeneous turbulence. Then the turbulence kinetic energy equation simplifies to Eq. (2.2). To test the validity of this assumption in the present measurements, sample calculations of the neglected terms, based on the streamwise and transverse profiles, have been made (Appendix A.1). The neglected terms are as high as 15% of the mean convection term, most of which is due to the streamwise production term. The deviations, although somewhat large, are not uncommon in turbulence studies. Moreover, it is possible to apply appropriate corrections to terms which are based on the simplified equation, such as the dissipation rate.

The transverse profiles (Figures 10 to 13) indicate that the flow is not necessarily symmetric about the tunnel centreline. Some of the results are also inconsistent with expectation; for instance, in Figure 10, the results at $M = 0.67$ feature a local min-

imum in mean velocity at the tunnel centreline. Some of this unexpected behaviour might be due to deviation in the mean flow direction from the tunnel axis. This is further borne out by the two-component measurement results, which indicate that V/U was as high as 0.01, corresponding to a flow angularity of to 0.6%. According to NRC personnel, flow angularities of up to 2% have been observed in the empty tunnel (the maximum occurring at $M \approx 0.6$), but this was likely reduced by the plate, which likely refracted the flow toward the tunnel axis.

5.2.3 Turbulence Gaussianity

Turbulence fluctuations in grid turbulence are known to have an approximately Gaussian probability density function (pdf). A typical velocity histogram (from MS1d) is provided in Figure 40. One condition of Gaussianity is that all odd moments of the pdf vanish. The third moment, called the skewness factor S, has been defined in Eq. (4.1). Figures 24 to 28 show that S was indeed close to zero in the present measurements, although on average slightly positive. The cases MS9a and MS9b (Figure 28) are exceptions, and are discussed further in Section 5.2.6.

Another property of Gaussian processes is that all even moments of the pdf beyond two are simple functions of the second moment. For instance, the flatness factor F, defined as

$$F = \frac{\overline{u^4}}{\overline{u'^4}}, \tag{5.1}$$

takes a value of three. In the current measurements, F was typically between 2.75 and 2.90 when samples beyond three standard deviations were rejected, and between 3.00 and 3.20 when no samples were rejected.

Based on these tests, it is concluded that the turbulence fluctuations in the moderate subsonic regime were approximately Gaussian.

5.2.4 Turbulence Isotropy

Isotropy of the turbulence fluctuations also has a number of implications for the turbulence statistics. For instance, by considering an x-axis reflection, it can be shown that S must vanish. As mentioned above, S was on average positive, perhaps due to the downstream energy decay, but close to zero. A second consequence of isotropy is that all turbulent shear stress correlation coefficients must vanish. The correlation coefficients at $M = 0.16$ and $M = 0.68$ have been presented in Figure 29, and are approximately zero.

These statistics indicate that the energy-containing eddies were approximately isotropic. More advanced tests for isotropy at other scales involve measurements of velocity autocorrelations, turbulence spectra, or velocity derivative skewnesses, all of which require a frequency response significantly higher than that obtained in the present tests.

Further evidence for isotropy is obtained by considering the number of eddy turnovers, N_{to}, which occur upstream of the measurement region. In grid turbulence studies, it is desirable to have a number of eddy turnovers, so that the eddies generated at the grid would be broken down and new, isotropic ones would form, thereby diminishing the dependence of the turbulence structure on the initial conditions. Isotropy is often assumed to be reached about 20 mesh lengths downstream of the grid. In the present flows, it is estimated that about one more eddy turnover occurred between that location and the measurement region (Appendix A.2), which strengthens the argument that the turbulence was indeed nearly isotropic.

5.2.5 Mean Velocity Profiles

In the absence of wind tunnel wall divergence to compensate for boundary layer growth, the mean velocity is expected to accelerate in the moderate subsonic regime. The measured profiles, presented in Figures 14 to 18, all display this trend, but also feature some unexpected behaviour. On one hand, they appear to accelerate more quickly than expected from boundary layer growth. This is evident from Figure 41, where representative profiles from throughout the moderate subsonic regime are plotted together with the expected profile at $M = 0.16$ based on zero-pressure-gradient boundary-layer growth along the four tunnel walls. Furthermore, the acceleration appears to increase with M, which is unexpected because turbulent boundary layers grow more slowly as $R_x = Ux/\nu$ increases. Compressibility acts to further slow turbulent boundary layer growth, although it is not expected to play a major role at subsonic speeds (Schlichting, 1979). Consequently, the observed accelerations appear inconsistent with boundary layer growth considerations.

The incongruity may have been due, at least partly, to flow angularity, which has been discussed in Section 5.2.2. Such non-axial flow development would lead to boundary layer developments which differ for each wall and also from the flat-plat case. If flow angularity was indeed responsible for the apparent anomaly, then the trend of increasing acceleration with M may also be explained, for the flow angularity was maximum at $M \approx 0.6$.

5.2.6 The Decay Law

Streamwise Velocity Variance Profiles

Streamwise velocity variance profiles have been presented in Figures 19 to 23. Representative cases from throughout the moderate subsonic regime are presented together in Figure 42. The axes are logarithmic, so that the slope of the best-fit curve through the points yields the exponent n of the decay law. The velocity variances generally decrease monotonically, although there is some scatter at $M = 0.37$. Similar scatter at $M = 0.24$ and $M = 0.46$ are evident from Figure 20. Given the degree of scatter, the slope of the curves appears to be roughly constant for $M \leq 0.58$, but significantly steeper at $M = 0.68$.

Before proceeding to a more complete discussion of the decay law, the cases MS9a and MS9b will be considered.

Some Anomalies

By comparing Figures 22 and 23, it is evident that MS9a and MS9b have decay curves which are much less steep than MS7a, MS7b, MS8a, and MS8b, despite having similar M. In this section we will show that MS9a and MS9b deviate significantly from the isotropic ideal.

That anisotropy exists in MS9a and MS9b is immediately evident from Figure 28, where S is large and positive, implying that the positive velocity fluctuations tend to be larger than the negative fluctuations. Further evidence for anomalous behaviour is obtained by considering the sensitivity of the moment calculations to the sample rejection criterion. For instance, Table 5.2 indicates that n is much more sensitive to the sample rejection criterion in MS9a and MS9b than in MS7a to MS8b. The

Table 5.2: Sensitivity of n to Sample Rejection Criterion

Rejection Criterion	n					
	MS7a	MS7b	MS8a	MS8b	MS9a	MS9b
$3u'$	1.64	1.53	1.51	1.42	1.00	0.92
$2u'$	1.62	1.55	1.55	1.45	0.84	1.32
% Change	-1.2%	1.3%	2.6%	2.1%	-16.0%	43.5%

rejected samples tended to have high velocities.

This behaviour was likely due to the wind tunnel behaviour, which for MS9a and MS9b lies on the curves shown in Figure 7. Prior to the moderate-to-high subsonic transition, at $P_{t0} \approx 150$ kPa, both M and u'/U were sensitive to P_{t0}, indicating that flow in the diffuser throat was not choked. MS9a and MS9b were taken at $P_{t0} = 150$ kPa, which was very close to the moderate-to-high subsonic transition. In contrast, the flow in the diffuser throat was choked for all other moderate subsonic cases, leading to a plateau over which M and u'/U were insensitive to P_{t0} (e.g. Figure 6 for MS7a and MS7b). It may be that the wind tunnel operated intermittently — most of the time in the moderate subsonic regime and part of the time in the high subsonic regime — during MS9a and MS9b, thereby leading to occassional large positive velocity fluctuations and the large S. Because these cases clearly involve inhomogeneous and anisotropic turbulence, they are excluded from further discussion.

Decay Law Parameters

The equation describing the decay of streamwise velocity variance has been presented in Eq. (2.6) as

$$\frac{u'^2}{U^2} = B\left(\frac{x - x_0}{m}\right)^{-n}, \tag{5.2}$$

which involves three emprical parameters: the decay coefficient B, the effective origin x_0, and the decay exponent n. The parameters are typically determined by varying x_0/m, calculating the corresponding values for B and n by the least squares method, and choosing as the optimal fit the parameters which fit the data over the widest range of x/m (Comte-Bellot and Corrsin, 1966). In the present measurements, the range of x/m was so narrow that a wide range of x_0/m provided equally good curve fits. For instance, the data for MS8b is plotted in Figure 43, together with two potential decay laws:

$$\frac{u'^2}{U^2} = 0.0739\left(\frac{x}{m}\right)^{-1.42} \tag{5.3}$$

and

$$\frac{u'^2}{U^2} = 0.00230\left(\frac{x}{m} - 30\right)^{-0.69}. \tag{5.4}$$

From the plot it appears that a unique optimal value for x_0 cannot be determined, and hence any discussion of the decay law must include an assumption for one of the its parameters.

The simplest assumption which can be made is that $x_0/m = 0$, which has often been found to be reasonable in incompressible grid turbulence experiments. The exponents which result from this assumption are shown in Figure 44, where the error bars on the plot correspond to the 90% confidence interval. Exponents obtained by Comte-Bellot and Corrsin (1966), Mohamed and LaRue (1990), and Kistler and Vrebalovich (1966) are also included; it should be noted that the range of x/m measured by Kistler and Vrebalovich was also rather narrow. The plot suggests that, if the assumption about x_0/m is true, then n remains roughly constant and close to unity for $M < 0.50$, after which it increases, particularly for $M > 0.60$.

There is, however, reason to doubt the assumption that $x_0/m = 0$. Experimentally, Comte-Bellot and Corrsin (1966) and Ling and Wan (1972) observed that n decreases with Reynolds number, which is the opposite of the trend observed in

Figure 44. Furthermore, George's (1992) analytical theory that n should decrease to unity as R_λ increases finds support in the high-Reynolds number experiments of Kistler and Vrebalovich (1966). In the present experiments, R_λ ranged between 100 and 200 which, although lower than in Kistler and Vrebalovich, is higher than in most grid turbulence studies. Therefore, it might be better to assume $n = 1$ than $x_0/m = 0$. The corresponding values of x_0/m are plotted in Figure 45. For $M < 0.5$, it is roughly constant and close to zero, even becoming negative in some cases; however, those cases have significant scatter, and their error bars in Figure 44 do not exclude the possibility that $n = 1$ at $x_0/m = 0$. For $M > 0.5$, x_0/m increases, particularly for $M > 0.60$.

Mathematically, x_0/m can be interpreted as the location at which an isotropic turbulence is generated with infinite kinetic energy. Experimentally, it accounts for the fact that the turbulence generated behind the grid requires some distance to develop to an approximately homogeneous and isotropic state. A large change in x_0 may be related to a shift in the nature of the turbulence structure near the grid, as is discussed further in Section 5.2.9.

The decay law parameters which result from the assumptions of $x_0/m = 0$ and of $n = 1$ are tabulated in Table 5.3.

5.2.7 Some Turbulence Parameters

In this section, various turbulence parameters, such as the dissipation rate, the integral length scale, the Taylor microscale, the Kolmogoroff microscale, and R_λ are presented. The estimates are tabulated together in Table 5.4.

The first parameter we consider is the dissipation rate of the turbulence kinetic energy, ϵ. A direct measurement of ϵ would require a measuring instrument capable

Table 5.3: Decay Law Parameters for the Moderate Subsonic Regime

Case	M	$x_0/m = 0$		$n = 1$	
		B	n	B	x_0/m
MS1a	0.164	0.031	1.10	0.019	5.0
MS1b	0.162	0.018	0.97	0.021	-2.0
MS1c	0.162	0.013	0.88	0.024	-8.0
MS1d	0.160	0.022	1.03	0.020	1.0
MS2	0.237	0.010	0.89	0.018	-7.0
MS3	0.369	0.010	0.88	0.020	-8.5
MS4	0.462	0.021	1.02	0.019	1.0
MS5a	0.517	0.062	1.32	0.013	14.0
MS5b	0.517	0.041	1.20	0.015	10.0
MS5c	0.525	0.032	1.09	0.020	5.0
MS5d	0.525	0.034	1.11	0.019	6.0
MS6	0.582	0.021	1.13	0.011	6.5
MS7a	0.639	0.129	1.64	0.0057	23.0
MS7b	0.640	0.080	1.53	0.0062	20.0
MS8a	0.679	0.097	1.51	0.0081	19.5
MS8b	0.683	0.074	1.42	0.0098	17.0

of resolving fluctuations in the dissipative range. However, it can also be calculated indirectly from the streamwise convection term of the streamwise Reynolds stress equation, provided the neglected terms are sufficiently small. In that case, upon combining with the decay law, the following expression for ϵ results:

$$\frac{\epsilon m}{U_m^3} = \frac{3nB}{2}\left(\frac{x-x_0}{m}\right)^{-n-1} . \tag{5.5}$$

However, as discussed in Appendix A.1, the streamwise production term was found to be as large as 15% of the streamwise convection term. The estimate for ϵ therefore incoporated a correction using the estimates provided in the appendix. The correction reduced the estimate for ϵ, because the production term was always negative. The values for $\epsilon m/U_m^3$ at $x/m = 58.5$, both with and without the correction, are plotted as a function of M in Figure 46. The non-dimensional group is approximately constant, indicating that ϵ itself increases strongly with U.

The size of the energy-containing eddies in a turbulent flow is characterized by the integral length scale, which is typically of the same order as the external geometry. The streamwise integral length scale, L_f, can be measured directly by integrating the streamwise velocity autocorrelation coefficient up to the first zero crossing. Since the temporal resolution was insufficient for such direct measurement, an indirect estimate was made using the observations of Sreenivasan (1984), who found that, for square-rod grid turbulence, $\epsilon L_f/u'^3$ asymptotes to unity for $R_\lambda > 50$. Physically, this implies that the ratio of the dissipation time scale to the energy-containing eddy time scale reaches a constant value. Although no similar trend was apparent for round-rod grids, and no results were available for perforated plates, it was nevertheless assumed to hold in the present experiments. Hence L_f was estimated using the equation:

$$L_f = \frac{u'^3}{\epsilon}, \tag{5.6}$$

where ϵ was corrected to account for streamwise production. The resulting values at

$x/m = 58.5$ are plotted in Figure 47. The error bars correspond to the uncertainty in the u' measurement. At low M, $L_f/m \approx 0.8$, which is larger than, but still comparable to, the value of 0.65 reported by Sreenivasan et al (1980) at the same $(x - x_0)/m$. At higher M, it is difficult to deduce how L_f changes with certainty, but the plot suggests it may decrease, which is consistent with the earlier speculation that x_0/m increases with M.

A second important length scale in turbulent flow is the Taylor microscale, λ, which is related to the second derivative of the velocity autocorrelation coefficient at its origin. Again, because of insufficient temporal resolution, it could not be measured directly. Instead, it was estimated indirectly from Eq. (2.4), assuming isotropy:

$$\lambda = \left(\frac{15\nu u'^2}{\epsilon}\right)^{1/2}. \tag{5.7}$$

The corrected values of ϵ were used. The resulting values at $x/m = 58.5$, normalized by m, are plotted in Figure 48. The error bars correspond to the uncertainty in the u' measurement. A monotonic decrease of λ with M is evident, which is consistent with the inverse relationship between λ and ϵ and, as we have already seen, ϵ increases with M.

The smallest scales of turbulence, on which viscous forces act to dissipate turbulence kinetic energy into thermal energy, are characterized by the Kolmogoroff microscale, η, which is found by dimensional analysis to be

$$\eta = \left(\frac{\nu^3}{\epsilon}\right)^{1/4}. \tag{5.8}$$

Figure 49, which shows the values at $x/m = 58.5$, indicates an inverse relationship between η and M. This seems reasonable because, as M increases, ϵ increases and ν decreases, so that the eddies must break down further before they can be dissipated by viscous forces.

Table 5.4: Turbulence Parameters in the Moderate Subsonic Regime [a]

Case	M	L_f/m	λ/m	η/m	$\epsilon m/U_m^3$ [b,c]	R_λ
MS1a	0.164	0.710	0.0883	0.00409	9.20×10^{-6}	120.
MS1b	0.162	0.821	0.0972	0.00441	7.62×10^{-6}	126.
MS1c	0.162	0.931	0.103	0.00450	7.03×10^{-6}	136.
MS1d	0.160	0.717	0.0945	0.00441	8.16×10^{-6}	119.
MS2	0.237	0.786	0.0848	0.00366	5.63×10^{-6}	139.
MS3	0.369	0.834	0.0724	0.00278	5.87×10^{-6}	175.
MS4	0.462	0.793	0.0637	0.00237	7.69×10^{-6}	188.
MS5a	0.517	0.550	0.0534	0.00219	9.00×10^{-6}	155.
MS5b	0.517	0.614	0.0560	0.00222	8.73×10^{-6}	164.
MS5c	0.525	0.779	0.0554	0.00216	9.39×10^{-5}	196.
MS5d	0.525	0.786	0.0597	0.00216	9.25×10^{-5}	198.
MS6	0.582	0.570	0.0551	0.00227	5.45×10^{-6}	155.
MS7a	0.639	0.347	0.0455	0.00217	6.04×10^{-6}	114.
MS7b	0.640	0.369	0.0475	0.00224	5.42×10^{-6}	116.
MS8a	0.679	0.422	0.0449	0.00192	7.07×10^{-6}	141.
MS8b	0.683	0.487	0.0392	0.00192	7.07×10^{-6}	130.

[a] $m = 14.5$ mm.
[b] Estimates for ϵ are corrected for the streamwise production term.
[c] U_m is tabulated in Table 5.1.

Information concerning the existence and width of an inertial subrange in isotropic turbulence is obtained from the turbulence Reynolds number, R_λ, defined as

$$R_\lambda = \frac{u'\lambda}{\nu}. \tag{5.9}$$

In grid turbulence, R_λ remains nearly constant, actually obeying a power law with an exponent $(-n+1)/2$. The values for the present cases are plotted in Figure 50, in which the error bars correspond to the ucertainties in u' and λ. The figure suggests that R_λ peaks at $M \approx 0.5$, and then decreases. At first glance, this appears surprising, because Corrsin (1963) showed that $R_\lambda \propto \sqrt{R_m}$, and R_m increases monotonically with M. In these experiments, however, R_λ decreases because of the drop in turbulence intensity beyond $M = 0.5$.

5.2.8 Applicability to Computational Turbulence Studies

One of the major current thrusts in turbulence research is the computational simulation and modelling of turbulent flows, for which experimental data are often used for comparison or calibration purposes. It is useful to consider the applicability of the present results for such studies. What most distinguishes the present study from previous grid turbulence experiments are the compressibility-induced changes in the flow near the grid. Using the results for computational studies would therefore require resolution of the details of the flow through the plate. At present, unfortunately, such resolution is beyond the capability of computational methods. In the future, however, the data may become useful for these purposes.

5.2.9 Flow near the Grid

The flow characteristics behind the grid, with downstream subsonic flow, have been presented for different rod geometries in Plates 10 to 13. At $M_{1d} = 0.46$, no density discontinuities are evident. As M_{1d} increased, the flow behind the rods became supersonic, featuring a complex system of shocks and expansions. The losses associated with the shocks forced the downstream flow to turn subsonic in all cases except two. The exceptions, which featured downstream supersonic flow, occurred at $A_{dt}/A = 0.95$ with the square rods II and the diamond rods, which had higher solidities than the other cases (see the final image of Plates 12 and 13).

The images also indicate that the characteristics of the wakes behind the rods changed as M_{1d} increased. At lower M, the wakes immediately behind the rods were relatively wide and, in at least one case (with the diamond rods), visibly unsteady. As M_{1d} increased, the individual jets became supersonic in the divergent region and were more resistant to separation. Furthermore, the wakes immediately behind the

rods became narrower and did not spread. Only downstream of the shocks, where the flow became subsonic, did the wakes spread out significantly.

The changes in the flow characteristics downstream of the grid suggest that the turbulence structure in that region may also have changed. This, in turn, may have affected the downstream turbulence characteristics. In fact, the range of Mach numbers over which the flow pattern behind the grid changed was about the same as that in which the downstream turbulence intensity dropped and the decay law parameters changed ($0.55 < M_{1d} < 0.68$).

5.3 High Subsonic Regime

In this section the results from the high subsonic regime are discussed. Qualitative information obtained from the flow visualization study is considered first, followed by a discussion of some quantitative results.

5.3.1 Qualitative Analysis

The shadowgraphs shown in Plates 5 and 6 reveal the presence of several bands which span much, but not all, of the test section width. The furthest upstream band was also the strongest, and featured oblique shocks which connected it with the boundary layer. The system was unstable, oscillating back and forth randomly, consistently with the phenomenon referred to here as the "quasi-normal shock". Such systems, rather than one-dimensional normal shocks, are the norm in ducts and wind tunnels (Shapiro, 1953). The two-dimensional effects at the walls were caused by shock-boundary layer interactions, similar to the flat-plate "λ-shocks" (Shapiro, 1953).

Generating a stable one-dimensional normal shock in a duct or wind tunnel requires special means. For instance, suction can be used to remove the boundary layers (Shapiro, 1953; Jacquin et al, 1991). Barre et al (1995) used wedges to generate a stable normal shock near the middle of the test section. In the present experiments, no attempt was made to stabilize the shock or remove the two-dimensional effects.

5.3.2 Quantitative Analysis

Quantitative analysis of the turbulence in this regime was difficult for two reasons. Firstly, the flow was very complex, being strongly anisotropic, and inhomogeneous. Secondly, there was some issue in deciding whether the quasi-normal shock oscillations were to be interpreted as turbulence. On one hand, the oscillations were one-dimensional, whereas turbulence is inherently three-dimensional. On the other hand, there was no apparent way to isolate the energy due to the oscillations. Whether the oscillations contributed to enhanced mixing rates is an open question. What is clear is that the "turbulence" intensity was much higher than in the moderate subsonic and supersonic regimes.

The quantitative results for two streamwise traverses which were taken in the high subsonic regime have already been presented as Figures 30 to 32. The profiles are inconsistent and difficult to explain. The mean velocity profile featured a minimum in the measurement window for HS1 but a maximum for HS2. The streamwise velocity variance decreased with x for HS1, but had a minimum for HS2. In both cases, S was large and positive, indicating that the flows were strongly anisotropic.

Because of the difficulty in interpreting the measurements, the high subsonic regime was not considered in further detail.

5.4 Supersonic Regime

In this section the flow in the supersonic regime is discussed. A qualitative understanding, based on the flow visualization study, is first provided, followed by a discussion of the quantitative results.

5.4.1 Qualitative Analysis

Shadowgraphs of the flow in the supersonic regime have been provided in Plates 7 to 9, which reveal diamond-shaped discontinuities in all cases. These discontinuities, referred to here as a "shock-diamond" pattern, must be compression waves, because they remain coalesced. They were inclined at approximately 35 to 40° to the mean flow, which, being very close to the flow Mach angle ($\sin^{-1}(1/M) = 40°$), suggests that they were nearly isentropic. The same conclusion may be reached by noting that static pressure rise across the window was small (Figure 8).

The waves appear to be reflected by the test section walls. The interaction of an oblique shock with a boundary layer is in general quite complex (Shapiro, 1953). For a turbulent boundary which remains attached, however, the region of interaction is quite small, and the interaction may be regarded as a regular reflection.

With the unmodified plates inserted in the standard orientation (the tops of Plates 7 and 9), a single set of waves dominated the flow. These relatively stronger waves are attributed to the metal blockages along the plate edges. With the modified MHP, for which the metal blockages were removed, and also with the unmodified plates inserted in the rotated orientation, the stronger waves were replaced by a distributed set of less intense waves.

Jacquin et al (1991) observed a similar pattern of compression waves in their

shock-turbulence interaction study. Recognizing that the abrupt exit from the grid was responsible for the waves, Barre et al (1995) used a multi-nozzle grid design (Pankhurst and Holder, 1952), resulting in waves of much lower intensity. In the same spirit, but independently, one aspect of the MHP modifications in the present study was the machining of chamfers around the holes at the downstream side of the plate. The chamfers resulted in a less abrupt flow exit from the plate, but noticeable waves were still generated.

The manner in which the compression waves were produced by the plate is considered further in Section 5.4.3.

5.4.2 Quantitative Analysis

The compression waves affected the LDV measurements, which are shown in Figures 33 to 38. The mean velocity and velocity variance profiles do not have monotonic trends, but rather fluctuate with x/m. The traverse profiles with smaller separation distances (SP1b, SP1c, SP2a, and SP2b) reveal smaller fluctuations, which are correlated with individual waves. This is illustrated more vividly in Figures 51 and 52, which show the profiles across a single wave (SP2c) with an expanded abscissa scale. The apparent smearing of the shock (15 mm in the mean velocity plot, and 25 mm in the velocity variance plot) was caused by particle inertia, as discussed in Section 5.5.2. The increase in downstream velocity variance may have been partly due to turbulence amplification, but was primarily caused by particle inertia.

The amplitude of the oscillations in the streamwise profiles is larger with the LHP than with the MHP, which is attributed to the modifications made to the MHP, resulting in the elimination of the strongest set of waves. The plate modifications may also have caused a turbulence intensity reduction, as is demonstrated in Table 5.5,

Table 5.5: Streamwise Turbulence Intensities in the Supersonic Regime

Plate	Budwig et al (1995)	Present Results
m = 14.5 mm, unmodified	1.29%	—
m = 14.5 mm, modified	—	0.81%
m = 14.5 mm, unmodified	1.37%	1.08%

where the average turbulence intensities (calculated as the average between the maximum and minimum intensities obtained with the 25.4 mm traverses) measured by Budwig et al (1995) are compared with the present results. The intensities with both plates dropped in the present experiments, the reason for which is discussed in Section 5.5.3. However, the drop is larger with the MHP, which is attributed to the addition of chamfers around the downstream side of the plate holes, This is an important point, for it implies that optimizing the plate design to minimize the wave intensity results in a turbulence intensity reduction.

The skewness factors, shown in Figure 37 and 38, are not zero. The flow is therefore anisotropic, which is not surprising given the degree of mean non-uniformity and turbulence inhomogeneity.

The decay exponents and their 90% confidence intervals are plotted for all regimes, assuming $x_0/m = 0$, in Figure 53. The exponents are much lower and more uncertain outside the moderate subsonic regime, due to flow non-stationarity in the high subsonic regime and to compression waves in the supersonic regime.

5.4.3 Flow near the Grid

Images of the flow near the grid as the supply pressure was increased have been presented in Plates 14 to 17. The first few frames show the flow turning subsonic through various shock waves. As the pressure increased, the shocks angles decreased,

indicating a weakening in their strength, and eventually became sufficiently weak that the downstream flow remained supersonic.

The images vividly show the coalescence of weaker oblique shocks to form fewer, relatively stronger, shocks. The final frame of each sequence (particularly Plate 15) shows that each internal rod sheds two oblique shocks — one towards the ceiling and one towards the floor. The two shocks travelling in the same direction have slightly different angles, eventually coalescing to form a single oblique shock (Plate 16 being an exception). For instance, with the round rods, the coalescence occurs close to the point of reflection from the test section walls. A joining may also be anticipated shortly downstream of the image border in the final frame of Plate 15.

The images also show the sensitivity of wave intensity to rod design, with the square rods appearing to shed the strongest waves, and the diamond rods the weakest. These results appear to confirm that the multi-nozzle design of Barre et al (1995) is effective in reducing wave intensity, and that the use of chamfers on the MHP in the present case is also helpful.

The images further suggest that the turbulence structure behind the grid in supersonic flow differs from the typical structure in incompressible flow. As with the subsonic cases at higher M, the wakes immediately behind the rods were narrow in extent and did not spread. The structure and intensity of the turbulence was also likely affected by the shocks.

5.4.4 Towards Generating Compressible Isotropic Turbulence

One of the objectives of the present work was to identify barriers which need to be overcome before an experimental approximation to compressible isotropic turbulence can be attained. The degree of turbulence compressibility is given by the turbu-

lence Mach number, M_t, which has been defined in Eq. (2.9). In the present results, $M_t \approx 0.03$, which is an order of magnitude smaller than that required for the dilatational dissipation rate to become significant, and the turbulence was far from the isotropic ideal. Clearly, improvements in both turbulence isotropy and intensity must be achieved before compressible isotropic turbulence can be experimentally realized.

A few options in improving the turbulence isotropy may be possible. The optimized grid of Barre et al (1995) has been found to be effective; however, it also appears to produce turbulence of relatively low intensity and therefore also low M_t. A second option is to separate the turbulence generator and sonic throat, by moving the grid upstream of a smooth converging-diverging nozzle. However, as the turbulence passes through the contraction, the turbulence will be damped, and it may also become inhomogeneous as it passes through the expansion. A third option, suggested by Dr. V. D. Nguyen (personal communication), is to permit waves to form at the grid, but then to remove them using porous test section walls. Turbulence intensity may potentially be increased using alternative grid designs, such as active grids (e.g. Gad-el-Hak and Corrsin, 1974).

Even if a compressible isotropic turbulence is achieved, a host of measurement difficulties remain. For instance, Taylor's hypothesis breaks down as M_t increases (Lee et al, 1992), which calls into question the validity of studying turbulence structure with single-point measurements.

5.5 Measurement Error and Uncertainty

Potential sources of error and techniques for estimating them were presented in Section 3.4. In this section, the resulting uncertainties in the measurements are esti-

mated.

5.5.1 Wind Tunnel Operation

Potential sources of measurement uncertainty due to the wind tunnel operation were considered in Section 3.4.1. The effects of storage tank pressure fluctuations were concluded to be insignificant, and error due to the operation of the 1.5 m tunnel was avoided. Nevertheless, measurement repeatability was difficult to attain. Scatter could occur while obtaining measurements at a single measuring location, within a run, from day-to-day, and over longer term periods.

The degree of scatter at a given measuring location was quantified by calculating the 95% confidence intervals for the ensemble-averaged moments. The earliest case, MS1a, had only five records per location, and hence had relatively large confidence intervals (0.44% for U and 2.43% for u'). Of the other cases, the largest confidence intervals for U were: in the moderate subsonic regime, 0.11% (MS5a); in the high subsonic regime, 0.18% (HS1); and in the supersonic regime, 0.10% (SP1b). The largest confidence intervals for u' were: in the moderate subsonic regime, 2.23% (MS5a); in the high subsonic regime, 4.66% (HS1); and in the supersonic regime, 3.51% (SP1c).

The effect of scatter within a run was minimized by randomizing the order in which measurement locations were visited, and was quantified by repeating measurements at one location two or three times during the run. The largest changes in U within a run were: in the moderate subsonic regime, 0.56% (MS5d); in the high subsonic regime, 0.32% (HS1); and in the supersonic regime, 1.28% (SP2c, much larger than the others). The largest variations in u' were: in the moderate subsonic regime, 3.8% (MS2); in the high subsonic regime, 7.2% (HS1); and in the supersonic regime, 8.5%

(SP1b).

There were also repeatability problems between runs and from one day to the next. For example, MS8a and MS8b were performed on the same day using identical wind tunnel settings, but u' was about 5% lower in MS8a. Similarly, MS9a and MS9b used identical wind tunnel settings and were performed five days apart, but u' was about 12% lower in MS9b.

Over longer periods, even stronger shifts or drifts in the wind tunnel characteristics occurred. For instance, MS8a and MS8b, which featured moderate subsonic flow, had the same wind tunnel settings as HS1, which was performed about a month later and featured high subsonic flow. The cause of these shift is unknown.

5.5.2 Particle Dynamics

Equations for estimating errors due to particle inertia have been derived in Section 3.4.2. The amount of apparent smear in a shock is described by Eq. (3.5). From Figure 52, the shock distance appears to be about 15 mm, from which we may conclude that the maximum particle size which affected the mean velocity calculation in the supersonic regime was about 1.5 μm, or twice the size of the average particle size generated by the atomizer (Figure 5). There are two possible reasons for the discrepency. Firstly, as the particles travelled from the atomizer into the settling chamber, they passed through various bends, which may have caused small particles to coalesce into larger particles (Menon and Lai, 1991). Secondly, the light scattered by the smaller particles may have had insufficient intensity to meet the minimum signal-to-noise ratio of the signal processor, as discussed later in Section 5.5.3.

The error in measured turbulence intensity due to particle inertia may be estimated by Eq. (3.8), using a range of frequencies characterized by ω_L, which in turn

Table 5.6: Estimated Error Due to Particle Inertia

M	L_f (mm)	ω_L (rad/s)	$d_p = 1.0$ μm			$d_p = 1.5$ μm		
			τ (s)	u'_p/u'		τ (s)	u'_p/u'	
				$10\omega_L$	$100\omega_L$		$10\omega_L$	$100\omega_L$
0.16	11.5	560	3.33×10^{-6}	1.000	0.983	7.19×10^{-6}	0.999	0.928
0.24	11.4	730	3.37×10^{-6}	1.000	0.971	7.58×10^{-6}	0.998	0.874
0.37	12.1	1120	3.41×10^{-6}	0.999	0.935	7.67×10^{-6}	0.996	0.760
0.46	11.5	1570	3.45×10^{-6}	0.999	0.880	7.76×10^{-6}	0.993	0.635
0.52	11.3	1920	3.48×10^{-6}	0.998	0.831	7.83×10^{-6}	0.989	0.554
0.58	8.27	2160	3.52×10^{-6}	0.997	0.796	7.92×10^{-6}	0.986	0.505
0.68	6.59	3190	3.55×10^{-6}	0.994	0.661	7.99×10^{-6}	0.969	0.365
1.55	6.59	7380	4.64×10^{-6}	0.946	0.280	1.04×10^{-5}	0.790	0.127

may be estimated from Eq. (3.9). Solving the equations suggests that particle inertia had a negligible effect for all relevant particles sizes at ω_L itself. However, higher frequencies also contribute to u', so calculations were carried out for $\omega = 10\omega_L$ and $\omega = 100\omega_L$. The resulting error estimates with $d_p = 1.0$ μm and $d_p = 1.5$ μm are shown in Table 5.6. Where measurements were made at similar M with both lenses, only the results with the 160 mm lens are shown. At $M = 1.55$, where L_f was unknown, the value from $M = 0.68$ was assumed; in reality, it was likely smaller because the turbulence was amplified, and consequently length scale growth suppressed, by the compression waves. At $M = 1.55$, the value for u' used to calculate ω_L was chosen to be twice its measured value, for it was known that the measured value was too low.

These estimates suggest that particle inertia error was an issue in the the turbulence measurements. In the supersonic regime, where earlier estimates showed that particles of $d_p = 1.5$ μm contribute to the moment calculations, the error was large. In the moderate subsonic regime, the number of smaller particles which are measured increases, and the error was much less serious.

Unfortunately, the error cannot be quantified further without knowing the shape of the Lagrangian spectrum and the size distribution of particles which trigger LDV bursts.

5.5.3 LDV System

Sources of error and uncertainty within the LDV system were discussed in Section 3.4.3, and included insufficient SNR, volume-averaging, and statistical bias. Statistical bias was found to be insignificant in the present study. Insufficient SNR was found to have a negligible direct contribution to uncertainty, because only those signals which exceeded the threshhold SNR triggered a burst. However, the parameters affecting the SNR could still indirectly affect the results. The reason is related to the incompatible requirements that the seed particle size must be both small enough to follow the flow and large enough to generate a signal that exceeds the threshhold SNR. For instance, suppose the signal generated by a small particle is too weak to register a burst. If the system parameters are changed to increase the signal strength, such that the same particle now registers a burst, the flow statistics could change, depending on how well the particles follow the flow.

In the present experiments, indirect effects of the signal strength were observed. In Section 5.4.2 it was noted that the turbulence intensity measured in the supersonic regime was lower than similar measurements performed by Budwig et al (1995). The drop is attributed to a degradation in laser power which was observed during the measurements, but not corrected until after the measurements were completed. That the turbulence intensities with the 243 mm lens were lower than with the 160 mm lens may also be an indirect effect of signal strength, for the scattered light intensity increases with the inverse square of the probe volume size (Menon and Lai, 1991).

Table 5.7: Estimated Error Due to Volume-Averaging

Case	Lens (mm)	u'_r/u'
MS1a	160	0.978
MS1b	160	0.980
MS1c	160	0.981
MS1d	160	0.979
MS2	160	0.979
MS3	160	0.980
MS4	160	0.979
MS5a	243	0.974
MS5b	243	0.976
MS5c	160	0.979
MS5d	160	0.979
MS6	243	0.974
MS7a	243	0.963
MS7b	243	0.964
MS8a	160	0.968
MS8b	160	0.970

An equation for estimating the error in measured turbulence intensity due to volume-averaging has been given as Eq. (3.11). Table 5.7 compiles the calculation results for the moderate subsonic cases. The calculation could not be performed in the high subsonic and supersonic regimes because ϵ was unknown. The results suggest that the error due to volume-averaging was relatively small.

5.5.4 Estimate of Uncertainty in Measured Turbulence Intensity

The above analysis suggests that particle inertia is the dominant source of error in these experiments, with a small contribution from volume-averaging. Both sources lead to an underestimation of the true turbulence intensity. Although the actual

error level could not be calculated, the maximum uncertainty was estimated, rather arbitrarily, as follows:

1. At $M = 0.16$, error due to particle inertia was negliglible. A 5% uncertainty was assumed, which is larger than the estimated 2% error due to volume-averaging.

2. At $M \approx 0.66$, the error due to volume-averaging was likely small relative to the particle inertia error, and the results with the 243 mm and 160 mm lens differed by about 16%. An uncertainty of 20% was assumed for the 160 mm lens, and 36% for the 243 mm lens.

3. The uncertainties at intermediate M was estimated assuming linear interpolation between the estimates at $M = 0.16$ and $M \approx 0.66$. Hence, at $M = 0.52$, it was estimated to be 15.4% with the 160 mm and 27.3% with the 243 mm lens. The difference between these two estimates agrees well with the observed difference of 11%.

4. In the supersonic regime, the error was likely much higher. The intensities measured by Budwig et al (1995) were about 30% higher than in the present tests, and particle inertia was also likely in that study. A reasonable uncertainty is set at 150%.

This procedure was used to obtain the error bars shown in Figure 39, and also used to estimate uncertainties in L_f, λ, and R_λ.

Chapter 6

Conclusions and Recommendations

6.1 Conclusions

The primary objective of this study was to study the effects of mean compressibility on the isotropy, homogeneity, and decay characteristics of grid turbulence. With respect to this objective, the results permit the following conclusions to be drawn:

1. With moderate subsonic conditions in the test section ($0.16 < M < 0.7$), the levels of homogeneity and isotropy were consistent with studies of grid turbulence in incompressible flow. Due to the limited range of x/m over which measurements were taken, it is more difficult to draw conclusions about the decay characteristics. However, the results are not inconsistent with previous high Reynolds-number experiments or the theory of George (1992).

   For $M > 0.5$, the turbulence intensity dropped and the decay parameters changed, with an increase in either the decay exponent or the effective origin. These shifts appear to be correlated with changes in the flow near the grid.

Unlike the flow at lower speeds, where the flow was subsonic throughout, the jets were choked between the rods, became supersonic in the ensuing expansion, and turned subsonic again via shocks. The wakes immediately behind the rods were much narrower in extent than those at lower speeds.

2. With high subsonic conditions ($0.7 < M < 1.0$), flow visualization revealed the presence of an unsteady quasi-normal shock in the test section, leading to strongly inhomogeneous and anisotropic turbulence with a large intensity. It is uncertain whether the unsteadiness in the shock system is to be interpreted as turbulence. The decay exponent was much lower than that in the moderate subsonic regime.

3. With supersonic conditions ($M = 1.55$), flow visualization revealed the presence of a shock-diamond structure, composed of weak oblique shocks, in the test section. The shocks resulted in inhomogeneous and anisotropic turbulence, and led to fluctuations in the downstream mean velocity and velocity variance profiles. Flow visualization near the grid indicated that the shocks were generated by the grid and were sensitive to grid geometry.

   Serious measurement error was encountered in this regime, due to particle inertia and leading to shock smearing, artificially high turbulence levels downstream of the shock, and underestimation of the turbulence intensity. Because of the shocks and measurement error, the measured decay exponent was much lower than that in the moderate subsonic regime.

A secondary objective of this study was to identify practical barriers to the experimental realization of compressible isotropic turbulence. It is concluded that the realization of such turbulence requires, on the one hand, an improvement of the homogeneity and isotropy of the turbulence, and on the other hand, an increase in the

turbulence intensity. Some possibilities on both of these fronts were suggested.

Regarding the applicability of the present results to computational turbulence studies, the measurements in the high subsonic regime and supersonic regime are not likely to be useful because of the measurement difficulties and the strong geometry-dependence of the flows. In the moderate subsonic regime, the results differ from previous grid turbulence studies primarily in the nature of the flow near the grid. Resolution of the details of the flow there is beyond the existing capability of computational methods, but the results may become useful in the future.

6.2 Recommendations for Further Research

Several modifications and enhancements could be made to the study, and the results suggest other potentially fruitful avenues for research. Some possibilities are listed below:

1. The biggest limitation in the study was the narrow range of x/m over which measurements could be obtained. If the range were extended, the decay law parameters could be obtained with more certainty. Extending the range of the facility used in the present measurements would require construction of a longer test section with transparent test section walls.

2. The spatial and temporal resolution of the LDV system precluded the measurement of velocity autocorrelations, derivatives, and turbulence spectra. Hot-wire anemometry measurements would be a useful supplement, permitting a more thorough analysis of the turbulence structure and better accuracy in the supersonic regime.

3. Velocity measurements and high-speed flow visualization near the grid would be useful to obtain further insight into the nature of the turbulence generation mechanism at supersonic and high subsonic speeds.

4. In the supersonic regime, alternative grid designs, which produce less intense shocks, could be investigated.

5. It was noticed that pressure loss varies strongly with M, but there was not enough information to calculate the static and total pressure loss coefficients. In incompressible flow, some studies have suggested a relationship between the geometry-dependent pressure loss coefficient and the decay coefficient (eg. Gad-el-Hak and Corrsin, 1974). These possibilities could be explored further.

6. The effects of contractions and expansions on turbulence have been studied in incompressible flow. Similar studies could be performed in compressible flow. One intriguing possibility is the generation of turbulence in supersonic flow by passing grid turbulence through a smooth converging-diverging nozzle.

7. Dr. V. D. Nguyen has suggested the possibility of generating a shock-free turbulence in supersonic flow by using porous test section walls. This possibility could be further explored.

Bibliography

Adrian, R. L. 1983. Laser velocimetry. In *Fluid Mechanics Measurements*, R. J. Goldstein, ed. Hemisphere Publishing Corporation, 155-244.

Annand, W. J. D. 1953. The resistance to air flow of wire gauzes. *Journal of the Royal Aeronautical Society* 57:141-146.

Anyiwo, J. C., Bushnell, D. M. 1984. Turbulence amplification in shock-wave boundary-layer interaction. *AIAA Journal* 20:893-899.

Ardonceau, P. L. 1984. The structure of turbulence in a supersonic shock-wave / boundary-layer interaction. *AIAA Journal* 22:1254-1262.

Baines, W. D., Peterson, E. G. 1951. An investigation of flow through screens. *Transactions of the ASME* 73:467-480.

Barre, S., Alem, D., Bonnet, J. P. 1995. Experimental study of a normal shock / homogeneous turbulence interaction. *AIAA 95-0579, 33rd Aerospace Sciences Meeting and Exhibit*, Reno.

Batchelor, G. K. 1948. Energy decay and self-preserving correlation functions in isotropic turbulence. *Quarterly of Applied Mathematics* 6:97-116.

Batchelor, G. K., Townsend, A. A. 1948. Decay of isotropic turbulence in the initial period. *Proceedings of the Royal Society of London, Series A* 193:539-558.

Blaisdell, G. A., Mansour, N. N., Reynolds, W. C. 1993. Compressibility effects on the growth and structure of homogeneous turbulence. *Journal of Fluid Mechanics* 256:443-485.

Blin, E., Jacquin, L., Geffroy, P. 1993. Etude experimentale sur l'interaction choc / turbulence libre. *Onera Report RTS no. 4/2496 AY006.*

Bloomberg, J. E. 1989. An investigation of particle dynamics effects related to LDV measurements in compressible flows. M. Sc. thesis, University of Illinois at Urbana-Champaign.

Bradshaw, P. 1977. Compressible turbulent shear layers. *Annual Review of Fluid Mechanics* 9:33-54.

Briassulis, G., Andreopoulos, J. 1994. Unsteady pressure field in shock wave interaction with grid generated turbulence in a shock tube. *AIAA 94-2277, 25th AIAA Fluid Dynamics Conference*, Colorado.

Buchhave, P., George, W. K., Lumley, J. L. 1979. The measurement of turbulence with the laser-Doppler anemometer. *Annual Review of Fluid Mechanics* 11:443-503.

Budwig, R., Zwart, P. J., Nguyen, V., Tavoularis, S. 1995. Grid-generated turbulence in compressible streams. *Second Symposium on Transitional and Turbulent Compressible Flows*, Hilton Head, South Carolina.

Chu, B. T., Kovasznay, L. S. G., 1958. Non-linear interactions in a viscous heat-conducting compressible gas. *Journal of Fluid Mechanics* 3:494-514.

Comte-Bellot, G., Corrsin, S. 1966. The use of a contraction to improve the isotropy of grid-generated turbulence. *Journal of Fluid Mechanics* 25:657-682.

Corrsin, S. 1963. Turbulence: experimental methods. *Handbuch der Physik*, Vol. VIII/2. S. Flugge, C. Truesdell, ed. Springer-Verlag.

Debieve, J. F., Lacharme, J. P. 1986. A shock-wave / free turbulence interaction. *Turbulent Shear Layer / Shock Wave Interactions*. J. Delery, ed. Springer-Verlag, 393-403.

de Souza, F. 1993. Experiments in highly sheared, nearly homogeneous turbulence. M. A. Sc. thesis, University of Ottawa, Ottawa, Canada.

de Souza, F, Nguyen, V., Tavoularis, S. 1995. The structure of highly sheared turbulence. *Journal of Fluid Mechanics* 303:155-167.

Durst, F., Mellig, A., Whitelaw, J. H. 1981. *Principles and Practice of Laser-Doppler Anemometry*. Academic Press, Inc.

Edwards, R. V. 1987. Report of the special panel on statistical particle bias problems in laser anemometry. *Journal of Fluids Engineering* 109:89-93.

Favre, A. 1967. Statistical equations of turbulent gases. *Problems of Hydrodynamics and Continuum Mechanics.* SIAM, 231-266.

Gad-el-Hak, M., Corrsin, S. 1974. Measurements of the nearly isotropic turbulence behind a uniform jet grid. *Journal of Fluid Mechanics* 62:115-143.

George, W. K. 1992. The decay of homogeneous isotropic turbulence. *Physics of Fluids A* 4:1492-1509.

Goldstein, R. J. 1983. Optical systems for flow measurements. In *Fluid Mechanics Measurements*, R. J. Goldstein, ed. Hemisphere Publishing Corporation, 155-244.

Grant, H. L., Nisbet, I. C. T. 1957. The inhomogeneity of grid turbulence. *Journal of Fluid Mechanics* 2:263-272.

Hannappel, R., Friedrich, R. 1993. Interaction of isotropic turbulence with a normal shock wave. *Applied Scientific Research* 51:507-512.

Hannappel, R., Friedrich, R. 1995. Direct numerical simulation of a Mach 2 shock interacting with isotropic turbulence. *Applied Scientific Research* 54:205-221.

Hinze, J. O. 1975. *Turbulence, 2nd ed.* McGraw-Hill Book Company.

Honkan, A., Andreopoulos, J. 1992. Rapid Compression of grid-generated turbulence by a moving shock wave. *Physics of Fluids A* 4:2562-2572.

Huang, M., Leonard, A. 1995. Velocity autocorrelations of decaying isotropic homogeneous turbulence. *Physics of Fluids A* 7:2455-2464.

Jacquin, L., Blin, E., Geffroy, P. 1991. An experiment on free turbulence / shock wave interaction. *Proceedings, Eighth Symposium on Turbulent Shear Flows.* F. Durst, ed. Springer-Verlag.

John, J. E. A. 1983. *Gas Dynamics, 2nd ed.* Allyn and Bacon.

von Kàrmàn, T., Howarth, L. 1938. On the statistical theory of isotropic turbulence. *Proceedings of the Royal Society* A164:192-215.

Keller, J., Merzkirch, W. 1990. Interaction of a normal shock wave with a compressible turbulent flow. *Experiments in Fluids* 8:241-248.

Kida, S., Orszag, S. A. 1992. Energy and spectral dynamics in decaying compressible turbulence. *Journal of Scientific Computing* 7:1-34.

Kistler, A. L., Vrebalovich, T. 1966. Grid turbulence at large Reynolds numbers. *Journal of Fluid Mechanics* 26:37-47.

Kolmogoroff, A. N. 1941. On degeneration of isotropic turbulence in an incompressible viscous liquid. *Comptes rendus (Doklady) de l'academie des sciences de l'U.R.S.S.* 31:538-540.

Kovasznay, L. S. G. 1950. The hot-wire anemometer in supersonic flow. *Journal of the Aeronautical Sciences* 17: 565-584.

Kovasznay, L. S. G. 1953. Turbulence in supersonic flow. *Journal of the Aeronautical Sciences* 20: 657-674.

Laws, E. M., Livesey, J. L. 1978. Flow through screens. *Annual Review of Fluid Mechanics* 10:247-266.

Lee, S., Lele, S. K., Moin, P. 1991. Eddy shocklets in decaying compressible turbulence. *Physics of Fluids A* 3:657-664.

Lee, S., Lele, S. K., Moin, P. 1992. Simulation of spatially evolving turbulence and the applicability of Taylor's hypothesis in compressible flow. *Physics of Fluids A* 4:1521-1530.

Lee, S., Lele, S. K., Moin, P. 1993. Direct numerical simulation of isotropic turbulence interacting with a weak shock wave. *Journal of Fluid Mechanics* 251:533-562.

Lele, S. K., Lee, S., Moin, P. 1992. Compressible Turbulence and Shock Waves. *Studies in Turbulence.* T. B. Gatski et al, ed. Springer-Verlag, 285-296.

Lele, S. K. 1994. Compressibility effects on turbulence. *Annual Review of Fluid Mechanics* 26:211-254.

Ling, S. C., Wan, C. A. 1972. Decay of Isotropic Turbulence Generated by a Mechanically Agitated Grid. *The Physics of Fluids* 15:1363-1369.

Loehrke, R. I., Nagib, H. M. 1972. Experiments on management of free-stream turbulence. *Agard Report No. R-598.*

Menon, R., Lai, W. T. 1991. Key considerations in the selection of seed particles for LDV measurements. *4th International Conference on Laser Anemometry, Advances and Applications* 2:719-730.

Micheli, F., D'Humieres, C., Papirnyk, O. 1991. Aerosol behaviour in supersonic flows. *4th International Conference on Laser Anemometry, Advances and Applications* 3:101-110.

Mohamed, M. S., LaRue, J. C. 1990. The decay power law in grid-generated turbulence. *Journal of Fluid Mechanics* 219:195-214.

Morkovin, M. V. 1961. Effects of compressibility on turbulent flows. *The Mechanics of Turbulence: International Symposium of the National Scientific Research Center.* A. Favre, ed. CNRS, 367-380.

Moyal, J. E. 1952. The spectra of turbulence in a compressible fluid; eddy turbulence and random noise. *Proceedings of the Cambridge Philosophical Society* 48:329-344.

Pankholster, R. C., Holder, D. W. 1952. *Wind-Tunnel Technique.* The Pitman Press.

Passot, T., Pouquet, A. 1987. Numerical simulation of compressible homogeneous flows in the turbulent regime. *Journal of Fluid Mechanics* 181:441-466.

Pinker, R. A., Herbert, M. V. 1967. Pressure loss associated with compressible flow through square-mesh wire gauzes. *Journal Mechanical Engineering Science* 9:11-23.

Ribner, H. S. 1953. Convection of a pattern of vorticity through a shock wave. *NACA TN-2864.*

Ristorcelli, J. R. 1995. A pseudo-sound constitutive relationship for the dilatational covariances in compressible turbulence: an analytical theory. *ICASE Report No. 95-22, NASA CR-195064.*

Rudoff, R. C., Bachalo, W. D. 1991. Seed particle response and size characterization in high speed flows. *4th International Conference on Laser Anemometry, Advances and Applications* 2:443-447.

Saffman, P. G. 1967a. The large-scale structure of homogeneous turbulence. *Journal of Fluid Mechanics* 27:581-593.

Saffman, P. G. 1967b. Note on decay of homogeneous turbulence. *The Physics of Fluids* 10:1349.

Sarkar, S., Erlebacher, G., Hussaini, M. Y., Kreiss, H. O. 1991. The analysis and modelling of dilatational terms in compressible turbulence. *Journal of Fluid Mechanics* 227:473-493.

Sarkar, S., Erlebacher, G., Hussaini, M. Y. 1992. Direct simulation of compressible turbulence in a shear flow. *Studies in Turbulence.* T. B. Gatski et al, ed. Springer-Verlag, 285-296.

Schedvin, J., Stegun, G. R., Gibson, C. H. 1966. Universal similarity at high grid Reynolds numbers. *Journal of Fluid Mechanics* 65:561-579.

Schlichting, H. 1979. *Boundary Layer Theory.* McGraw-Hill Book Company.

Shlien, D. J., Corrsin, S. A measurement of Lagrangian velocity autocorrelation in approximately isotropic turbulence. *Journal of Fluid Mechanics* 62:255-271.

Simmons, L. F. G., Salter, C. 1934. Experimental investingation and analysis of the velocity variations in turbulent flow. *Proceedings of the Royal Society* A145:212-234.

Sreenivasan, K. R., Tavoularis, S., Henry, R., Corrsin, S. 1980. Temperature fluctuations and scales in grid-generated turbulence. *Journal of Fluid Mechanics* 100:597-621.

Sreenivasan, K. R. 1984. On the scaling of the turbulence energy dissipation rate. *The Physics of Fluids* 27:1048-1051.

Shapiro, A. H. 1953. *The Dynamics and Thermodynamics of Compressible Fluid Flow, Vols. 1 and 2.* The Ronald Press Company.

Tan-atichat, J., Nagib, H. M., Loehrke, R. I. 1982. Interaction of free-stream turbulence with screens and grids: a balance between turbulence scales. *Journal of Fluid Mechanics* 114:501-528.

Tassa, Y., Kamotani, Y. 1975. Experiments on turbulence behind a grid with jet injection in downstream and upstream direction. *The Physics of Fluids* 18:411-414.

Taylor, G. I. 1935. Statistical theory of isotropic turbulence. *Proceedings of the Royal Society* A151:421-478.

Tennekes, H., Lumley, J. L. 1972. *A First Course in Turbulence.* The MIT Press.

Trolier, J. W., Duffy, R. E. 1985. Turbulence measurements in shock-induced flows. *AIAA Journal* 23:1172-1178.

Uberoi, M. S., Kovasznay, L. S. G. 1955. Analysis of turbulent density fluctuations by the shadow method. *Journal of Applied Physics* 26:19-24.

Uberoi, M. S., Wallis, S. 1966. Small axisymmetric contraction of grid turbulence. *Journal of Fluid Mechanics* 24:539-543.

Zang, T. A., Hussaini, M. Y., Bushnell, D. M. 1984. Numerical computations of turbulence amplification in shock-wave interactions. *AIAA Journal* 22:13-21.

Zeman, O. 1990. Dilatation dissipation: The concept and application in modeling compressible mixing layers. *Physics of Fluids A* 2:178-188.

Zeman, O. 1991. On the decay of compressible isotropic turbulence. *Physics of Fluids A* 3:951-955.

Zeman, O. 1992. Toward a constitutive relation in compressible turbulence. *Studies in Turbulence.* T. B. Gatski et al, ed. Springer-Verlag, 285-296.

Plates

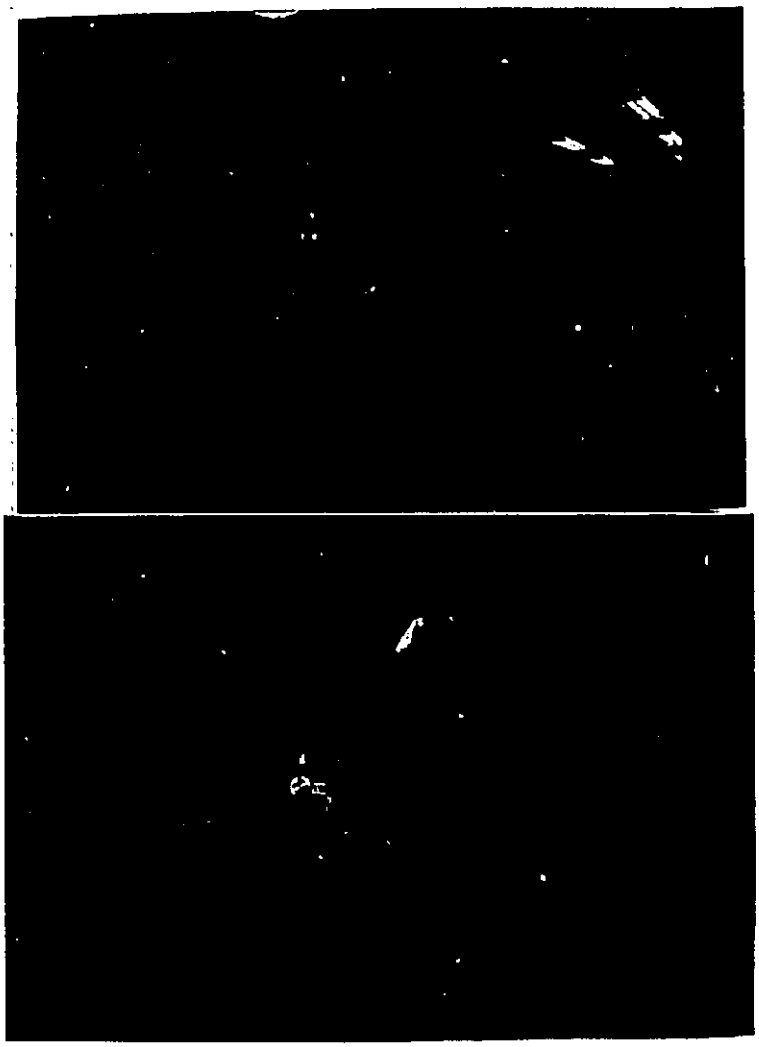

Plate 1: Photographs of the wind tunnel facility.

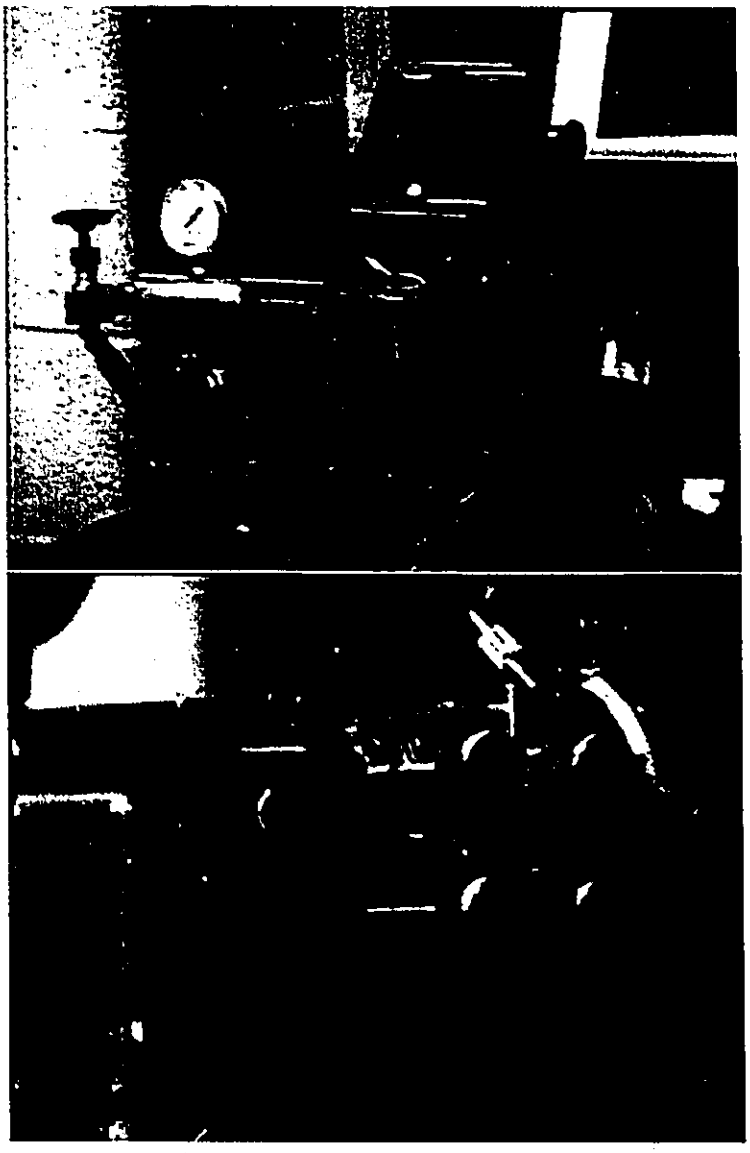

Plate 2: Photographs of the demonstration nozzle.

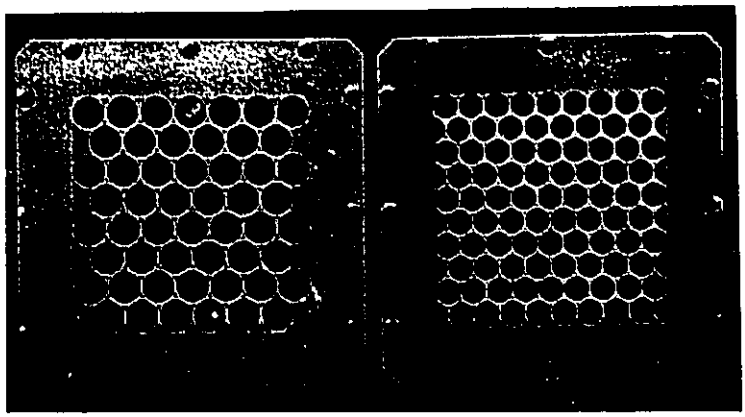

Plate 3: Photograph of the perforated plates. On the left is the LHP ($m = 18.4$ mm) and on the right is the modified MHP ($m = 14.5$ mm).

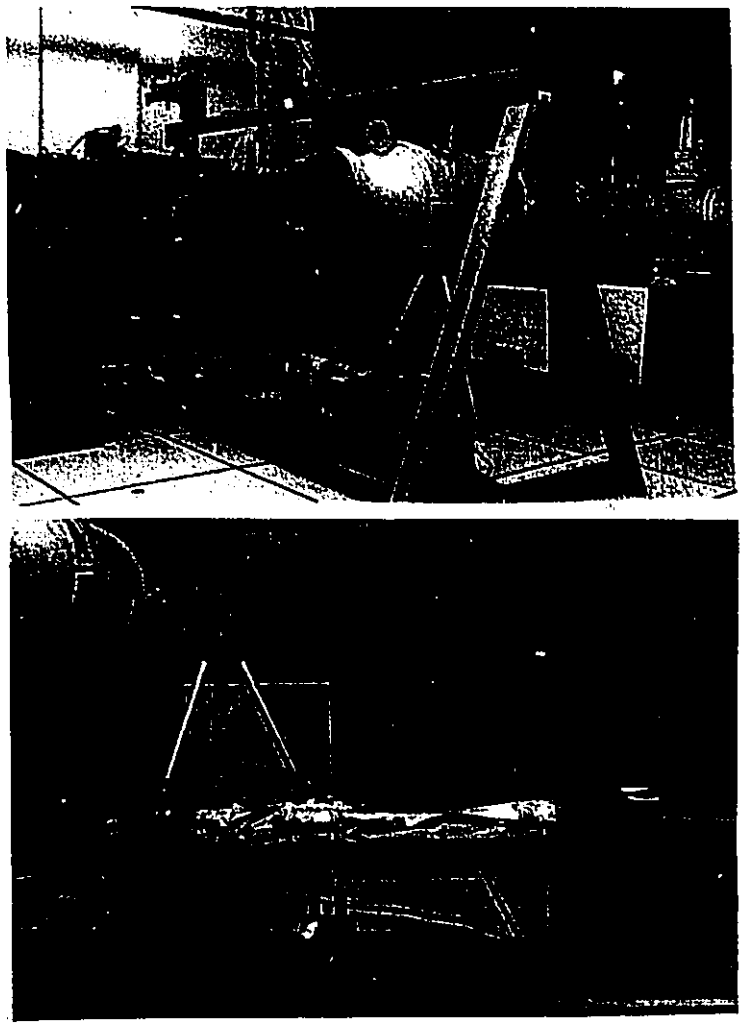

Plate 4: Photographs of the wind tunnel with the flow visualization system.

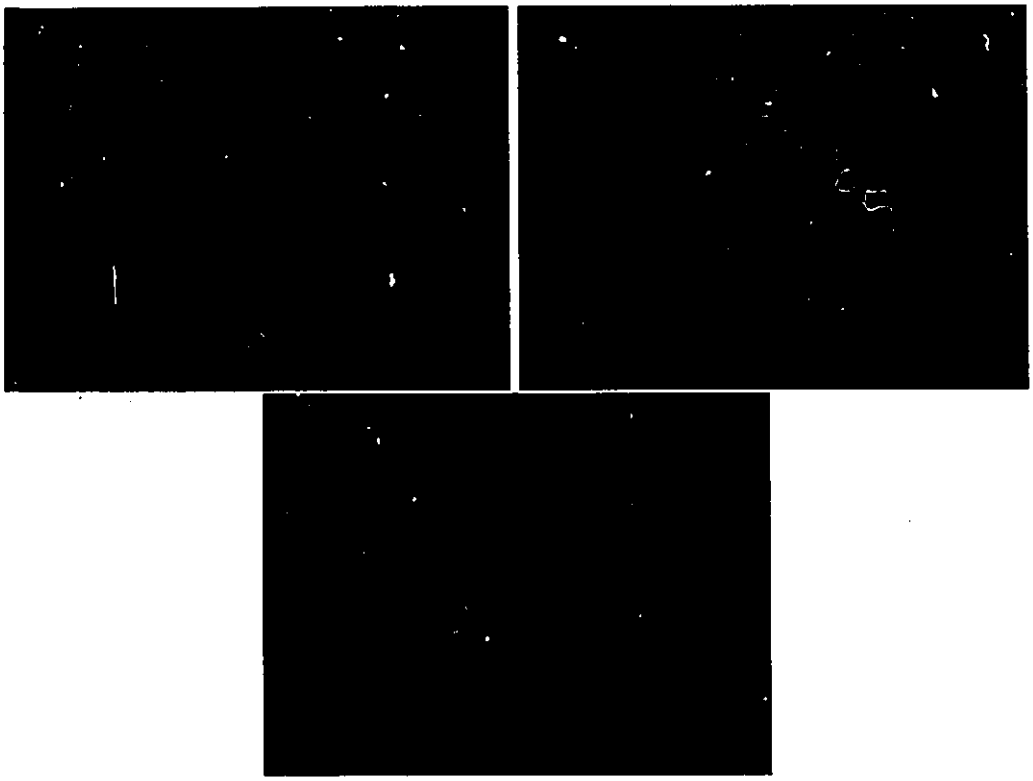

Plate 5: Shadowgraphs of the quasi-normal shock, $A_{dt}/A = 0.94$. Top left: P_{t0}=29.0 psi; top right: P_{t0}=32.0 psi; bottom: P_{t0}=35.0 psi.

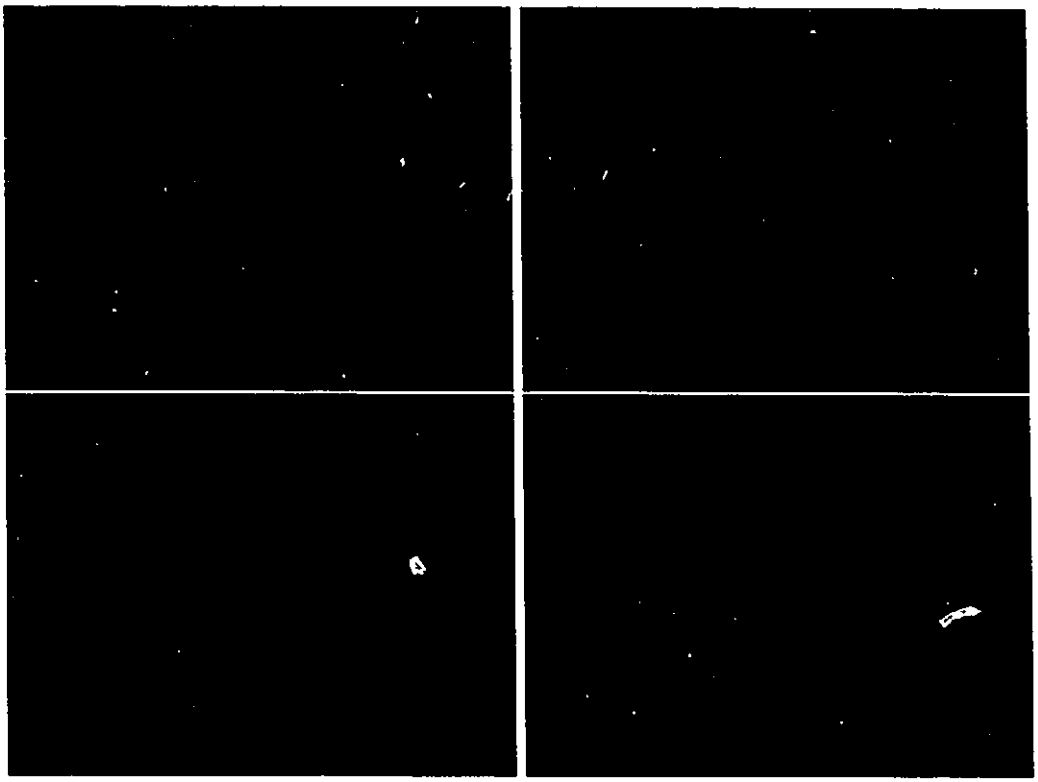

Plate 6: Shadowgraphs of the quasi-normal shock, $A_{dt}/A = 0.98$. Top left: P_{t0}=22.4 psi; top right: P_{t0}=22.6 psi; bottom left: P_{t0}=22.8 psi; bottom right: P_{t0}=23.0 psi.

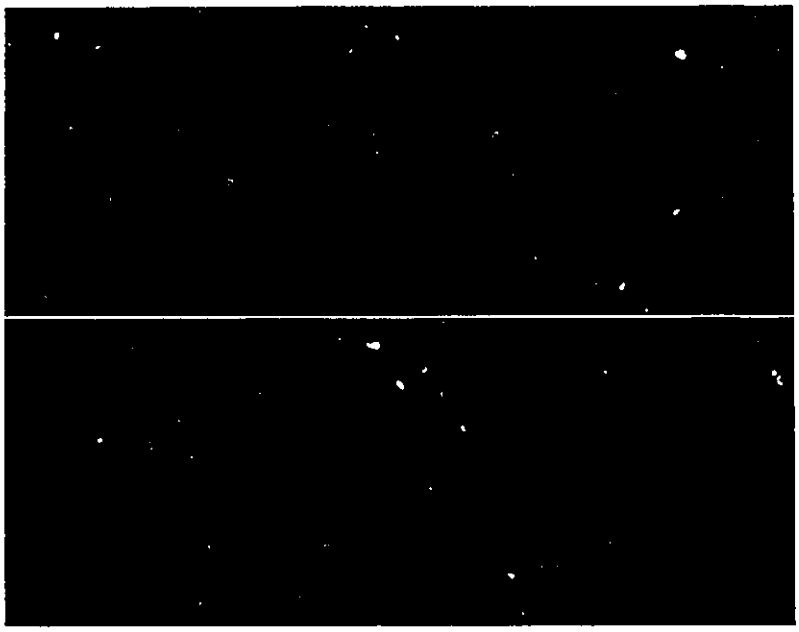

Plate 7: Shadowgraph images with the unmodified MHP. Top: plate in standard orientation; bottom: plate in rotated orientation.

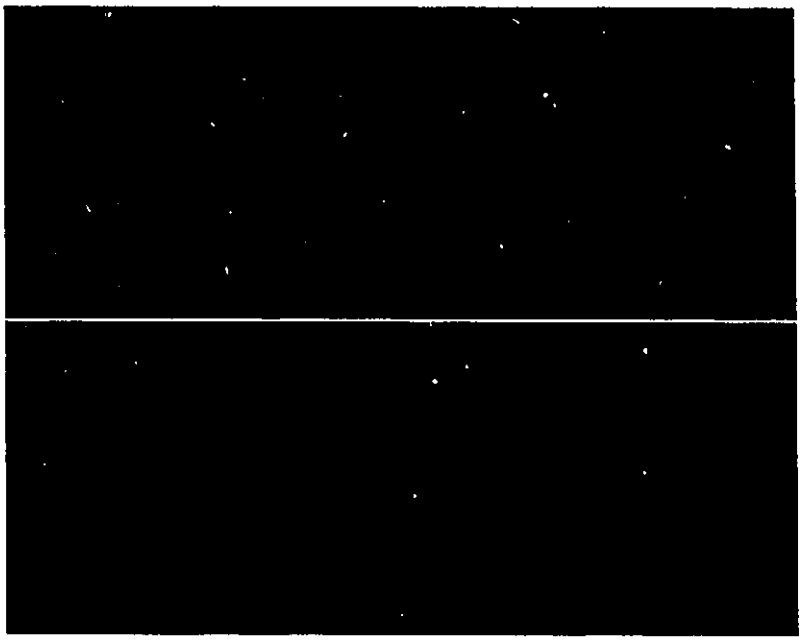

Plate 8: Shadowgraph images with the modified MHP. Top: plate in standard orientation; bottom: plate in rotated orientation.

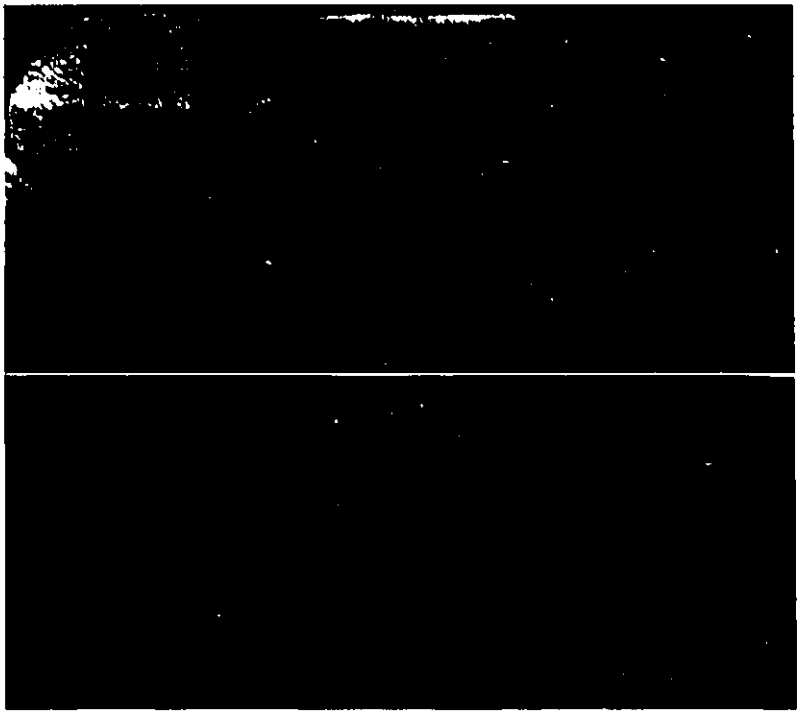

Plate 9: Shadowgraph images with the LHP. Top: plate in standard orientation; bottom: plate in rotated orientation.

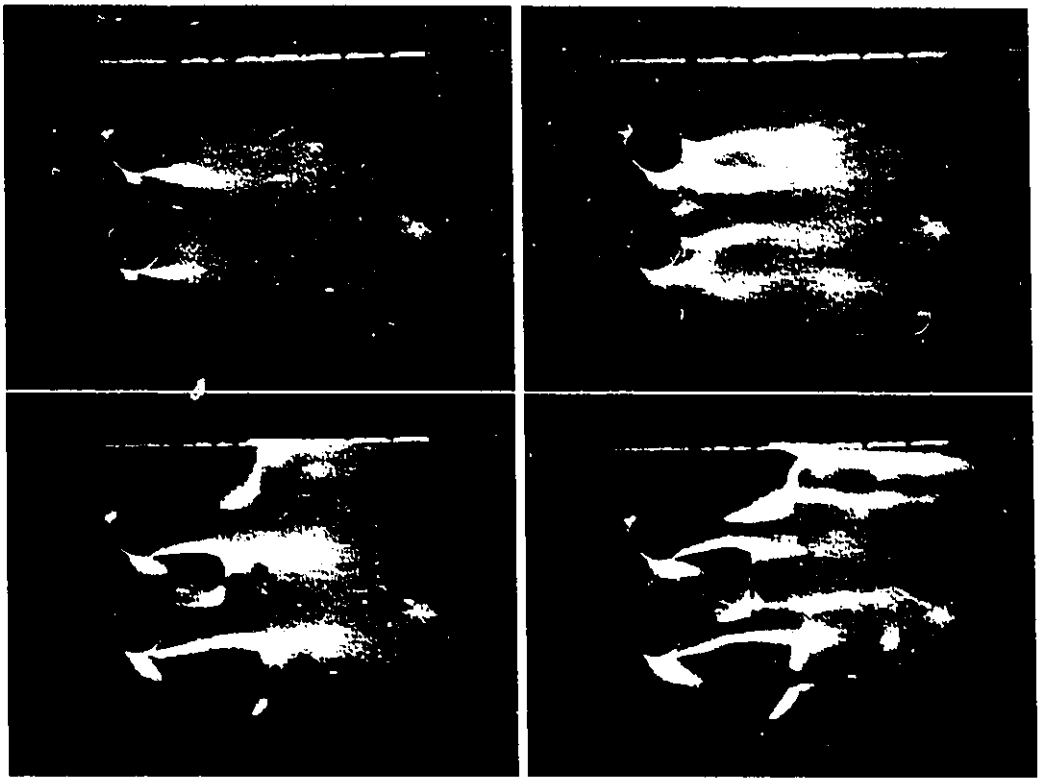

Plate 10: Schlieren images in the demonstration nozzle with round rods (1). Top left: $M_{1d} = 0.46$; top right: $M_{1d} = 0.55$; bottom left: $M_{1d} = 0.68$; bottom right: $M_{1d} = 0.77$.

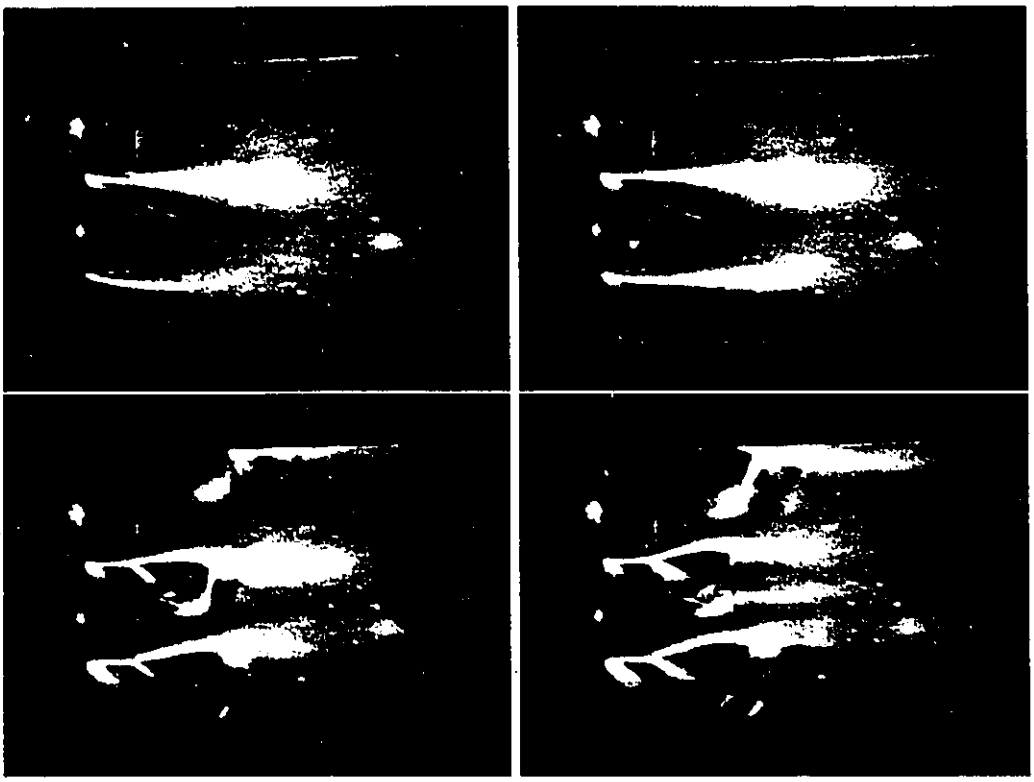

Plate 11: Schlieren images in the demonstration nozzle with square rods I (1). Top left: $M_{1d} = 0.46$; top right: $M_{1d} = 0.55$; bottom left: $M_{1d} = 0.68$; bottom right: $M_{1d} = 0.77$.

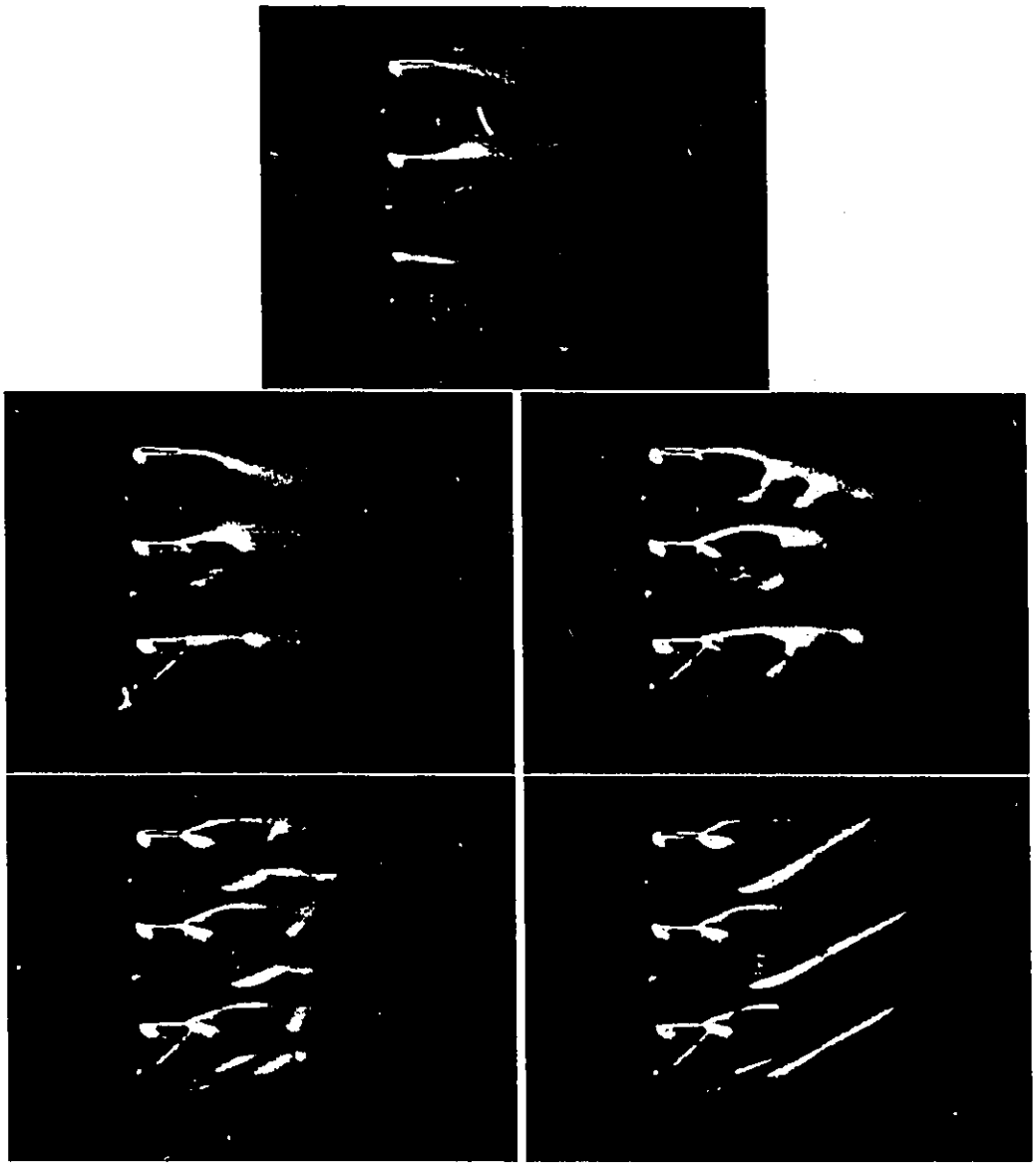

Plate 12: Schlieren images in the demonstration nozzle with square rods II (1). Top: $M_{1d} = 0.38$; middle left: $M_{1d} = 0.46$; middle right: $M_{1d} = 0.55$; bottom left: $M_{1d} = 0.68$; bottom right: $M_{1d} = 2.2$.

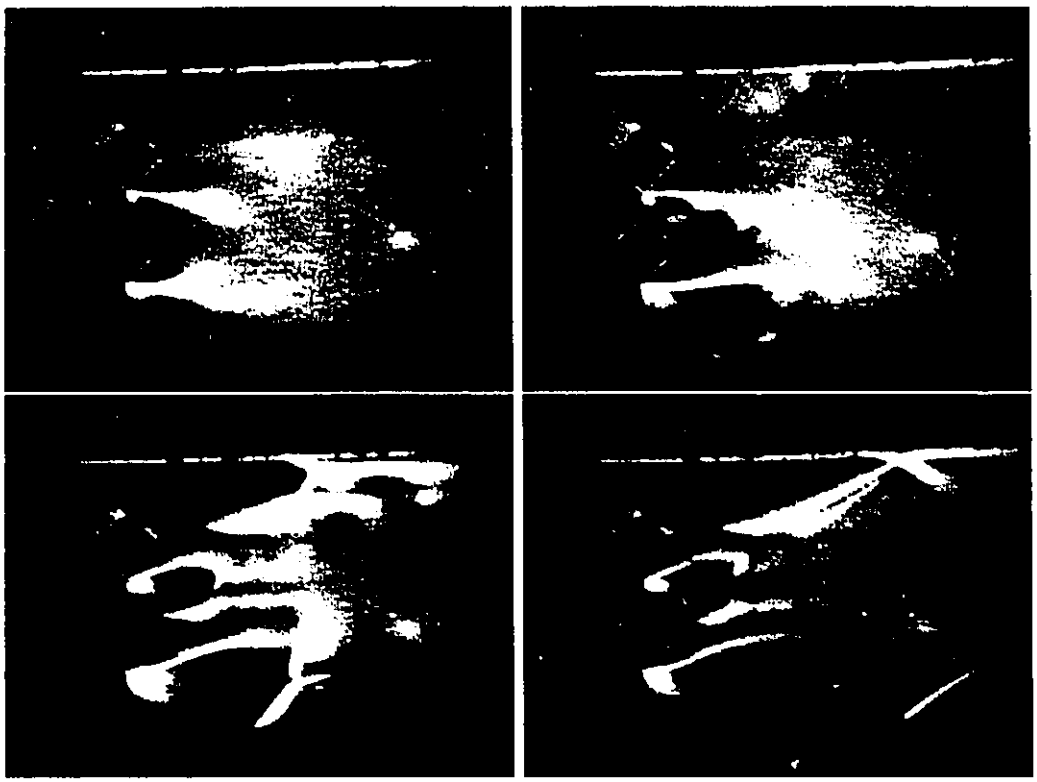

Plate 13: Schlieren images in the demonstration nozzle with diamond rods (1). Top left: $M_{1d} = 0.46$; top right: $M_{1d} = 0.55$; bottom left: $M_{1d} = 0.68$; bottom right: $M_{1d} = 2.2$.

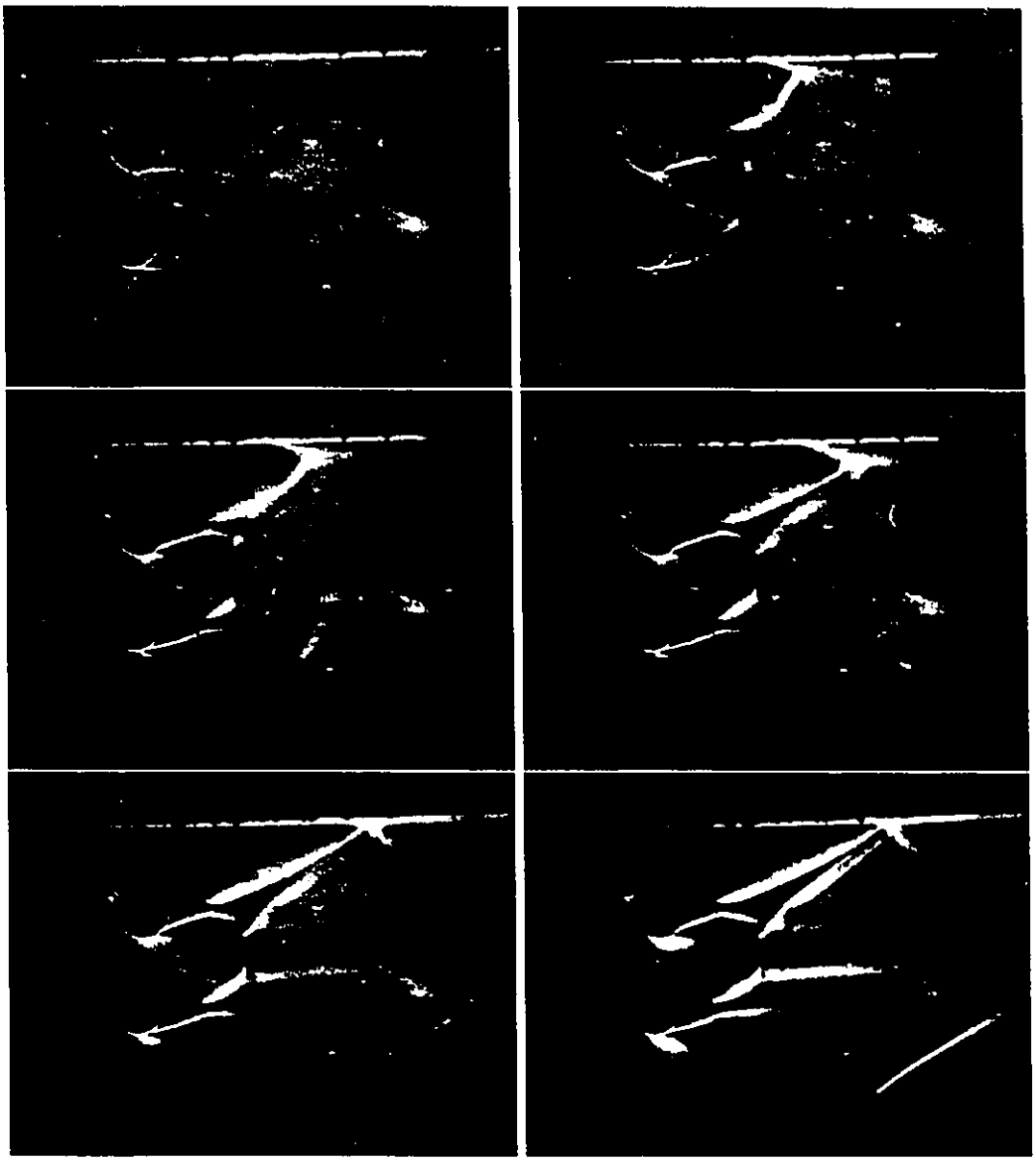

Plate 14: Schlieren images in the demonstration nozzle with round rods (2). The sequence of images shows the formation of oblique shocks by the rods, with the second throat wide open, as the pressure is increased.

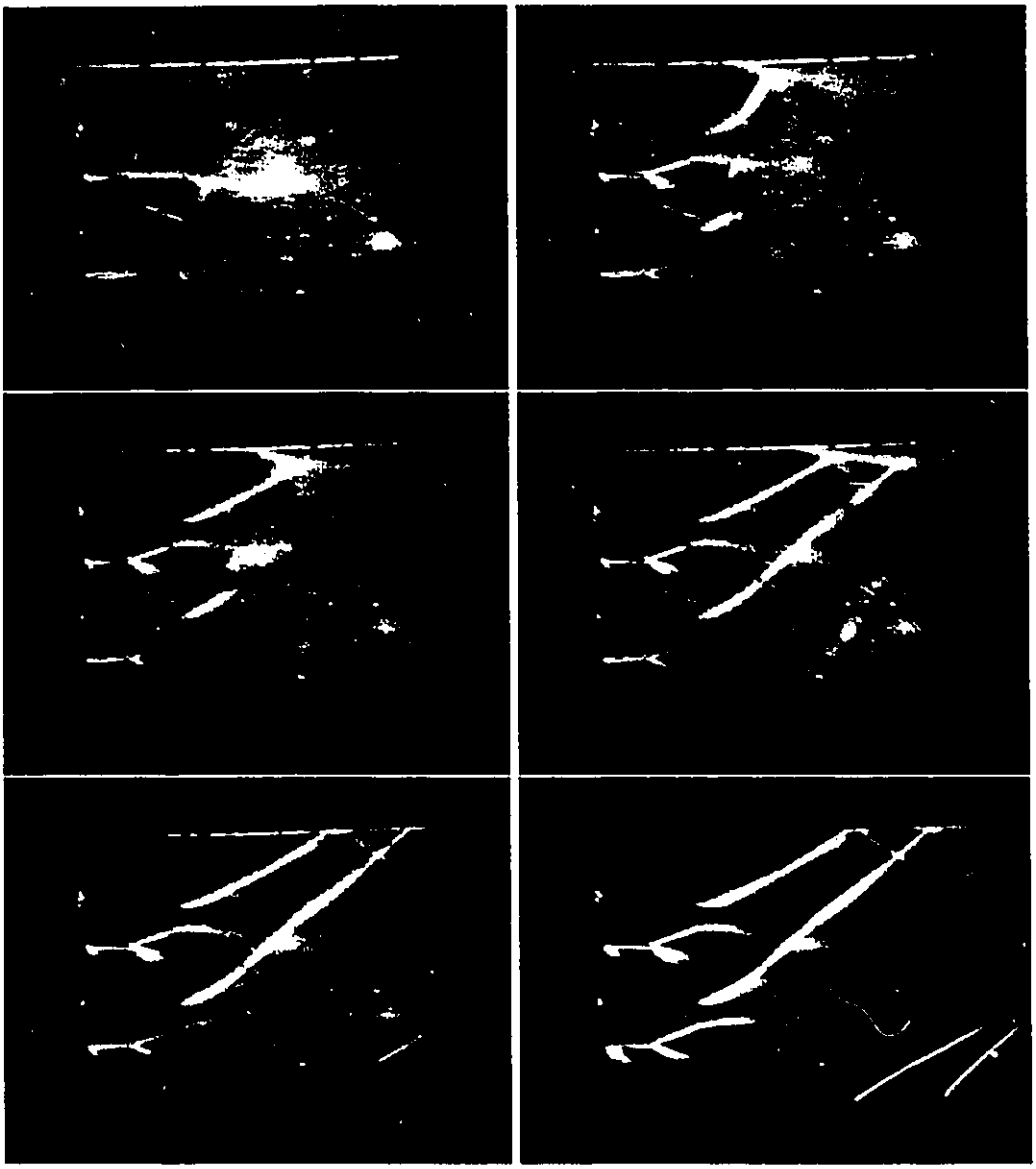

Plate 15: Schlieren images in the demonstration nozzle with square rods I (2). The sequence of images shows the formation of oblique shocks by the rods, with the second throat wide open, as the pressure is increased.

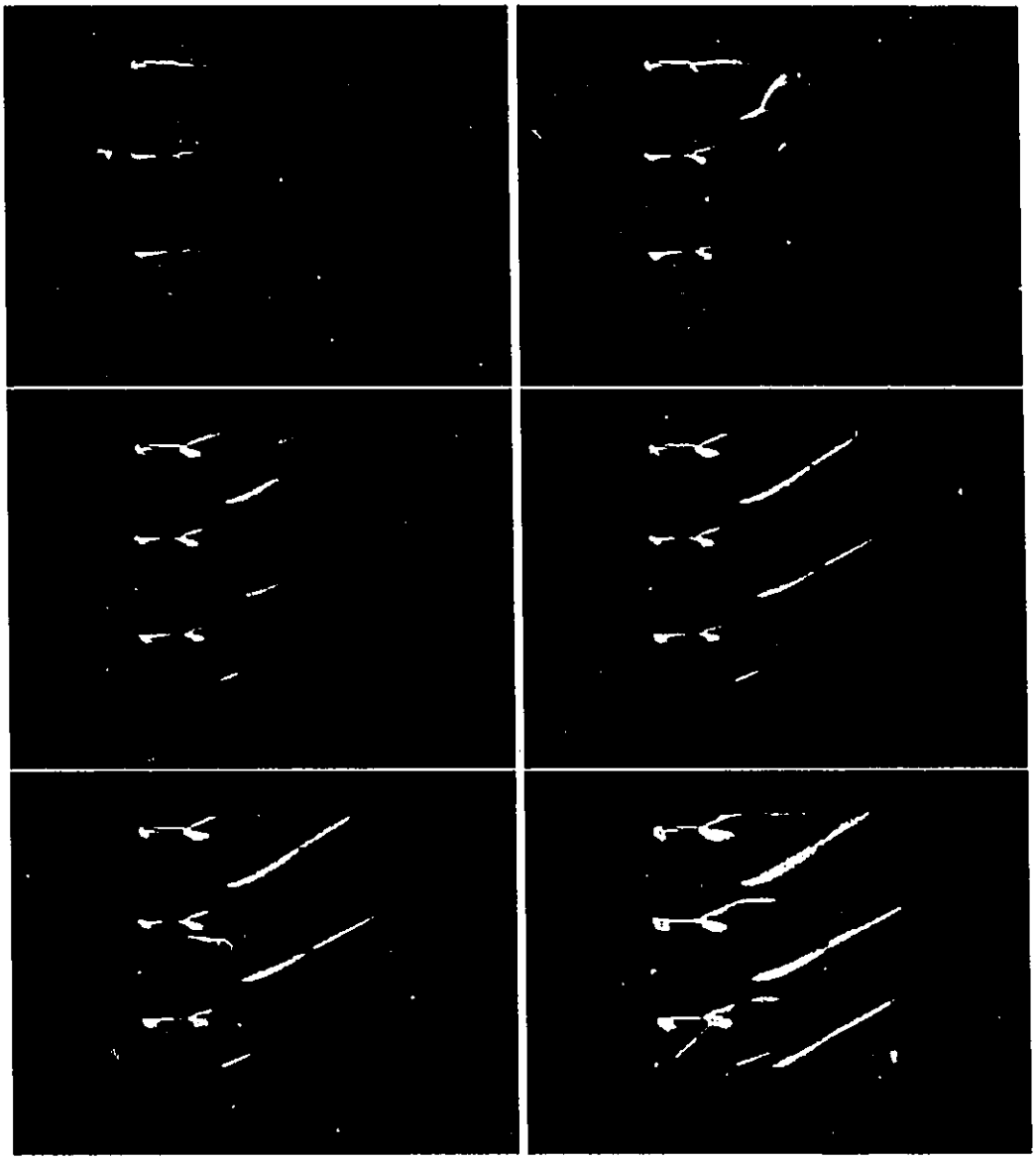

Plate 16: Schlieren images in the demonstration nozzle with square rods II (2). The sequence of images shows the formation of oblique shocks by the rods, with the second throat wide open, as the pressure is increased.

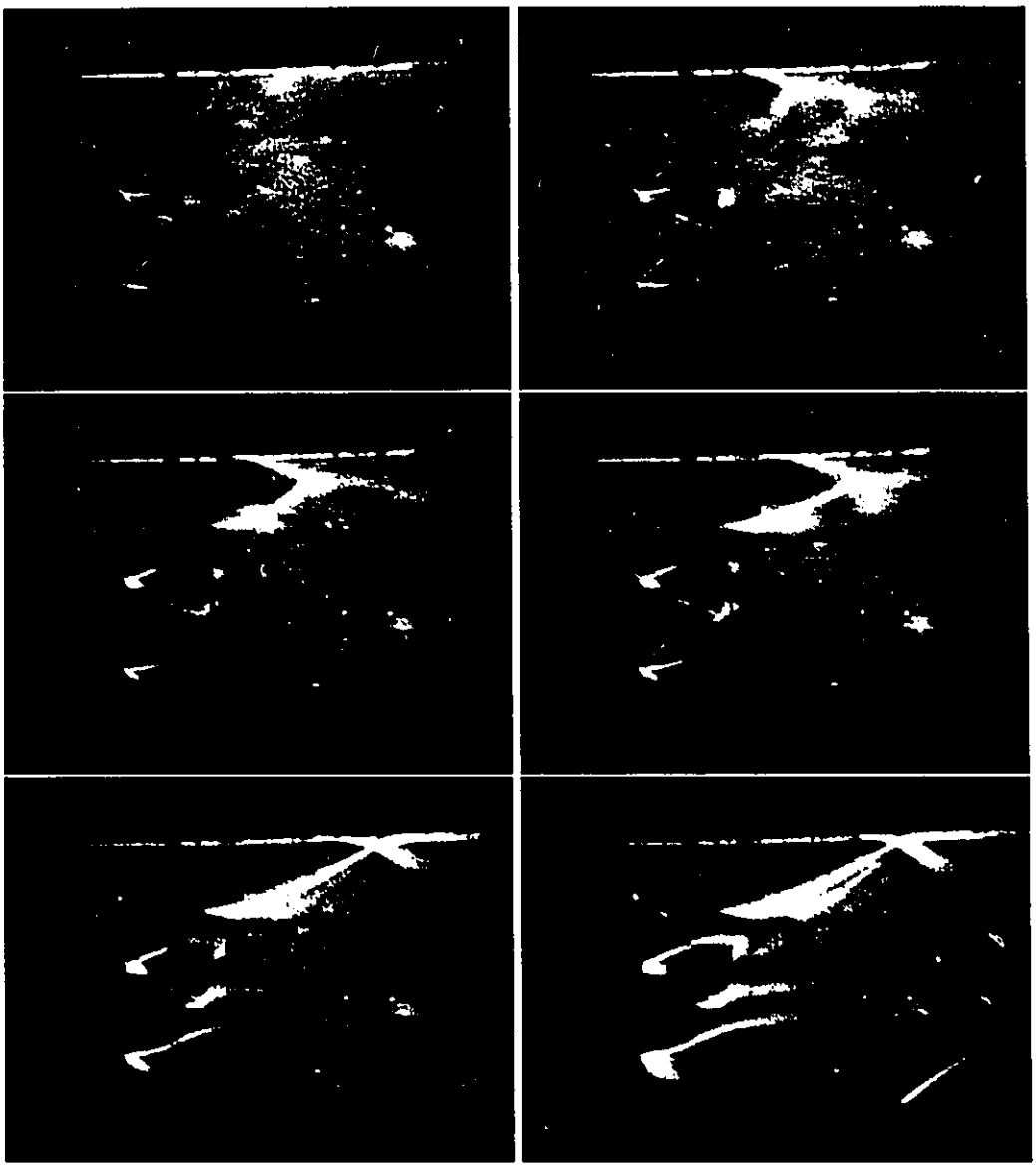

Plate 17: Schlieren images in the demonstration nozzle with diamond rods (2). The sequence of images shows the formation of oblique shocks by the rods, with the second throat wide open, as the pressure is increased.

Figures

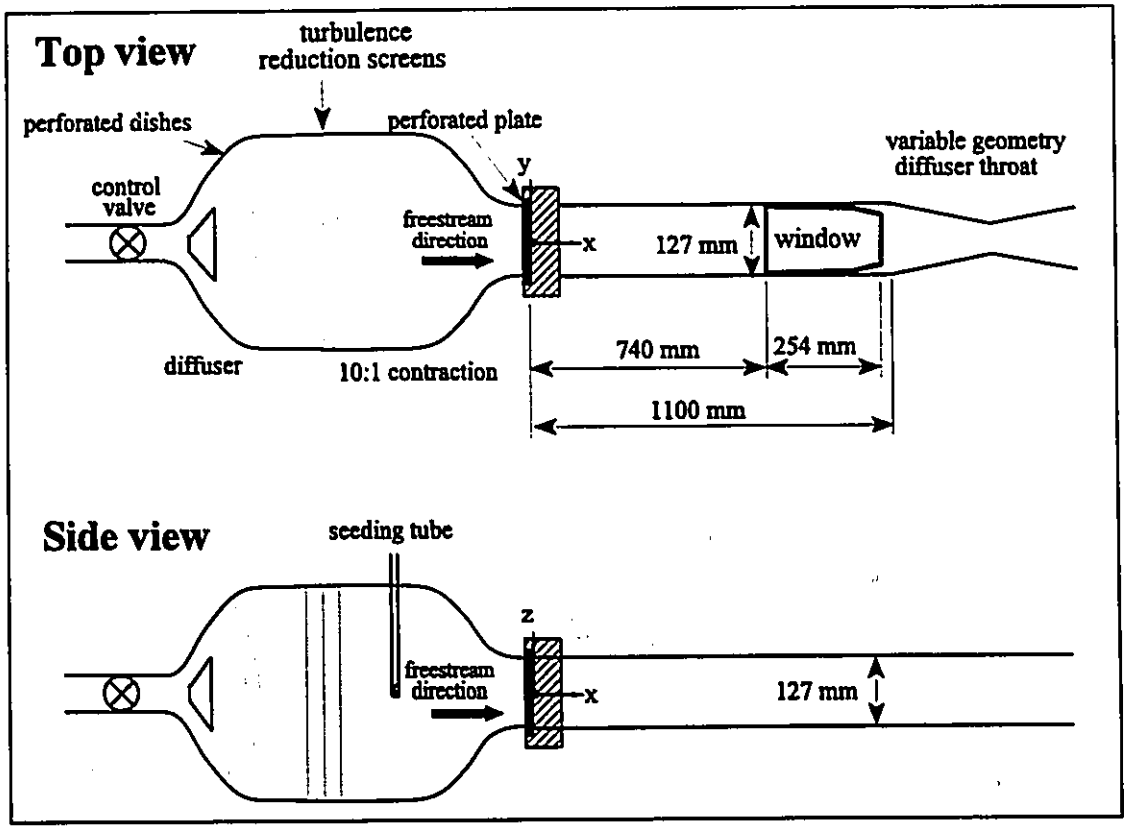

Figure 1: Schematic of the wind tunnel facility.

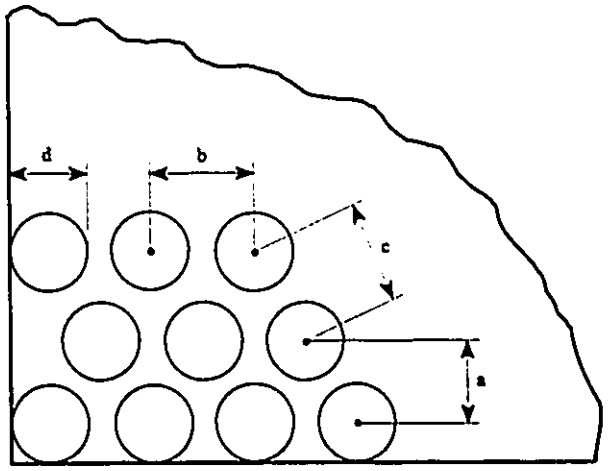

Figure 2: Schematic of a perforated plate.

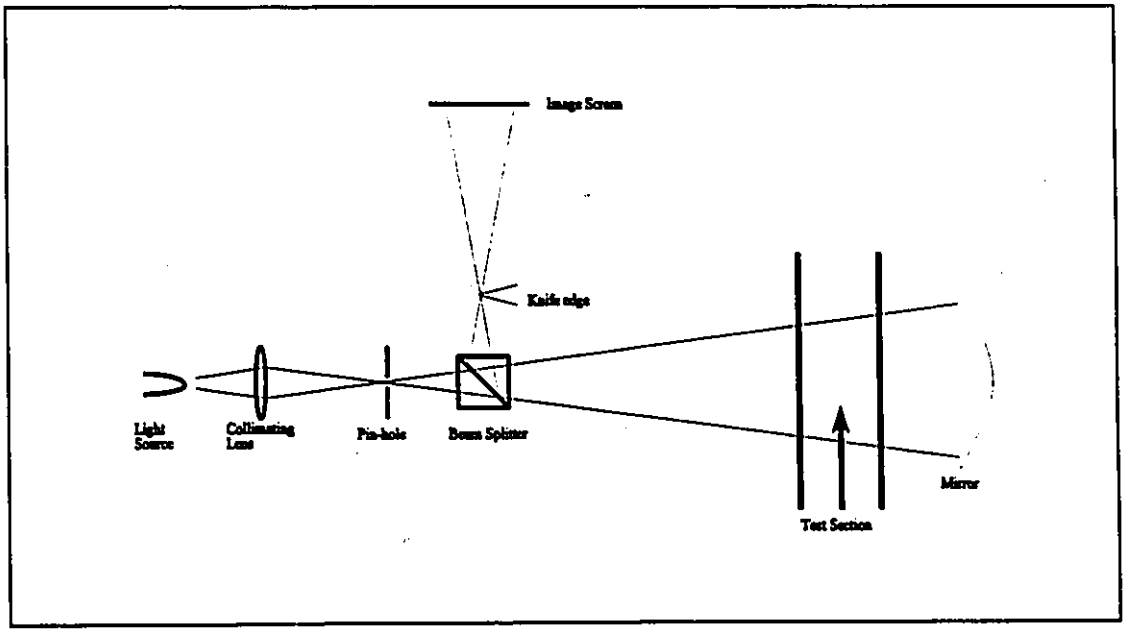

Figure 3: Schematic of the flow visualization system.

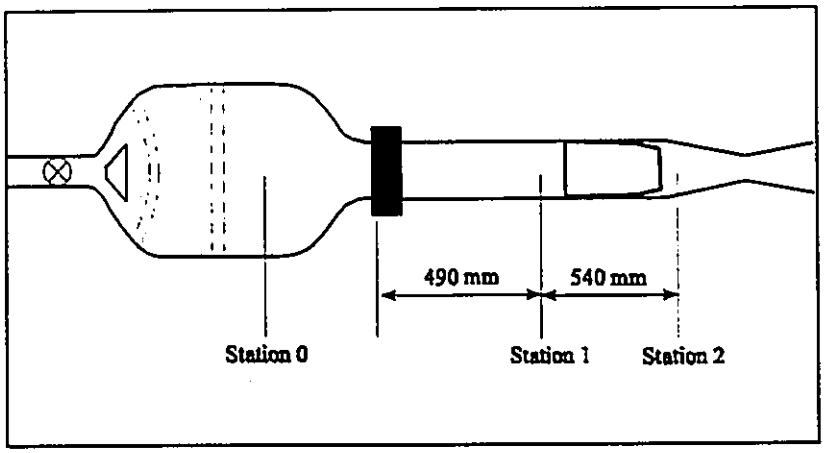

Figure 4: Locations of the wind tunnel measuring stations.

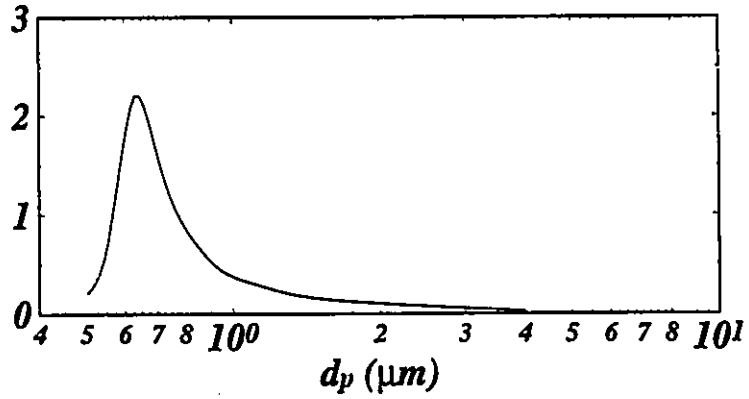

Figure 5: Distribution of particle sizes in polyethylene glycol aerosol. The abscissa represents the particle aerodynamic diameter.

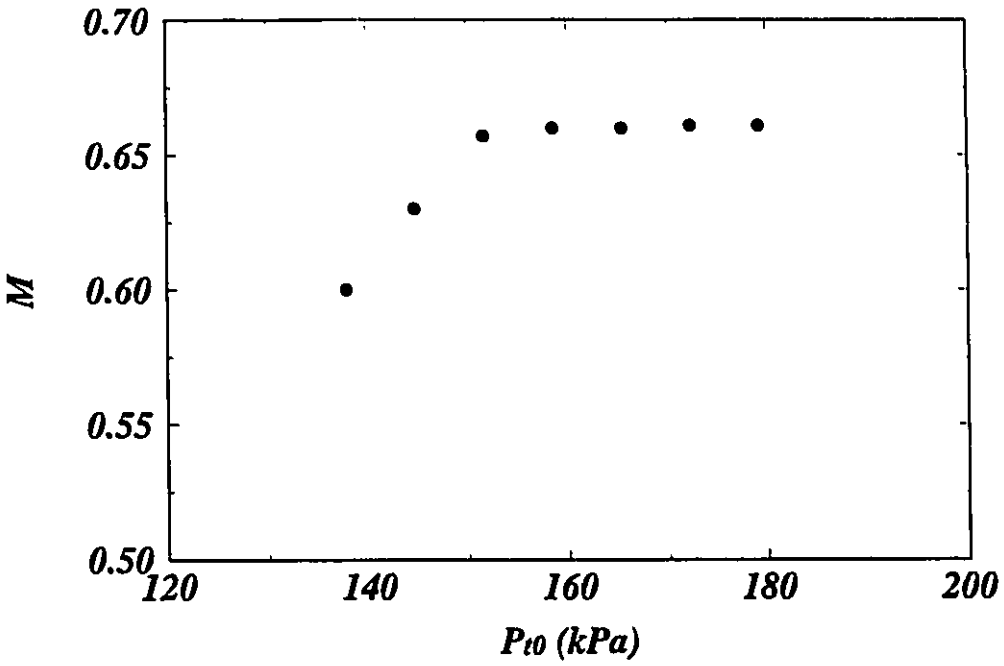

Figure 6: Typical wind tunnel characteristics in the moderate subsonic regime. $A_{dt}/A = 0.90$.

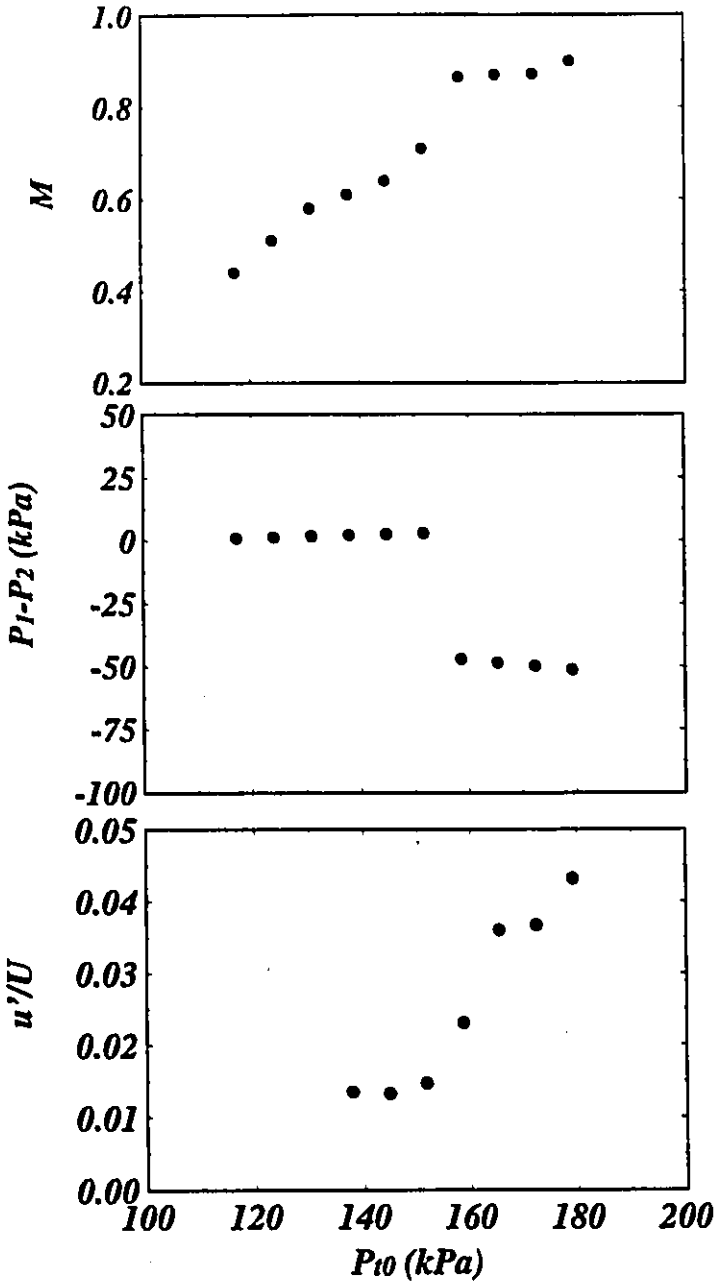

Figure 7: Typical wind tunnel characteristics to the high subsonic regime. $A_{dt}/A = 0.92$.

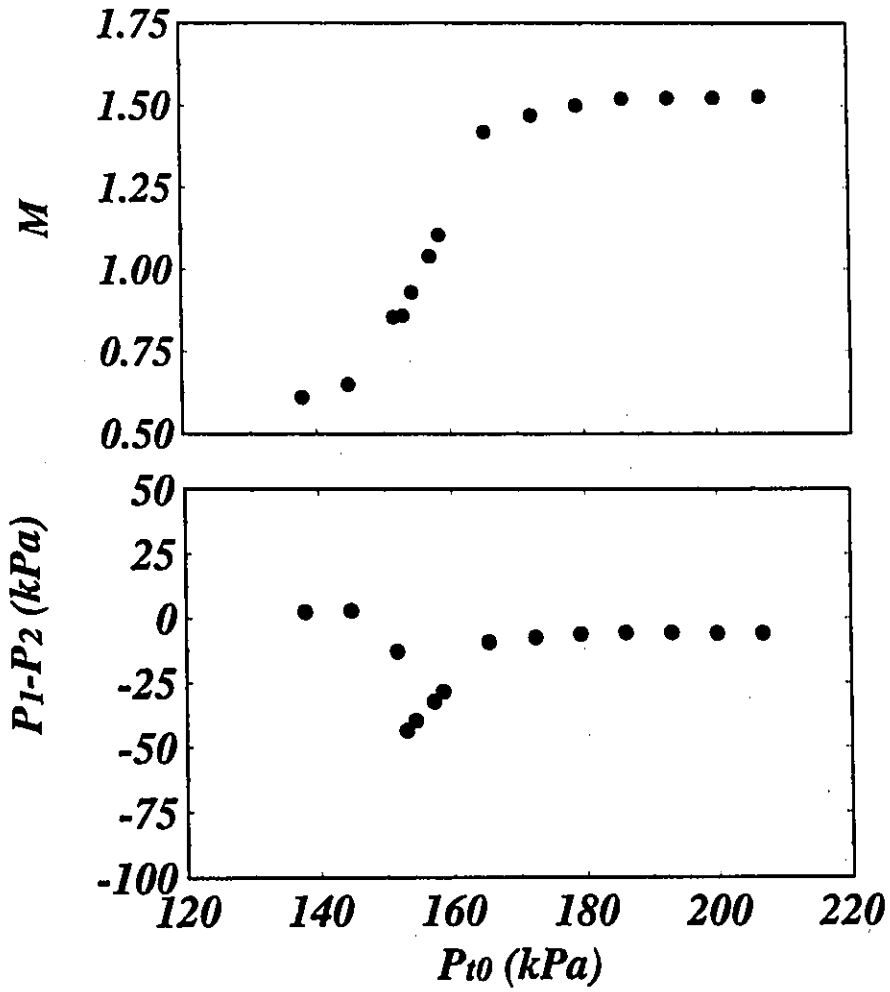

Figure 8: Typical wind tunnel characteristics to the supersonic regime. $A_{dt}/A = 0.98$.

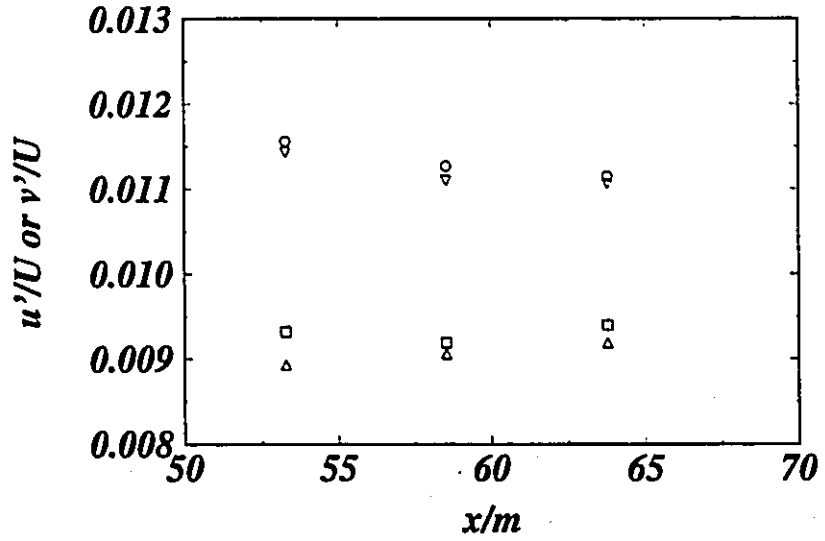

Figure 9: Background turbulence intensities, $M = 0.69$. $\square$ u'/U, $P_{t0} = 120$ kPa; $\circ$ v'/U, $P_{t0} = 120$ kPa; $\triangle$ u'/U, $P_{t0} = 165$ kPa; $\triangledown$ v'/U, $P_{t0} = 165$ kPa.

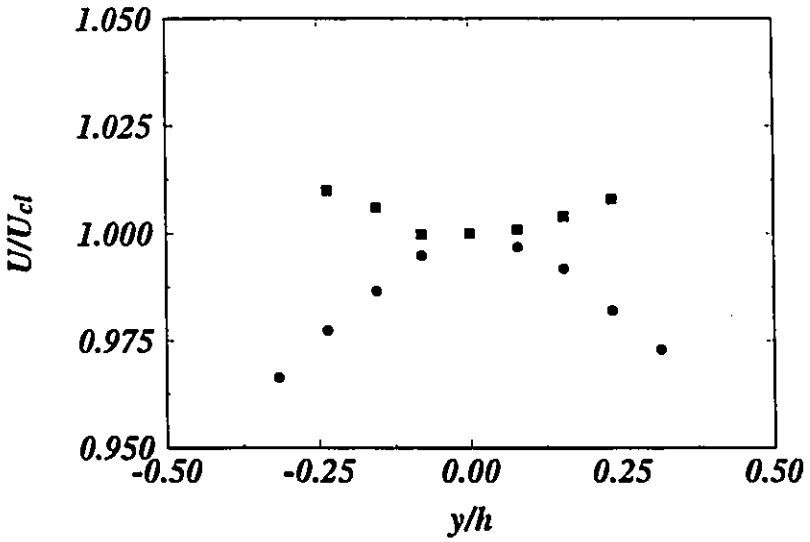

Figure 10: Transverse mean velocity profiles, y-traverse. ● $M = 0.16$, $U_{cl} = 55.4$ m/s; ■ $M = 0.67$, $U_{cl} = 221.8$ m/s.

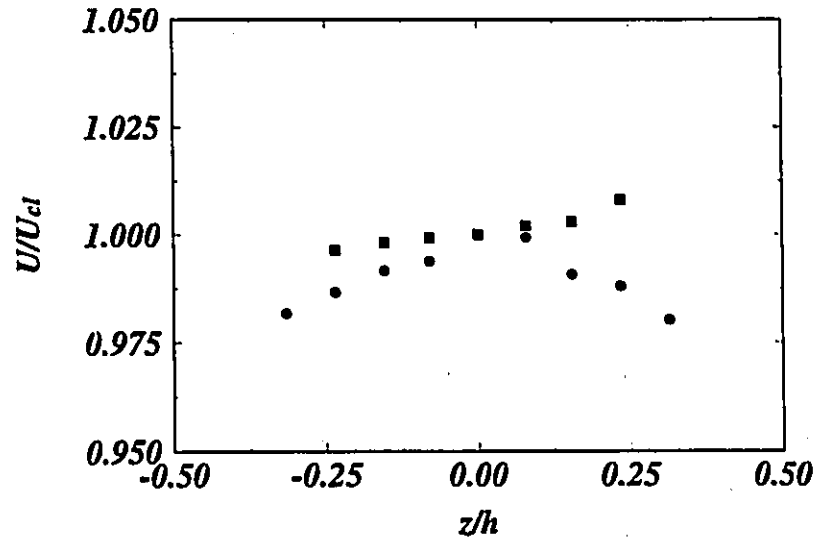

Figure 11: Transverse mean velocity profiles, z-traverse. ● $M = 0.16$, $U_{cl} = 55.4$ m/s; ■ $M = 0.67$, $U_{cl} = 222.1$ m/s.

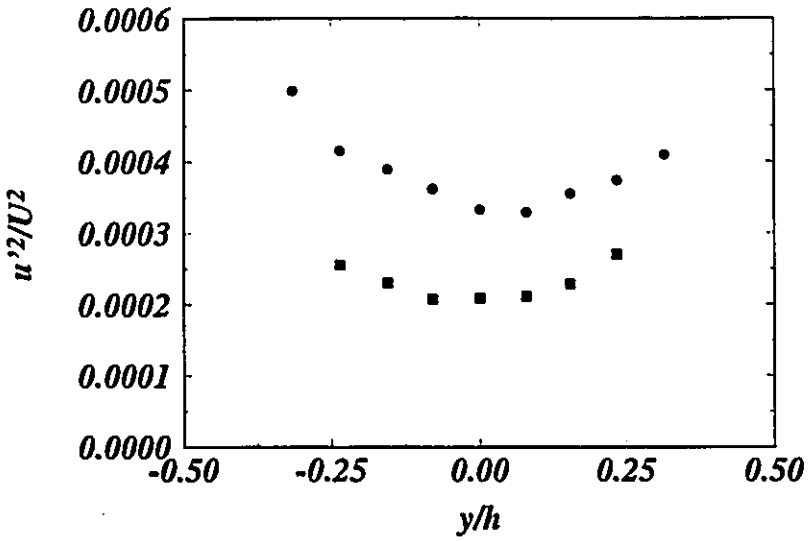

Figure 12: Streamwise velocity variances, y-traverse. ● $M = 0.16$; ■ $M = 0.67$.

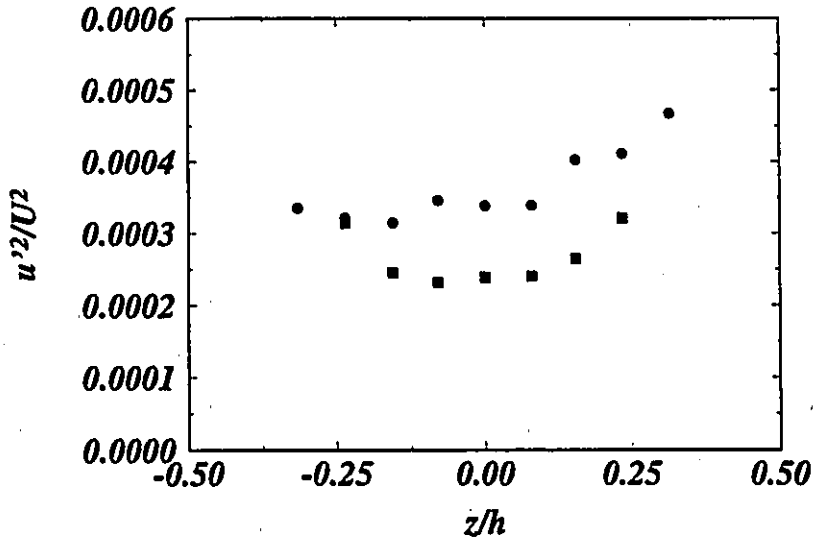

Figure 13: Streamwise velocity variances, z-traverse. ● $M = 0.16$; ■ $M = 0.67$.

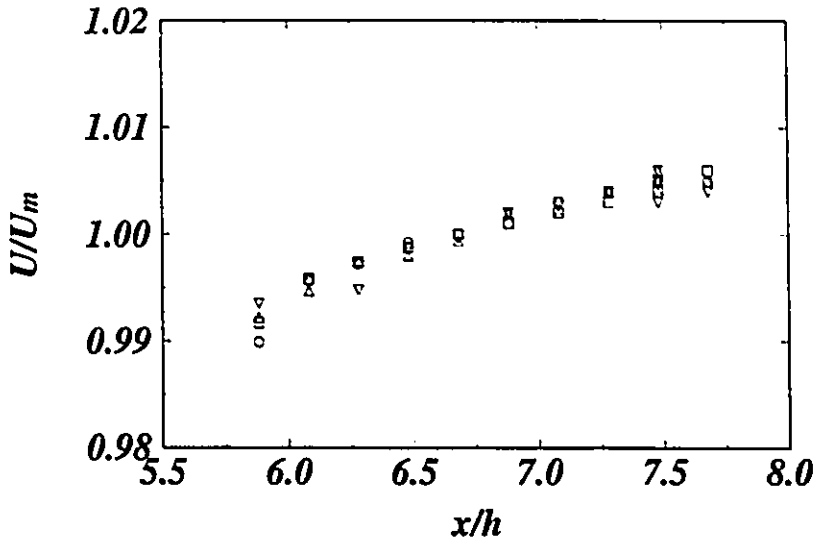

Figure 14: Mean velocity profiles for $M = 0.16$. □ MS1a ($U_m = 55.0$ m/s); ○ MS1b ($U_m = 55.7$ m/s); △ MS1c ($U_m = 55.6$ m/s); ▽ MS1d ($U_m = 55.4$ m/s).

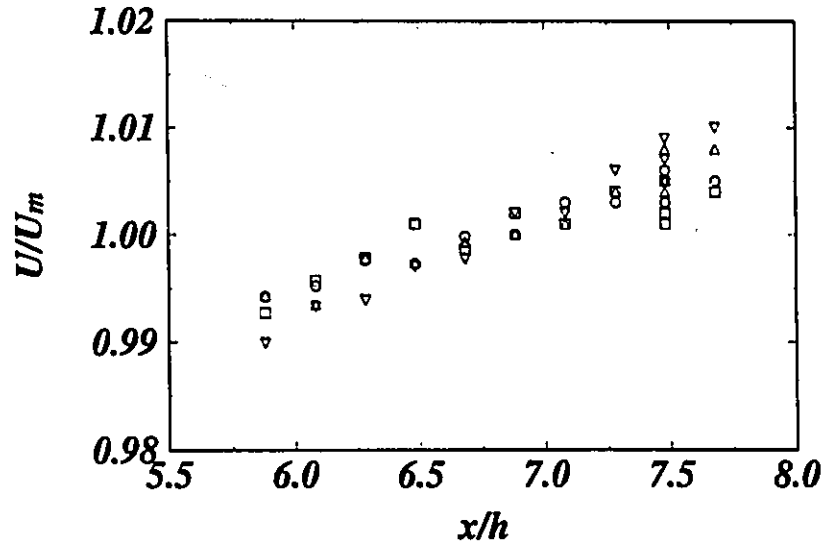

Figure 15: Mean velocity profiles for $0.24 \leq M \leq 0.58$. □ MS2 ($M = 0.24$, $U_m = 81.1$ m/s); ○ MS3 ($M = 0.37$, $U_m = 126.2$ m/s); △ MS4 ($M = 0.46$, $U_m = 156.8$ m/s); ▽ MS6 ($M = 0.58$, $U_m = 194.6$ m/s).

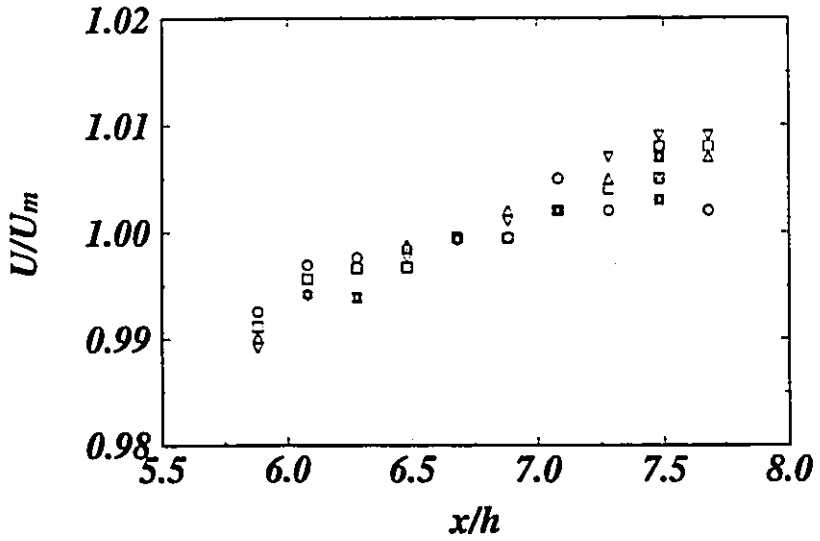

Figure 16: Mean velocity profiles for $M = 0.52$. □ MS5a ($U_m = 174.8$ m/s); ○ MS5b ($U_m = 175.3$ m/s); △ MS5c ($U_m = 178.0$ m/s); ▽ MS5d ($U_m = 177.7$ m/s).

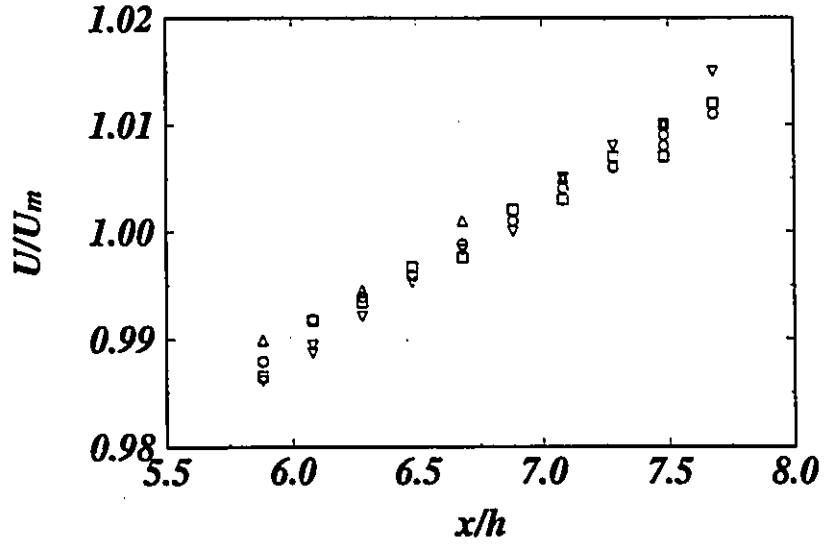

Figure 17: Mean velocity profiles for $0.64 \leq M \leq 0.68$. □ MS7a, $M = 0.64$ ($U_m = 213.6$ m/s); ○ MS7b ($M = 0.64$, $U_m = 214.5$ m/s); △ MS8a ($M = 0.68$, $U_m = 226.3$ m/s); ▽ MS8b ($M = 0.68$, $U_m = 227.5$ m/s).

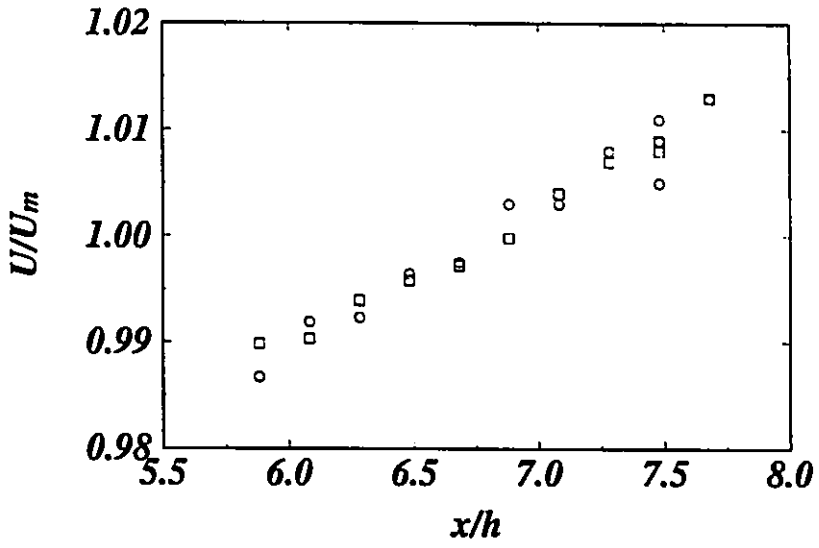

Figure 18: Mean velocity profiles for anomalous cases, $M = 0.66$. □ MS9a (U_m = 222.3 m/s); ○ MS9b ($U_m = 214.5$ m/s).

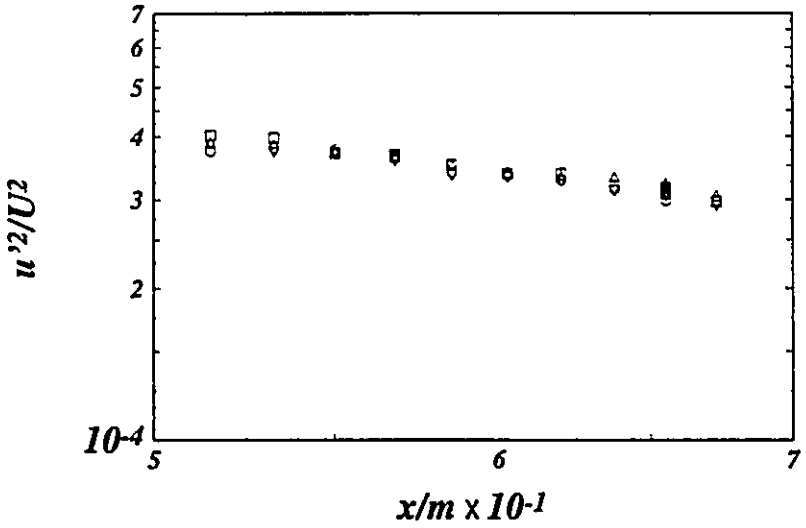

Figure 19: Streamwise velocity variances profiles for $M = 0.16$. □ MS1a; ○ MS1b; △ MS1c; ▽ MS1d.

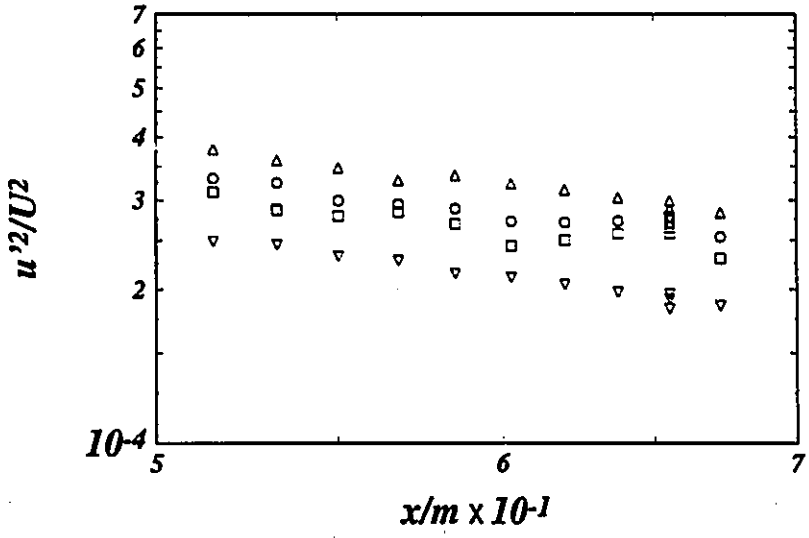

Figure 20: Streamwise velocity variance profiles for $0.24 \leq M \leq 0.58$. □ MS2 ($M = 0.24$); ○ MS3 ($M = 0.37$); △ MS4 ($M = 0.46$); ▽ MS6 ($M = 0.58$).

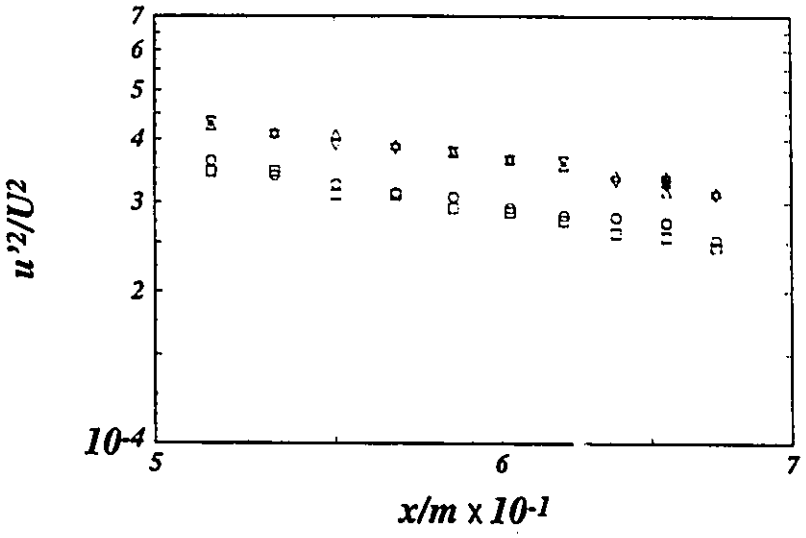

Figure 21: Streamwise velocity variance profiles for $M = 0.52$. □ MS5a (160 mm lens); ○ MS5b (160 mm lens); △ MS5c (243 mm lens); ▽ MS5d (243 mm lens).

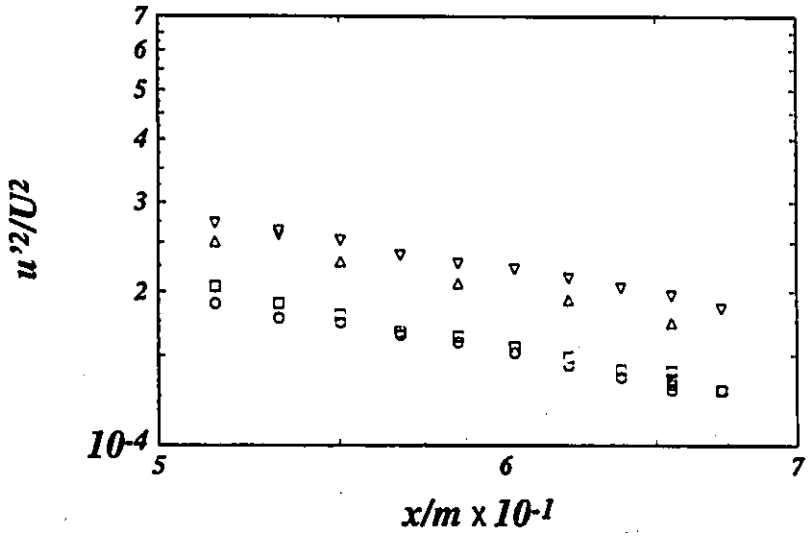

Figure 22: Streamwise velocity variance profiles for $0.64 \leq M \leq 0.68$. □ MS7a ($M = 0.64$, 160 mm lens); ○ MS7b ($M = 0.64$, 160 mm lens); △ MS8a ($M = 0.68$, 243 mm lens); ▽ MS8b ($M = 0.68$, 243 mm lens).

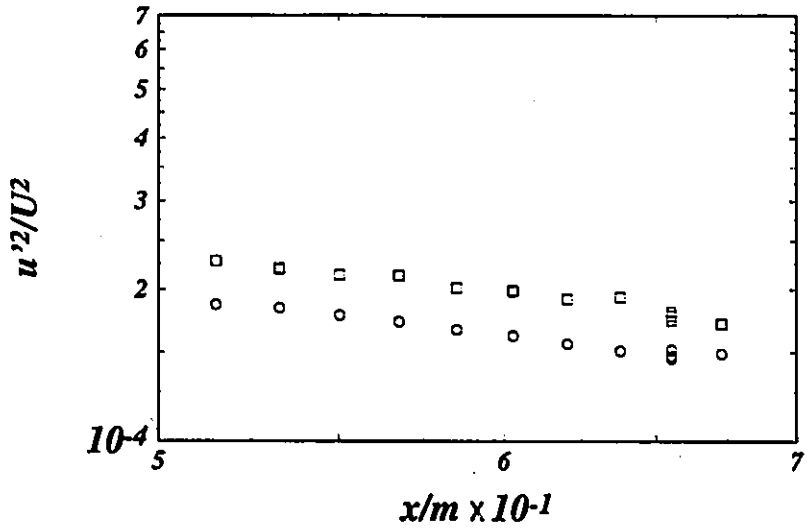

Figure 23: Streamwise velocity variance profiles for anomalous cases, $M = 0.66$. □ MS9a; O MS9b.

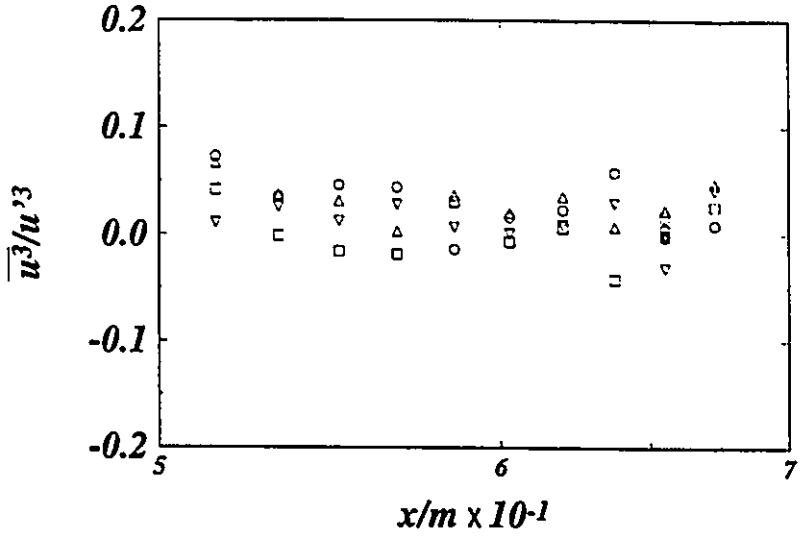

Figure 24: Skewness factors for $M = 0.16$. □ MS1a; ○ MS1b; △ MS1c; ▽ MS1d.

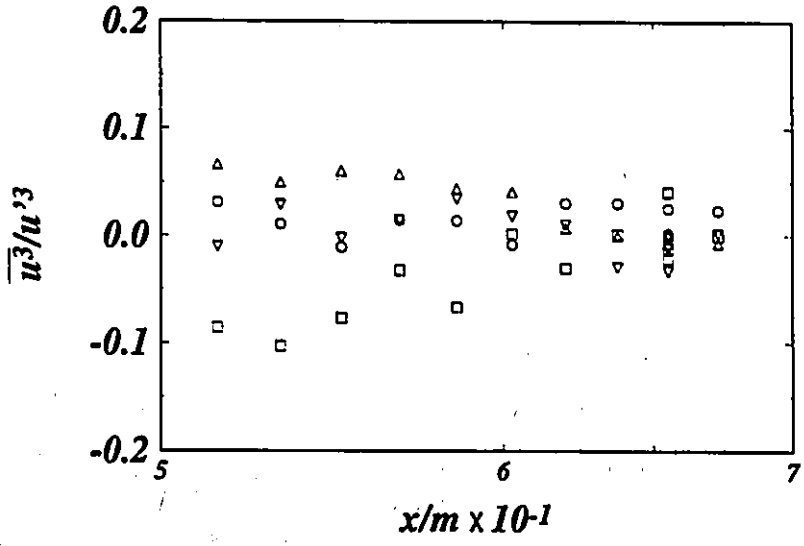

Figure 25: Skewness factors for $0.24 \leq M \leq 0.58$. □ MS2 ($M = 0.24$); ○ MS3 ($M = 0.37$); △ MS4 ($M = 0.46$); ▽ MS6 ($M = 0.58$).

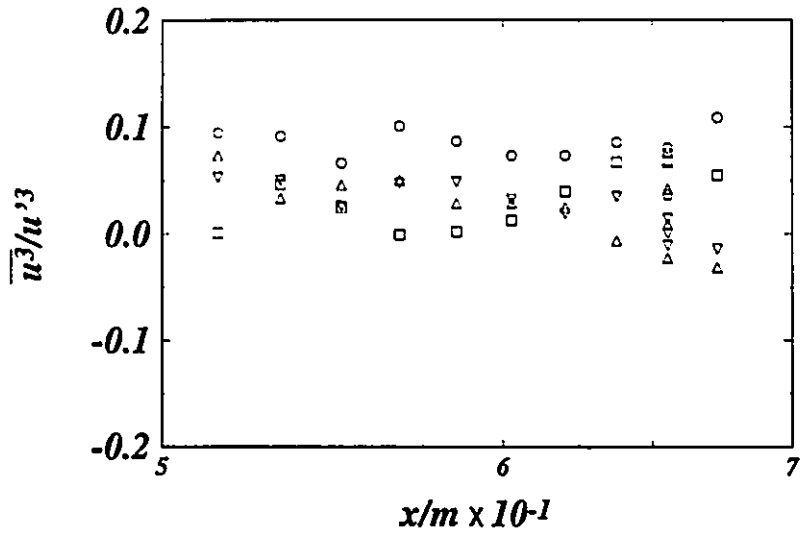

Figure 26: Skewness factors for $M = 0.52$. □ MS5a; ○ MS5b; △ MS5c; ▽ MS5d.

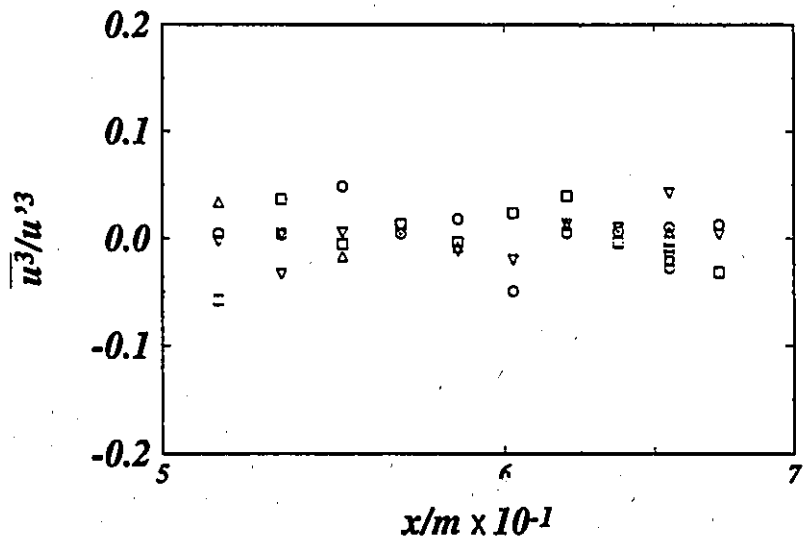

Figure 27: Skewness factors for $0.64 \leq M \leq 0.68$. □ MS7a ($M = 0.64$); ○ MS7b ($M = 0.64$); △ MS8a ($M = 0.68$); ▽ MS8b ($M = 0.68$).

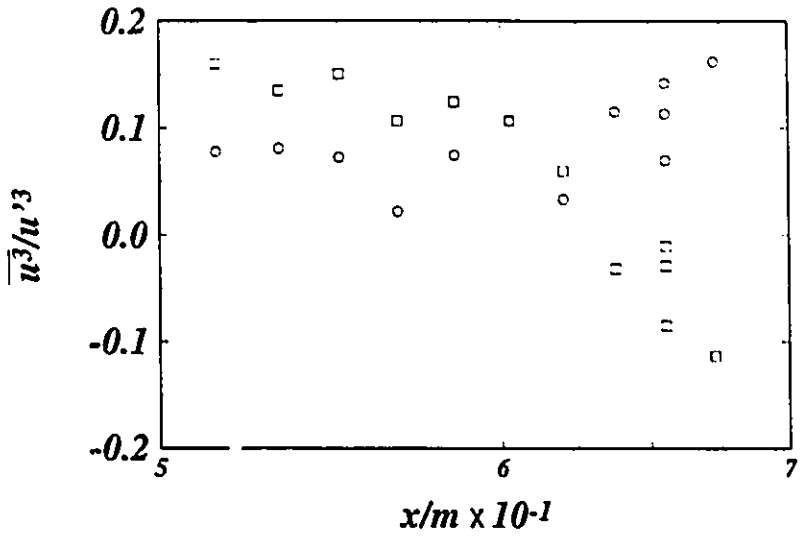

Figure 28: Skewness factors for anomalous cases, $M = 0.66$. □ MS9a; ○ MS9b.

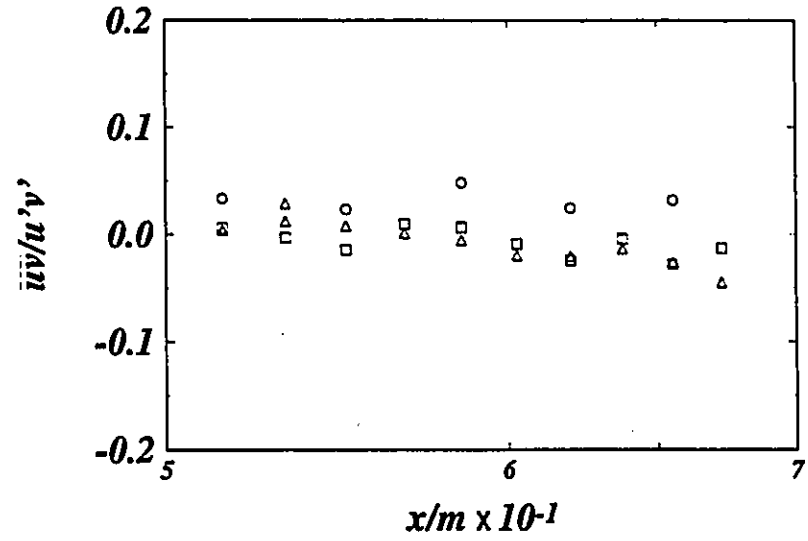

Figure 29: Turbulent shear stress correlation coefficients in the moderate subsonic regime. □ MS1a ($M = 0.16$); ○ MS8a ($M = 0.68$); △ MS8b ($M = 0.68$).

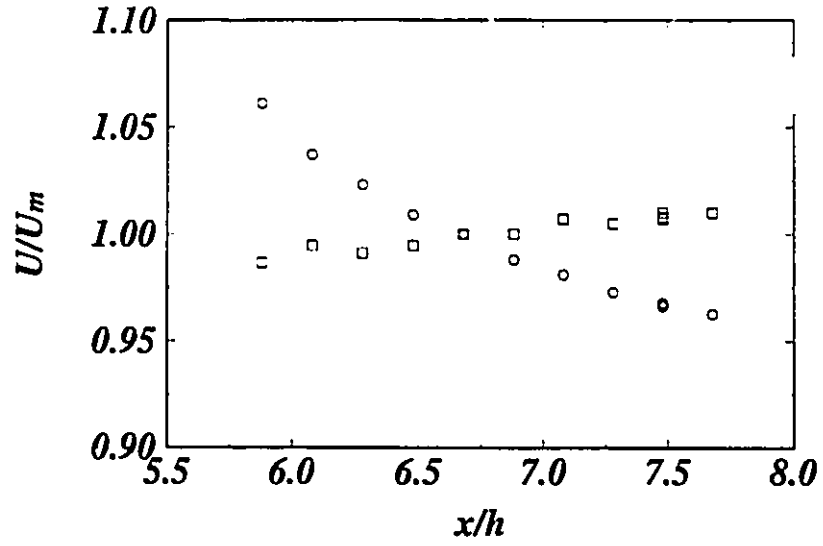

Figure 30: Mean velocity profiles in the high subsonic regime. □ HS1 ($M = 0.69$, $U_m = 227.4$ m/s); ○ HS2 ($M = 0.92$, $U_m = 294.3$ m/s).

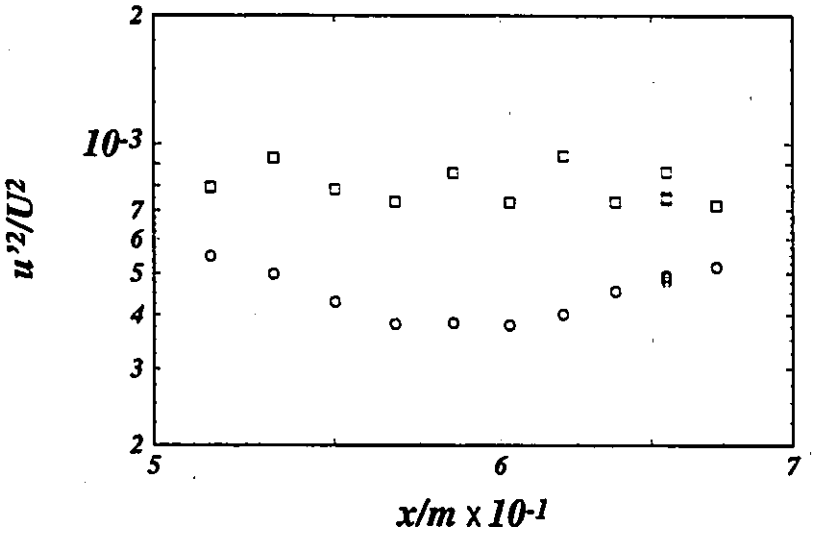

Figure 31: Velocity variances in the high subsonic regime. □ HS1 ($M = 0.69$); ○ HS2 ($M = 0.92$).

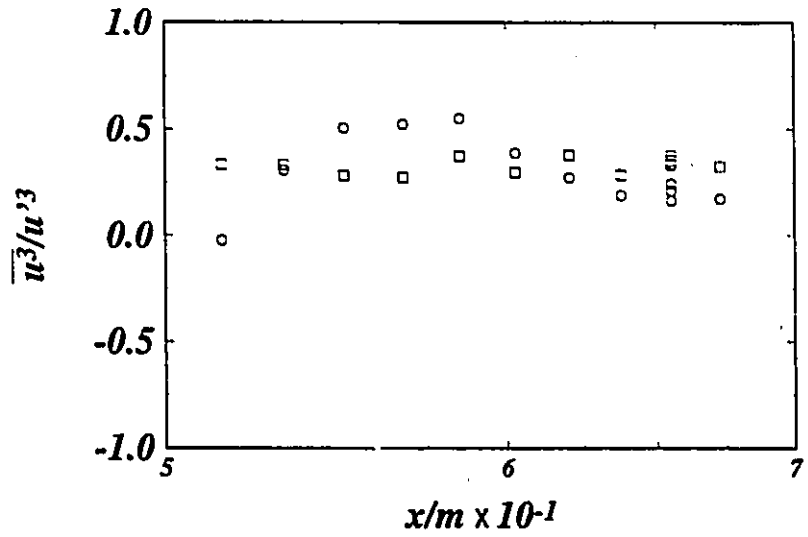

Figure 32: Skewness factors in the high subsonic regime. □ HS1 ($M = 0.69$); ○ HS2 ($M = 0.92$).

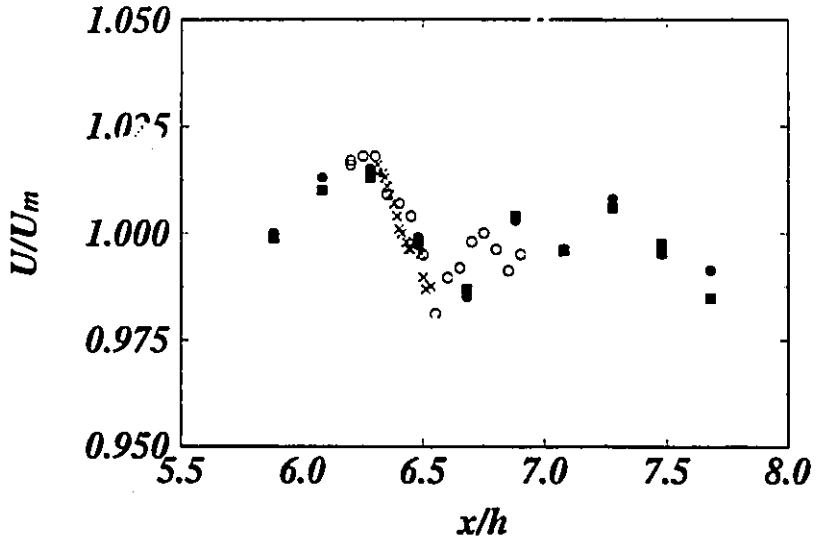

Figure 33: Mean velocity profiles in the supersonic regime, MHP, $M = 1.55$, $U_m = 447.8$ m/s. ■ SP1a ($\Delta x_t/m = 1.75$ (1)); ● SP1b ($\Delta x_t/m = 1.75$ (2)); ○ SP1c ($\Delta x_t/m = 0.438$); × SP1d ($\Delta x_t/m = 0.110$, $y/h = -0.035$).

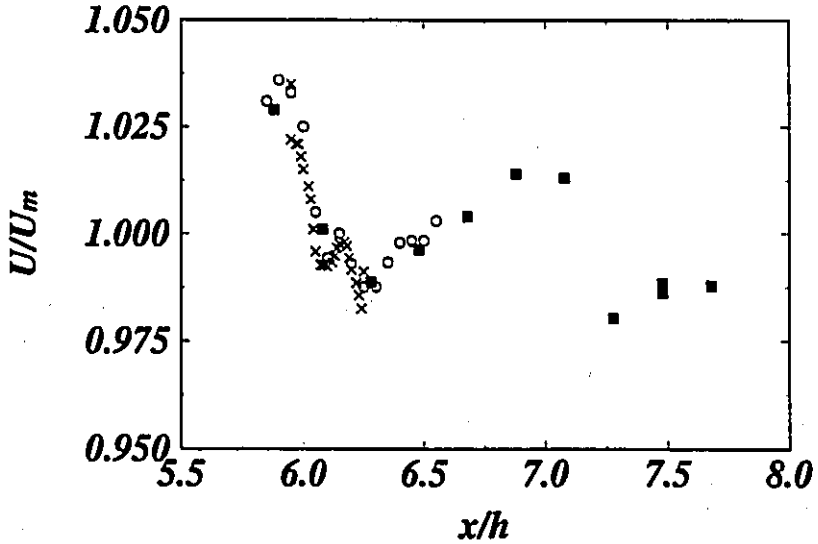

Figure 34: Mean velocity profiles in the supersonic regime, LHP, $M = 1.57$, $U_m = 446.0$ m/s. ■ SP2a ($\Delta x_t/m = 1.38$); ○ SP2b ($\Delta x_t/m = 0.345$); × SP2c ($\Delta x_t/m = 0.086$, $y/h = -0.051$).

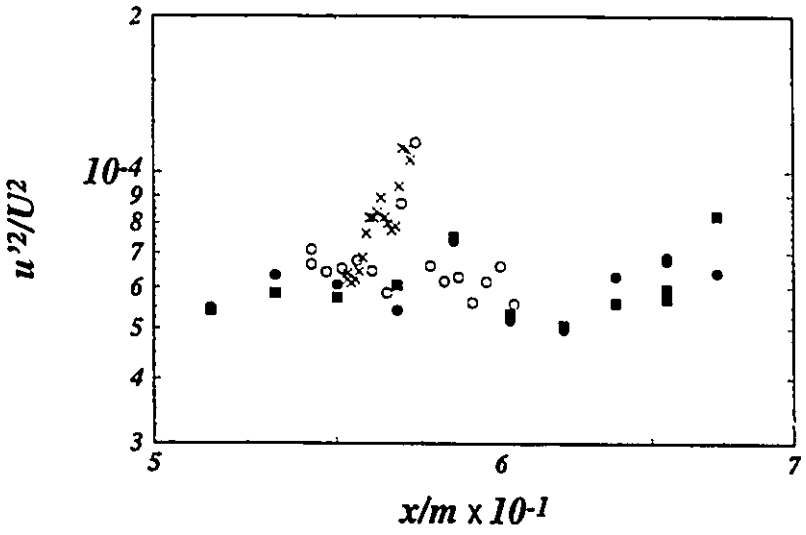

Figure 35: Streamwise velocity variance profiles in the supersonic regime, MHP, $M = 1.55$. ■ SP1a ($\Delta x_t/m = 1.75$ (1)); ● SP1b ($\Delta x_t/m = 1.75$ (2)); ○ SP1c ($\Delta x_t/m = 0.438$); × SP1d ($\Delta x_t/m = 0.110$, $y/h = -0.035$).

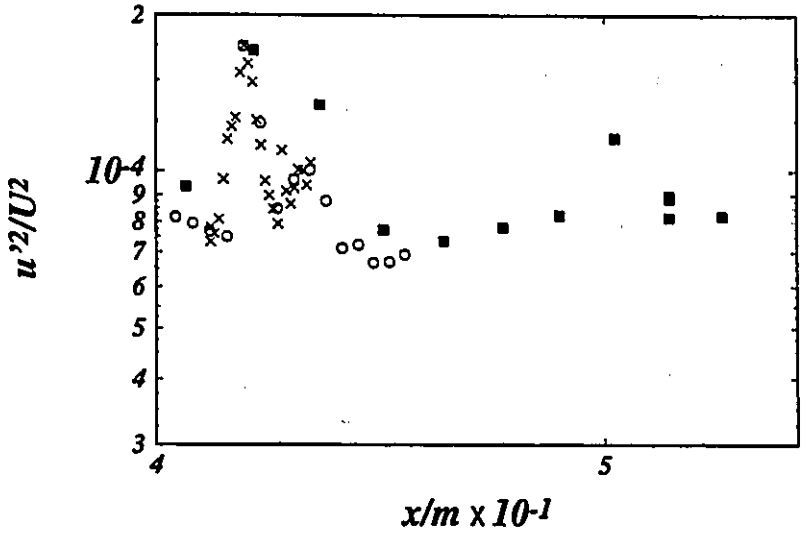

Figure 36: Streamwise velocity variance profiles in the supersonic regime, LHP, $M = 1.57$. ■ SP2a ($\Delta x_t/m = 1.38$); ○ SP2b ($\Delta x_t/m = 0.345$); × SP2c ($\Delta x_t/m = 0.086$, $y/h = -0.051$).

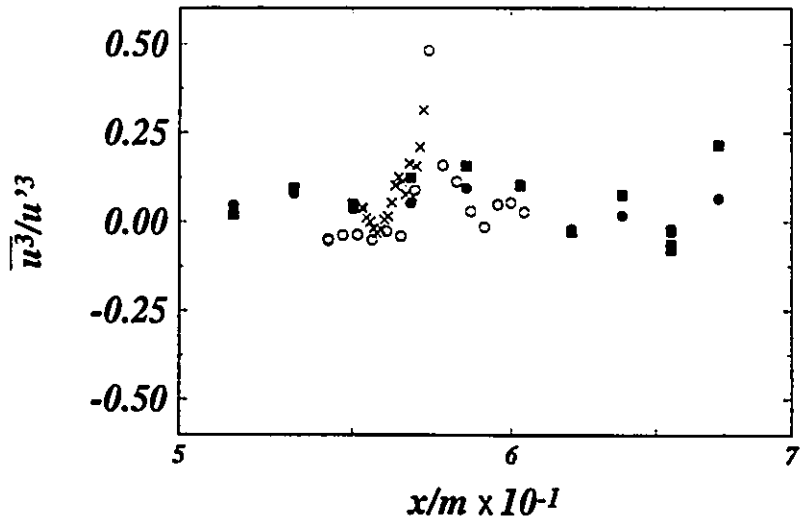

Figure 37: Skewness factors in the supersonic regime, MHP, $M = 1.55$. ■ SP1a ($\Delta x_t/m = 1.75$ (1)); ● SP1b ($\Delta x_t/m = 1.75$ (2)); ○ SP1c ($\Delta x_t/m = 0.438$); × SP1d ($\Delta x_t/m = 0.110$, $y/h = -0.035$).

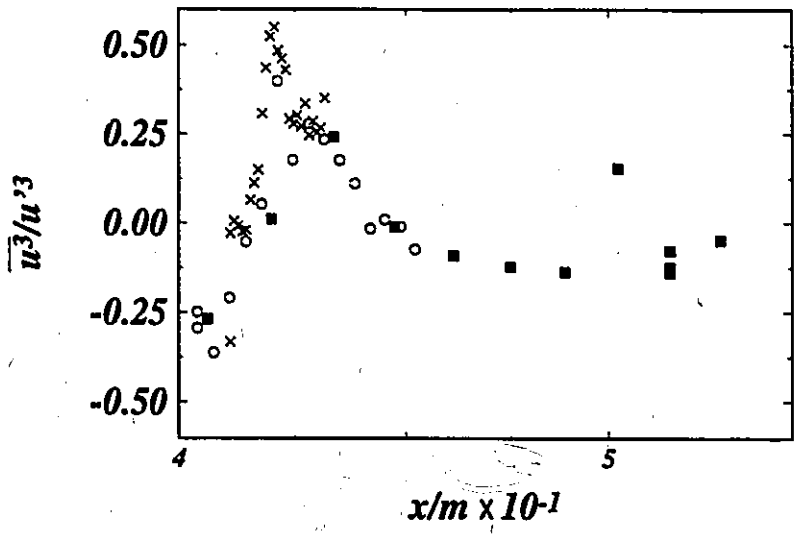

Figure 38: Skewness factors in the supersonic regime, LHP, $M = 1.57$. ■ SP2a ($\Delta x_t/m = 1.38$); ○ SP2b ($\Delta x_t/m = 0.345$); × SP2c ($\Delta x_t/m = 0.086$, $y/h = -0.051$).

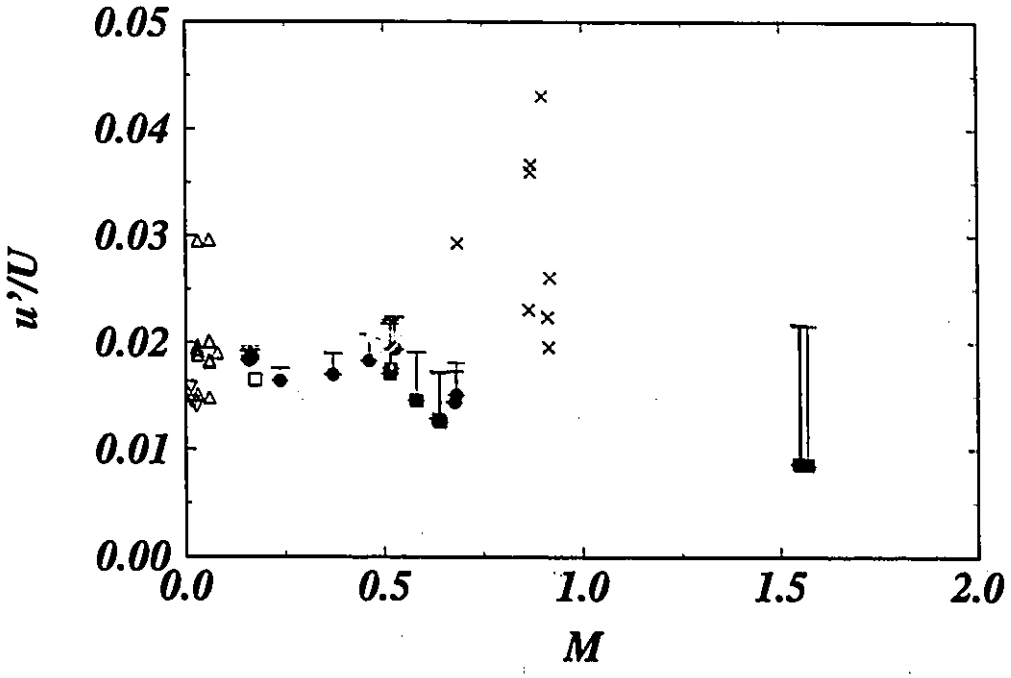

Figure 39: Turbulence intensities at $x/m = 58.5$. ● Steady flow, 160 mm lens; ■ Stationary flow, 243 mm lens; × Non-stationary flow (high subsonic regime); △ Comte-Bellot and Corrsin (1966); ▽ Mohamed and LaRue (1990); □ Kistler and Vrebalovich (1966). The error bars indicate the maximum uncertainty.

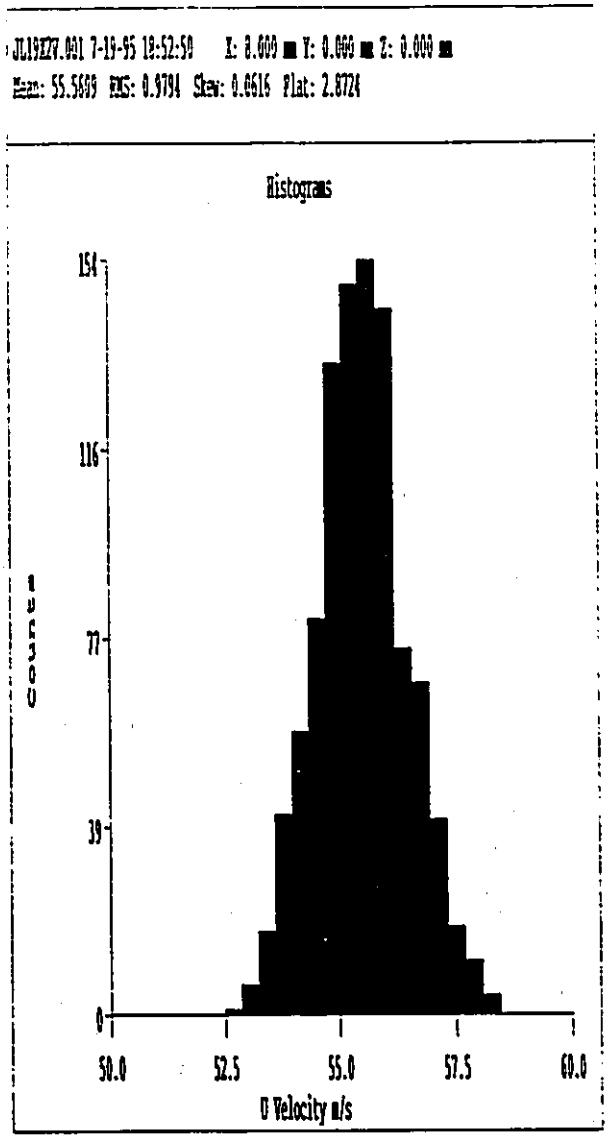

Figure 40: A typical velocity histogram, taken from MS1d.

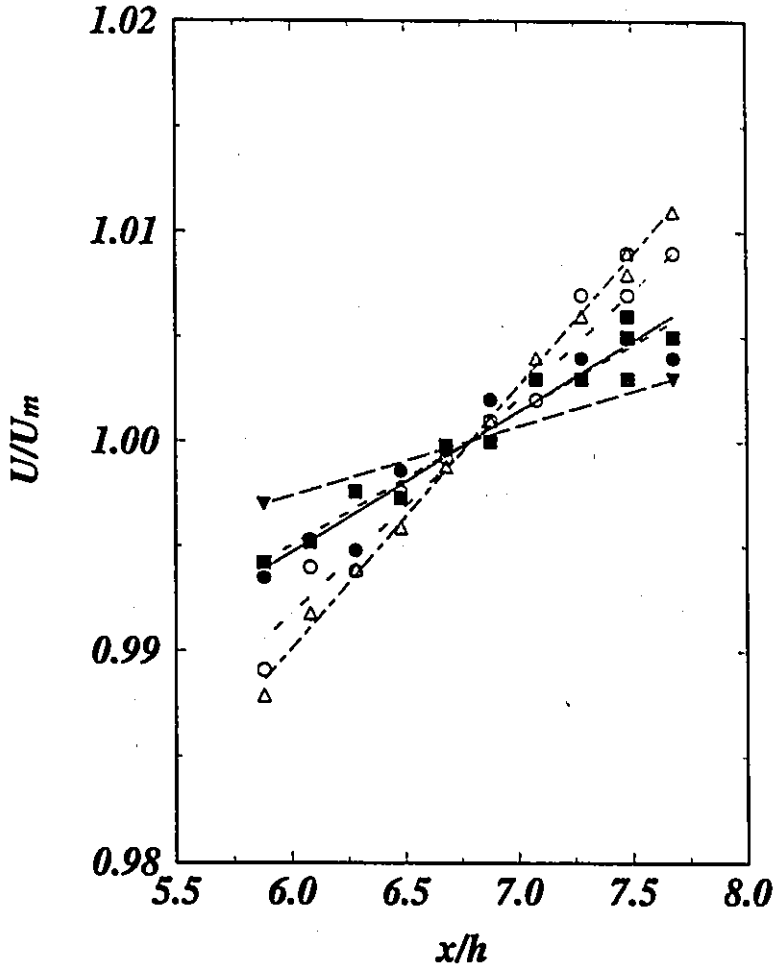

Figure 41: Typical mean velocities in the moderate subsonic regime. ● MS1d (M = 0.16, U_m = 55 m/s); ■ MS3 (M = 0.37, U_m = 126 m/s); ○ MS5d (M = 0.52, U_m = 178 m/s); △ MS8b (M = 0.68, U_m = 227.5 m/s); ▼ flat plate boundary layer growth, M = 0.16.

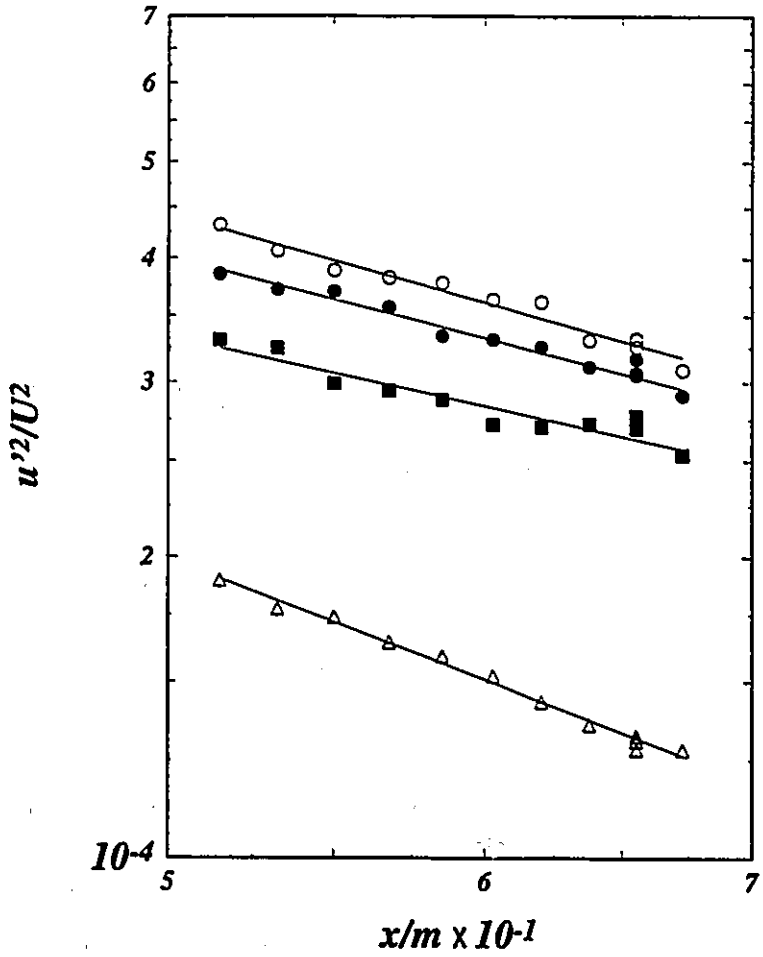

Figure 42: Typical streamwise velocity variance profiles in the moderate subsonic regime. ● MS1d ($M = 0.16$); ■ MS3 ($M = 0.37$); ○ MS5d ($M = 0.52$); △ MS8b ($M = 0.68$).

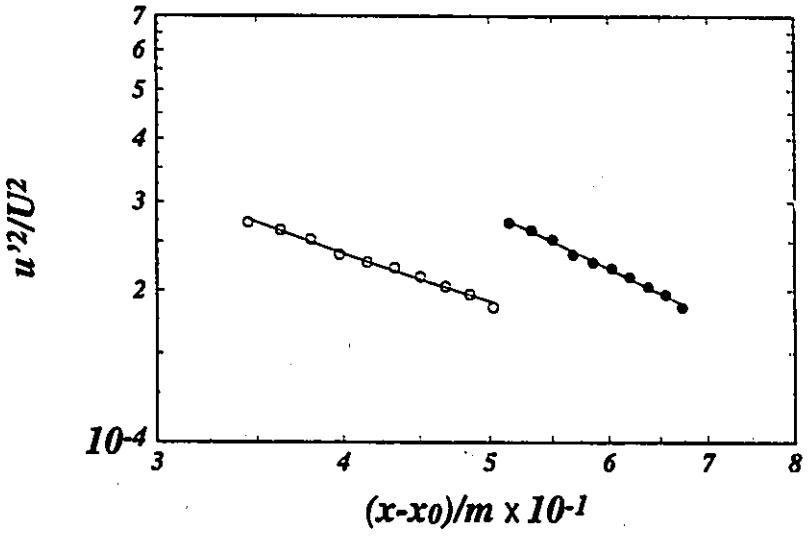

Figure 43: Two potential decay laws for MS8b. ● $x_0/m = 0$; ○ $x_0/m = 30$.

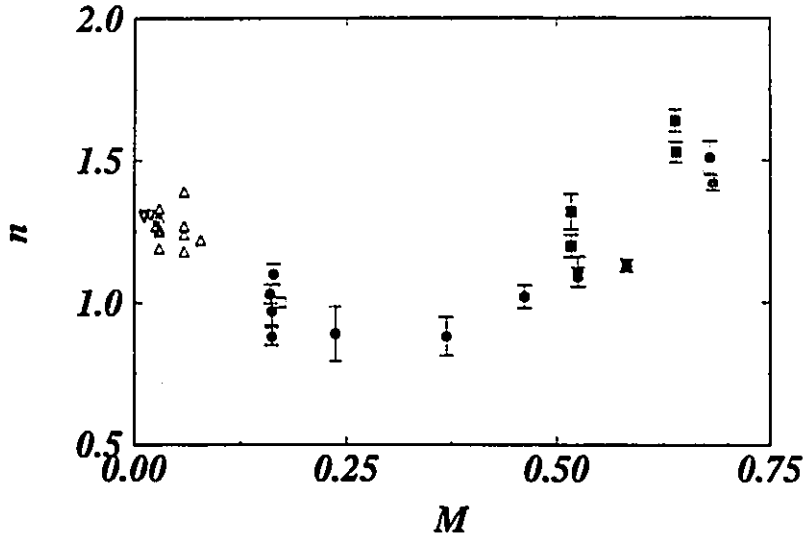

Figure 44: Decay exponents in the moderate subsonic regime, assuming $x_0/m = 0$ for the present results. Error bars correspond to 90% confidence intervals. ● Present results, 160 mm lens; ■ Present results, 243 mm lens; △ Comte-Bellot and Corrsin (1966); ▽ Mohamed and LaRue (1990); □ Kistler and Vrebalovich (1966).

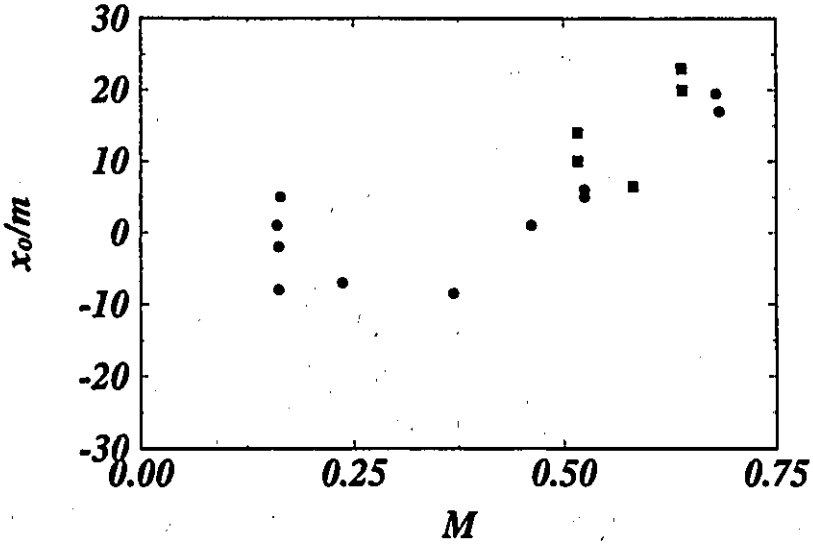

Figure 45: Effective origins in the moderate subsonic regime, assuming $n = 1$. ● 160 mm lens; ■ 243 mm lens.

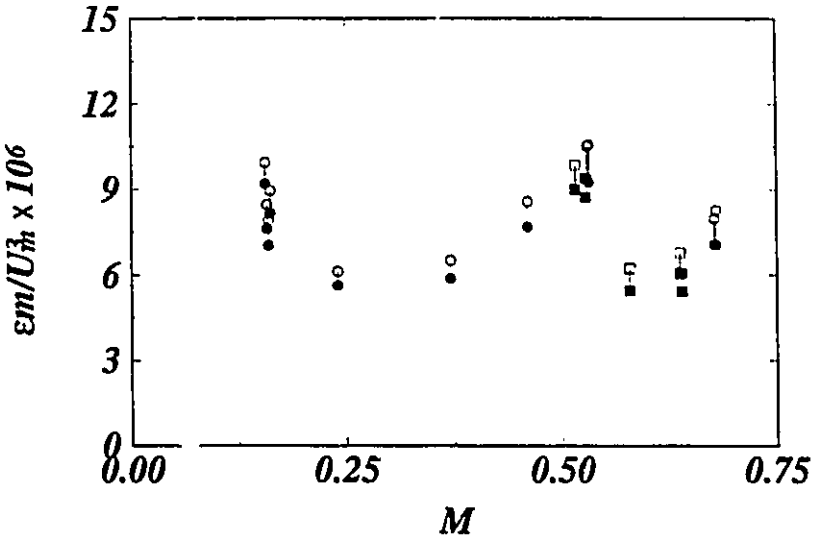

Figure 46: Dissipation rates at $x/m = 58.5$ in the moderate subsonic regime. ● 160 mm lens, corrected for the streamwise production term; ■ 243 mm lens, corrected; ○ 160 mm lens, uncorrected; □ 243 mm lens, uncorrected.

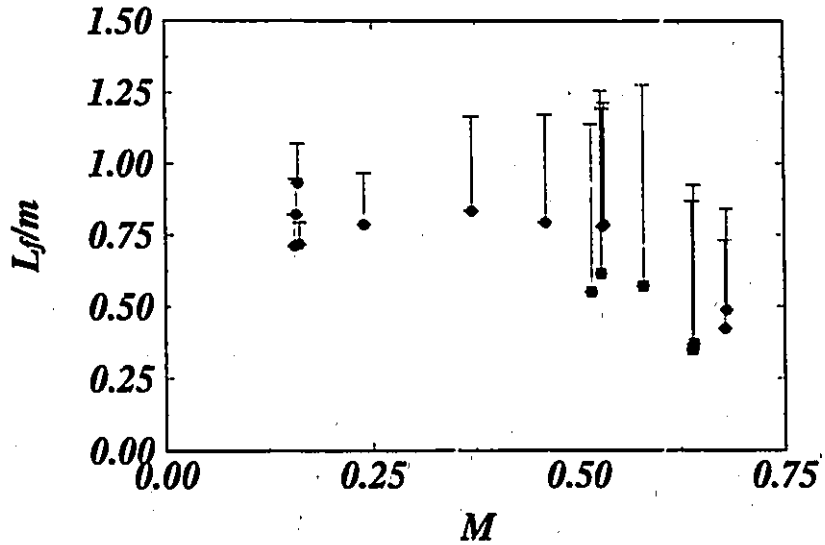

Figure 47: Integral length scales at $x/m = 58.5$ in the moderate subsonic regime. ● 160 mm lens; ■ 243 mm lens. The error bars correspond to the uncertainty in the u' measurement.

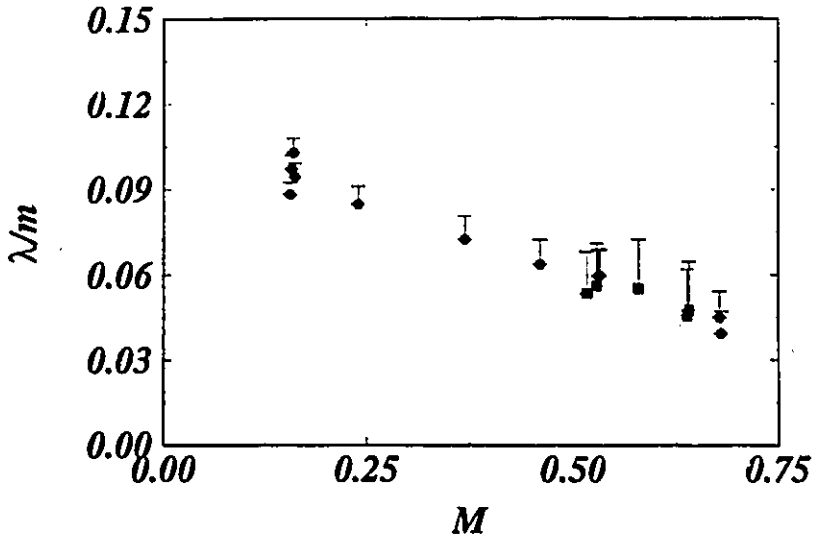

Figure 48: Taylor microscales at $x/m = 58.5$ in the moderate subsonic regime. ● 160 mm lens; ■ 243 mm lens. The error bars correspond to the uncertainty in the u' measurement.

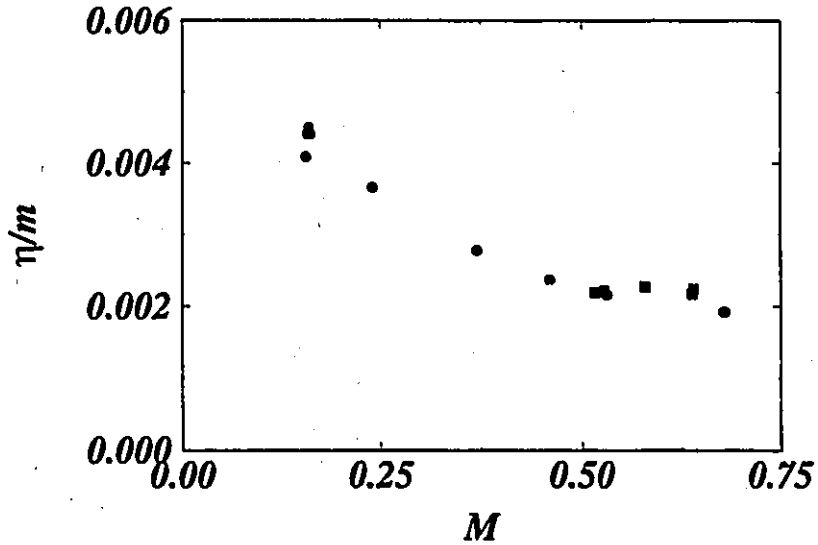

Figure 49: Kolmogoroff microscales at $x/m = 58.5$ in the moderate subsonic regime. ● 160 mm lens; ■ 243 mm lens.

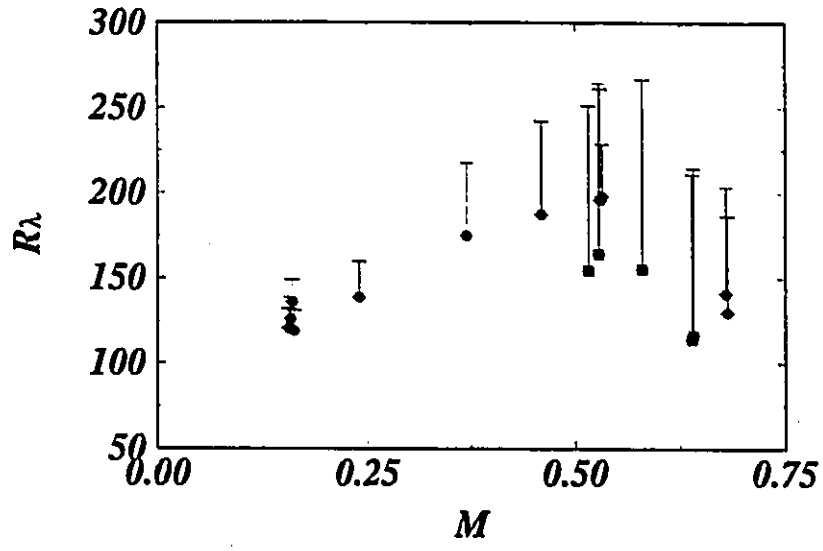

Figure 50: Turbulence Reynolds numbers at $x/m = 58.5$ in the moderate subsonic regime. ● 160 mm lens; ■ 243 mm lens. The error bars correspond to the uncertainty in the u' measurement.

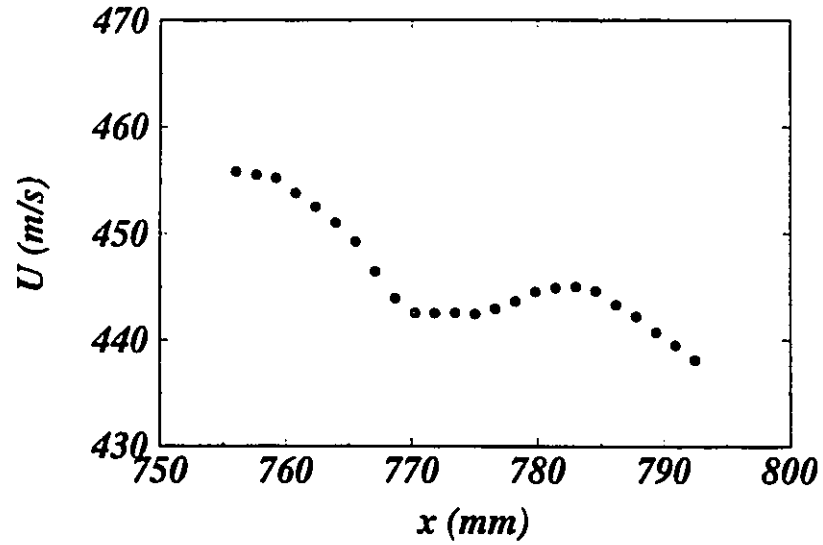

Figure 51: Mean velocity profile across a wave (SP2c).

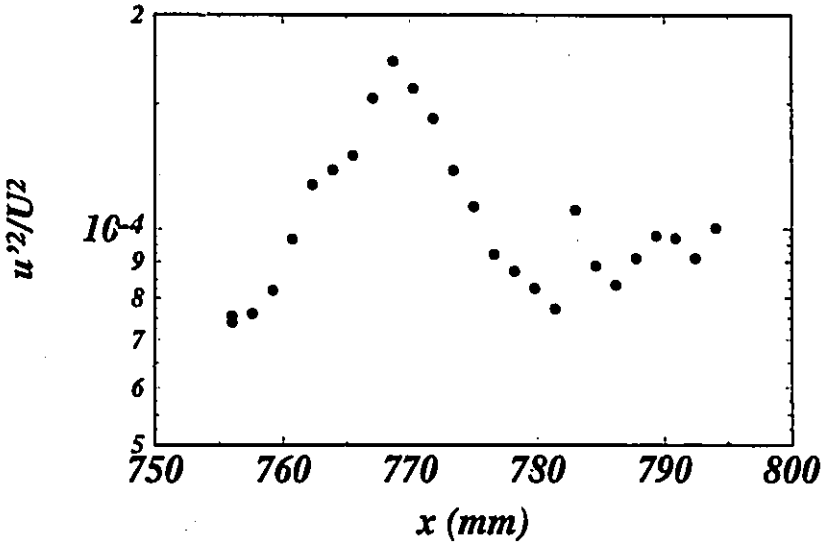

Figure 52: Velocity variance profile across a wave (SP2c).

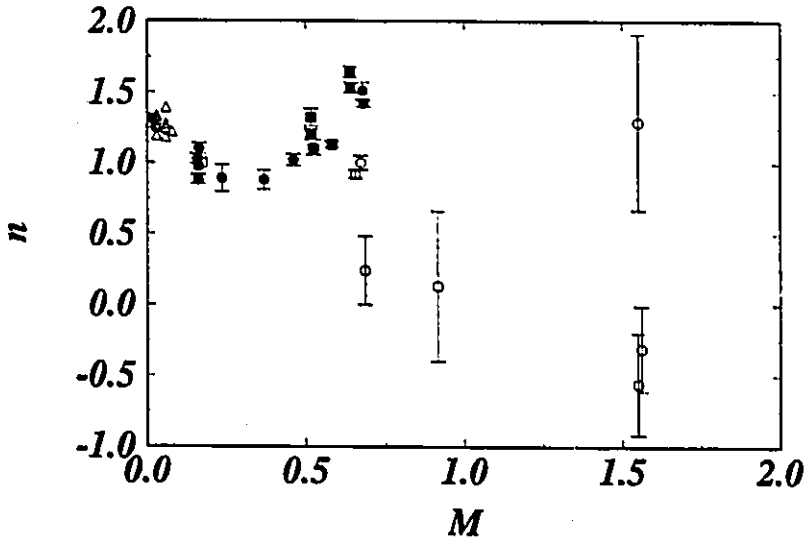

Figure 53: Decay exponents in all regimes, assuming $x_0/m = 0$ for the present results. Error bars correspond to 90% confidence intervals. ● Present results, 160 mm lens; ■ Present results, 243 mm lens; ○ Present results, anisotropic flow; △ Comte-Bellot and Corrsin (1966); ▽ Mohamed and LaRue (1990); □ Kistler and Vrebalovich (1966).

Appendix A

Further Tests of the Flow Homogeneity and Isotropy

A.1 Estimates of the Neglected Terms in the Streamwise Reynolds Stress Equation

The transport equation for the streamwise Reynolds stress in incompressible flow may be expressed as:

$$\frac{\partial \overline{u^2}}{\partial t} + \underbrace{U\frac{\partial \overline{u^2}}{\partial x} + V\frac{\partial \overline{u^2}}{\partial y} + W\frac{\partial \overline{u^2}}{\partial z}}_{C=C_x+C_y+C_z} = \underbrace{-2\overline{u^2}\frac{\partial U}{\partial x} - 2\overline{uv}\frac{\partial U}{\partial y} - 2\overline{uw}\frac{\partial U}{\partial z}}_{P=P_x+P_y+P_z} - \underbrace{\frac{2}{\rho}\overline{u\frac{\partial p}{\partial x}}}_{W_p}$$
$$- \underbrace{\left(\frac{\partial \overline{u^3}}{\partial x} + \frac{\partial \overline{u^2v}}{\partial y} + \frac{\partial \overline{u^2w}}{\partial z}\right)}_{D_t=D_{tx}+D_{ty}+D_{tz}} + \underbrace{2\nu\left(\overline{u\frac{\partial^2 u}{\partial x^2}} + \overline{u\frac{\partial^2 u}{\partial y^2}} + \overline{u\frac{\partial^2 u}{\partial z^2}}\right)}_{D_\nu - 2\epsilon/3}, \qquad \text{(A.1)}$$

where C represents the convective rate of change, P represents the production by mean velocity gradients, W_p represents the work due to pressure fluctuations, D_t rep-

Table A.1: Estimates of the Neglected Terms in the Streamwise Reynolds Stress Equation at $M = 0.16$

C_y/C_x	P_x/C_x	P_y/C_x	D_{tx}/C_x	D_{ty}/C_x
0.013	0.073	-0.008	0.003	-0.003

resents diffusion by turbulence, D_v represents viscous diffusion, and ϵ is the dissipation rate of turbulence kinetic energy, assuming local isotropy. In studies of decaying turbulence it is desirable to have all terms other than C_x and ϵ to be small. The degree to which this ideal is realized for the moderate subsonic cases in the present study is considered in this appendix. The incompressible equation is considered sufficient for the moderate subsonic cases because the density gradients in the free-stream are very small.

The unsteady term was zero for the present flows, and W_p and D_v were assumed to be small. C_z, P_z, and D_{tz} could not be determined because W and w were not measured; however, they were assumed to be of the same order as the corresponding terms in the y-direction. The remaining terms — C_x, C_y, P_x, P_y, D_{tx}, and D_{ty} — were estimated from the streamwise (SB1a) and transverse (Figures 10 and 12; case `j5x7` in Appendix D) profiles at $M = 0.16$. The streamwise gradients were estimated from least-squares curve fits through the measured data points, and the transverse gradients using central differencing between the data points adjacent to the tunnel centreline. The estimate for P_y required a shear stress correlation coefficient, for which a value of 0.05 (the maximum measured value) was used. The estimate for D_{tx} assumed a skewness factor S of 0.1, which is larger than any measured value. The estimates for various terms, non-dimensionalized by C_x, are tabulated in Table A.1.

From these estimates it is apparent that the largest non-dissipative term is due to production by the streamwise velocity gradient. The same term was calculated for the

Table A.2: Estimates of the Streamwise Production Term in the Moderate Subsonic Regime

Case	P_x/C_x
SB1a	0.073
SB1b	0.102
SB1c	0.108
SB1d	0.086
SB2	0.079
SB3	0.097
SB4	0.103
SB5a	0.085
SB5b	0.071
SB5c	0.106
SB5d	0.125
SB6	0.125
SB7a	0.109
SB7b	0.111
SB8a	0.114
SB8b	0.146

remainder of the moderate subsonic cases, and the results are shown in Table A.2. In all cases both P_x and C_x were negative. The estimates were used to apply a correction to the calculation of ϵ.

A.2 Estimate of the Number of Eddy Turnovers

The number of eddy turnovers, N_{to}, which occur between the grid and the measurement region is a measure of the influence of initial conditions on the turbulence. It is a function of the dissipation and convection time scales. The dissipation time scale, also called the *eddy turnover time*, is calculated from

$$\tau_e = \frac{k}{\epsilon}. \tag{A.2}$$

The convection time scale, or the time required for an eddy to be convected from the grid to a location x, is

$$\tau_c = \frac{x}{U}. \tag{A.3}$$

Because τ_e may change significantly with x, N_{to} must be calculated from

$$N_{to} = \int_0^x \frac{d\tau_c}{\tau_e}, \tag{A.4}$$

where $d\tau_c$ is the time required for an eddy to be convected through a distance dx. Unfortunately, τ_e is unknown near the grid. A conservative estimate can be made by considering only the region where the decay power law applies, say $x > x_1$. Then

$$N_{to} = n \ln \left(\frac{x - x_0}{x_1 - x_0} \right). \tag{A.5}$$

In low-speed grid turbulence studies, isotropy is often assumed to be reached at $x/m \approx 20$. The same assumption has been made here. If it is further assumed that $x_0 = 0$, and choosing x to be at the first measurement location, we obtain $N_{to} = 0.95 \approx 1$. Hence eddies produced at the location where the turbulence is typically assumed to become isotropic have dissipated completely by the time they are convected to the measurement region, which provides further support that the turbulence in the measurement region is approximately isotropic.

Appendix B

LDV Equipment: Some Practical Considerations

The LDV equipment is described in some detail in the various DANTEC manuals, and operation of the software in the FLOware manual. This appendix is meant to provide a guide to the more common equipment adjustments and software choices.

B.1 Hardware

The LDV hardware is costly, and contains several components which can be aligned only at DANTEC facilities. For this reason the equipment should be handled with extreme care. The laser beams can cause serious eye damage if they, or their spectral reflections, are viewed directly. Safety goggles are available for eye protection.

B.1.1 Description

The LDV hardware consists of the following components:

Laser The laser is a 100 mW Argon-ion laser. It is harder on the laser to turn it off and on than to leave it on; hence it should not be needlessly turned off and on. The laser produces a single cyan beam, composed mainly of green (514.5 nm) and blue (488 nm) wavelengths.

Beam Splitter A beam splitter splits the cyan beam into two cyan beams of equal intensity.

Bragg Cell A Bragg cell shifts the frequency of one of the two cyan beams by 40 MHz. The other beam passes through a glass rod to ensure the optical pathlengths are equal. The Bragg cell is powered by the signal processor, which is controlled by the `FLOware` software. Hence, for frequency shifting to be guaranteed to occur, the signal processor must be on, the software must specify that power is supplied to the Bragg cell, and the software must be in "Setup and Acquire" mode.

The Bragg cell actually produces a diffraction pattern, consisting of several beams, each mode of which has a different frequency shift. The central beam is unshifted, the modes to each side of the centre are shifted by ± 40 MHz, and so on. The distribution of power among the various modes is controlled by the "Bragg cell angle" Allen key. It is currently set to maximize power to the first-order mode, which has a 40 MHz shift. However, the Bragg cell angle should rarely need to be changed. For measurements of low speed flows, a 40 MHz shift is usually used. For some higher speed flows, the unshifted beam may be needed; however, this beam is obtained not by changing the Bragg cell angle, but by not powering the Bragg cell at all, in which case the incident beam passes through without change.

There is no fundamental difference between a shift of 40 MHz and a shift of -40 MHz, such that an effective shift of -40 MHz can be obtained by rotating the probe by 180°.

From the above it is apparent that two beams exit from the Bragg cell: an unshifted cyan beam, which passes through the glass rod, and a (potentially) shifted cyan beam, which passes through the Bragg cell proper.

Colour Separator The shifted cyan beam is split into green and blue beams by a colour separator. The direction of the outgoing beams is controlled by prisms, which can be adjusted with Allen keys. When changing from zero-order mode to first-order mode, or vice versa, these prisms must be adjusted, as discussed later in this section.

Hence three beams exit from the colour separator: an unshifted cyan beam, which is unaffected by the colour separator proper, a (potentially) shifted green beam, and a (potentially) shifted blue beam.

Coupling to Fibre Optic Cables Fibre optic cables transmit each of the beams. The beams are directed onto the fibre optic cables using two additional components:

- The fibre optic cable ends, onto which the laser beams are directed, are attached to fibre optic plugs, which plug into the manipulators, discussed

next. The plugs can be removed from the manipulators by loosening two Allen keys (but not the Allen key for the locking screw). A notch on the locking screw ensures that the angular position of the plug, and consequently the beam polarization, will be preserved when the plug is re-inserted. Beam polarization is discussed further in Section B.1.3.

- The fibre optic cable coupling efficiency is very sensitive to directional and, even more important, angular alignment between the beam and the cable. Fine-tune control is provided by the fibre optic cable manipulators. Each manipulator has four independent thumb screws. Two thumb screws control the angular alignment and two control the directional alignment. Each thumb screw has a corresponding Allen key, which must be loosened and tightened before and after the thumb screw adjustment.

Probe Distribution Box The three cables carry the three beams to a probe distribution box, which combines the fibre optics into a single cable.

Fibre Optic Cable A fibre optic cable transmits the beams to the probe. As discussed in Section B.1.3, there is some issue about the integrity of this cable.

Probe Head This cable transmits the three beams to the probe head. The probe head is pre-aligned by DANTEC and can only be re-aligned at DANTEC facilities.

Beam Expander A 1.9× beam expander may be used to expand the beam diameters and separations by a factor of 1.9. It also reduce the probe volume dimensions and increases the light intensity at the probe volume, yielding a higher SNR. The beam expander couples only with the DANTEC 310 mm and 600 mm lenses.

Adaptors Only the DANTEC 160 mm lens fastens directly to the probe. For the 310 mm and 600 mm lenses, an adaptor is required if the beam expander is not used. For the TSI lenses another adaptor is available.

Lenses Lenses are required to focus the beams. Various lenses, listed in Tables B.1 and B.2, are available. The corresponding velocity ranges which they can measure are also included; these velocity ranges differ slightly for the blue and green beams. Only the DANTEC lenses are achromats, so only they are suitable for two-component measurements.

Probe Volume The intersection of the beams is called the probe volume and is ellipsoidal in shape. If the probe is properly aligned, the green-cyan intersection should be at exactly the same location as the blue-cyan intersection. This can be

Table B.1: Velocity Ranges with the Green Beam

Lens	Velocity range (m/s)		
	40 MHz shift	No shift	-40 MHz shift
DANTEC 160 mm	-18.4–92.2	104.5–215.1	227.4–338.0
DANTEC 310 mm	-35.6–178.2	202.0–415.9	439.7–653.5
DANTEC 310 mm 1.9× beam expansion	-18.8–94.0	106.6–219.4	232.0–344.8
DANTEC 600 mm	-68.9–344.7	390.7–804.4	850.3–1264.
DANTEC 600 mm 1.9× beam expansion	-36.3–181.6	205.8–423.7	447.9–665.8
TSI 103 mm	-11.9–56.7	67.6–139.2	147.2–218.8
TSI 104 mm	-12.0–60.2	68.3–140.6	148.6–220.9
TSI 243 mm	-28.0–139.8	158.4–326.2	344.8–512.6
TSI 553 mm	-63.5–317.7	360.1–741.4	783.7–1165.
TSI 580 mm	-66.6–333.2	377.7–777.6	822.0–1221.

Table B.2: Velocity Ranges with the Blue Beam

Lens (mm)	Velocity range (m/s)		
	40 MHz shift	No shift	-40 MHz shift
DANTEC 160 mm	-17.5–87.4	99.1–204.0	215.7–320.6
DANTEC 310 mm	-33.8–169.1	191.6–394.5	417.0–619.9
DANTEC 310 mm 1.9× beam expansion	-17.8–89.2	101.1–208.1	220.0–327.1
DANTEC 600 mm	-65.4–327.0	370.6–762.9	806.5–1198.
DANTEC 600 mm 1.9× beam expansion	-34.4–172.2	195.2–401.8	424.8–631.5
TSI 103 mm	-11.3–56.6	64.1–132.0	139.6–207.5
TSI 104 mm	-11.4–57.1	64.7–133.3	140.9–209.5
TSI 243 mm	-26.5–132.6	150.3–309.4	327.1–486.2
TSI 553 mm	-60.3–301.4	341.6–703.2	743.4–1105.
TSI 580 mm	-63.2–316.1	358.2–737.5	779.7–1159.

verified by magnifying the probe volume onto a wall using a diverging lens, one of which is included with the LDV equipment. Currently the blue-cyan intersection occurs slightly closer to the probe than the green-cyan intersection, indicating a slight misalignment. However, because the probe volume is elongated in the height-direction, the two intersections have a lot of overlap and two-dimensional measurements are still possible. When the LDV system is operated in zero-order mode (i.e. no frequency shifting) and the probe volume is magnified onto a wall or screen, two sets of orthogonal fringes due to the beam intersections should be visible.

Receiving Optics When the LDV system is operated in back-scatter mode, the Doppler signal is received into the probe head and carried via the fibre optic cable to the photomultiplier tubes mounted on the laser bench. When the LDV system is operated in forward-scatter mode, the receiving optics must be placed on the opposite side of the flow as the probe. In this case a receiving lens is attached to the photomultiplier tubes (PMTs). The eyepiece should be placed slightly off-axis, so that none of the three incident beams strikes the lens directly. The PMTs should be perpendicular to the eyepiece for optimum receiving efficiency.

Receiving efficiency is extremely sensitive to the alignment of the receiving optics. When initially setting up the optics, a rough alignment should be obtained by setting the distance between the probe volume and the front plane of the receiving lens to approximately 24.5 cm, and the receiving lens should point directly at the probe volume. When this is done, and when the flow is seeded, the three beams and their intersections should be visible through the eyepiece.

Next, the alignment should be further tuned. The distance between the receiving optics and the probe volume should be adjusted so that the beams intersect at the same probe volume, which should be in sharp focus and positioned at the centre of the eyepiece; the concentric circles in the eyepiece are an aid for this. As this procedure is being followed, the signal processor should be monitored to ensure that the red PMT overload lights do not flash. The PMT lifetimes are shortened by overloading; if they do overload the applied voltage must be reduced via the `FLOware` software.

Fine-tuning should be done with the `FLOware` software in "Continuous Run" mode, and should be done both viewing the probe volume through the eyepiece and monitoring the data rate and validation levels reported by the software. There are three independent controls on the receiving optics used to fine-tune the alignment. The lens can be rotated to optimize the distance between the lens and the probe volume. Two thumb screws rotate the lens about the two

axes perpendicular to the axis through the lens, and thereby move the position of the probe volume in the eyepiece. The alignment is optimized when the net data rate (the data rate multiplied by the validation percentage) is maximized for a given set of software settings.

Signal Processor The burst information is processed with the DANTEC 55N10 Flow Velocity Analyzer (FVA). Before connecting the cables to the FVA, it is necessary to choose which beam will correspond to which velocity channel. This choice is governed by two factors. First, the green beam is somewhat more intense, and therefore produces a stronger signal, than the blue beam. Second, the bursts are triggered when the U-signal reaches a certain threshold. Consequently, if the green beam is connected to the U-channel, more bursts will be registered, but the validation percentage will suffer due the the weaker V-signal. On the other hand, if the blue beam is connected to the U-channel, the data rate will fall, but the validation percentage will increase. For two-dimensional measurements in which both velocities components are to be validated, the choice does not matter much.

Two coaxial cables connect each PMT to the signal processor. A coaxial cable also connects the signal processor to the Bragg cell. Another cable connects the signal processor to the host computer. Finally, if the system is to be run with an encoder (which synchronizes operation with an external trigger), a cable connects the signal processor to the external trigger.

Computer Hardware Two pieces of hardware are required for the host computer. Firstly, a board must be installed into the host computer, which includes a port permitting communication with the signal processor. Secondly, a hardware identification key must be attached to the printer port.

B.1.2 Changing the System Order

In this section the technique for changing the system from first-order mode to zero-order mode is described. Changing from zero-order mode to first-order mode is the inverse. First the "long", more systematic procedure is described. Then a short-cut is suggested. Both procedures, however, are relatively short: the longer procedure takes perhaps 5 minutes for each colour.

The systematic approach, which is performed for both the green and blue beams, is as follows:

1. Loosen the Allen keys for the fibre optic plug.

2. Remove the fibre optic plug. A series of beams will appear. The most intense beam should be the first-order (shifted) beam. This is the beam which is currently fed into the cable. The zero-order beam, which is to be directed into the fibre optic cable, can be identified by turning off the power to the Bragg cell using the FLOware software.

3. Insert and tighten the alignment tool (a hollow tube with a cross at one end) into the fibre optic plug socket. The cross intersection should be located close to the first-order beam.

4. Adjust the colour separator prisms so that the zero-order beam moves to the cross intersection. For the blue beam, only the transverse direction needs to be adjusted. For the green beam, only the in/out direction needs to be adjusted. For both beams, an Allen key rotation of approximately $\frac{1}{8}$ of a turn is required. When moving to zero-order mode, the rotations are counter-clockwise; when returning to first-order mode, the rotations are clockwise.

5. Remove the alignment tool and re-insert the fibre plug. Ensure the Bragg cell is off so that the zero-order beam has full power.

6. Optimize the alignment between the beam and fibre optic cable using the thumb screws on the fibre optic manipulator. This can be done visually by directing the beam at a wall and maximizing the beam intensity.

7. Ensure the frequency shift specified in the software (found in the "Bandwidths" section of the "Setup" menu) is set to 0 MHz rather than 40 MHz or -40 MHz. This ensures the correct velocities are calculated.

The following short-cut technique is also possible:

1. Turn off power to the Bragg cell.

2. Adjust the Allen keys for the colour separator prisms, by the amounts specified in Step (4) above.

3. Maximize the beam intensities using the thumb screws on the fibre optic cable manipulators.

4. Ensure the frequency shift specified in the software (found in the "Bandwidths" section of the "Setup" menu) is set to 0 MHz rather than 40 MHz.

B.1.3 Beam Polarization

To achieve the maximum possible SNR, the three beams must be polarized in the same plane. The polarization can be roughly optimized by inspecting the interference fringes, which requires the system to be operated in zero-order mode (Section B.1.2. Then, using the small diverging lens to project the probe volume on the wall, the polarizations should be adjusted so that the fringes in both directions are of maximum intensity. This can be done only approximately by eye, since the intensity perceived by the eye is non-linearly related to the actual light intensity. Fine-tuning requires monitoring of the data rate and validation levels while taking measurements.

The polarization of a given beam is adjusted by rotating its fibre optic plug, which requires that the Allen key screw for the locking screw be loosened first. The beam intensitities may need to be re-optimized (using the thumb screws on the fibre manipulator) after rotating the plug.

Observations made during the measurements of Budwig et al (1995) suggest that the cables may not preserve the beam polarizations correctly, for under certain conditions, the data rate and validation level were sensitive to cable position, such that moving or twisting the cable slightly could cause an order-of-magnitude change in the net data rate. This occurred when the TSI 253 mm lens was used. Later I observed the same phenomenon with the DANTEC 310 mm lens.

B.1.4 Sign Convention

A sign convention must be specified in order to identify the direction of fluid motion with respect to the beams. The convention depends upon the frequency shift:

1. In zero-order mode, the direction of particle motion cannot be determined because particles travelling in both directions produce identical detected frequencies.

2. In first-order mode, with the software frequency shift for the channel under consideration set to 40 MHz, the sign convention is such that a particle moving from the shifted beam (green or blue) toward the cyan beam has a positive velocity. This convention is the opposite of that given in the manual, which could indicate that the frequency shift is actually -40 MHz rather than 40 MHz.

3. In first-order mode, with the software frequency shift for the channel under consideration set to -40 MHz, the sign convention is such that a particle moving

from the cyan beam toward the shifted beam (green or blue) has a positive velocity.

B.2 The FLOware Software

In this section some guidelines for operating version 3.0 of FLOware Attention is limited to the "Setup and Acquire" module. Only those parameters which I found necessary to adjust in my work are discussed. For other options, and for further information on the parameters discussed here, consult the FLOware manual. The discussion is subdivided into the various menus under the "Setup and Acquire" module.

Note that an existing set of parameters may be loaded by opening the appropriate parameter file, using the "Files" option in the "Setup and Acquire" menu. By the same token, the current parameters may be saved using the same option.

B.2.1 Setup

The setup menu includes the following options:

Electronics In this screen parameters such as the number of dimensions, the power to the Bragg cell, the burst detector mode, and the type of photomultiplier tubes are set.

The Bragg cell setting should be consistent with the mode of operation of the Bragg cell and driver used to power it. If the Bragg cell is operated in zero-order mode, both drivers should be set to off. If it is operated in first-order mode, power should be supplied to the appropriate driver.

For the burst detector mode, I had it set to the "Trigger on U1/external inhibit" option, in which case a burst is triggered when the U1-voltage exceeds a certain threshold and is below a certain plateau between bursts.

The default base address is correct.

The photomultiplier tubes are of type 55x08.

Optics This menu sets various optics parameters for each channel, including the beam wavelength, the Gaussian beam diameter, the beam expansion ratio, the beam separation, and the lens focal length. From this it calculates the fringe spacing, the number of fringes in the probe volume, and the size of the probe volume.

Table B.3: Probe Volume Data for the Green Beam

f (mm)	Exp. ratio	No. of fringes	Fringe spacing(μm)	Probe volume dim. (mm)		
				Length	Width	Height
160	1.0	25	3.074	0.0777	0.0776	1.238
310	1.0	25	5.941	0.1505	0.1504	4.635
310	1.9	25	3.135	0.0793	0.0791	1.287
600	1.0	25	11.49	0.2911	0.2911	17.32
600	1.9	25	6.052	0.1533	0.1532	4.809
103	1.0	25	1.989	0.0502	0.0499	0.515
104	1.0	25	2.008	0.0506	0.0504	0.525
243	1.0	25	4.660	0.1180	0.1179	2.849
558	1.0	25	10.59	0.2685	0.2683	14.74
580	1.0	25	11.11	0.2814	0.2814	16.21

The wavelengths for the channels should be set consistent with the cable connections between the PMTs and the signal processor. Blue has a wavelength of 488 nm and green has a wavelength of 514.5 nm.

The laser beam has a diameter (at the $1/e^2$ locus of points) of 1.30 mm. This value holds regardless of whether or not a beam expander is used.

A beam collimator is not used and the ratio is therefore unity.

The beam expander increases the beam diameter and beam separation distance. by a factor of 1.9. If it is used, the expansion ratio should be set to this value; else it should be set to unity.

The beam separation gives the green/cyan and blue/cyan separation distances at the front lens on the probe. Without a beam expander, these are 26.87 mm; with a beam expander they are 51.05 mm.

The lens focal length should be given in mm.

The size of the probe volume can be displayed by typing `<ctrl>v`. For convenience, the probe volume data are provided as functions of the lens focal length and beam expansion ratio in Table B.3 for the green beam and in Table B.4 for the blue beam.

Traverse This option permits specification of the traverse positions at which data are to be collected. With a traverse operated manually, as I had, the traverse mode should be set to "User-Input" rather than "Automatic" or "Manual". Grids for various coordinate systems can be generated; points can also be added, deleted,

Table B.4: Probe Volume Data for the Blue Beam

f (mm)	Exp. ratio	No. of fringes	Fringe spacing(μm)	Probe volume dim. (mm)		
				Length	Width	Height
160	1.0	25	2.916	0.0737	0.0736	1.174
310	1.0	25	5.635	0.1427	0.1426	4.395
310	1.9	25	2.973	0.0752	0.0750	1.221
600	1.0	25	10.90	0.2761	0.2761	16.46
600	1.9	25	5.741	0.1454	0.1453	4.562
103	1.0	25	1.866	0.0476	0.0474	0.489
104	1.0	25	1.904	0.0480	0.0478	0.498
243	1.0	25	4.420	0.1119	0.1118	2.703
553	1.0	25	10.05	0.2545	0.2545	13.98
580	1.0	25	10.54	0.2669	0.2669	15.38

or modified manually. I performed an entire run with a single traverse file; i.e., the first 20 points (say) were for all records at the first position, the next 20 points were for all records at the next position, and so on.

Bandwidths This option permits specification of the bandwidth, or range of acceptable frequencies detected by the signal processor, for each channel. It should be as narrow as possible without truncating the velocity histogram.

The optical frequency shift is also set in this screen; it should be set consistent with the mode of operation of the Bragg cell. If the Bragg cell is used in zero-order mode, it should be set to 0 MHz; if the Bragg cell is used in first-order mode, it should be set to 40 MHz or -40 MHz, depending on the desired velocity range and probe orientation (see the "Sign Convention" discussion in the previous section.)

B.2.2 Acquire

Several options are available in the "Acquire" menu; of these, only the following are discussed:

Validation This option permits specification of validation type and level. The validation criteria can be applied to any or none of the active velocity channels. There are two types of signal validation. The first is based upon the signal-to-noise ratio. A rule of thumb for the cut-off ratio is provided in the FLOware

manual, based upon the number of fringes in the probe volume. In my case, there were (for example) 25 fringes in the probe volume, for which a cut-off SNR ratio of -3 dB is appropriate. A second type of validation is based upon the number of fringes crossed by the particle. In contrast to the manual, DANTEC personel say that the range should always be set wide (0-150 fringes).

High Voltage This is an important option which determines the voltage level to be applied to the PMTs. Increasing the applied voltage leads to a stronger signal and additional noise, leading to a higher data rate but a higher rejection rate. If the high voltage is increased too far, the PMTs will overload (the PM Overload light on the front face of the FVA flashes accordingly), leading to a shorter lifetime.

The optimum high voltage level is determined by trial and error, but typically falls in the range of 1000-1500 V. The applied voltage may be suspended in the "Acquire" menu by pressing `<ctrl>h`.

Bandwidths This option is the same as in the "Setup" menu.

Run Actual data acquisition is performed using this option. During data acquisition, histograms of the mean and fluctuating velocities are displayed on-line. There are two modes of operation of this menu: repetitive and continuous. In repetitive mode, the data is displayed but not saved, which is useful for optimizing the FLOware parameters and optics alignment. In continuous mode, the data is saved to files which can be later processed. If a traverse file was created in the "Traverse" option of the "Setup" menu, it is used for continuous mode.

There are various parameters to be set in the "Run" option. Dead-time mode can be used to force a certain time interval between samples. Data acquisition is halted at a traverse position if the maximum number of samples (either attempted or validated) is met or if the time limit is exceeded.

On some occassions, it is useful to angle the laser beams with respect to the reference frame, in order to measure velocities which would otherwise be out of range of the lenses. If this is the case, the velocities must be transformed to the original reference frame, which is possible with the "Transform" option in the "Edit" menu. Then the matrix which transforms the measured (U' and V') velocities to the desired (U and V) velocities may be modified; however, the on-line histograms and any data files which are written still use untransformed velocities.

Error Display This option displays useful diagnostic information such as the anode current in the PMTs and the validation levels, including the causes of sample rejections.

Appendix C

Computer Program Used for Data Processing

```
/*****************************************************************************

   program ldv

   This program reads and processes LDV data stored in binary data files,
   generated by the FLOware software developed by DANTEC.  Input parameters
   are read from ldv.inp, of which a sample is provided later.  Each data file
   corresponds to a single record (of which there are parms.nrec per
   measurement location) at a single measurement location (of which there are
   parms.npos).  Each record contains point.nval velocity samples.  For each
   record, the samples are read, averaged, and (if desired) outliers rejected.
   Various averaging procedures are available.  Subsequently, all records at
   a given measuring location are ensemble-averaged and (if desired) outliers
   rejected.  Then various turbulence parameters are calculated, including a
   curve fit to the decay law.  Finally, the data is written to various output
   files, some of which are summaries to be read, and some of which are data
   files which can be imported and plotted by a graphics program (eg. Axum).

   A sample input file ldv.inp:

        j20x2
        11        20
        1
        14.5    747.0     25.4     -1.
        13.23    17.55    539.
        3      2     1     1
        3.     2.5     17
        j20x2
        4     7 0     9 0     9 1    9 2
        1     10

        The above information provides the following information:
        1. Filename (no v or extension).
        2. Number of traverse positions / Number of records per position.
        3. Traverse direction (x/y/z/p).
        4. Mesh size / x-value of position 0 / x-increment / U-norm.
        5. Static pressure / Total pressure / Total temperature.
        6. Transformation method / Weighting method / Reject outliers / Sort data.
        7. Sample·sd / Record sd / z0.
        8. Output filename.
        9. Number of records to be excluded, followed by list (ipos, irec).
        10. Number of positions to be excluded, followed by list.

    Program written by Philip Zwart, 1995.

*****************************************************************************/

#include <stdio.h>
```

```
#include <math.h>
#include <string.h>

#define MAX_SAMPLES 3000
#define MAX_POS 30
#define MAX_REC 20
#define MAX_FILES (MAX_POS*MAX_REC)
#define FALSE 0
#define TRUE  1
#define X  0
#define Y  1
#define Z  2
#define P  3
#define EPS  1.e-8

typedef struct {
   char  finp[75];
   char  fout[75];
   int   npos;
   int   nrec;
   int   nfil;
   int   dim;
   float mesh_length;
   float reff;
   float x_inc;
   float u_norm;
   float h;
   float p;
   float p0;
   float t0;
   int   dirn;
   int   transform;
   int   rem_outliers;
   int   sort;
   int   weight_method;
   float sample_sd;
   float record_sd;
   float x0;
} Parms;

typedef struct {
   float at;
   float tt;
   float u;
   float v;
   float wt;
   int   reject;
} Sample;

typedef struct {
   int   aval[MAX_POS];
   int   arej[MAX_POS];
   int   reject[MAX_POS];
   float pval[MAX_POS];
   float data_rate[MAX_POS];
   float xpos[MAX_POS];
   float ypos[MAX_POS];
   float zpos[MAX_POS];
   float pos[MAX_POS];
   float dist1[MAX_POS];
   float dist2[MAX_POS];
} Point;

typedef struct {
   float u_mean[MAX_POS];
   float u_rms[MAX_POS];
   float u_skew[MAX_POS];
   float u_flat[MAX_POS];
   float v_mean[MAX_POS];
   float v_rms[MAX_POS];
   float v_skew[MAX_POS];
   float v_flat[MAX_POS];
   float uv[MAX_POS];
} Moment;

typedef struct {
   float data_rate[MAX_POS];
   float aval[MAX_POS];
   float pval[MAX_POS];
   float sam_rej[MAX_POS];
   int   ptr[MAX_POS];
```

```
   int   nrej[MAX_POS];
   int   reject[MAX_POS];
   float dist1[MAX_POS];
   float dist2[MAX_POS];
   float u_mean    [MAX_POS];
   float u_mean_err[MAX_POS];
   float u_ms    [MAX_POS];
   float u_ms_err[MAX_POS];
   float u_ms_reg[MAX_POS];
   float u_rms    [MAX_POS];
   float u_rms_err[MAX_POS];
   float u_skew    [MAX_POS];
   float u_skew_err[MAX_POS];
   float u_flat    [MAX_POS];
   float u_flat_err[MAX_POS];
   float v_mean    [MAX_POS];
   float v_mean_err[MAX_POS];
   float v_ms    [MAX_POS];
   float v_ms_err[MAX_POS];
   float v_ms_reg[MAX_POS];
   float v_rms    [MAX_POS];
   float v_rms_err[MAX_POS];
   float v_skew    [MAX_POS];
   float v_skew_err[MAX_POS];
   float v_flat    [MAX_POS];
   float v_flat_err[MAX_POS];
   float uv    [MAX_POS];
   float uv_err[MAX_POS];
   float uov   [MAX_POS];
   float integral[MAX_POS];
   float tay    [MAX_POS];
   float diss   [MAX_POS];
   float kol    [MAX_POS];
   float re_tay [MAX_POS];
   float zeros  [MAX_POS];
} Ensemble;

typedef struct {
   int   nrej;
   float u_mean;
   float u_norm;
   float re_m;
   float u_exp;
   float u_coef;
   float u_ci;
   float u_cor;
   float v_exp;
   float v_coef;
   float v_ci;
   float v_cor;
   float nu;
   float rho;
   float mach_p;
   float mach_u;
} Global;

void  get_parms(void);
void  initialize(void);
void  read_vfile(int ipos, int irec);
void  calc_weight(int ipos, int irec);
void  calc_moment(int ipos, int irec);
void  reject_samples(int ipos, int irec);
void  normalize(int ipos, int irec);
void  ensemble_average(int ipos);
void  reject_records(int ipos);
void  confidence_interval(int ipos);
void  global_average(void);
void  power_law(void);
void  curve_fit(float x0);
void  calc_scales(void);
void  bubble_sort(void);
void  write_data(void);
void  write_sum(void);
void  write_inp(FILE *fid);
void  write_rec(FILE *fid);
void  write_ens(FILE *fid);
void  write_file(char *ext, float *dist, float *udat, float *udat_err,
        float *udat_reg, float *vdat, float *vdat_err, float *vdat_reg);
void  wrap_up(void);

Parms    parms              = {0};
```

```
Sample   sample[MAX_SAMPLES] = {0},
Point    point[MAX_REC]      = {0},
Moment   moment[MAX_REC]     = {0},
Moment   norm[MAX_REC]       = {0},
Ensemble ensemble            = {0},
Global   global              = {0};

float    ci_factor[MAX_REC] = {0.00, 6.31, 2.92, 2.35, 2.13, 2.02, 1.94, 1.90,
                               1.86, 1.83, 1.81, 1.80, 1.78, 1.77, 1.76, 1.75,
                               1.75, 1.74, 1.73, 1.73};

FILE     *frej;
char     text[MAX_FILES][3] = { {"000"},{"001"},{"002"},{"003"},{"004"},
                                {"005"},{"006"},{"007"},{"008"},{"009"},
                                {"00a"},{"00b"},{"00c"},{"00d"},{"00e"},
                                {"00f"},{"00g"},{"00h"},{"00i"},{"00j"},
                                {"00k"},{"00l"},{"00m"},{"00n"},{"00o"},
                                {"00p"},{"00q"},{"00r"},{"00s"},{"00t"},
                                {"00u"},{"00v"},{"00w"},{"00x"},{"00y"},
                                {"00z"},{"010"},{"011"},{"012"},{"013"},
                                {"014"},{"015"},{"016"},{"017"},{"018"},
                                {"019"},{"01a"},{"01b"},{"01c"},{"01d"},
                                {"01e"},{"01f"},{"01g"},{"01h"},{"01i"},
                                {"01j"},{"01k"},{"01l"},{"01m"},{"01n"},
                                {"01o"},{"01p"},{"01q"},{"01r"},{"01s"},
                                {"01t"},{"01u"},{"01v"},{"01w"},{"01x"},
                                {"01y"},{"01z"},{"020"},{"021"},{"022"},
                                {"023"},{"024"},{"025"},{"026"},{"027"},
                                {"028"},{"029"},{"02a"},{"02b"},{"02c"},
                                {"02d"},{"02e"},{"02f"},{"02g"},{"02h"},
                                {"02i"},{"02j"},{"02k"},{"02l"},{"02m"},
                                {"02n"},{"02o"},{"02p"},{"02q"},{"02r"},
                                {"02s"},{"07t"},{"02u"},{"02v"},{"02w"},
                                {"02x"},{"02y"},{"02z"},{"030"},{"031"},
                                {"032"},{"033"},{"034"},{"035"},{"036"},
                                {"037"},{"038"},{"039"},{"03a"},{"03b"},
                                {"03c"},{"03d"},{"03e"},{"03f"},{"03g"},
                                {"03h"},{"03i"},{"03j"},{"03k"},{"03l"},
                                {"03m"},{"03n"},{"03o"},{"03p"},{"03q"},
                                {"03r"},{"03s"},{"03t"},{"03u"},{"03v"},
                                {"03w"},{"03x"},{"03y"},{"03z"},{"040"},
                                {"041"},{"042"},{"043"},{"044"},{"045"},
                                {"046"},{"047"},{"048"},{"049"},{"04a"},
                                {"04b"},{"04c"},{"04d"},{"04e"},{"04f"},
                                {"04g"},{"04h"},{"04i"},{"04j"},{"04k"},
                                {"04l"},{"04m"},{"04n"},{"04o"},{"04p"},
                                {"04q"},{"04r"},{"04s"},{"04t"},{"04u"},
                                {"04v"},{"04w"},{"04x"},{"04y"},{"04z"},
                                {"050"},{"051"},{"052"},{"053"},{"054"},
                                {"055"},{"056"},{"057"},{"058"},{"059"},
                                {"05a"},{"05b"},{"05c"},{"05d"},{"05e"},
                                {"05f"},{"05g"},{"05h"},{"05i"},{"05j"},
                                {"05k"},{"05l"},{"05m"},{"05n"},{"05o"},
                                {"05p"},{"05q"},{"05r"},{"05s"},{"05t"},
                                {"05u"},{"05v"},{"05w"},{"05x"},{"05y"},
                                {"05z"},{"060"},{"061"},{"062"},{"063"},
                                {"064"},{"065"},{"066"},{"067"},{"068"},
                                {"069"},{"06a"},{"06b"},{"06c"},{"06d"},
                                {"06e"},{"06f"},{"06g"},{"06h"},{"06i"},
                                {"06j"},{"06k"},{"06l"},{"06m"},{"06n"},
                                {"06o"},{"06p"},{"06q"},{"06r"},{"06s"},
                                {"06t"},{"06u"},{"06v"},{"06w"},{"06x"},
                                {"06y"},{"06z"},{"070"},{"071"},{"072"},
                                {"073"},{"074"},{"075"},{"076"},{"077"},
                                {"078"},{"079"},{"07a"},{"07b"},{"07c"},
                                {"07d"},{"07e"},{"07f"},{"07g"},{"07h"},
                                {"07i"},{"07j"},{"07k"},{"07l"},{"07m"},
                                {"07n"},{"07o"},{"07p"},{"07q"},{"07r"},
                                {"07s"},{"07t"},{"07u"},{"07v"},{"07w"},
                                {"07x"},{"07y"},{"07z"},{"080"},{"081"},
                                {"082"},{"083"},{"084"},{"085"},{"086"},
                                {"087"},{"088"},{"089"},{"08a"},{"08b"} };

/*************************************************************************/

main()
{
   int ifil, irec, ipos;
   char frejx[80];
   FILE *frej;
```

```
    get_parms();
    initialize();

    for (ipos = 0; ipos < parms.npos; ipos++) {
       printf("Position %d.\n", ipos);
       for (irec = 0; irec < parms.nrec; irec++) {
          read_vfile(ipos, irec);
 calc_weight(ipos, irec);
 calc_moment(ipos, irec);
          if (parms.rem_outliers == TRUE) {
             reject_samples(ipos, irec);
    calc_weight(ipos, irec);
             calc_moment(ipos, irec);
 }
          normalize(ipos, irec);
       }
       ensemble_average(ipos);
       if (parms.rem_outliers == TRUE) {
          reject_records(ipos);
 ensemble_average(ipos);
       }
       confidence_interval(ipos);
    }
    global_average();
    if (parms.dirn == 2) {
       power_law();
       calc_scales();
    }
    bubble_sort();
    write_data();
    wrap_up();

    return;
}


/*************************************************************************/

void get_parms(void)

/* This subroutine sets or reads in parameters, including:
   - Filename
   - Number of traverse positions
   - Number of records per traverse position
   - Mesh size and reference position for turbulence generator
   - Static pressure, total pressure, and total temperature
   - Velocity transformation method
   - Weighting method to be used when calculating moments
   - Whether outliers should be removed
   - Number of acceptable standard deviations for samples
   - Number of acceptable standard deviations for records
   - Whether output data should be sorted
   - Output filename
   - Confidence interval multiplying factor (from t-distribution)
   - Records to be excluded from calculations
   - Positions to be excluded from decay law calculation
.....................................................................*/
{
   int found, nrej, i, ipos, irec;
   FILE *fid;

   if ((fid = fopen("ldv.inp","r")) == NULL)
      printf("*** Error opening input file ldv.inp.\n");
   else
      printf("Reading input data from ldv.inp.");

   fscanf(fid, "%s", &parms.finp[0]);

   fscanf(fid, "%d", &parms.npos);
   if (parms.npos > MAX_POS) {
      printf("*** Warning: Number of traverse positions reduced to %d.", MAX_REC);
      parms.npos = MAX_POS;
   }

   fscanf(fid, "%d", &parms.nrec);
   if (parms.nrec > MAX_REC) {
      printf("*** Warning: Number of records reduced to %d.", MAX_REC);
      parms.nrec = MAX_REC;
   }

   parms.nfil = parms.nrec * parms.npos;
```

```
  parms.h = 127;

  found = FALSE;
  while (!found) {
     switch ( fgetc(fid) ) {
        case 'x': case 'X':
           parms.dirn = X;
   found = TRUE;
           break;
        case 'y': case 'Y':
           parms.dirn = Y;
   found = TRUE;
           break;
        case 'z': case 'Z':
           parms.dirn = Z;
   found = TRUE;
           break;
        case 'p': case 'P':
           parms.dirn = P;
   found = TRUE;
           break;
        default:
           break;
     }
  }

  fscanf(fid, "%f", &parms.mesh_length);
  fscanf(fid, "%f", &parms.xeff);
  fscanf(fid, "%f", &parms.x_inc);
  fscanf(fid, "%f", &parms.u_norm);
  fscanf(fid, "%f", &parms.p);
  fscanf(fid," %f", &parms.p0);
  fscanf(fid, "%f", &parms.t0);
  fscanf(fid, "%d", &parms.transform);
  fscanf(fid, "%d", &parms.weight_method);
  fscanf(fid, "%d", &parms.rem_outliers);
  if (parms.rem_outliers != TRUE && parms.rem_outliers != FALSE) {
      printf("\nInvalid assignment for rem_outliers; FALSE value assumed");
      parms.rem_outliers = FALSE;
  }
  fscanf(fid, "%d", &parms.sort);
  if (parms.sort != TRUE && parms.sort != FALSE) {
      printf("\nInvalid assignment for sort; FALSE value assumed");
      parms.sort = FALSE;
  }
  fscanf(fid, "%f", &parms.sample_sd);
  fscanf(fid, "%f", &parms.record_sd);
  fscanf(fid, "%f", &parms.x0);

  fscanf(fid, "%s", parms.fout);

                              /* Read records to be rejected a priori */
  fscanf(fid,"%d",&nrej);
  for (i=0; i<nrej; i++) {
    fscanf(fid,"%d %d", &ipos, &irec);
    point[irec].reject[ipos] = TRUE;
    ensemble.nrej[ipos] += 1;
  }

                              /* Read positions to be rejected a priori */
  fscanf(fid,"%d",&nrej);
  for (i=0; i<nrej; i++) {
    fscanf(fid,"%d", &ipos);
    ensemble.reject[ipos] = TRUE;
    global.nrej += 1;
  }

  if (fclose(fid) == EOF)
     puts("  Error closing input file ldv.inp.");

  return;
}


/*************************************************************************/

void initialize(void)

/* This subroutine performs some initialization
.........................................................................*/
{
```

```
   char frejx[80];

   strcpy(frejx, parms.fout);
   strcat(frejx, ".rej");

   if ((frej = fopen(frejx,"w")) == NULL)
      printf("*** Error opening sample rejection file %s.\n", frejx);
   else
      printf("\nRejected samples will be written to %s.\n\n", frejx);

   return;
}


/*************************************************************************/

void read_vfile(int ipos, int irec)

/* This subroutine reads in header and sample data from the FLOware
   velocity files.
.........................................................................*/
{
   int    i, ifil;
   int    old_dim;
   char   finpx[80];  /* Input file name with extension */
   int    idum;       /* dummy integer variable */
   char   cdum[128];  /* dummy character variable */
   long   ldum;       /* long dummy variable */
   float  fdum;       /* dummy float variable */
   float  u,v;
   long   natt;       /* attempted samples */
   FILE  *fid;        /* input file number */

   ifil = irec + ipos*parms.nrec;

   strcpy(finpx, &parms.finp[0]);
   strcat(finpx, "v.");
   strncat(finpx, &fext[ifil][0], 3);
   if ((fid = fopen(finpx,"rb")) == NULL)
      printf("*** Error opening input file %s.\n", finpx);
   else
      printf("  Reading and processing %s.\n", finpx);

   for (i = 0; i < 6; i++)                    /* Ignore date and time */
      fread(&idum, sizeof(short), 1, fid);

   old_dim = parms.dim;
   fread(&parms.dim, sizeof(short), 1, fid);          /* Read dimension */
   if (ifil > 0 && old_dim != parms.dim) {
      puts("  Warning: inconsistent dimensions.  Lower value used.");
      parms.dim = ( parms.dim <= old_dim ? parms.dim : old_dim );
   }
   for ( i= 0; i < 3; i++)                    /* Ignore diam, encoder info */
      fread(&idum, sizeof(short), 1, fid);

   fread(&natt, sizeof(long), 1, fid);                     /* Read attempted samples */
   fread(&point[irec].nval[ipos], sizeof(long), 1, fid);   /* Read validated samples */
   point[irec].pval[ipos] = 100. * point[irec].nval[ipos] / (natt+EPS);   /* Calculate % validation */
   if (point[irec].nval[ipos] > MAX_SAMPLES) {
      printf("  Warning: the number of samples read in will be truncated.\n"
             "     %d samples are in file, but MAX_SAMPLES is set to %d.\n",
             point[irec].nval[ipos], MAX_SAMPLES);
      point[irec].nval[ipos] = MAX_SAMPLES;
   }

   fread(&ldum, sizeof(long), 1, fid);                 /* Ignore sph_accepted */
   fread(&point[irec].data_rate[ipos], sizeof(float), 1, fid); /* Read data rate */
   point[irec].data_rate[ipos] *= 1000.;                       /* Convert to Hz */

   fread(&fdum, sizeof(float), 1, fid);             /* Ignore elapsed time */
   fread(&point[irec].xpos[ipos], sizeof(float), 1, fid);
   fread(&point[irec].ypos[ipos], sizeof(float), 1, fid);
   fread(&point[irec].zpos[ipos], sizeof(float), 1, fid);

   /* Normalize distance variable (dist1 for mean velocity, dist2 for mean-square
      quantities.  Tunnel width/height is normalizing length for dist1 and for
      dist2 with y- and z-traverses; mesh size for dist2 with x-traverses; no
      normalization done for pressure traverses */
   switch (parms.dirn) {
      case 1:
         point[irec].dist1[ipos] = (parms.x_inc*point[irec].zpos[ipos] + parms.xoff)
```

```
                                        / parms.mesh_length;
        point[irec].dist2[ipos] = (parms.x_inc*point[irec].xpos[ipos] + parms.xoff)
                                / parms.h;
point[irec].pos[ipos] = point[irec].xpos[ipos];
break;
     case Y:
        point[irec].dist1[ipos] = 10*point[irec].ypos[ipos] / parms.h;
        point[irec].dist2[ipos] = point[irec].dist1[ipos];
point[irec].pos[ipos]   = point[irec].ypos[ipos];
break;
     case Z:
        point[irec].dist1[ipos] = 10*point[irec].zpos[ipos] / parms.h;
        point[irec].dist2[ipos] = point[irec].dist1[ipos];
point[irec].pos[ipos]   = point[irec].zpos[ipos];
break;
     case P:
point[irec].dist1[ipos] = point[irec].xpos[ipos];
point[irec].dist2[ipos] = point[irec].xpos[ipos];
point[irec].pos[ipos]   = point[irec].xpos[ipos];
break;
     default:
        break;
  }

  for (i = 0; i < 8; i++)
     fread (&fdum, sizeof(float), 1, fid);    /* Ignore 8 floats */

  for (i = 3; i < 12; i++)
     fread (&idum, sizeof(short), 1, fid);    /* Ignore 12 integers */

  fread (cdum, sizeof(char), 128, fid);       /* Ignore 128-char string */

  for (i = 0; i < point[irec].nval[ipos]; i++) {     /* Read velocity data */
     fread (&fdum, sizeof(float), 1, fid);          /* Ignore status word */
     fread (&xsample[i].at, sizeof(float), 1, fid);   /* Read arrival time  */
     fread (&xsample[i].tt, sizeof(float), 1, fid);   /* Read transit time  */
     fread (&u, sizeof(float), 1, fid);               /* Read U-velocity    */
     if (parms.dim == 2)
        fread (&v, sizeof(float), 1, fid);            /* Read V-velocity    */
     switch (parms.transform) {
case 1 :
   sample[i].u = u;
   sample[i].v = v;
   break;
case 2 :
   sample[i].u =  u;
   sample[i].v = -v;
   break;
case 3 :
   sample[i].u = 0.707107*u + 0.707107*v;
   sample[i].v = 0.707107*u - 0.707107*v;
   break;
default :
   break;
     }
     sample[i].reject = 0;                /* Initialize to unrejected */
  }

  if (fclose(fid) == EOF)
     printf("  Error closing input file %s.", finpx);

  return;
}


/*****************************************************************************/

void calc_weight(int ipos, int irec)

/* This subroutine calculates the weighting factors for the velocity samples.
.....................................................................*/
{
   float wt, sum;
   int   i, nval, nrej;

   nval = point[irec].nval[ipos];
   nrej = point[irec].nrej[ipos];

   switch(parms.weight_method) {
      case 1:                          /* Unweighted */
         wt = 1/ (float) (nval - nrej);
```

```
      for (i = 0; i < nval; i++)
         sample[i].wt = wt * (TRUE - sample[i].reject);
      break;
   case 2                              /* Residence time weighting */
      for (i = 0, sum = 0; i < nval; i++) {
         sample[i].wt = sample[i].tt * (TRUE - sample[i].reject);
         sum += sample[i].wt;
      }
      for (i = 0; i < nval; i++)
         sample[i].wt /= sum;
      break;
   case 3:                             /* Interval time weighting */
                                       /* Does not work when samples rejected */
      sample[0].wt = sample[0].at;
      for (i = 1, sum = sample[0].at; i < nval; i++) {
         sample[i].wt = sample[i].at - sample[i-1].at;
         sum += sample[i].wt;
      }
      for (i = 0; i < nval; i++)
         sample[i].wt /= sum;
      break;
   default:
      break;
  }

  return;
}


/*****************************************************************************/

void calc_moment(int ipos, int irec)

/* This subroutine calculates the moment data at each point.
------------------------------------ ------------------------------------*/
{
  int i, nval;
  float u_mean, u_ms, u_skew, u_flat;
  float v_mean, v_ms, v_skew, v_flat, uv;

  nval = point[irec].nval[ipos];

  for (i=0, u_mean=0; i < nval; i++)
     u_mean += sample[i].u * sample[i].wt;

  for (i=0, u_ms=0, u_skew=0, u_flat=0; i < nval; i++) {
     u_ms   += pow( sample[i].u - u_mean, 2) * sample[i].wt;
     u_skew += pow( sample[i].u - u_mean, 3) * sample[i].wt;
     u_flat += pow( sample[i].u - u_mean, 4) * sample[i].wt;
  }
  moment[irec].u_mean[ipos] = u_mean;
  moment[irec].u_rms[ipos]  = sqrt( u_ms );
  moment[irec].u_skew[ipos] = u_skew;
  moment[irec].u_flat[ipos] = u_flat;

  if (parms.dim == 2) {
     for (i=0, v_mean=0; i < nval; i++)
        v_mean += sample[i].v * sample[i].wt;

     for (i=0, v_ms=0, v_skew=0, v_flat=0, uv=0; i < nval; i++) {
        v_ms   += pow( sample[i].v - v_mean, 2) * sample[i].wt;
       v_skew += pow( sample[i].v - v_mean, 3) * sample[i].wt;
        v_flat += pow( sample[i].v - v_mean, 4) * sample[i].wt;
        uv     += (sample[i].u - u_mean)*(sample[i].v - v_mean)*sample[i].wt;
     }
     moment[irec].v_mean[ipos] = v_mean;
     moment[irec].v_rms[ipos]  = sqrt( v_ms );
     moment[irec].v_skew[ipos] = v_skew;
     moment[irec].v_flat[ipos] = v_flat;
     moment[irec].uv[ipos]     = uv;
  }

  return;
}


/*****************************************************************************/

void reject_samples(int ipos, int irec)

/* This subroutine removes outliers from the list of samples used in the
```

```
   calculations.  Rejected samples are written to [name].rej
.....                                                                  */
{
   float u_max, u_min, v_max, v_min, sd;
   int i;

   sd = parms.sample_sd;
   u_max = moment[irec].u_mean[ipos] + sd*moment[irec].u_rms[ipos] + EPS;
   u_min = moment[irec].u_mean[ipos] - sd*moment[irec].u_rms[ipos] - EPS;
   v_max = moment[irec].v_mean[ipos] + sd*moment[irec].v_rms[ipos] + EPS;
   v_min = moment[irec].v_mean[ipos] - sd*moment[irec].v_rms[ipos] - EPS;

   if (parms.dim == 1) {
      for (i = 0; i < point[irec].nval[ipos]; i++)
         if (sample[i].u > u_max || sample[i].u < u_min) {
            sample[i].reject = TRUE;
            point[irec].nrej[ipos] += 1;
            fprintf(frej, "\n %2d %2d %7.4f", ipos, irec,
                     sample[i].u - moment[irec].u_mean[ipos]);
         }
   }

   if (parms.dim == 2) {
      for (i = 0; i < point[irec].nval[ipos]; i++)
         if (sample[i].u > u_max || sample[i].u < u_min ||
             sample[i].v > v_max || sample[i].v < v_min) {
            sample[i].reject = TRUE;
            point[irec].nrej[ipos] += 1;
            fprintf(frej, "\n %2d %2d %7.4f %7.4f", ipos, irec,
        sample[i].u-moment[irec].u_mean[ipos], sample[i].v-moment[irec].v_mean[ipos]);
         }
   }

   return;
}


/**************************************************************************/

void normalize(int ipos, int irec)

/* This subroutine normalizes all the point data except the mean velocities.
.....*/
{
   norm[irec].u_mean[ipos] = moment[irec].u_mean[ipos];
   norm[irec].u_rms[ipos]  = moment[irec].u_rms[ipos] /
                             ( sqrt( pow(moment[irec].u_mean[ipos], 2) +
  pow(moment[irec].v_mean[ipos], 2) ) + EPS);
   norm[irec].u_skew[ipos] = moment[irec].u_skew[ipos] /
                             ( pow( moment[irec].u_rms[ipos], 3) + EPS);
   norm[irec].u_flat[ipos] = moment[irec].u_flat[ipos] /
                             ( pow( moment[irec].u_rms[ipos], 4) + EPS);

   if (parms.dim == 2) {
      norm[irec].v_mean[ipos] = moment[irec].v_mean[ipos];
      norm[irec].v_rms[ipos]  = moment[irec].v_rms[ipos] /
                             ( sqrt( pow(moment[irec].u_mean[ipos], 2) +
  pow(moment[irec].v_mean[ipos], 2) ) + EPS);
      norm[irec].v_skew[ipos] = moment[irec].v_skew[ipos] /
                                ( pow( moment[irec].v_rms[ipos], 3) + EPS);
      norm[irec].v_flat[ipos] = moment[irec].v_flat[ipos] /
                                ( pow( moment[irec].v_rms[ipos], 4) + EPS);
      norm[irec].uv[ipos]     = moment[irec].uv[ipos] /
                                ( moment[irec].u_rms[ipos] *
     moment[irec].v_rms[ipos] + EPS);
   }

   return;
}


/**************************************************************************/

void ensemble_average(int ipos)

/* This subroutine performs ensemble averaging at the current
   traverse position.
.....*/
{
   int irec, nrec;
   int wt;
```

```
 nrec = parms.nrec - ensemble.nrej[ipos];
 ensemble.dist1[ipos] = point[0].dist1[ipos];
 ensemble.dist2[ipos] = point[0].dist2[ipos];

 for (irec = 0, ensemble.data_rate[ipos]=0, ensemble.pval[ipos]=0,
              ensemble.nval[ipos]=0, ensemble.sam_rej[ipos]=0,
ensemble.u_mean[ipos]=0, ensemble.u_ms[ipos]=0,
              ensemble.u_rms[ipos]=0, ensemble.u_skew[ipos]=0,
ensemble.u_flat[ipos]=0; irec < parms.nrec; irec++) {
    wt = 1 - point[irec].reject[ipos];
    ensemble.data_rate[ipos] += wt * point[irec].data_rate[ipos];
    ensemble.pval[ipos]      += wt * point[irec].pval[ipos];
    ensemble.nval[ipos]      += wt * point[irec].nval[ipos];
    ensemble.sam_rej[ipos]   += wt * point[irec].nrej[ipos];
    ensemble.u_mean[ipos] += wt * norm[irec].u_mean[ipos];
    ensemble.u_ms[ipos]   += wt * pow( norm[irec].u_rms[ipos], 2);
    ensemble.u_rms[ipos]  += wt * moment[irec].u_rms[ipos];
    ensemble.u_skew[ipos] += wt * norm[irec].u_skew[ipos];
    ensemble.u_flat[ipos] += wt * norm[irec].u_flat[ipos];
 }
 ensemble.data_rate[ipos] /= nrec;
 ensemble.pval[ipos]      /= nrec;
 ensemble.nval[ipos]      /= nrec;
 ensemble.sam_rej[ipos]   /= nrec;
 ensemble.u_mean[ipos] /= nrec;
 ensemble.u_ms[ipos]   /= nrec;
 ensemble.u_rms[ipos]  /= nrec;
 ensemble.u_skew[ipos] /= nrec;
 ensemble.u_flat[ipos] /= nrec;

 for (irec = 0, ensemble.u_mean_err[ipos]=0, ensemble.u_ms_err[ipos]=0,
              ensemble.u_rms_err[ipos]=0, ensemble.u_skew_err[ipos]=0,
ensemble.u_flat_err[ipos]=0; irec < parms.nrec; irec++) {
    wt = 1 - point[irec].reject[ipos];
    ensemble.u_mean_err[ipos] += wt * pow(ensemble.u_mean[ipos] -
                                     norm[irec].u_mean[ipos], 2);
    ensemble.u_ms_err[ipos]   += wt * pow(ensemble.u_ms[ipos] -
                                     pow(norm[irec].u_rms[ipos], 2), 2);
    ensemble.u_rms_err[ipos]  += wt * pow(ensemble.u_rms[ipos] -
                                      moment[irec].u_rms[ipos], 2);
    ensemble.u_skew_err[ipos] += wt * pow(ensemble.u_skew[ipos] -
                                     norm[irec].u_skew[ipos], 2);
    ensemble.u_flat_err[ipos] += wt * pow(ensemble.u_flat[ipos] -
                                     norm[irec].u_flat[ipos], 2);
 }
 ensemble.u_mean_err[ipos] = sqrt( ensemble.u_mean_err[ipos] / (nrec-1+EPS) );
 ensemble.u_ms_err[ipos]   = sqrt( ensemble.u_ms_err[ipos]   / (nrec-1+EPS) );
 ensemble.u_rms_err[ipos]  = sqrt( ensemble.u_rms_err[ipos]  / (nrec-1+EPS) );
 ensemble.u_skew_err[ipos] = sqrt( ensemble.u_skew_err[ipos] / (nrec-1+EPS) );
 ensemble.u_flat_err[ipos] = sqrt( ensemble.u_flat_err[ipos] / (nrec-1+EPS) );

 if (parms.dim == 2) {
   for (irec = 0, ensemble.v_mean[ipos]=0, ensemble.v_ms[ipos]=0,
                ensemble.v_rms[ipos]=0, ensemble.v_skew[ipos]=0,
  ensemble.v_flat[ipos]=0, ensemble.uv[ipos]=0;
  irec < parms.nrec; irec++) {
      wt = 1 - point[irec].reject[ipos];
      ensemble.v_mean[ipos] += wt * norm[irec].v_mean[ipos];
      ensemble.v_ms[ipos]   += wt * pow( norm[irec].v_rms[ipos], 2);
      ensemble.v_rms[ipos]  += wt * moment[irec].v_rms[ipos];
      ensemble.v_skew[ipos] += wt * norm[irec].v_skew[ipos];
      ensemble.v_flat[ipos] += wt * norm[irec].v_flat[ipos];
      ensemble.uv[ipos]     += wt * norm[irec].uv[ipos];
   }
   ensemble.v_mean[ipos] /= nrec;
   ensemble.v_ms[ipos]   /= nrec;
   ensemble.v_rms[ipos]  /= nrec;
   ensemble.v_skew[ipos] /= nrec;
   ensemble.v_flat[ipos] /= nrec;
   ensemble.uv[ipos]     /= nrec;

   ensemble.uev[ipos] = ensemble.u_rms[ipos] / (ensemble.v_rms[ipos]+EPS);

   for (irec = 0, ensemble.v_mean_err[ipos]=0, ensemble.v_ms_err[ipos]=0,
                ensemble.v_rms_err[ipos]=0, ensemble.v_skew_err[ipos]=0,
  ensemble.v_flat_err[ipos]=0, ensemble.uv_err[ipos]=0;
  irec < parms.nrec; irec++) {
      wt = 1 - point[irec].reject[ipos];
      ensemble.v_mean_err[ipos] += wt * pow(ensemble.v_mean[ipos] -
                                      norm[irec].v_mean[ipos], 2);
```

```
            ensemble.v_ms_err[ipos]    += wt * pow(ensemble.v_ms[ipos] -
                                              pow(norm[irec].v_rms[ipos],2) , 2),
            ensemble.v_rms_err[ipos]   += wt * pow(ensemble.v_rms[ipos] -
                                              moment[irec].v_rms[ipos], 2);
            ensemble.v_skew_err[ipos]  += wt * pow(ensemble.v_skew[ipos] -
                                              norm[irec].v_skew[ipos], 2),
            ensemble.v_flat_err[ipos]  += wt * pow(ensemble.v_flat[ipos] -
                                              norm[irec].v_flat[ipos], 2);
            ensemble.uv_err[ipos]      += wt * pow(ensemble.uv[ipos] -
                                              norm[irec].uv[ipos], 2),
         }
         ensemble.v_mean_err[ipos] = sqrt(ensemble.v_mean_err[ipos] / (nrec-1+EPS));
         ensemble.v_ms_err[ipos]   = sqrt(ensemble.v_ms_err[ipos]   / (nrec-1+EPS));
         ensemble.v_rms_err[ipos]  = sqrt(ensemble.v_ms_err[ipos]   / (nrec-1+EPS));
         ensemble.v_skew_err[ipos] = sqrt(ensemble.v_skew_err[ipos] / (nrec-1+EPS));
         ensemble.v_flat_err[ipos] = sqrt(ensemble.v_flat_err[ipos] / (nrec-1+EPS));
         ensemble.uv_err[ipos]     = sqrt(ensemble.uv_err[ipos]     / (nrec-1+EPS));
      }

      return;
}


/*************************************************************************/

void reject_records(ipos)

/* This subroutine removes outliers from the list of records used in the
   calculations.
.........................................................................*/
{
   float umn_max, umn_min, ums_max, ums_min, sd;
   int irec;

   sd = parms.record_sd;
   umn_max = ensemble.u_mean[ipos] + sd*ensemble.u_mean_err[ipos];
   umn_min = ensemble.u_mean[ipos] - sd*ensemble.u_mean_err[ipos];

   for (irec = 0; irec < parms.nrec; irec++)
      if (point[irec].reject[ipos] == FALSE)
         if (norm[irec].u_mean[ipos] > umn_max ||
     norm[irec].u_mean[ipos] < umn_min ) {
            point[irec].reject[ipos] = TRUE;
            ensemble.nrej[ipos] += 1;
         }

   return;
}


/*************************************************************************/

void confidence_interval(int ipos)

/* This subroutine calculates the confidence interval for the ensemble means.
.........................................................................*/
{
   int nrec;

   nrec = parms.nrec - ensemble.nrej[ipos];

   ensemble.u_mean_err[ipos] *= ci_factor[nrec-1] / sqrt( nrec );
   ensemble.u_ms_err[ipos]   *= ci_factor[nrec-1] / sqrt( nrec );
   ensemble.u_rms_err[ipos]  *= ci_factor[nrec-1] / sqrt( nrec );
   ensemble.u_skew_err[ipos] *= ci_factor[nrec-1] / sqrt( nrec );
   ensemble.u_flat_err[ipos] *= ci_factor[nrec-1] / sqrt( nrec );

   if (parms.dim == 2) {
      ensemble.v_mean_err[ipos] *= ci_factor[nrec-1] / sqrt( nrec );
      ensemble.v_ms_err[ipos]   *= ci_factor[nrec-1] / sqrt( nrec );
      ensemble.v_rms_err[ipos]  *= ci_factor[nrec-1] / sqrt( nrec );
      ensemble.v_flat_err[ipos] *= ci_factor[nrec-1] / sqrt( nrec );
      ensemble.uv_err[ipos]     *= ci_factor[nrec-1] / sqrt( nrec );
   }

   return;
}


/*************************************************************************/
```

```
void global_average(void)

/* This subroutine calculates the global mean velocity and grid Reynolds number
.....*/
{
   int ipos, nrej;
   float u_norm, t, t0, mu;

   t0 = parms.t0 / 1.8;
   t = t0 * pow( parms.p / parms.p0, 0.285714 );
   global.rho = parms.p * 101325 / ( 14.7 * 287 * t);
   mu = 1.716e-5 * pow( t/273, 1.5) * 384 / (t+111);
   global.nu = mu / global.rho;

   for (ipos = 0, global.u_mean = 0; ipos < parms.npos; ipos++)
      global.u_mean += (1 - ensemble.reject[ipos]) * ensemble.u_mean[ipos];

   global.u_mean /= parms.npos - global.nrej;
   global.re_m = global.u_mean * parms.mesh_length / (1000. * global.nu);

   global.u_norm = ( parms.u_norm == -1 ? global.u_mean : parms.u_norm );
   for (ipos = 0; ipos < parms.npos; ipos++) {
      ensemble.u_mean[ipos]     /= global.u_norm;
      ensemble.u_mean_err[ipos] /= global.u_norm;
      ensemble.v_mean[ipos]     /= global.u_norm;
      ensemble.v_mean_err[ipos] /= global.u_norm;
   }

   global.mach_p = sqrt( 5 * (t0/t - 1) );
   global.mach_u = global.u_mean / sqrt( 1.4 * 287 * t );

   return;
}


/*****************************************************************************/

void power_law(void)

/* This subroutine calculates least-squares curve fits for various values of
   the effective origin.  Data is written to [name].reg.
.....*/
{
   float x0;
   int i, ipos;
   char fregx[80];
   FILE *fid;

   strcpy(fregx, parms.fout);
   strcat(fregx, ".reg");

   if ((fid = fopen(fregx,"w")) == NULL)
      printf("*** Error opening regression file %s.\n", fregx);
   else
      printf("\n\nWriting regression summary %s.\n", fregx);

   fprintf(fid, "\n   x0    u-coef    u-exp    u-ci    u-cor");
   for (i=-10; i<=25; i++) {
       x0 = 1. * i;
       curve_fit( x0);
       fprintf(fid, "\n %5.1f  %7.4f  %7.4f  %7.4f  %7.4f",
                x0, global.u_coef, global.u_exp, global.u_ci, global.u_cor);
   }
   curve_fit( parms.x0 );

   for (ipos=0; ipos < parms.npos; ipos++)
      ensemble.u_ms_reg[ipos] = global.u_coef *
                          pow(ensemble.dist1[ipos]-parms.x0, -global.u_exp);

   if (parms.dim == 2)
      for (ipos=0; ipos < parms.npos; ipos++)
         ensemble.v_ms_reg[ipos] = global.v_coef *
                          pow(ensemble.dist1[ipos]-parms.x0, -global.v_exp);

   printf("\nMach-p = %7.3f; Mach-u = %7.3f", global.mach_p, global.mach_u);
   printf("\nU-mean = %7.3f; Re_m = %8.f", global.u_mean, global.re_m);
   printf("\nU-coef = %7.5f; U-exp = %7.4f", global.u_coef, global.u_exp);
   printf("; U-exp-ci = %7.4f; U-cor = %7.4f", global.u_ci, global.u_cor);
   printf("\nV-coef = %7.5f; V-exp = %7.4f", global.v_coef, global.v_exp);
   printf("; V-exp-ci = %7.4f; V-cor = %7.4f", global.v_ci, global.v_cor);
```

```
   if (fclose(fid) == EOF)
      printf("  Error closing output file %s ", fregx);

   return;
}


/*************************************************************************/

void curve_fit(float x0)

/* This subroutine calculates the decay law exponent and coefficient
   using the least squares curve fit in log-log space.
   ..........................................................................*/
{
   float log_u2, log_v2, log_x;
   float sum_x, sum_y, sum_xx, sum_xy, sum_yy;
   float sxx, syy, sxy;
   int ipos, npos;

   npos = parms.npos - global.nrej;
   for (ipos=0, sum_x=0, sum_y=0, sum_xx=0, sum_xy=0, sum_yy=0;
                                        ipos < parms.npos; ipos++) {
      log_x  = (1-ensemble.reject[ipos]) * log10( ensemble.dist1[ipos] - x0 );
      log_u2 = (1-ensemble.reject[ipos]) * log10( ensemble.u_ms[ipos] );
      sum_x += log_x;
      sum_y += log_u2;
      sum_xx += log_x * log_x;
      sum_xy += log_x * log_u2;
      sum_yy += log_u2 * log_u2;
   }
   sxy  = (sum_xy - sum_x*sum_y/npos );
   sxx  = (sum_xx - sum_x*sum_x/npos );
   syy  = (sum_yy - sum_y*sum_y/npos );
   global.u_exp  = sxy / sxx;
   global.u_coef = pow(10, (sum_y - global.u_exp*sum_x) / npos);
   global.u_cor  = sxy / sqrt( sxx * syy + EPS);
   global.u_ci   = ci_factor[npos-2] * sqrt( (syy-sxx*pow(global.u_exp,2))
                    / ( (npos-2) * (npos-1) * sxx) );

   if (parms.dim == 2) {
      for (ipos=0, sum_x=0, sum_y=0, sum_xx=0, sum_xy=0, sum_yy=0;
                                        ipos < parms.npos; ipos++) {
         log_x  = (1-ensemble.reject[ipos]) * log10( ensemble.dist1[ipos] - x0 );
         log_v2 = (1-ensemble.reject[ipos]) * log10( ensemble.v_ms[ipos] );
         sum_x += log_x;
         sum_y += log_v2;
         sum_xx += log_x * log_x;
         sum_xy += log_x * log_v2;
         sum_yy += log_v2 * log_v2;
      }
      sxy  = (sum_xy - sum_x*sum_y/npos );
      sxx  = (sum_xx - sum_x*sum_x/npos );
      syy  = (sum_yy - sum_y*sum_y/npos );
      global.v_exp  = sxy / sxx;
      global.v_coef = pow(10, (sum_y - global.v_exp*sum_x) / npos);
      global.v_cor  = sxy / sqrt( sxx * syy + EPS);
      global.v_ci   = ci_factor[npos-2] * sqrt( (syy-sxx*pow(global.v_exp,2))
                       / ( (npos-2) * (npos-1) * sxx) );
   }

   global.u_exp *= -1;
   global.v_exp *= -1;

   return;
}


/*************************************************************************/

void calc_scales(void)

/* This subroutine calculates various turbulence scales and characteristics.
   ..........................................................................*/
{
   float dist;
   int ipos;

   for (ipos = 0; ipos < parms.npos; ipos++) {
       dist = ensemble.dist1[ipos] - parms.x0) * parms.mesh_length / 1000;
       ensemble.tay[ipos] = sqrt( 10 * global.nu * dist /
```

```
                        ( global.u_exp * ensemble.u_mean[ipos] *
    global.u_norm) ),
       ensemble.re_tay[ipos] = sqrt( ensemble.u_ms_reg[ipos] *
                               pow( ensemble.u_mean[ipos] * global.u_norm, 2)) *
                               ensemble.tay[ipos] / global.nu,
       ensemble.diss[ipos] = 1.5 * 1000 *
                               pow( ensemble.u_mean[ipos]*global.u_norm, 3) *
     global.u_exp * global.u_coef / parms.mesh_length *
                               pow( ensemble.dist1[ipos] - parms.x0, -global.u_exp-1 ),
       ensemble.kol[ipos] = pow( (pow(global.nu, 3) / ensemble.diss[ipos]), 0.25),
       ensemble.integral[ipos] = pow( ensemble.u_ms_reg[ipos] *
                                 pow( ensemble.u_mean[ipos]*global.u_norm, 2), 1.5) /
 ensemble.diss[ipos];
    }

    return;
}


/*****************************************************************************/

void bubble_sort(void)

/* This subroutine sorts the ensemble data in increasing order of distance
.....................................................................*/
{
    int i, j, temp;

    for (i = 0; i < parms.npos; i++)
       ensemble.ptr[i] = i;

    if (parms.sort == TRUE) {
       for (i = 0; i < parms.npos-1; i++)
          for (j = 0; j < parms.npos-1; j++)
              if (ensemble.dist1[ensemble.ptr[j]] >
                    ensemble.dist1[ensemble.ptr[j+1]] ) {
         temp = ensemble.ptr[j];
         ensemble.ptr[j] = ensemble.ptr[j+1];
         ensemble.ptr[j+1] = temp;
       }
    }

    return;
}


/*****************************************************************************/

void write_data(void)

/* This subroutine controls writing of the output data.  Files for graphing
   are:
      [name]_mn.dat     (mean velocities)
      [name]_ms.dat     (mean-square velocities)
      [name]_sk.dat     (skewness factors)
      [name]_fl.dat     (flatness factors)
      [name]_uv.dat     (shear stress correlation coefficients)
      [name]_sc.dat     (turbulence scales)
   The columns (except for uv and sc) are:
      Column 1:  position (dist1 or dist2)
      Column 2:  number of rejected records.
      Column 3:  ensemble mean; first component.
      Column 4:  confidence interval for mean; first component.
      Column 5:  regression value (for ms only); first component
      Column 6,7,8:  same as 4,5,6, but for second component (if measured).

.....................................................................*/
{
    write_sum();

    write_file("_mn.dat", ensemble.dist2, ensemble.u_mean, ensemble.u_mean_err,
                          ensemble.zeros, ensemble.v_mean, ensemble.v_mean_err,
 ensemble.zeros);
    write_file("_ms.dat", ensemble.dist1, ensemble.u_ms, ensemble.u_ms_err,
                          ensemble.u_ms_reg, ensemble.v_ms, ensemble.v_ms_err,
 ensemble.v_ms_reg);
    write_file("_sk.dat", ensemble.dist1, ensemble.u_skew, ensemble.u_skew_err,
                          ensemble.zeros, ensemble.v_skew, ensemble.v_skew_err,
 ensemble.zeros);
    write_file("_fl.dat", ensemble.dist1, ensemble.u_flat, ensemble.u_flat_err,
                          ensemble.zeros, ensemble.v_flat, ensemble.v_flat_err,
```

```
 ensemble zeros),
   write_file("_uv dat", ensemble.dist1, ensemble.uv, ensemble.uv_err,
                         ensemble.zeros, ensemble.uov, ensemble.zeros,
 ensemble zeros),
   write_file("_sc dat", ensemble.dist1, ensemble integral, ensemble.tay,
                         ensemble.ksl,  ensemble.diss, ensemble re_tay,
 ensemble zeros),

   return,
}


/*********************************.*****************************************/

void write_sum(void)

/* This subroutine writes a summary of the input data and the point data.
. . . . . .  . . . . . .....................................................*/
{
   char foutx[80], fsumx[80];
   FILE *fid;

   strcpy(foutx, parms.fout);
   strcat(foutx, ".out");

   if ((fid = fopen(foutx,"w")) == NULL)
      printf("*** Error opening record output file %s.\n", foutx);
   else
      printf("\n\nWriting record output summary %s.", foutx);

   write_inp(fid);
   write_rec(fid);

   if (fclose(fid) == EOF)
      printf("*** Error closing record output file %s.", foutx);

   strcpy(fsumx, parms.fout);
   strcat(fsumx, ".sum");

   if ((fid = fopen(fsumx,"w")) == NULL)
      printf("*** Error opening ensemble output file %s.\n", fsumx);
   else
      printf("\n\nWriting ensemble output summary %s.\n\n", fsumx);

   write_inp(fid);
   write_ens(fid);

   if (fclose(fid) == EOF)
      printf("*** Error closing ensemble output file %s.", foutx);

   return;
}



/*************************************************************************/

void write_inp(FILE *fid)

/* This subroutine writes a summary of the input and global data.
.....................................................................*/
{
   fprintf(fid,
     "------------------------------ Input Parameters ------------------------------");
   fprintf(fid, "\n  Input filename       = %s"         , parms.finp);
   fprintf(fid, "\n  Number of positions  = %2d        ", parms.npos);
   fprintf(fid, "    Number of records    = %d"         , parms.nrec);
   fprintf(fid, "\n  Starting position    = %5.1f mm  " , parms.xoff);
   fprintf(fid, "    Increment            = %6.4f mm"   , parms.x_inc);
   fprintf(fid, "\n  Mesh length          = %5.2f mm  " , parms.mesh_length);
   fprintf(fid, "    Normalizing velocity = %5.1f m/s"  , parms.u_norm);
   fprintf(fid, "\n  Static pressure      = %6.2f psi"  , parms.p);
   fprintf(fid, "    Total pressure       = %6.2f psi"  , parms.p0);
   fprintf(fid, "\n  Traverse direction   = %c         ", parms.dirn='x');
   fprintf(fid, "    Total temperature    = %6.2f R"    , parms.t0);
   fprintf(fid, "\n  Transform method     = %d         ", parms.transform);
   fprintf(fid, "    Weighting method     = %d"         , parms.weight_method);
   fprintf(fid, "\n  x0/m                 = %5.2f     " , parms.x0);

   if (parms.rem_outliers == TRUE) {
      fprintf(fid, "\n  Outliers removed:");
```

```
      fprintf(fid, "  Sample st  dev  = %6.2f," , parms.sample_sd),
      fprintf(fid, "  Record st  dev  = %6.2f"      , parms.record_sd),
   } else
      fprintf(fid, "\n  Outliers not removed ");

   fprintf(fid,
     "\n\n------------------------------ Global Information ----------------------------");
   fprintf(fid, "\n  nu = %11.3e kg/(m s)         "  , global.nu),
   fprintf(fid, "; rho = %11.3e kg/m3"              , global.rho);
   fprintf(fid, "\n  Mach-p = %7.3f; Mach-u = %6.3f", global.mach_p, global.mach_u),
   fprintf(fid, "; U-mean   = %7.3f; Re_m  = %7.f"  , global.u_mean, global.re_m);
   fprintf(fid, "\n  U-coef = %7.5f; U-exp = %7.4f" , global.u_coef, global.u_exp);
   fprintf(fid, "; U-exp-ci = %7.4f; U-cor = %7.4f" , global.u_ci, global.u_cor);
   fprintf(fid, "\n  V-coef = %7.5f; V-exp = %7.4f" , global.v_coef, global.v_exp);
   fprintf(fid, "; V-exp-ci = %7.4f; V-cor = %7.4f" , global.v_ci, global.v_cor);

   return;
}


/*************************************************************************/

void write_rec(FILE *fid)

/* This subroutine writes a summary of the record data.
.........................................................................*/
{
   int ipos, irec;

   fprintf(fid,
     "\n\n------------------------------ Record Information ----------------------------");
   fprintf(fid, "\npos nsam out rate  pc R");
   fprintf(fid, "   umean   urms  uskew  vmean   vrms  vskew    uv   usv");
   for (ipos = 0; ipos < parms.npos; ipos++) {
      for (irec = 0; irec < parms.nrec; irec++) {
         fprintf(fid,"\n %2.f %4d %3d %4.f %3.f %1d",
     point[irec].pos[ipos], point[irec].nval[ipos],
     point[irec].nrej[ipos], point[irec].data_rate[ipos],
     point[irec].pval[ipos], point[irec].reject[ipos]);
fprintf(fid," %7.2f %6.3f %6.3f %6.2f %6.3f %6.3f %6.3f",
     moment[irec].u_mean[ipos], moment[irec].u_rms[ipos],
     moment[irec].u_skew[ipos], moment[irec].v_mean[ipos],
     moment[irec].v_rms[ipos], moment[irec].v_skew[ipos],
     moment[irec].uv[ipos]);
      }
   }

   return;
}


/*************************************************************************/

void write_ens(FILE *fid)

/* This subroutine writes a summary of the ensemble-averaged data.
.........................................................................*/
{
   int ipos, ptr;

   fprintf(fid,
     "\n\n------------------------------ Ensemble Information ----------------------------");
   fprintf(fid, "\n pos  Order  nsam  Rate(avg)  %%Val(avg)  nrej(avg)  Rec_rej");
   for (ipos = 0; ipos < parms.npos; ipos++) {
      ptr = ensemble.ptr[ipos];
      fprintf(fid, "\n%5.2f  %2d  %6.f  %6.f  %10.1f  %8.1f  %7d",
   ensemble.dist1[ptr], ptr, ensemble.nval[ptr],
   ensemble.data_rate[ptr], ensemble.pval[ptr],
   ensemble.sam_rej[ptr], ensemble.nrej[ptr]);
   }

   fprintf(fid, "\n\n pos      U    U_ci    u'   u'_ci");
   fprintf(fid, "    V   V_ci    v'   v'_ci uv/u'v' u'/v' u_sk   u_fl");
   for (ipos = 0; ipos < parms.npos; ipos++) {
      ptr = ensemble.ptr[ipos];
      fprintf(fid, "\n%5.2f  %6.2f %5.2f  %5.3f  %5.3f",
   ensemble.dist1[ptr], ensemble.u_mean[ptr]*global.u_norm,
   ensemble.u_mean_err[ptr]*global.u_norm,
   ensemble.u_rms[ptr], ensemble.u_rms_err[ptr] );
```

```
      fprintf(fid, " %5.2f %5.2f  %5.3f  %5.3f %6.3f  %4.2f %6.3f  %4.2f",
   ensemble.v_mean[ptr]*global.u_norm,
   ensemble.v_mean_err[ptr]*global.u_norm,
   ensemble.v_rms[ptr], ensemble.v_rms_err[ptr], ensemble.uv[ptr],
   ensemble.uev[ptr], ensemble.u_skew[ptr], ensemble.u_flat[ptr] );
   }

   fprintf(fid, "\n\n pos     U/Um     u'2/U2");
   fprintf(fid, "    integral    taylor     kolmog   diss rate  Re_tay");
   for (ipos = 0; ipos < parms.npos; ipos++) {
      ptr = ensemble.ptr[ipos];
      fprintf(fid, "\n%5.2f  %6.3f %11.3e",
           ensemble.dist[ptr], ensemble.u_mean[ptr], ensemble.u_ms[ptr] );
      fprintf(fid, " %10.3e %10.3e %10.3e %10.3e   %5.1f",
   ensemble.integral[ptr], ensemble.tay[ptr], ensemble.kol[ptr],
   ensemble.diss[ptr], ensemble.re_tay[ptr] );
   }

   fprintf(fid,
     "\n\n---------------------------------- Comments ----------------------------------");

   return;
}


/*************************************************************************/

void write_file(char *ext, float *dist, float *udat, float *udat_err,
          float *udat_reg, float *vdat, float *vdat_err, float *vdat_reg)

/* This subroutine writes individual output files.
.........................................................................*/

{
   int ipos, ptr;
   char foutx[80];
   FILE *fid;

   strcpy(foutx, parms.fout);
   strcat(foutx, ext);

   if ((fid= fopen(foutx,"w")) == NULL)
      printf("*** Error opening output file %s.\n", foutx);
   else
      printf("Writing output file %s.\n", foutx);

   for (ipos = 0; ipos < parms.npos; ipos++) {
      ptr = ensemble.ptr[ipos];
      if (ensemble.reject[ptr] == FALSE)
         fprintf(fid, "%5.2f %1d %11.3e %11.3e %11.3e %11.3e %11.3e %11.3e\n",
                dist[ptr], ensemble.nrej[ptr],
 udat[ptr], udat_err[ptr], udat_reg[ptr],
 vdat[ptr], vdat_err[ptr], vdat_reg[ptr] );
   }

   fprintf(fid, "\n");
   for (ipos = 0; ipos < parms.npos; ipos++) {
      ptr = ensemble.ptr[ipos];
      if (ensemble.reject[ptr] == TRUE)
         fprintf(fid, "%5.2f %1d %11.3e %11.3e %11.3e %11.3e %11.3e %11.3e\n",
                dist[ptr], ensemble.nrej[ptr],
 udat[ptr], udat_err[ptr], udat_reg[ptr],
 vdat[ptr], vdat_err[ptr], vdat_reg[ptr] );
   }

   if (fclose(fid) == EOF)
      printf("  Error closing output file %s.", foutx);

   return;
}


/*************************************************************************/

void wrap_up(void)

/* This subroutine wraps things up.
.........................................................................*/
{
```

```
    if (fclose(frej) == EOF)
       printf("  Error closing rejection file.");

    return;
}
```

Appendix D

Detailed Measurement Data

In this appendix, the results of most mesurements are tabulated. The results for each case are compiled on a different page. An explanation of some of the parameters and headings is given below:

- `Input filename` - the label given to the case, ordered by date; eg., `j28x2` was the second experiment taken on June 28.
- `Normalizing velocity` - the value for U_m when normalizing the mean velocity. If -1 is specified, the program calculates it as the average over all measuring locations.
- `Transform method` - gives transformation matrix for measured velocities. Options are: untransformed (1), change sign of V-velocity (2), or rotate by 45°(3).
- `Weighting method` - unweighted (1), transit-time-weighted (2), or inter-arrival time-weighted (3).
- `Sample st. dev.` - the number of standard deviations beyond which velocity samples are rejected.
- `Record st. dev.` - the number of standard deviations beyond which records are rejected.
- `nu, rho` - kinematic viscosity and density
- `Mach-p, Mach-u` - the Mach numbers calculated from the pressure ratio and mean velocity, respectively.

- `U-mean` - velocity averaged over all measuring locations.
- `Re_m` - Reynolds number based on U-mean and mesh length.
- `U-coef, V-coef` - coefficients of decay law.
- `U-exp, V-exp` - exponents of decay law.
- `U-exp-ci, V-exp-ci` - 90% confidence interval for U-exp and V-exp.
- `U-cor, V-cor` - correlation coefficients of curve fit.
- `pos` - x/m (x-traverses), y/h (y-traverses), z/h (z-traverses), or P_{t0} (pressure traverses).
- `Order` - the order in which the positions were traversed.
- `Rate` - data rate (Hz), averaged over all records at that location.
- `%Val` - the validation level, averaged over all records at that location.
- `nrej` - the number of samples rejected, averaged over all records at that location.
- `Rec_rej` - the number of records rejected at that location.
- `U, V, U_ci, V_ci` - mean velocities and 95% confidence intervals.
- `u', v', u'_ci, v'_ci` - rms velocities and 95% confidence intervals.

The remaining headings are considered self-explanatory. Unless otherwise noted, all units are SI. The length scales and dissipation rate are calculated from the decay law.

```
------------------------------ Input Parameters ------------------------------
  Input filename       = j5z1
  Number of positions  = 10            Number of records    = 5
  Starting position    = 747.0 mm      Increment            = 25.4000 mm
  Mesh length          = 14.50 mm      Normalizing velocity =  -1.0 m/s
  Static pressure      =  21.20 psi    Total pressure       =  22.00 psi
  Traverse direction   = z             Total temperature    = 547.50 R
  Transform method     = 2             Weighting method     = 2
  x0/m                 =  5.00
  Outliers removed.  Sample st. dev. =   3.00.  Record st. dev. =   2.50

------------------------------ Global Information ----------------------------
  nu =  1.094e-005 kg/(m s)        ; rho =  1.692e+000 kg/m3
  Mach-p =   0.231; Mach-u =  0.158; U-mean   =  55.015; Re_m =   72891
  U-coef = 0.01931; U-exp =  1.0064; U-exp-ci =  0.0336; U-cor = -0.9886
  V-coef = 0.01215; V-exp =  0.9048; V-exp-ci =  0.0296; V-cor = -0.9890

---------------------------- Ensemble Information ---------------------------
 pos  Order  nsam  Rate(avg)  %Val(avg)  nrej(avg)  Rec_rej
51.52   0    3000     5862        29.0       17.2        0
53.27   1    3000     7377        43.9       13.8        0
55.02   2    3000     7051        47.4       13.8        0
56.77   3    3000     7004        48.4       13.4        0
58.52   4    3000     6412        47.9       18.0        0
60.28   5    3000     6797        52.5       17.4        0
62.03   6    3000     5943        52.1       17.2        0
63.78   7    3000     6510        53.2       15.6        0
65.53   8    3000     5783        54.9       17.2        0
67.28   9    3000     2811        60.3       16.8        0

 pos      U    U_ci    u'    u'_ci    V    V_ci    v'    v'_ci uv/u'v' u'/v' u_sk   u_fl
51.52  54.56  0.21  1.094  0.016  0.28  0.08  1.070  0.002  0.006  1.02  0.041  2.82
53.27  54.78  0.22  1.091  0.014  0.24  0.08  1.044  0.002 -0.003  1.05 -0.002  2.81
55.02  54.87  0.19  1.054  0.009  0.22  0.08  1.022  0.002 -0.015  1.03 -0.016  2.79
56.77  54.95  0.23  1.054  0.011  0.24  0.06  1.009  0.002  0.010  1.04 -0.019  2.79
58.52  55.03  0.22  1.031  0.010  0.30  0.07  1.003  0.002  0.006  1.03  0.030  2.80
60.28  55.06  0.24  1.011  0.015  0.27  0.07  0.987  0.001 -0.009  1.03 -0.007  2.82
62.03  55.12  0.19  1.012  0.016  0.29  0.09  0.979  0.001 -0.024  1.03  0.006  2.80
63.78  55.20  0.20  0.986  0.024  0.27  0.08  0.956  0.001 -0.005  1.03 -0.042  2.88
65.53  55.22  0.19  0.980  0.013  0.31  0.11  0.951  0.001 -0.028  1.03  0.017  2.82
67.28  55.35  0.22  0.953  0.011  0.32  0.06  0.949  0.001 -0.013  1.00  0.026  2.87

 pos     U/Um     u'2/U2     integral     tayler     kolmog   diss rate  Re_tay
51.52   0.992  4.018e-004  8.99e-003  1.16e-003  5.46e-005  1.47e+002   116.3
53.27   0.996  3.967e-004  9.16e-003  1.18e-003  5.55e-005  1.38e+002   116.6
55.02   0.997  3.688e-004  9.32e-003  1.20e-003  5.64e-005  1.29e+002   116.6
56.77   0.999  3.679e-004  9.48e-003  1.22e-003  5.73e-005  1.21e+002   116.7
58.52   1.000  3.508e-004  9.64e-003  1.24e-003  5.82e-005  1.14e+002   116.8
60.28   1.001  3.373e-004  9.80e-003  1.26e-003  5.92e-005  1.07e+002   116.8
62.03   1.002  3.371e-004  9.95e-003  1.28e-003  6.00e-005  1.01e+002   116.9
63.78   1.003  3.189e-004  1.01e-002  1.30e-003  6.09e-005  9.53e+001   116.9
65.53   1.004  3.149e-004  1.02e-002  1.31e-003  6.18e-005  9.00e+001   116.9
67.28   1.006  2.964e-004  1.04e-002  1.33e-003  6.26e-005  8.56e+001   117.1

--------------------------------- Comments ---------------------------------
- DT = 1.2 (24%); CJ = 5.0; PO = 22 psi
- 160 mm lens; 40 MHz frequency shift
- ensemble average of 5 separate traverses (y = -.5,0..5; z=-.5,0,.5)
- Thesis label: HS1a
```

---------- Input Parameters ----------

Input filename	= j5x6		
Number of positions	= 9	Number of records	= 1
Starting position	= 747.0 mm	Increment	= 25.4000 mm
Mesh length	= 14.50 mm	Normalizing velocity	= 55.4 m/s
Static pressure	= 21.20 psi	Total pressure	= 22.00 psi
Traverse direction	= z	Total temperature	= 547.50 F
Transform method	= 2	Weighting method	= 2
x0/m	= 0.00		

Outliers removed: Sample st. dev. = 3.00; Record st. dev. = 2.50

---------- Global Information ----------

nu = 1.094e-005 kg/(m s) ; rho = 1.692e+000 kg/m3

Mach-p = 0.231; Mach-u = 0.158, U-mean = 54.818; Re_m = 72629

U-coef = 0.00000; U-exp = 0.0000; U-exp-ci = 0.0000; U-cor = 0.0000

V-coef = 0.00000; V-exp = 0.0000; V-exp-ci = 0.0000; V-cor = 0.0000

---------- Ensemble Information ----------

pos	Order	nsam	Rate(avg)	%Val(avg)	nrej(avg)	Rec_rej
-0.31	0	3000	229	84.3	13.0	0
-0.24	1	3000	763	72.1	19.0	0
-0.16	2	3000	892	47.9	25.0	0
-0.08	3	3000	5331	39.5	17.0	0
0.00	4	3000	4531	31.2	15.0	0
0.08	5	1764	757	7.8	7.0	0
0.16	6	3000	3972	30.2	26.0	0
0.24	7	3000	681	16.7	17.0	0
0.31	8	3000	3012	40.3	30.0	0

pos	U	U_ci	u'	u'_ci	V	V_ci	v'	v'_ci	uv/u'v'	u'/v'	u_sk	u_fl
-0.31	54.35	0.00	0.995	0.000	0.05	0.00	0.931	0.000	6.001	1.07	0.066	2.87
-0.24	54.62	0.00	0.979	0.000	0.19	0.00	0.945	0.000	-0.055	1.04	0.003	2.76
-0.16	54.89	0.00	0.974	0.000	0.19	0.00	0.948	0.000	-0.001	1.03	-0.004	2.88
-0.08	55.01	0.00	1.023	0.000	0.27	0.00	0.972	0.000	0.007	1.05	-0.020	2.85
0.00	55.36	0.00	1.019	0.000	0.21	0.00	1.035	0.000	-0.009	0.98	0.039	2.96
0.08	55.33	0.00	1.019	0.000	0.11	0.00	1.040	0.000	-0.002	0.98	0.013	2.99
0.16	54.84	0.00	1.100	0.000	0.16	0.00	1.085	0.000	0.059	1.01	0.025	2.81
0.24	54.70	0.00	1.109	0.000	0.01	0.00	1.154	0.000	0.050	0.96	0.024	2.72
0.31	54.27	0.00	1.173	0.000	0.09	0.00	1.163	0.000	0.056	1.01	-0.055	2.84

pos	U/Um	u'2/U2	integral	taylor	kolmog	diss rate	Re_tay
-0.31	0.982	3.350e-004	0.00e+000	0.00e+000	0.00e+000	0.00e+000	0.0
-0.24	0.987	3.214e-004	0.00e+000	0.00e+000	0.00e+000	0.00e+000	0.0
-0.16	0.992	3.146e-004	0.00e+000	0.00e+000	0.00e+000	0.00e+000	0.0
-0.08	0.994	3.459e-004	0.00e+000	0.00e+000	0.00e+000	0.00e+000	0.0
0.00	1.000	3.386e-004	0.00e+000	0.00e+000	0.00e+000	0.00e+000	0.0
0.08	0.999	3.391e-004	0.00e+000	0.00e+000	0.00e+000	0.00e+000	0.0
0.16	0.991	4.025e-004	0.00e+000	0.00e+000	0.00e+000	0.00e+000	0.0
0.24	0.988	4.111e-004	0.00e+000	0.00e+000	0.00e+000	0.00e+000	0.0
0.31	0.980	4.674e-004	0.00e+000	0.00e+000	0.00e+000	0.00e+000	0.0

---------- Comments ----------

- DT = 1.2 (24%); CJ = 5.0; P0 = 22 psi
- 160 mm lens; 40 MHz frequency shift
- same conditions as j5x1
- z-traverse

```
------------------------------ Input Parameters ------------------------------
  Input filename        = j5z7
  Number of positions   =  9            Number of records     = 1
  Starting position     = 747.0 mm      Increment             = 25.4000 mm
  Mesh length           = 14.50 mm      Normalizing velocity =  55.3 m/s
  Static pressure       =  21.20 psi    Total pressure        =  22.00 psi
  Traverse direction    = y             Total temperature     = 547.50 R
  Transform method      = 2             Weighting method      = 2
  z0/m                  =  0.00
  Outliers removed   Sample st. dev  =   3.00;  Record st. dev. =   2.50

------------------------------ Global Information ----------------------------
  nu =  1.094e-005 kg/(m s)        ; rho =  1.692e+000 kg/m3
  Mach-p =   0.231, Mach-u =  0.157; U-mean    =  54.541; Re_m  =   72263
  U-coef = 0.00000, U-exp =  0.0000; U-exp-ci =  0.0000; U-cor =  0.0000
  V-coef = 0.00000, V-exp =  0.0000, V-exp-ci =  0.0000, V-cor =  0.0000

---------------------------- Ensemble Information ----------------------------
 pos  Order  nsam  Rate(avg)  %Val(avg)  nrej(avg)  Rec_rej
-0.31   0     687      244         4.7        3.0        0
-0.24   1    3000      770         9.0       18.0        0
-0.16   2    3000     1866        16.0       22.0        0
-0.08   3    3000     3010        22.4       18.0        0
 0.00   4    3000     4173        32.4        7.0        0
 0.08   5    3000     3929        35.7       22.0        0
 0.16   6    3000     2539        41.4       13.0        0
 0.24   7    3000     1236        52.1       20.0        0
 0.31   8    3000      503        59.4       17.0        0

 pos      U    U_ci     u'    u'_ci     V    V_ci     v'    v'_ci uv/u'v' u'/v' u_sk   u_fl
-0.31   53.48  0.00  1.195  0.000 -0.47  0.00  0.944  0.000 -0.199  1.27  0.087  2.77
-0.24   54.10  0.00  1.102  0.000 -0.24  0.00  1.006  0.000 -0.175  1.10 -0.020  2.73
-0.16   54.60  0.00  1.077  0.000 -0.12  0.00  0.972  0.000 -0.161  1.11  0.007  2.73
-0.08   55.06  0.00  1.047  0.000  0.05  0.00  0.950  0.000 -0.121  1.10  0.016  2.79
 0.00   55.35  0.00  1.009  0.000  0.20  0.00  0.943  0.000 -0.028  1.07 -0.026  2.96
 0.08   55.17  0.00  1.000  0.000  0.50  0.00  0.926  0.000  0.050  1.08 -0.040  2.88
 0.16   54.90  0.00  1.034  0.000  0.58  0.00  0.947  0.000  0.132  1.09 -0.071  2.79
 0.24   54.35  0.00  1.051  0.000  0.71  0.00  0.912  0.000  0.096  1.15 -0.028  2.78
 0.31   53.85  0.00  1.090  0.000  0.75  0.00  0.950  0.000  0.176  1.15  0.033  2.72

 pos     U/Um     u'2/U2     integral     taylor      kolmog     diss rate  Re_tay
-0.31   0.966  4.988e-004  0.00e+000  0.00e+000  0.00e+000  0.00e+000      0.0
-0.24   0.977  4.152e-004  0.00e+000  0.00e+000  0.00e+000  0.00e+000      0.0
-0.16   0.986  3.889e-004  0.00e+000  0.00e+000  0.00e+000  0.00e+000      0.0
-0.08   0.995  3.616e-004  0.00e+000  0.00e+000  0.00e+000  0.00e+000      0.0
 0.00   1.000  3.325e-004  0.00e+000  0.00e+000  0.00e+000  0.00e+000      0.0
 0.08   0.997  3.288e-004  0.00e+000  0.00e+000  0.00e+000  0.00e+000      0.0
 0.16   0.992  3.550e-004  0.00e+000  0.00e+000  0.00e+000  0.00e+000      0.0
 0.24   0.982  3.735e-004  0.00e+000  0.00e+000  0.00e+000  0.00e+000      0.0
 0.31   0.973  4.094e-004  0.00e+000  0.00e+000  0.00e+000  0.00e+000      0.0

---------------------------------- Comments ----------------------------------
- DT = 1.2 (24%); CJ = 5.0; PO = 22 psi
- 160 mm lens; 40 KHz frequency shift
- same conditions as j5z1
- y-traverse
```

---------- Input Parameters ----------

Input filename	= j5x10		
Number of positions	= 10	Number of records	= 5
Starting position	= 747.0 mm	Increment	= 25.4000 mm
Mesh length	= 18.40 mm	Normalizing velocity	= -1.0 m/s
Static pressure	= 12.71 psi	Total pressure	= 17.03 psi
Traverse direction	= x	Total temperature	= 547.50 R
Transform method	= 2	Weighting method	= 2
x0/m	= 0.00		

Outliers removed: Sample st. dev. = 3.00; Record st. dev. = 2.50

---------- Global Information ----------

nu = 1.603e-005 kg/(m s) ; rho = 1.091e+000 kg/m3

Mach-p = 0.660; Mach-u = 0.172; U-mean = 57.780; Re_m = 66308

U-coef = 0.01129; U-exp = 0.8744; U-exp-ci = 0.0638; U-cor = -0.9488

V-coef = 0.00540; V-exp = 0.6758; V-exp-ci = 0.0416; V-cor = -0.9627

---------- Ensemble Information ----------

pos	Order	nsam	Rate(avg)	%Val(avg)	nrej(avg)	Rec_rej
40.60	0	3000	8087	33.6	23.6	0
41.98	1	3000	7769	45.6	28.6	0
43.36	2	3000	7994	48.2	24.6	0
44.74	3	3000	7802	47.7	27.4	0
46.12	4	3000	6818	48.9	26.4	0
47.50	5	3000	8077	53.9	28.4	0
48.88	6	3000	7986	53.5	33.2	0
50.26	7	3000	8429	54.6	29.6	0
51.64	8	3000	7381	56.4	27.4	0
53.02	9	3000	3558	60.9	32.4	0

pos	U	U_ci	u'	u'_ci	V	V_ci	v'	v'_ci	uv/u'v'	u'/v'	u_sk	u_fl
40.60	57.40	0.04	1.232	0.029	0.13	0.08	1.206	0.002	0.006	1.02	-0.166	2.82
41.98	57.61	0.03	1.180	0.020	0.10	0.10	1.204	0.002	0.008	0.98	-0.155	2.91
43.36	57.67	0.05	1.182	0.026	0.09	0.07	1.178	0.001	0.020	1.00	-0.128	2.95
44.74	57.77	0.05	1.147	0.033	0.10	0.06	1.177	0.002	0.013	0.97	-0.147	3.04
46.12	57.77	0.07	1.156	0.037	0.21	0.13	1.180	0.002	0.037	0.98	-0.197	3.09
47.50	57.84	0.05	1.117	0.036	0.11	0.08	1.148	0.002	0.016	0.97	-0.142	3.09
48.88	57.82	0.08	1.115	0.025	0.11	0.09	1.129	0.002	-0.005	0.99	-0.160	3.08
50.26	57.91	0.05	1.123	0.035	0.13	0.08	1.122	0.002	0.027	1.00	-0.139	3.18
51.64	57.96	0.06	1.113	0.027	0.11	0.12	1.124	0.002	0.009	0.99	-0.134	3.25
53.02	58.06	0.05	1.081	0.016	0.14	0.09	1.128	0.003	-0.010	0.96	-0.175	3.23

pos	U/Um	u'2/U2	integral	taylor	kolmog	diss rate	Re_tay
40.60	0.993	4.613e-004	1.20e-002	1.54e-003	7.28e-005	1.47e+002	116.4
41.98	0.997	4.195e-004	1.22e-002	1.57e-003	7.37e-005	1.40e+002	116.8
43.36	0.998	4.200e-004	1.24e-002	1.59e-003	7.48e-005	1.32e+002	117.1
44.74	1.000	3.946e-004	1.27e-002	1.62e-003	7.58e-005	1.25e+002	117.5
46.12	1.000	4.009e-004	1.29e-002	1.64e-003	7.69e-005	1.18e+002	117.7
47.50	1.001	3.736e-004	1.31e-002	1.66e-003	7.79e-005	1.12e+002	118.0
48.88	1.001	3.723e-004	1.33e-002	1.69e-003	7.89e-005	1.06e+002	118.2
50.26	1.002	3.767e-004	1.35e-002	1.71e-003	7.99e-005	1.01e+002	118.5
51.64	1.003	3.691e-004	1.37e-002	1.73e-003	8.09e-005	9.64e+001	118.7
53.02	1.005	3.469e-004	1.39e-002	1.76e-003	8.18e-005	9.23e+001	119.0

---------- Comments ----------

- DT = 1.2 (24%); CJ = 5.0; PO = 22 psi
- 160 mm lens; 40 MHz frequency shift
- Large-hole plate
- ensemble average of 5 separate traverses (y = -.5,0,.5; z=-.5,0,.5)

```
------------------------------ Input Parameters ------------------------------
  Input filename       = j5x16
  Number of positions  = 9              Number of records    = 1
  Starting position    = 747.0 mm       Increment            = 25.4000 mm
  Mesh length          = 18.40 mm       Normalizing velocity = -1.0 m/s
  Static pressure      =  21.20 psi     Total pressure       =  22.00 psi
  Traverse direction   = x              Total temperature    = 547.50 R
  Transform method     = 2              Weighting method     = 2
  z0/m                 =  0.00
  Outliers removed.  Sample st. dev  =   3.00;  Record st. dev. =   2.50

------------------------------ Global Information ----------------------------
  nu =  1.094e-005 kg/(m s)        ; rho =  1.692e+000 kg/m3
  Mach-p =   0.231, Mach-u =  0.166; U-mean   =  57.802; Re_m  =   97180
  U-coef = 0.00000; U-exp =  0.0000; U-exp-ci =  0.0000; U-cor =  0.0000
  V-coef = 0.00000; V-exp =  0.0000; V-exp-ci =  0.0000; V-cor =  0.0000

------------------------------ Ensemble Information --------------------------
 pos  Order  nsam  Rate(avg)  %Val(avg)  nrej(avg)  Rec_rej
-0.31   0    3000     198        84.6       35.0        0
-0.24   1    3000    1247        77.2       27.0        0
-0.16   2    3000    2293        60.8       24.0        0
-0.08   3    3000     794        11.8       41.0        0
 0.00   4    3000    4280        24.3       21.0        0
 0.08   5    3000    1066         9.8       33.0        0
 0.16   6    3000    1130        15.8       25.0        0
 0.24   7    3000    5555        35.0       46.0        0
 0.31   8    3000    2416        32.3       64.0        0

 pos      U    U_ci    u'    u'_ci    V    V_ci    v'    v'_ci uv/u'v' u'/v' u_sk   u_fl
-0.31   57.91  0.00  1.161  0.000  0.13  0.00  1.112  0.000 -0.052  1.04 -0.088  3.22
-0.24   58.29  0.00  1.035  0.000  0.18  0.00  1.018  0.000 -0.016  1.02 -0.090  3.22
-0.16   58.43  0.00  1.064  0.000  0.14  0.00  1.048  0.000 -0.038  1.02  0.084  3.06
-0.08   58.27  0.00  1.052  0.000  0.10  0.00  1.159  0.000  0.045  0.91  0.026  3.23
 0.00   57.90  0.00  1.110  0.000  0.09  0.00  1.224  0.000  0.018  0.91 -0.135  2.99
 0.08   57.83  0.00  1.155  0.000  0.03  0.00  1.259  0.000  0.009  0.92 -0.034  3.13
 0.16   57.55  0.00  1.217  0.000  0.13  0.00  1.294  0.000  0.034  0.94 -0.094  2.99
 0.24   57.59  0.00  1.313  0.000  0.20  0.00  1.248  0.000  0.007  1.05 -0.192  3.17
 0.31   56.46  0.00  2.024  0.000  0.29  0.00  1.601  0.000  0.015  1.26 -0.801  3.81

 pos     U/Um     u'2/U2     integral     taylor     kolmog     diss rate  Re_tay
-0.31   1.002  4.018e-004  0.00e+000  0.00e+000  0.00e+000  0.00e+000      0.0
-0.24   1.008  3.151e-004  0.00e+000  0.00e+000  0.00e+000  0.00e+000      0.0
-0.16   1.011  3.319e-004  0.00e+000  0.00e+000  0.00e+000  0.00e+000      0.0
-0.08   1.008  3.257e-004  0.00e+000  0.00e+000  0.00e+000  0.00e+000      0.0
 0.00   1.002  3.675e-004  0.00e+000  0.00e+000  0.00e+000  0.00e+000      0.0
 0.08   1.001  3.991e-004  0.00e+000  0.00e+000  0.00e+000  0.00e+000      0.0
 0.16   0.996  4.471e-004  0.00e+000  0.00e+000  0.00e+000  0.00e+000      0.0
 0.24   0.996  5.197e-004  0.00e+000  0.00e+000  0.00e+000  0.00e+000      0.0
 0.31   0.977  1.285e-003  0.00e+000  0.00e+000  0.00e+000  0.00e+000      0 0

---------------------------------- Comments ----------------------------------
- DT = 1.2 (24%); CJ = 5.0; P0 = 22 psi
- 160 mm lens; 40 MHz frequency shift
- Large-hole plate
- same conditions as j5x10
- x-traverse
```

---------- Input Parameters ----------

Input filename	= j5x17		
Number of positions	= 9	Number of records	= 1
Starting position	= 747.0 mm	Increment	= 25.4000 mm
Mesh length	= 18.40 mm	Normalizing velocity	= -1.0 m/s
Static pressure	= 21.20 psi	Total pressure	= 22.00 psi
Traverse direction	= y	Total temperature	= 547.50 R
Transform method	= 2	Weighting method	= 2
x0/m	= 0.00		

Outliers removed: Sample st. dev. = 3.00; Record st. dev. = 2.50

---------- Global Information ----------

nu = 1.094e-005 kg/(m s) ; rho = 1.692e+000 kg/m3

Mach-p = 0.231; Mach-u = 0.160; U-mean = 55.641; Re_m = 93548

U-coef = 0.00000; U-exp = 0.0000; U-exp-ci = 0.0000; U-cor = 0.0000

V-coef = 0.00000; V-exp = 0.0000; V-exp-ci = 0.0000; V-cor = 0.0000

---------- Ensemble Information ----------

pos	Order	nsam	Rate(avg)	IVal(avg)	nrej(avg)	Rec_rej
-0.31	0	1970	468	7.0	14.0	0
-0.24	1	3000	723	12.3	40.0	0
-0.16	2	3000	961	15.4	76.0	0
-0.08	3	3000	1521	25.7	36.0	0
0.00	4	3000	2712	35.2	27.0	0
0.08	5	3000	2553	34.0	32.0	0
0.16	6	3000	1575	40.0	57.0	0
0.24	7	3000	681	46.9	47.0	0
0.31	8	3000	284	58.9	25.0	0

pos	U	U_ci	u'	u'_ci	V	V_ci	v'	v'_ci	uv/u'v'	u'/v'	u_sk	u_fl
-0.31	52.02	0.00	3.092	0.000	-1.04	0.00	2.164	0.000	-0.309	1.43	-0.307	2.73
-0.24	54.84	0.00	2.631	0.000	-0.85	0.00	1.805	0.000	-0.255	1.46	-0.653	3.18
-0.16	56.99	0.00	1.667	0.000	-0.58	0.00	1.385	0.000	-0.158	1.20	-0.601	3.67
-0.08	57.88	0.00	1.188	0.000	-0.21	0.00	1.172	0.000	-0.071	1.01	-0.159	3.30
0.00	57.99	0.00	1.097	0.000	0.03	0.00	1.103	0.000	0.050	0.99	-0.135	3.10
0.08	57.75	0.00	1.158	0.000	0.38	0.00	1.166	0.000	0.093	0.99	-0.226	3.11
0.16	56.68	0.00	1.635	0.000	0.75	0.00	1.323	0.000	0.149	1.24	-0.621	3.59
0.24	54.64	0.00	2.361	0.000	1.08	0.00	1.655	0.000	0.270	1.43	-0.570	3.16
0.31	51.98	0.00	2.920	0.000	1.35	0.00	2.035	0.000	0.304	1.44	-0.400	2.84

pos	U/Um	u'2/U2	integral	tayler	kolmog	diss rate	Re_tay
-0.31	0.935	3.531e-003	0.00e+000	0.00e+000	0.00e+000	0.00e+000	0.0
-0.24	0.986	2.301e-003	0.00e+000	0.00e+000	0.00e+000	0.00e+000	0.0
-0.16	1.024	8.560e-004	0.00e+000	0.00e+000	0.00e+000	0.00e+000	0.0
-0.08	1.040	4.212e-004	0.00e+000	0.00e+000	0.00e+000	0.00e+000	0.0
0.00	1.042	3.581e-004	0.00e+000	0.00e+000	0.00e+000	0.00e+000	0.0
0.08	1.038	4.020e-004	0.00e+000	0.00e+000	0.00e+000	0.00e+000	0.0
0.16	1.019	8.316e-004	0.00e+000	0.00e+000	0.00e+000	0.00e+000	0.0
0.24	0.982	1.867e-003	0.00e+000	0.00e+000	0.00e+000	0.00e+000	0.0
0.31	0.934	3.154e-003	0.00e+000	0.00e+000	0.00e+000	0.00e+000	0.0

---------- Comments ----------

- DT = 1.2 (24%); CJ = 5.0; PO = 22 psi
- 160 mm lens; 40 KHz frequency shift
- Large-hole plate
- same conditions as j5x10
- y-traverse

---------- Input Parameters ----------

Input filename	= j27x1		
Number of positions	= 10	Number of records	= 20
Starting position	= 747.0 mm	Increment	= 25.4000 mm
Mesh length	= 14.50 mm	Normalizing velocity	= -1.0 m/s
Static pressure	= 13.30 psi	Total pressure	= 17.50 psi
Traverse direction	= x	Total temperature	= 542.00 R
Transform method	= 3	Weighting method	= 2
z0/m	= 0.00		

Outliers removed. Sample st. dev. = 3.00; Record st. dev. = 2.50

---------- Global Information ----------

nu = 1.519e-005 kg/(m s) ; rho = 1.147e+000 kg/m3

Mach-p = 0.639; Mach-u = 0.679; U-mean = 227.152; Re_m = 216853

U-coef = 0.20294; U-exp = 1.6865; U-exp-ci = 0.0377; U-cor = -0.9948

V-coef = 0.91719; V-exp = 2.0934; V-exp-ci = 0.0899; V-cor = -0.9813

---------- Ensemble Information ----------

pos	Order	nsam	Rate(avg)	ZVal(avg)	nrej(avg)	Rec_rej
51.52	0	1000	691	52.9	5.2	0
53.27	1	1000	1353	42.2	5.2	0
55.02	2	1000	1651	44.7	6.1	0
56.77	3	1000	1442	41.0	4.8	0
58.52	4	1000	1251	37.7	4.8	0
60.28	5	1000	761	37.7	5.4	0
62.03	6	1000	708	33.1	6.7	2
63.78	7	1000	531	36.9	7.2	0
65.53	8	949	237	27.5	6.8	0
67.28	9	951	211	27.4	5.8	0

pos	U	U_ci	u'	u'_ci	V	V_ci	v'	v'_ci	uv/u'v'	u'/v'	u_sk	u_fl
51.52	224.10	0.05	3.629	0.033	2.22	0.04	3.428	0.000	0.011	1.06	-0.004	2.79
53.27	224.90	0.05	3.516	0.035	2.11	0.04	3.329	0.000	0.025	1.06	-0.033	2.79
55.02	225.46	0.04	3.468	0.032	2.31	0.03	3.250	0.000	0.027	1.07	-0.025	2.79
56.77	226.14	0.05	3.377	0.027	2.42	0.05	3.159	0.000	0.003	1.07	-0.032	2.83
58.52	226.93	0.07	3.306	0.030	2.74	0.07	3.102	0.000	-0.002	1.07	-0.043	2.82
60.28	227.02	0.05	3.248	0.024	2.36	0.04	3.013	0.000	-0.008	1.08	-0.018	2.83
62.03	228.59	0.19	3.209	0.049	2.45	0.04	2.948	0.000	-0.011	1.09	-0.027	2.89
63.78	229.48	0.06	3.113	0.033	2.62	0.04	2.902	0.000	-0.029	1.07	-0.018	2.88
65.53	229.52	0.09	3.044	0.037	2.24	0.06	2.779	0.000	-0.037	1.10	0.020	2.87
67.28	229.38	0.09	2.924	0.038	2.18	0.06	2.567	0.000	-0.037	1.14	0.013	2.88

pos	U/Um	u'2/U2	integral	taylor	kolmog	diss rate	Re_tay
51.52	0.987	2.623e-004	4.79e-003	5.48e-004	2.43e-005	1.00e+004	131.1
53.27	0.990	2.445e-004	4.82e-003	5.56e-004	2.48e-005	9.27e+003	129.9
55.02	0.993	2.368e-004	4.84e-003	5.65e-004	2.53e-005	8.56e+003	128.6
56.77	0.996	2.231e-004	4.86e-003	5.73e-004	2.58e-005	7.94e+003	127.4
58.52	0.999	2.123e-004	4.89e-003	5.80e-004	2.62e-005	7.39e+003	126.3
60.28	0.999	2.047e-004	4.91e-003	5.89e-004	2.68e-005	6.84e+003	125.1
62.03	1.006	1.973e-004	4.93e-003	5.95e-004	2.71e-005	6.46e+003	124.3
63.78	1.010	1.841e-004	4.95e-003	6.02e-004	2.76e-005	6.07e+003	123.3
65.53	1.010	1.760e-004	4.97e-003	6.11e-004	2.81e-005	5.65e+003	122.2
67.28	1.010	1.627e-004	4.99e-003	6.19e-004	2.86e-005	5.25e+003	121.1

---------- Comments ----------

- DT = 4.6 (92%); CJ = 6.2; PO = 24 psi
- 160 mm lens at 45 degrees to mean flow; 0 MHz frequency shift
- window fogged badly during run, affecting data rate
- no holes repeated to check for repeatability

---------- Input Parameters ----------

Input filename	= j28x1		
Number of positions	= 5	Number of records	= 20
Starting position	= 747.0 mm	Increment	= 25.4000 mm
Mesh length	= 14.50 mm	Normalizing velocity	= -1.0 m/s
Static pressure	= 13.23 psi	Total pressure	= 17.55 psi
Traverse direction	= x	Total temperature	= 539.00 R
Transform method	= 3	Weighting method	= 2
x0/m	= 19.50		

Outliers removed: Sample st. dev. = 3.00; Record st. dev. = 2.50

---------- Global Information ----------

nu = 1.506e-005 kg/(m s) ; rho = 1.150e+000 kg/m3

Mach-p = 0.648; Mach-u = 0.679; U-mean = 226.340; Re_m = 217983

U-coef = 0.00608; U-exp = 0.9996; U-exp-ci = 0.0474; U-cor = -0.9975

V-coef = 0.00485; V-exp = 0.9216; V-exp-ci = 0.0841; V-cor = -0.9911

---------- Ensemble Information ----------

pos	Order	nsam	Rate(avg)	%Val(avg)	nrej(avg)	Rec_rej
51.52	4	1000	300	84.8	7.3	0
55.02	3	1000	790	91.6	7.2	0
58.52	2	1000	1103	92.8	7.5	1
62.03	1	1000	1054	92.4	7.3	0
65.53	0	1000	1029	92.8	8.2	0

pos	U	U_ci	u'	u'_ci	V	V_ci	v'	v'_ci	uv/u'v'	u'/v'	u_sk	u_fl
51.52	224.05	0.06	3.546	0.031	1.89	0.05	3.146	0.000	0.033	1.13	0.034	2.86
55.02	225.08	0.06	3.406	0.041	1.91	0.04	3.060	0.000	0.023	1.11	-0.017	2.78
58.52	226.52	0.05	3.263	0.037	2.03	0.03	2.881	0.000	0.048	1.13	-0.008	2.82
62.03	227.55	0.03	3.188	0.026	1.94	0.03	2.832	0.000	0.024	1.11	0.012	2.86
65.53	228.50	0.05	3.009	0.029	1.91	0.04	2.721	0.000	0.032	1.11	0.006	2.88

pos	U/Um	u'2/U2	integral	tayler	kolmog	diss rate	Re_tay
51.52	0.990	2.507e-004	4.92e-003	5.59e-004	2.47e-005	9.18e+003	132.1
55.02	0.994	2.291e-004	5.18e-003	5.87e-004	2.59e-005	7.56e+003	132.4
58.52	1.001	2.076e-004	5.43e-003	6.13e-004	2.70e-005	6.38e+003	132.9
62.03	1.005	1.926e-004	5.67e-003	6.39e-004	2.81e-005	5.45e+003	133.2
65.53	1.010	1.735e-004	5.90e-003	6.63e-004	2.92e-005	4.71e+003	133.5

---------- Comments ----------

- DT = 4.6 (92%); CJ = 6.2; PO = 24 psi
- 160 mm lens at 45 degrees to mean flow; 0 MHz frequency shift
- 5 holes measured in reverse order to check for repeatability of j27x1
- Thesis label: HSBa

```
------------------------------ Input Parameters ------------------------------
  Input filename       = j28x2
  Number of positions  = 11            Number of records    = 20
  Starting position    = 747.0 mm      Increment            = 25.4000 mm
  Mesh length          = 14.50 mm      Normalizing velocity =  -1.0 m/s
  Static pressure      =  13.23 psi    Total pressure       =  17.55 psi
  Traverse direction   = x             Total temperature    = 539.00 R
  Transform method     = 3             Weighting method     = 2
  x0/s                 = 17.00
  Outliers removed:  Sample st. dev. =   3.00;  Record st. dev. =   2.50

------------------------------ Global Information ------------------------------
  nu =  1.506e-005 kg/(m s)        ; rho =  1.150e+000 kg/m3
  Mach-p =   0.648; Mach-u =  0.683; U-mean   = 227.468; Re_m  =  219070
  U-coef = 0.00977; U-exp =  1.0076; U-exp-ci =  0.0178; U-cor = -0.9967
  V-coef = 0.01586; V-exp =  1.1952; V-exp-ci =  0.0399; V-cor = -0.9886

------------------------------ Ensemble Information ----------------------------
 pos  Order  nsam  Rate(avg)  %Val(avg)  nrej(avg)  Rec_rej
51.52   0    1000     798        90.7        8.1        0
53.27   1    1000    1316        90.2        7.1        0
53.27  10    1000     716        91.7        7.2        0
55.02   2    1000    1480        88.6        8.7        0
56.77   3    1000    1430        85.2        9.2        0
58.52   4    1000    1378        83.7        8.6        0
60.28   5    1000    1010        85.0        7.7        0
62.03   6     981    2361        88.5        8.1        0
63.78   7    1000    2893        90.8        9.8        1
65.53   8    1000    2890        92.8        8.1        0
67.28   9    1000     711        90.4        8.7        3

 pos      U    U_ci     u'    u'_ci     V    V_ci     v'    v'_ci uv/u'v' u'/v' u_sk   u_fl
51.52  224.30  0.06  3.702  0.031  1.83  0.04  3.340  0.000  0.004  1.11 -0.003  2.81
53.27  225.05  0.05  3.652  0.036  1.89  0.04  3.354  0.000  0.012  1.09 -0.034  2.85
53.27  224.90  0.05  3.616  0.034  1.73  0.04  3.228  0.000  0.029  1.12  0.004  2.85
55.02  225.68  0.06  3.586  0.036  1.70  0.04  3.220  0.000  0.008  1.11  0.005  2.85
56.77  226.41  0.05  3.475  0.033  1.72  0.05  3.172  0.000  0.001  1.10  0.007  2.84
58.52  227.08  0.06  3.422  0.034  1.71  0.03  3.085  0.000 -0.006  1.11 -0.012  2.86
60.28  227.53  0.06  3.386  0.034  1.73  0.04  3.053  0.000 -0.020  1.11 -0.020  2.88
62.03  228.60  0.15  3.333  0.040  1.74  0.03  2.941  0.000 -0.021  1.13  0.013  2.92
63.78  229.40  0.08  3.272  0.037  2.03  0.04  2.895  0.000 -0.014  1.13  0.010  2.89
65.53  229.83  0.07  3.219  0.035  1.75  0.05  2.877  0.000 -0.026  1.12  0.042  2.83
67.28  230.80  0.15  3.142  0.027  2.00  0.06  2.744  0.000 -0.045  1.15  0.004  2.84

 pos     U/Um     u'2/U2     integral     tayler      kolmog    diss rate  Re_tay
51.52  0.986  2.725e-004  5.80e-003  5.77e-004  2.46e-005  9.38e+003   142.8
53.27  0.989  2.635e-004  5.63e-003  5.91e-004  2.51e-005  8.58e+003   143.0
53.27  0.989  2.587e-004  5.63e-003  5.91e-004  2.51e-005  8.56e+003   142.9
55.02  0.992  2.526e-004  5.77e-003  6.04e-004  2.57e-005  7.87e+003   143.1
56.77  0.995  2.357e-004  5.90e-003  6.17e-004  2.62e-005  7.26e+003   143.3
58.52  0.998  2.273e-004  6.02e-003  6.29e-004  2.67e-005  6.72e+003   143.5
60.28  1.000  2.216e-004  6.15e-003  6.42e-004  2.72e-005  6.22e+003   143.7
62.03  1.005  2.128e-004  6.27e-003  6.53e-004  2.77e-005  5.83e+003   144.0
63.78  1.008  2.035e-004  6.39e-003  6.65e-004  2.81e-005  5.45e+003   144.2
65.53  1.010  1.963e-004  6.51e-003  6.76e-004  2.86e-005  5.09e+003   144.3
67.28  1.015  1.853e-004  6.62e-003  6.87e-004  2.90e-005  4.80e+003   144.6

------------------------------------ Comments ------------------------------------
- DT = 4.6 (92%); CJ = 6.2; PO = 24 psi
- 160 mm lens at 45 degrees to mean flow; 0 MHz frequency shift
- At this point, the practice of repeating a hole to check for repeatability
  started.  Subsequent tests also scattered the measuring order.
- Thesis label: M58b
```

```
------------------------------ Input Parameters ------------------------------
  Input filename       = j15x2
  Number of positions  =  3            Number of records    = 10
  Starting position    = 747.0 mm      Increment            = 25.4000 mm
  Mesh length          = 14.50 mm      Normalizing velocity =  -1.0 m/s
  Static pressure      =  13.20 psi    Total pressure       =  17.50 psi
  Traverse direction   = x             Total temperature    = 540.00 R
  Transform method     = 3             Weighting method     = 2
  x0/m                 =  0.00
  Outliers removed:  Sample st. dev. =   3.00;  Record st. dev. =   2.50

------------------------------ Global Information ----------------------------
  nu =  1.514e-005 kg/(m s)        ; rho =  1.145e+000 kg/m3
  Mach-p =   0.648; Mach-u =  0.686; U-mean   = 228.862; Re_m  =  219120
  U-coef = 0.00005; U-exp = -0.1150; U-exp-ci =  1.2044; U-cor =  0.3895
  V-coef = 0.00062; V-exp =  0.3903; V-exp-ci =  0.5798, V-cor = -0.9458

---------------------------- Ensemble Information ----------------------------
 pos  Order  nsam  Rate(avg)  %Val(avg)  nrej(avg)  Rec_rej
53.27   0    1000     2393        36.7       11.2        0
58.52   1    1000     2903        42.6       13.8        0
63.78   2    1000     2690        40.9       12.3        0

 pos      U    U_ci    u'    u'_ci    V   V_ci    v'   v'_ci uv/u'v' u'/v' u_sk   u_fl
53.27  227.47 0.04  2.110  0.026  2.40  0.05  2.608  0.001 -0.217  0.81  0.032  2.98
58.52  228.85 0.05  2.090  0.027  2.46  0.09  2.552  0.001 -0.228  0.82  0.055  3.11
63.78  230.27 0.04  2.159  0.034  2.48  0.05  2.550  0.000 -0.203  0.85  0.082  3.12

 pos     U/Um     u'2/U2     integral     taylor     kolmog   diss rate  Re_tay
53.27   0.994  8.609e-005 -4.13e-002  0.00e+000  0.00e+000 -2.23e+002     0.0
58.52   1.000  8.347e-005 -4.56e-002  0.00e+000  0.00e+000 -2.09e+002     0.0
63.78   1.006  8.799e-005 -4.99e-002  0.00e+000  0.00e+000 -1.97e+002     0.0

--------------------------------- Comments ---------------------------------
- DT = 4.6 (92%); CJ = 6.2; PO = 17.5 psi
- 160 mm lens at 45 degrees to mean flow; 0 MHz frequency shift
- no plate, to check for background turbulence levels at 17.5 psi.
- transformed results (may be slightly incorrect, due to blue beam degradation)



------------------------------ Input Parameters ------------------------------
  Input filename       = j15x3
  Number of positions  =  3            Number of records    = 10
  Starting position    = 747.0 mm      Increment            = 25.4000 mm
  Mesh length          = 14.50 mm      Normalizing velocity =  -1.0 m/s
  Static pressure      =  13.20 psi    Total pressure       =  17.50 psi
  Traverse direction   = x             Total temperature    = 540.00 R
  Transform method     = 3             Weighting method     = 2
  x0/m                 =  0.00
  Outliers removed:  Sample st. dev. =   3.00;  Record st. dev. =   2.50

------------------------------ Global Information ----------------------------
  nu =  1.514e-005 kg/(m s)        ; rho =  1.145e+000 kg/m3
  Mach-p =   0.648; Mach-u =  0.695; U-mean   = 231.720; Re_m  =  221857
  U-coef = 0.00002; U-exp = -0.3599; U-exp-ci =  0.1592; U-cor =  0.9911
  V-coef = 0.00056; V-exp =  0.3718; V-exp-ci =  0.5946; V-cor = -0.9381

---------------------------- Ensemble Information ----------------------------
 pos  Order  nsam  Rate(avg)  %Val(avg)  nrej(avg)  Rec_rej
53.27   0    1000     1447        43.9       13.7        0
58.52   1    1000     1830        44.3       13.1        0
63.78   2    1000     1120        29.4       12.3        0

 pos      U    U_ci    u'    u'_ci    V   V_ci    v'   v'_ci uv/u'v' u'/v' u_sk   u_fl
53.27  230.33 0.03  2.040  0.040  2.41  0.05  2.615  0.001 -0.200  0.78 -0.003  3.16
58.52  231.61 0.05  2.081  0.016  2.52  0.05  2.557  0.001 -0.231  0.81  0.052  3.06
63.78  233.22 0.03  2.134  0.042  2.89  0.05  2.561  0.001 -0.267  0.83  0.028  2.98

 pos     U/Um     u'2/U2     integral     taylor     kolmog   diss rate  Re_tay
53.27   0.994  7.851e-005 -1.27e-002  0.00e+000  0.00e+000 -6.69e+002     0.0
58.52   1.000  8.070e-005 -1.42e-002  0.00e+000  0.00e+000 -6.40e+002     0.0
63.78   1.006  8.378e-005 -1.57e-002  0.00e+000  0.00e+000 -6.19e+002     0.0

--------------------------------- Comments ---------------------------------
- DT = 4.6 (92%); CJ = 6.2; PO = 24.0 psi
- 160 mm lens at 45 degrees to mean flow; 0 MHz frequency shift
- no plate, to check for background turbulence levels at 24.0 psi.
- transformed results (may be slightly incorrect, due to blue beam degradation)
```

---------- Input Parameters ----------

Input filename	= j118z1		
Number of positions	= 12	Number of records	= 15
Starting position	= 747.0 mm	Increment	= 25.4000 mm
Mesh length	= 14.50 mm	Normalizing velocity	= -1.0 m/s
Static pressure	= 19.31 psi	Total pressure	= 19.79 psi
Traverse direction	= x	Total temperature	= 532.00 R
Transform method	= 2	Weighting method	= 2
x0/m	= -2.00		

Outliers removed: Sample st. dev. = 3.00; Record st. dev. = 2.50

---------- Global Information ----------

nu = 1.149e-005 kg/(m s) ; rho = 1.580e+000 kg/m3

Mach-p = 0.188; Mach-u = 0.162; U-mean = 55.666; Re_m = 70239

U-coef = 0.02078; U-exp = 0.9996; U-exp-ci = 0.0509; U-cor = -0.9740

V-coef = 0.00297; V-exp = 0.4531; V-exp-ci = 0.0451; V-cor = -0.9104

---------- Ensemble Information ----------

pos	Order	nsam	Rate(avg)	%Val(avg)	nrej(avg)	Rec_rej
51.52	1	1000	665	17.2	14.9	0
53.27	6	1000	1638	38.5	9.9	4
55.02	2	1000	1790	41.8	8.7	0
56.77	7	1000	1253	42.4	8.7	0
58.52	3	1000	1461	46.2	8.7	0
60.28	8	1000	1540	43.1	8.1	0
62.03	4	1000	1717	42.0	7.7	0
63.78	9	1000	1943	37.9	9.1	0
65.53	0	1000	1727	33.8	10.1	0
65.53	5	1000	1595	37.1	9.3	0
65.53	11	1000	1364	35.1	9.0	0
67.28	10	1000	298	37.2	10.9	0

pos	U	U_ci	u'	u'_ci	V	V_ci	v'	v'_ci	uv/u'v'	u'/v'	u_sk	u_fl
51.52	55.10	0.02	1.065	0.013	0.53	0.02	1.206	0.001	-0.007	0.88	0.072	2.86
53.27	55.42	0.02	1.079	0.017	0.64	0.02	1.222	0.001	0.024	0.88	0.035	2.79
55.02	55.51	0.02	1.076	0.012	0.61	0.02	1.204	0.001	0.018	0.89	0.046	2.72
56.77	55.62	0.02	1.061	0.014	0.59	0.02	1.216	0.001	0.028	0.87	0.044	2.78
58.52	55.67	0.02	1.025	0.011	0.68	0.02	1.207	0.001	-0.003	0.85	-0.014	2.86
60.28	55.72	0.02	1.018	0.012	0.60	0.02	1.188	0.001	0.031	0.86	0.016	2.82
62.03	55.82	0.02	1.011	0.013	0.63	0.02	1.172	0.001	0.015	0.86	0.023	2.79
63.78	55.88	0.01	0.991	0.012	0.61	0.01	1.191	0.001	-0.010	0.83	0.058	2.78
65.53	55.92	0.02	0.965	0.010	0.58	0.02	1.196	0.001	-0.002	0.81	0.006	2.79
65.53	55.96	0.01	0.979	0.011	0.62	0.01	1.181	0.001	0.000	0.83	0.005	2.78
65.53	55.93	0.01	0.986	0.012	0.56	0.02	1.199	0.001	0.019	0.82	-0.002	2.77
67.28	55.96	0.02	0.966	0.008	0.60	0.01	1.153	0.001	0.022	0.84	0.009	2.83

pos	U/Um	u'2/U2	integral	taylor	kolmog	diss rate	Re_tay
51.52	0.990	3.737e-004	1.02e-002	1.27e-003	5.89e-005	1.26e+002	120.3
53.27	0.996	3.792e-004	1.04e-002	1.29e-003	5.96e-005	1.20e+002	120.7
55.02	0.997	3.758e-004	1.05e-002	1.31e-003	6.05e-005	1.13e+002	120.8
56.77	0.999	3.641e-004	1.07e-002	1.33e-003	6.13e-005	1.07e+002	120.9
58.52	1.000	3.391e-004	1.09e-002	1.35e-003	6.22e-005	1.01e+002	120.9
60.28	1.001	3.342e-004	1.10e-002	1.36e-003	6.31e-005	9.60e+001	121.0
62.03	1.003	3.282e-004	1.12e-002	1.38e-003	6.39e-005	9.13e+001	121.1
63.78	1.004	3.147e-004	1.13e-002	1.40e-003	6.47e-005	8.68e+001	121.2
65.53	1.005	2.981e-004	1.15e-002	1.42e-003	6.55e-005	8.25e+001	121.2
65.53	1.005	3.059e-004	1.15e-002	1.42e-003	6.55e-005	8.27e+001	121.3
65.53	1.005	3.109e-004	1.15e-002	1.42e-003	6.55e-005	8.25e+001	121.2
67.28	1.005	2.982e-004	1.16e-002	1.44e-003	6.63e-005	7.85e+001	121.2

---------- Comments ----------

- DT = 1.2 (24%); CJ = 5.0; P0 = 20.0 psi
- 160 mm lens; 40 MHz frequency shift
- x = -1.3 by accident
- 2-component results obtained, but blue beam performance was poor
- after this point, only 1-component measurements were obtained, since the blue beam results could not be trusted
- Thesis label (U-results only): M51b

---------- Input Parameters ----------

Input filename	= j118x2		
Number of positions	= 12	Number of records	= 15
Starting position	= 747.0 mm	Increment	= 25.4000 mm
Mesh length	= 14.50 mm	Normalizing velocity	= -1.0 m/s
Static pressure	= 19.31 psi	Total pressure	= 19.79 psi
Traverse direction	= x	Total temperature	= 532.00 R
Transform method	= 2	Weighting method	= 2
x0/m	= -8.00		

Outliers removed: Sample st. dev. = 3.00; Record st. dev. = 2.50

---------- Global Information ----------

nu = 1.149e-005 kg/(m s) ; rho = 1.580e+000 kg/m3

Mach-p = 0.188; Mach-u = 0.162; U-mean = 55.557; Re_m = 70102

U-coef = 0.02349; U-exp = 1.0006; U-exp-ci = 0.0333; U-cor = -0.9886

V-coef = 0.00000; V-exp = 0.0000; V-exp-ci = 0.0000; V-cor = 0.0000

---------- Ensemble Information ----------

pos	Order	nsam	Rate(avg)	%Val(avg)	nrej(avg)	Rec_rej
51.52	1	1000	262	100.0	1.4	1
53.27	6	1000	944	100.0	1.2	0
55.02	2	1000	1035	100.0	1.6	0
56.77	7	1000	873	100.0	0.6	2
58.52	3	1000	1385	100.0	1.6	1
60.28	8	1000	1072	100.0	1.7	0
62.03	4	1000	1935	100.0	1.5	0
63.78	9	1000	1270	100.0	1.3	0
65.53	0	1000	1499	100.0	1.3	0
65.53	5	1000	1591	100.0	1.9	0
65.53	11	1000	771	100.0	0.7	0
67.28	10	1000	186	100.0	1.6	0

pos	U	U_ci	u'	u'_ci	V	V_ci	v'	v'_ci	uv/u'v'	u'/v'	u_sk	u_fl
51.52	55.13	0.01	1.088	0.012	0.00	0.00	0.000	0.000	0.000	0.00	0.066	2.81
53.27	55.26	0.03	1.085	0.012	0.00	0.00	0.000	0.000	0.000	0.00	0.037	2.78
55.02	55.42	0.02	1.069	0.014	0.00	0.00	0.000	0.000	0.000	0.00	0.031	2.74
56.77	55.45	0.02	1.058	0.008	0.00	0.00	0.000	0.000	0.000	0.00	0.003	2.78
58.52	55.52	0.02	1.040	0.011	0.00	0.00	0.000	0.000	0.000	0.00	0.036	2.80
60.28	55.65	0.02	1.024	0.010	0.00	0.00	0.000	0.000	0.000	0.00	0.020	2.74
62.03	55.69	0.02	1.018	0.012	0.00	0.00	0.000	0.000	0.000	0.00	0.035	2.80
63.78	55.78	0.02	1.016	0.010	0.00	0.00	0.000	0.000	0.000	0.00	0.007	2.80
65.53	55.84	0.01	0.991	0.012	0.00	0.00	0.000	0.000	0.000	0.00	-0.002	2.79
65.53	55.86	0.02	1.003	0.011	0.00	0.00	0.000	0.000	0.000	0.00	0.023	2.78
65.53	55.79	0.02	1.002	0.011	0.00	0.00	0.000	0.000	0.000	0.00	0.000	2.74
67.28	55.81	0.02	0.975	0.010	0.00	0.00	0.000	0.000	0.000	0.00	0.047	2.79

pos	U/Um	v'2/U2	integral	taylor	kolmog	diss rate	Re_tay
51.52	0.992	3.894e-004	1.14e-002	1.34e-003	6.03e-005	1.15e+002	127.6
53.27	0.995	3.855e-004	1.16e-002	1.36e-003	6.11e-005	1.09e+002	127.8
55.02	0.997	3.726e-004	1.17e-002	1.38e-003	6.18e-005	1.04e+002	127.9
56.77	0.998	3.640e-004	1.19e-002	1.39e-003	6.26e-005	9.85e+001	128.0
58.52	0.999	3.512e-004	1.21e-002	1.41e-003	6.34e-005	9.38e+001	128.1
60.28	1.002	3.386e-004	1.22e-002	1.43e-003	6.41e-005	8.96e+001	128.2
62.03	1.002	3.341e-004	1.24e-002	1.45e-003	6.49e-005	8.54e+001	128.3
63.78	1.004	3.320e-004	1.25e-002	1.46e-003	6.57e-005	8.17e+001	128.4
65.53	1.005	3.154e-004	1.27e-002	1.48e-003	6.64e-005	7.81e+001	128.4
65.53	1.006	3.228e-004	1.27e-002	1.48e-003	6.64e-005	7.82e+001	128.5
65.53	1.004	3.227e-004	1.27e-002	1.48e-003	6.64e-005	7.79e+001	128.4
67.28	1.005	3.051e-004	1.28e-002	1.50e-003	6.72e-005	7.44e+001	128.4

---------- Comments ----------

- same run as j118x1 (previous page), but only 1-component measurements taken
- Thesis label: M31c

---------- Input Parameters ----------

Input filename	= jl19z1		
Number of positions	= 12	Number of records	= 15
Starting position	= 747.0 mm	Increment	= 25.4000 mm
Mesh length	= 14.50 mm	Normalizing velocity	= -1.0 m/s
Static pressure	= 18.62 psi	Total pressure	= 19.46 psi
Traverse direction	= x	Total temperature	= 532.00 R
Transform method	= 1	Weighting method	= 2
z0/m	= -7.00		

Outliers removed: Sample st. dev. = 3.00; Record st. dev. = 2.50

---------- Global Information ----------

nu = 1.180e-005 kg/(m s) ; rho = 1.532e+000 kg/m3

Mach-p = 0.252; Mach-u = 0.237; U-mean = 81.055; Re_m = 99604

U-coef = 0.01756; U-exp = 0.9992; U-exp-ci = 0.1074; U-cor = -0.8978

V-coef = 0.00000; V-exp = 0.0000; V-exp-ci = 0.0000; V-cor = 0.0000

---------- Ensemble Information ----------

pos	Order	nsam	Rate(avg)	%Val(avg)	nrej(avg)	Rec_rej
51.52	1	1000	761	100.0	2.8	1
53.27	6	1000	1156	100.0	2.9	0
55.02	2	1000	1351	100.0	2.9	0
56.77	7	1000	1069	100.0	3.3	0
58.52	3	1000	1131	100.0	3.6	0
60.28	8	1000	957	100.0	4.2	0
62.03	4	1000	737	100.0	3.5	0
63.78	9	1000	1097	100.0	3.3	0
65.53	0	1000	1041	100.0	2.7	0
65.53	5	1000	508	100.0	4.3	0
65.53	11	1000	1324	100.0	3.1	0
67.28	10	1000	131	100.0	3.1	0

pos	U	U_ci	u'	u'_ci	V	V_ci	v'	v'_ci	uv/u'v'	u'/v'	u_sk	u_fl
51.52	80.46	0.03	1.418	0.021	0.00	0.00	0.000	0.000	0.000	0.00	-0.086	2.97
53.27	80.70	0.02	1.367	0.017	0.00	0.00	0.000	0.000	0.000	0.00	-0.103	2.99
55.02	80.88	0.03	1.351	0.012	0.00	0.00	0.000	0.000	0.000	0.00	-0.077	3.01
56.77	81.14	0.05	1.367	0.019	0.00	0.00	0.000	0.000	0.000	0.00	-0.033	3.06
58.52	80.95	0.03	1.327	0.021	0.00	0.00	0.000	0.000	0.000	0.00	-0.067	3.07
60.28	81.24	0.02	1.267	0.019	0.00	0.00	0.000	0.000	0.000	0.00	0.002	3.10
62.03	81.14	0.03	1.283	0.018	0.00	0.00	0.000	0.000	0.000	0.00	-0.031	3.05
63.78	81.40	0.01	1.306	0.015	0.00	0.00	0.000	0.000	0.000	0.00	0.001	3.06
65.53	81.16	0.02	1.354	0.015	0.00	0.00	0.000	0.000	0.000	0.00	-0.022	3.06
65.53	81.24	0.02	1.304	0.013	0.00	0.00	0.000	0.000	0.000	0.00	-0.011	3.12
65.53	81.44	0.03	1.325	0.015	0.00	0.00	0.000	0.000	0.000	0.00	0.041	3.03
67.28	81.40	0.05	1.234	0.011	0.00	0.00	0.000	0.000	0.000	0.00	0.000	3.08

pos	U/Um	u'2/U2	integral	taylor	kolmog	diss rate	Re_tay
51.52	0.993	3.108e-004	9.82e-003	1.12e-003	4.94e-005	2.77e+002	132.0
53.27	0.996	2.869e-004	9.97e-003	1.13e-003	5.00e-005	2.63e+002	132.2
55.02	0.998	2.792e-004	1.01e-002	1.15e-003	5.06e-005	2.50e+002	132.3
56.77	1.001	2.843e-004	1.03e-002	1.16e-003	5.12e-005	2.39e+002	132.6
58.52	0.999	2.691e-004	1.04e-002	1.18e-003	5.20e-005	2.25e+002	132.4
60.28	1.002	2.436e-004	1.05e-002	1.19e-003	5.25e-005	2.16e+002	132.6
62.03	1.001	2.502e-004	1.07e-002	1.21e-003	5.33e-005	2.04e+002	132.6
63.78	1.004	2.576e-004	1.08e-002	1.22e-003	5.38e-005	1.96e+002	132.8
65.53	1.001	2.784e-004	1.09e-002	1.24e-003	5.46e-005	1.85e+002	132.6
65.53	1.002	2.578e-004	1.09e-002	1.24e-003	5.45e-005	1.86e+002	132.6
65.53	1.005	2.650e-004	1.09e-002	1.23e-003	5.44e-005	1.87e+002	132.8
67.28	1.004	2.299e-004	1.11e-002	1.25e-003	5.51e-005	1.78e+002	132.8

---------- Comments ----------

- DT = 1.8 (36%); CJ = 5.0; P0 = 20.0 psi
- 160 mm lens; 40 MHz frequency shift
- Thesis label: HS2

---------- Input Parameters ----------

Input filename	= jl19x2		
Number of positions	= 12	Number of records	= 15
Starting position	= 747.0 mm	Increment	= 25.4000 mm
Mesh length	= 14.50 mm	Normalizing velocity	= -1.0 m/s
Static pressure	= 19.45 psi	Total pressure	= 19.79 psi
Traverse direction	= x	Total temperature	= 538.00 R
Transform method	= 1	Weighting method	= 2
x0/m	= 1.00		

Outliers removed: Sample st. dev. = 3.00; Record st. dev. = 2.50

---------- Global Information ----------

nu = 1.168e-005 kg/(m s) ; rho = 1.571e+000 kg/m3

Mach-p = 0.158; Mach-u = 0.160; U-mean = 55.360; Re_m = 68723

U-coef = 0.02037; U-exp = 1.0092; U-exp-ci = 0.0338; U-cor = -0.9885

V-coef = 0.00000; V-exp = 0.0000; V-exp-ci = 0.0000; V-cor = 0.0000

---------- Ensemble Information ----------

pos	Order	ns_n	Rate(avg)	%Val(avg)	nrej(avg)	Rec_rej
51.52	1	1000	1161	100.0	2.9	0
53.27	6	1000	1518	100.0	2.1	0
55.02	2	1000	1580	100.0	2.2	0
56.77	7	1000	1401	100.0	0.9	0
58.52	3	1000	1940	100.0	1.6	0
60.28	8	1000	1843	100.0	1.7	0
62.03	4	1000	1959	100.0	1.8	1
63.78	9	1000	1300	100.0	1.7	0
65.53	0	1000	1659	100.0	1.8	0
65.53	5	1000	1585	100.0	1.8	0
65.53	11	1000	1406	100.0	1.9	1
67.28	10	1000	178	100.0	1.4	1

pos	U	U_ci	u'	u'_ci	V	V_ci	v'	v'_ci	uv/u'v'	u'/v'	u_sk	u_fl
51.52	55.00	0.01	1.079	0.013	0.00	0.00	0.000	0.000	0.000	0.00	0.010	2.75
53.27	55.10	0.02	1.062	0.017	0.00	0.00	0.000	0.000	0.000	0.00	0.025	2.77
55.02	55.07	0.06	1.060	0.012	0.00	0.00	0.000	0.000	0.000	0.00	0.012	2.79
56.77	55.28	0.02	1.045	0.014	0.00	0.00	0.000	0.000	0.000	0.00	0.028	2.81
58.52	55.34	0.02	1.012	0.011	0.00	0.00	0.000	0.000	0.000	0.00	0.007	2.81
60.28	55.47	0.01	1.009	0.016	0.00	0.00	0.000	0.000	0.000	0.00	0.001	2.82
62.03	55.51	0.02	1.002	0.008	0.00	0.00	0.000	0.000	0.000	0.00	0.008	2.79
63.78	55.59	0.02	0.980	0.010	0.00	0.00	0.000	0.000	0.000	0.00	0.029	2.82
65.53	55.55	0.02	0.988	0.012	0.00	0.00	0.000	0.000	0.000	0.00	-0.032	2.82
65.53	55.64	0.02	0.974	0.011	0.00	0.00	0.000	0.000	0.000	0.00	-0.004	2.83
65.53	55.69	0.01	0.973	0.010	0.00	0.00	0.000	0.000	0.000	0.00	-0.001	2.82
67.28	55.61	0.01	0.948	0.009	0.00	0.00	0.000	0.000	0.000	0.00	0.041	2.85

pos	U/Um	u'2/U2	integral	tayler	kolmog	diss rate	Re_tay
51.52	0.993	3.852e-004	9.54e-003	1.24e-003	5.88e-005	1.34e+002	115.3
53.27	0.995	3.719e-004	9.70e-003	1.26e-003	5.97e-005	1.26e+002	115.4
55.02	0.995	3.705e-004	9.86e-003	1.28e-003	6.07e-005	1.17e+002	115.3
56.77	0.999	3.573e-004	1.00e-002	1.30e-003	6.15e-005	1.11e+002	115.5
58.52	1.000	3.343e-004	1.02e-002	1.32e-003	6.25e-005	1.05e+002	115.6
60.28	1.002	3.313e-004	1.03e-002	1.34e-003	6.33e-005	9.95e+001	115.7
62.03	1.003	3.257e-004	1.05e-002	1.36e-003	6.42e-005	9.41e+001	115.7
63.78	1.004	3.111e-004	1.06e-002	1.38e-003	6.50e-005	8.92e+001	115.8
65.53	1.003	3.166e-004	1.08e-002	1.40e-003	6.60e-005	8.42e+001	115.7
65.53	1.005	3.069e-004	1.08e-002	1.40e-003	6.59e-005	8.46e+001	115.8
65.53	1.006	3.053e-004	1.08e-002	1.39e-003	6.58e-005	8.49e+001	115.9
67.28	1.004	2.910e-004	1.09e-002	1.41e-003	6.68e-005	8.01e+001	115.8

---------- Comments ----------

- DT = 1.2 (24%); CJ = 5.0; P0 = 20.0 psi
- 160 mm lens; 40 MHz frequency shift
- same conditions as jl18x1 and jl18x2, except x = 0
- Thesis label: HS1d

---------- Input Parameters ----------

Input filename	= j120s1		
Number of positions	= 12	Number of records	= 15
Starting position	= 747.0 mm	Increment	= 25.4000 mm
Mesh length	= 14.50 mm	Normalizing velocity	= -1.0 m/s
Static pressure	= 11.65 psi	Total pressure	= 18.67 psi
Traverse direction	= x	Total temperature	= 531.00 R
Transform method	= 1	Weighting method	= 2
z0/m	= 0.00		

Outliers removed: Sample st. dev. = 3.00; Record st. dev. = 2.50

---------- Global Information ----------

nu = 1.517e-005 kg/(m s) ; rho = 1.079e+000 kg/m3

Mach-p = 0.858; Mach-u = 0.916; U-mean = 294.296; Re_m = 281269

U-coef = 0.00075; U-exp = 0.1299; U-exp-ci = 0.3320; U-cor = -0.0854

V-coef = 0.00000; V-exp = 0.0000; V-exp-ci = 0.0000; V-cor = 0.0000

---------- Ensemble Information ----------

pos	Order	nsam	Rate(avg)	%Val(avg)	nrej(avg)	Rec_rej
51.52	1	1000	3126	99.6	2.8	0
53.27	6	1000	3348	99.7	5.1	0
55.02	2	1000	3586	99.9	9.1	0
56.77	7	1000	3798	99.8	11.8	0
58.52	3	1000	3946	99.8	11.9	0
60.28	8	1000	3150	99.8	11.2	0
62.03	4	1000	3725	99.8	10.9	0
63.78	9	1000	2364	99.6	9.2	0
65.53	0	1000	3479	99.8	9.1	0
65.53	5	1000	3059	99.7	8.3	0
65.53	11	1000	4527	99.7	8.9	1
67.28	10	1000	1308	99.7	8.7	0

pos	U	U_ci	u'	u'_ci	V	V_ci	v'	v'_ci	uv/u'v'	u'/v'	u_sk	u_fl
51.52	312.37	0.22	7.298	0.186	0.00	0.00	0.000	0.000	0.000	0.00	-0.024	2.89
53.27	305.11	0.24	6.800	0.176	0.00	0.00	0.000	0.000	0.000	0.00	0.305	3.03
55.02	301.05	0.26	6.224	0.193	0.00	0.00	0.000	0.000	0.000	0.00	0.504	3.35
56.77	296.89	0.18	5.786	0.154	0.00	0.00	0.000	0.000	0.000	0.00	0.522	3.47
58.52	294.29	0.18	5.757	0.150	0.00	0.00	0.000	0.000	0.000	0.00	0.550	3.58
60.28	290.74	0.17	5.651	0.161	0.00	0.00	0.000	0.000	0.000	0.00	0.387	3.52
62.03	288.69	0.16	5.773	0.178	0.00	0.00	0.000	0.000	0.000	0.00	0.272	3.44
63.78	286.31	0.18	6.097	0.090	0.00	0.00	0.000	0.000	0.000	0.00	0.189	3.27
65.53	284.60	0.15	6.286	0.078	0.00	0.00	0.000	0.000	0.000	0.00	0.209	3.21
65.53	284.25	0.10	6.220	0.107	0.00	0.00	0.000	0.000	0.000	0.00	0.165	3.11
65.53	284.83	0.20	6.323	0.164	0.00	0.00	0.000	0.000	0.000	0.00	0.244	3.22
67.28	283.25	0.14	6.433	0.111	0.00	0.00	0.000	0.000	0.000	0.00	0.172	3.10

pos	U/Um	u'2/U2	integral	tayler	kolmog	diss rate	Re_tay
51.52	1.061	5.475e-004	8.14e-002	1.67e-003	3.14e-005	3.59e+003	731.0
53.27	1.037	4.981e-004	8.40e-002	1.72e-003	3.23e-005	3.22e+003	733.1
55.02	1.023	4.291e-004	8.66e-002	1.76e-003	3.29e-005	2.98e+003	738.5
56.77	1.009	3.809e-004	8.92e-002	1.80e-003	3.35e-005	2.76e+003	743.4
58.52	1.000	3.838e-004	9.18e-002	1.84e-003	3.41e-005	2.60e+003	750.0
60.28	0.988	3.791e-004	9.43e-002	1.87e-003	3.46e-005	2.42e+003	755.1
62.03	0.981	4.015e-004	9.69e-002	1.91e-003	3.51e-005	2.30e+003	761.9
63.78	0.973	4.539e-004	9.94e-002	1.94e-003	3.56e-005	2.17e+003	768.0
65.53	0.967	4.882e-004	1.02e-001	1.97e-003	3.60e-005	2.07e+003	774.8
65.53	0.966	4.795e-004	1.02e-001	1.98e-003	3.61e-005	2.06e+003	774.3
65.53	0.968	4.941e-004	1.02e-001	1.97e-003	3.60e-005	2.07e+003	775.1
67.28	0.962	5.165e-004	1.05e-001	2.01e-003	3.64e-005	1.98e+003	781.9

---------- Comments ----------

- DT = 4.7 (94%); CJ = 5.6; PO = 24.0 psi
- 243 mm lens; 0 MHz frequency shift
- Thesis label: M52

---------- Input Parameters ----------

Input filename	= j121x1		
Number of positions	= 3	Number of records	= 5
Starting position	= 747.0 mm	Increment	= 25.4000 mm
Mesh length	= 14.50 mm	Normalizing velocity	= -1.0 m/s
Static pressure	= 11.60 psi	Total pressure	= 18.90 psi
Traverse direction	= x	Total temperature	= 531.00 R
Transform method	= 1	Weighting method	= 2
x0/m	= 0.00		

Outliers removed: Sample st. dev. = 3.00; Record st. dev. = 2.50

---------- Global Information ----------

nu = 1.504e-005 kg/(m s) ; rho = 1.086e+000 kg/m3

Mach-p = 0.865; Mach-u = 0.913; U-mean = 293.002; Re_m = 282395

U-coef = 0.00000; U-exp = -1.9012; U-exp-ci = 3.8326; U-cor = 0.9112

V-coef = 0.00000; V-exp = 0.0000; V-exp-ci = 0.0000; V-cor = 0.0000

---------- Ensemble Information ----------

pos	Order	nsam	Rate(avg)	IVal(avg)	nrej(avg)	Rec_rej
53.27	0	3000	3269	99.9	18.4	0
60.28	1	3000	2971	99.3	23.6	0
65.53	2	3000	2680	99.7	20.4	0

pos	U	U_ci	u'	u'_ci	V	V_ci	v'	v'_ci	uv/u'v'	u'/v'	u_sk	u_fl
53.27	303.92	0.20	6.504	0.195	0.00	0.00	0.000	0.000	0.000	0.00	0.336	3.12
60.28	290.70	0.26	6.509	0.231	0.00	0.00	0.000	0.000	0.000	0.00	0.324	3.28
65.53	284.39	0.50	7.484	0.262	0.00	0.00	0.000	0.000	0.000	0.00	0.278	3.06

pos	U/Um	u'2/U2	integral	taylor	kolmog	diss rate	Re_tay
53.27	1.037	4.583e-004	-5.68e-003	0.00e+000	0.00e+000	-4.56e+004	0.0
60.28	0.992	5.019e-004	-7.23e-003	0.00e+000	0.00e+000	-4.46e+004	0.0
65.53	0.971	6.932e-004	-8.51e-003	0.00e+000	0.00e+000	-4.50e+004	0.0

---------- Comments ----------

- DT = 4.7 (94%); CJ = 5.6; PO = 24.0 psi
- 243 mm lens; 0 KHz frequency shift
- same conditions as j120x1
- 10000 samples/record taken for spectral analysis with FLOware. However, no fixed frequency of pseudo-shock oscillation was evident.
- here only the first 3000 samples are processed due to memory limitations in my program

```
------------------------------ Input Parameters ------------------------------
  Input filename        = j121a2
  Number of positions   =  1            Number of records     =  5
  Starting position     =  747 0 mm     Increment             =  25 4000 mm
  Mesh length           =  14 10 mm     Normalizing velocity  =  -1 0 m/s
  Static pressure       =  11 60 psi    Total pressure        =  18.90 psi
  Traverse direction    =  y            Total temperature     =  531 00 R
  Transform method      =  1            Weighting method      =  2
  s0/m                  =  0 00
  Outliers removed   Sample st. dev  =   3.00,  Record st. dev  =   2.50

------------------------------ Global Information ------------------------------
  nu =  1 504e-005 kg/(m s)        , rho =  1.086e+000 kg/m3
  Mach-p =   0 865, Mach-u =  0 930, U-mean   = 298.694, Re_m  =  287880
  U-coef =  0 00000, U-exp =  0 0000, U-exp-ci =  0 0000, U-cor =  0 0000
  V-coef =  0 00000, V-exp =  0 0000, V-exp-ci =  0.0000, V-cor =  0 0000

------------------------------ Ensemble Information ------------------------------
 pos  Order  mean  Rate(avg)  %Val(avg)  nrej(avg)  Rec_rej
-0 16    0   1000       361      100.0        4.6        0
-0 08    1   1000      1468       99 9        0 8        0
 0 00    2   1000      2475       99 9        5.4        0
 0 08    3   1000      1647       99.9        7.6        0
 0.16    4   1000       699       99.9        7.0        0

 pos       U    U_ci     u'   u'_ci     V    V_ci     v'   v'_ci uv/u'v' u'/v' u_sk   u_fl
-0 16  309 47  0 40  8 315  0.288  0.00  0.00  0.000  0.000  0.000  0.00 -0.415  3.04
-0 08  301 09  0 57  9 023  0.113  0 00  0.00  0.000  0.000  0.000  0.00  0.159  2.49
 0 00  295 25  0 10  7.694  0.339  0.00  0.00  0.000  0.000  0.000  0.00  0.561  3.13
 0 08  294 00  0.27  5 741  0.358  0.00  0.00  0.000  0.000  0 000  0.00  0.344  3.22
 0 16  293 66  0.30  5.660  0.017  0.00  0.00  0.000  0.000  0.000  0.00  0.070  3.05

 pos     U/Um     u'2/U2     integral     taylor     kolmog   diss rate  Re_tay
-0 16  1.036  7.229e-004  0.00e+000  0.00e+000  0.00e+000  0.00e+000     0.0
-0 08  1.008  8 981e-004  0 00e+000  0.00e+000  0.00e+000  0.00e+000     0.0
 0 00  0 988  6.802e-004  0.00e+000  0.00e+000  0.00e+000  0.00e+000     0.0
 0 08  0.984  3 826e-004  0.00e+000  0.00e+000  0.00e+000  0.00e+000     0.0
 0 16  0 983  3.715e-004  0.00e+000  0.00e+000  0.00e+000  0.00e+000     0.0

---------------------------------- Comments ----------------------------------
- same run as j121a1
- y-traverse to check for homogeneity
```

```
------------------------------ Input Parameters ------------------------------
  Input filename       = j121x3
  Number of positions  = 12              Number of records     = 15
  Starting position    = 747.0 mm        Increment             = 25.4000 mm
  Mesh length          = 14.50 mm        Normalizing velocity = 447.8 m/s
  Static pressure      =  6.01 psi       Total pressure        =  21.21 psi
  Traverse direction   = x               Total temperature     = 538.00 R
  Transform method     = 1               Weighting method      = 2
  x0/m                 = 0.00
  Outliers removed:  Sample st. dev. =  3.00;  Record st. dev. =  2.50

------------------------------ Global Information ----------------------------
  nu =  1.988e-005 kg/(m s)        ; rho =  6.924e-001 kg/m3
  Mach-p =   1.473; Mach-u =  1.546; U-mean   = 447.573; Re_m  =  326481
  U-coef = 0.00001; U-exp = -0.5634; U-exp-ci =  0.3556; U-cor =  0.3280
  V-coef = 0.00000; V-exp =  0.0000; V-exp-ci =  0.0000; V-cor =  0.0000

------------------------------ Ensemble Information --------------------------
 pos  Order  nsam  Rate(avg)  %Val(avg)  nrej(avg)  Rec_rej
51.52   1    1000     3221        99.3        5.5        0
53.27   6    1000     1818        99.6        4.1        1
55.02   2    1000     2175        99.7        3.9        0
56.77   7    1000     2523        99.5        5.1        0
58.52   3    1000     3077        98.8        5.3        0
60.28   8    1000     2760        99.5        4.5        0
62.03   4    1000     2899        99.5        4.5        0
63.78   9    1000     2398        99.6        4.3        0
65.53   0    1000     2746        99.5        4.1        0
65.53   5    1000     2658        99.4        4.4        0
65.53  11    1000     3387        99.3        3.7        0
67.28  10    1000      779        97.9        5.1        0

 pos      U    U_ci    u'   u'_ci    V   V_ci    v'   v'_ci uv/u'v' u'/v' u_sk   u_fl
51.52 447.31  0.10  3.291  0.045  0.00  0.00  0.000  0.000  0.000  0.00  0.019  3.04
53.27 452.52  0.09  3.456  0.068  0.00  0.00  0.000  0.000  0.000  0.00  0.094  2.80
55.02 453.61  0.06  3.435  0.043  0.00  0.00  0.000  0.000  0.000  0.00  0.049  2.83
56.77 446.71  0.07  3.476  0.033  0.00  0.00  0.000  0.000  0.000  0.00  0.123  3.02
58.52 441.92  0.07  3.829  0.058  0.00  0.00  0.000  0.000  0.000  0.00  0.156  3.12
60.28 449.70  0.05  3.282  0.029  0.00  0.00  0.000  0.000  0.000  0.00  0.102  2.94
62.03 446.02  0.07  3.172  0.061  0.00  0.00  0.000  0.000  0.000  0.00 -0.027  2.94
63.78 450.30  0.06  3.369  0.039  0.00  0.00  0.000  0.000  0.000  0.00  0.075  2.87
65.53 445.82  0.05  3.363  0.033  0.00  0.00  0.000  0.000  0.000  0.00 -0.078  2.86
65.53 446.62  0.07  3.419  0.058  0.00  0.00  0.000  0.000  0.000  0.00 -0.070  3.01
65.53 446.71  0.09  3.445  0.051  0.00  0.00  0.000  0.000  0.000  0.00 -0.063  2.97
67.28 441.03  0.09  4.005  0.067  0.00  0.00  0.000  0.000  0.000  0.00  0.216  3.03

 pos     U/Um     u'2/U2     integral     taylor      kolmog     diss rate  Re_tay
51.52   0.999  5.416e-005 -6.58e-003  0.00e+000  0.00e+000 -5.62e+003      0.0
53.27   1.010  5.843e-005 -6.87e-003  0.00e+000  0.00e+000 -5.73e+003      0.0
55.02   1.013  5.737e-005 -7.16e-003  0.00e+000  0.00e+000 -5.69e+003      0.0
56.77   0.997  6.056e-005 -7.46e-003  0.00e+000  0.00e+000 -5.36e+003      0.0
58.52   0.987  7.514e-005 -7.75e-003  0.00e+000  0.00e+000 -5.12e+003      0.0
60.28   1.004  5.328e-005 -8.05e-003  0.00e+000  0.00e+000 -5.33e+003      0.0
62.03   0.996  5.068e-005 -8.35e-003  0.00e+000  0.00e+000 -5.14e+003      0.0
63.78   1.006  5.602e-005 -8.66e-003  0.00e+000  0.00e+000 -5.22e+003      0.0
65.53   0.995  5.693e-005 -8.96e-003  0.00e+000  0.00e+000 -5.01e+003      0.0
65.53   0.997  5.868e-005 -8.96e-003  0.00e+000  0.00e+000 -5.04e+003      0.0
65.53   0.997  5.955e-005 -8.96e-003  0.00e+000  0.00e+000 -5.04e+003      0.0
67.28   0.985  8.257e-005 -9.27e-003  0.00e+000  0.00e+000 -4.78e+003      0.0

------------------------------ Comments --------------------------------------
- DT = 4.9 (98%); CJ = 5.6; P0 = 24.0 psi
- 243 mm lens; -40 MHz frequency shift
- Thesis label: SP1a
```

---------- Input Parameters ----------

Input filename	= j121x4		
Number of positions	= 12	Number of records	= 15
Starting position	= 747.0 mm	Increment	= 25.4000 mm
Mesh length	= 14.50 mm	Normalizing velocity	= 447.8 m/s
Static pressure	= 5.85 psi	Total pressure	= 21.37 psi
Traverse direction	= x	Total temperature	= 540.00 R
Transform method	= 1	Weighting method	= 2
x0/m	= 0.00		
Outliers removed	Sample st. dev. = 3.00;	Record st. dev. =	2.50

---------- Global Information ----------

nu = 2.019e-005 kg/(m s) ; rho = 6.781e-001 kg/m3
Mach-p = 1.497; Mach-u = 1.553; U-mean = 448.117; Re_m = 321810
U-coef = 0.00002; U-exp = -0.3051; U-exp-ci = 0.3037; U-cor = 0.2150
V-coef = 0.00000; V-exp = 0.0000; V-exp-ci = 0.0000; V-cor = 0.0000

---------- Ensemble Information ----------

pos	Order	nsam	Rate(avg)	%Val(avg)	nrej(avg)	Rec_rej
51.52	1	1000	3636	99.7	4.3	1
53.27	6	1000	1975	99.8	2.6	1
55.02	2	1000	3181	99.6	3.1	0
56.77	7	1000	2564	99.5	4.9	0
58.52	3	1000	3249	98.3	5.6	0
60.28	8	1000	2136	99.7	4.3	0
62.03	4	1000	2228	99.2	4.5	0
63.78	9	1000	2168	99.7	3.9	0
65.53	0	1000	3313	99.2	5.2	0
65.53	5	1000	2396	99.2	3.9	0
65.53	11	1000	3171	99.4	4.9	1
67.28	10	999	445	98.5	5.3	0

pos	U	U_ci	u'	u'_ci	V	V_ci	v'	v'_ci	uv/u'v'	u'/v'	u_sk	u_fl
51.52	447.86	0.06	3.314	0.060	0.00	0.00	0.000	0.000	0.000	0.00	0.046	3.04
53.27	453.57	0.07	3.608	0.030	0.00	0.00	0.000	0.000	0.000	0.00	0.078	2.85
55.02	454.48	0.07	3.539	0.040	0.00	0.00	0.000	0.000	0.000	0.00	0.035	2.82
56.77	447.38	0.08	3.291	0.049	0.00	0.00	0.000	0.000	0.000	0.00	0.052	3.05
58.52	441.15	0.08	3.789	0.054	0.00	0.00	0.000	0.000	0.000	0.00	0.094	3.12
60.28	449.30	0.08	3.233	0.041	0.00	0.00	0.000	0.000	0.000	0.00	0.106	3.00
62.03	446.19	0.13	3.146	0.030	0.00	0.00	0.000	0.000	0.000	0.00	-0.021	2.98
63.78	451.58	0.06	3.583	0.040	0.00	0.00	0.000	0.000	0.000	0.00	0.017	2.85
65.53	445.68	0.07	3.660	0.038	0.00	0.00	0.000	0.000	0.000	0.00	-0.072	2.91
65.53	445.72	0.10	3.690	0.048	0.00	0.00	0.000	0.000	0.000	0.00	-0.030	2.96
65.53	446.41	0.45	3.401	0.075	0.00	0.00	0.000	0.000	0.000	0.00	-0.019	2.93
67.28	443.93	0.13	3.550	0.041	0.00	0.00	0.000	0.000	0.000	0.00	0.066	3.00

pos	U/Um	u'2/U2	integral	taylor	kolmog	diss rate	Re_tay
51.52	1.000	5.482e-005	-1.24e-002	0.00e+000	0.00e+000	-3.16e+003	0.0
53.27	1.013	6.328e-005	-1.29e-002	0.00e+000	0.00e+000	-3.21e+003	0.0
55.02	1.015	6.065e-005	-1.33e-002	0.00e+000	0.00e+000	-3.16e+003	0.0
56.77	0.999	5.418e-005	-1.38e-002	0.00e+000	0.00e+000	-2.95e+003	0.0
58.52	0.985	7.383e-005	-1.43e-002	0.00e+000	0.00e+000	-2.77e+003	0.0
60.28	1.003	5.183e-005	-1.48e-002	0.00e+000	0.00e+000	-2.86e+003	0.0
62.03	0.996	4.972e-005	-1.53e-002	0.00e+000	0.00e+000	-2.75e+003	0.0
63.78	1.008	6.300e-005	-1.58e-002	0.00e+000	0.00e+000	-2.79e+003	0.0
65.53	0.995	6.747e-005	-1.63e-002	0.00e+000	0.00e+000	-2.64e+003	0.0
65.53	0.995	6.861e-005	-1.63e-002	0.00e+000	0.00e+000	-2.64e+003	0.0
65.53	0.997	5.819e-005	-1.63e-002	0.00e+000	0.00e+000	-2.65e+003	0.0
67.28	0.991	6.399e-005	-1.68e-002	0.00e+000	0.00e+000	-2.56e+003	0.0

---------- Comments ----------

- DT = 4.9 (98%); CJ = 5.6; P0 = 24.0 psi
- 243 mm lens; -40 kHz frequency shift
- same conditions as j121x3 (but different run), to check for consistency
- Thesis label: SP1b

---------- Input Parameters ----------

Input filename	= j125x1		
Number of positions	= 16	Number of records	= 10
Starting position	= 787.0 mm	Increment	= 6.3500 mm
Mesh length	= 14.50 mm	Normalizing velocity	= 447.9 m/s
Static pressure	= 6.44 psi	Total pressure	= 20.84 psi
Traverse direction	= x	Total temperature	= 540.00 R
Transform method	= 1	Weighting method	= 2
x0/m	= 0.00		

Outliers removed: Sample st. dev. = 3.00; Record st. dev. = 2.50

---------- Global Information ----------

nu = 1.955e-005 kg/(m s) ; rho = 7.211e-001 kg/m3

Mach-p = 1.412; Mach-u = 1.528; U-mean = 448.563; Re_m = 332672

U-coef = 0.00790; U-exp = 1.1754; U-exp-ci = 0.4936; U-cor = -0.2982

V-coef = 0.00000; V-exp = 0.0000; V-exp-ci = 0.0000; V-cor = 0.0000

---------- Ensemble Information ----------

pos	Order	nsam	Rate(avg)	%Val(avg)	nrej(avg)	Rec_rej
54.28	0	1000	1569	99.5	4.0	0
54.28	15	1000	2067	99.4	3.9	0
54.71	1	1000	2003	99.6	3.3	0
55.15	2	1000	2109	99.3	4.7	0
55.59	3	1000	2248	99.3	4.8	0
56.03	4	1000	2824	99.6	2.6	0
56.47	5	1000	2352	99.0	3.8	0
56.90	6	1000	2807	99.1	3.0	0
57.34	7	1000	2952	98.6	5.7	0
57.78	8	1000	2752	99.3	4.8	0
58.22	9	1000	2741	99.2	3.6	0
58.66	10	1000	2423	99.5	2.5	0
59.09	11	1000	2203	98.4	3.4	0
59.53	12	1000	2609	99.3	4.1	0
59.97	13	1000	2639	99.2	4.3	0
60.41	14	1000	2713	99.4	3.6	0

pos	U	U_ci	u'	u'_ci	V	V_ci	v'	v'_ci	uv/u'v'	u'/v'	u_sk	u_fl
54.28	455.97	0.13	3.715	0.076	0.00	0.00	0.000	0.000	0.000	0.00	-0.189	2.85
54.28	455.93	0.09	3.562	0.085	0.00	0.00	0.000	0.000	0.000	0.00	-0.101	2.85
54.71	454.29	0.09	3.558	0.075	0.00	0.00	0.000	0.000	0.000	0.00	-0.036	2.88
55.15	454.73	0.08	3.499	0.045	0.00	0.00	0.000	0.000	0.000	0.00	-0.034	2.86
55.59	452.31	0.11	3.743	0.078	0.00	0.00	0.000	0.000	0.000	0.00	-0.053	2.93
56.03	448.84	0.07	4.009	0.064	0.00	0.00	0.000	0.000	0.000	0.00	0.064	2.83
56.47	445.93	0.13	4.085	0.054	0.00	0.00	0.000	0.000	0.000	0.00	0.194	2.87
56.90	444.99	0.08	4.213	0.071	0.00	0.00	0.000	0.000	0.000	0.00	0.154	2.90
57.34	443.67	0.13	3.865	0.052	0.00	0.00	0.000	0.000	0.000	0.00	0.283	3.13
57.78	444.93	0.05	3.683	0.034	0.00	0.00	0.000	0.000	0.000	0.00	0.179	2.98
58.22	445.76	0.12	3.590	0.056	0.00	0.00	0.000	0.000	0.000	0.00	0.113	2.86
58.66	447.45	0.09	3.543	0.052	0.00	0.00	0.000	0.000	0.000	0.00	0.038	2.85
59.09	446.95	0.13	3.637	0.144	0.00	0.00	0.000	0.000	0.000	0.00	-0.010	2.88
59.53	447.78	0.12	3.426	0.049	0.00	0.00	0.000	0.000	0.000	0.00	0.033	2.94
59.97	447.27	0.10	3.498	0.048	0.00	0.00	0.000	0.000	0.000	0.00	0.031	2.88
60.41	447.57	0.05	3.423	0.046	0.00	0.00	0.000	0.000	0.000	0.00	0.003	2.82

pos	U/Um	u'2/U2	integral	taylor	kolmog	diss rate	Re_tay
54.28	1.018	6.647e-005	3.80e-003	5.36e-004	2.64e-005	1.54e+004	106.2
54.28	1.018	6.114e-005	3.80e-003	5.36e-004	2.64e-005	1.53e+004	106.2
54.71	1.014	6.140e-005	3.81e-003	5.39e-004	2.66e-005	1.49e+004	106.0
55.15	1.015	5.922e-005	3.82e-003	5.41e-004	2.67e-005	1.47e+004	106.0
55.59	1.010	6.856e-005	3.83e-003	5.44e-004	2.69e-005	1.42e+004	105.6
56.03	1.002	7.984e-005	3.85e-003	5.49e-004	2.72e-005	1.37e+004	105.1
56.47	0.996	8.397e-005	3.86e-003	5.53e-004	2.74e-005	1.32e+004	104.7
56.90	0.994	8.968e-005	3.87e-003	5.55e-004	2.76e-005	1.29e+004	104.5
57.34	0.991	7.592e-005	3.88e-003	5.58e-004	2.78e-005	1.25e+004	104.3
57.78	0.993	6.854e-005	3.89e-003	5.60e-004	2.78e-005	1.24e+004	104.4
58.22	0.995	6.492e-005	3.91e-003	5.61e-004	2.79e-005	1.23e+004	104.4
58.66	0.999	6.274e-005	3.92e-003	5.62e-004	2.79e-005	1.23e+004	104.5
59.09	0.998	6.652e-005	3.93e-003	5.65e-004	2.81e-005	1.20e+004	104.4
59.53	1.000	5.858e-005	3.94e-003	5.66e-004	2.82e-005	1.19e+004	104.4
59.97	0.999	6.120e-005	3.95e-003	5.69e-004	2.83e-005	1.17e+004	104.3
60.41	0.999	5.853e-005	3.97e-003	5.71e-004	2.84e-005	1.15e+004	104.3

---------- Comments ----------

- DT = 4.9 (98%); CJ = 5.6; PO = 24.0 psi
- 243 mm lens; -40 MHz frequency shift
- y = -0.4 cm by accident
- 1/4" traverse

```
------------------------------ Input Parameters ------------------------------
  Input filename       = j125x2
  Number of positions  = 19              Number of records    = 10
  Starting position    = 802.0 mm        Increment            = 1.5875 mm
  Mesh length          = 14.50 mm        Normalizing velocity = 447.9 m/s
  Static pressure      =  6.27 psi       Total pressure       =  21.11 psi
  Traverse direction   = x               Total temperature    = 538.00 R
  Transform method     = 1               Weighting method     = 2
  xO/m                 = 0.00
  Outliers removed:  Sample st. dev. =  3.00;  Record st. dev. =  2.50

------------------------------ Global Information ----------------------------
  nu = 1.953e-005 kg/(m s)        ; rho = 7.127e-001 kg/m3
  Mach-p =  1.440; Mach-u =  1.539; U-mean  = 448.349; Re_m  =  332828
  U-coef = 0.00000; U-exp = -16.1933; U-exp-ci =  0.8503; U-cor =  0.8962
  V-coef = 0.00000; V-exp =  0.0000; V-exp-ci =  0.0000; V-cor =  0.0000

---------------------------- Ensemble Information ---------------------------
 pos  Order  nsam  Rate(avg)  %Val(avg)  nrej(avg)  Rec_rej
55.31   0    1000     1796       99.8        4.5        0
55.31  18    1000     1568       99.3        4.6        0
55.42   1    1000     1821       99.6        3.7        0
55.53   2    1000     1778       99.6        4.0        0
55.64   3    1000     1706       99.6        4.9        0
55.75   4    1000     1807       99.7        3.5        0
55.86   5    1000     1938       99.5        2.7        0
55.97   6    1000     2077       99.4        2.8        0
56.08   7    1000     2160       99.5        2.7        0
56.19   8    1000     2155       99.4        2.7        0
56.30   9    1000     2336       99.4        2.8        0
56.41  10    1000     2242       99.2        3.7        0
56.51  11    1000     1968       99.0        4.1        0
56.62  12    1000     1990       99.1        4.5        0
56.73  13    1000     1770       99.4        3.7        0
56.84  14    1000     1964       98.9        4.0        0
56.95  15    1000     2109       98.6        2.7        0
57.06  16    1000     2415       98.6        3.7        0
57.17  17    1000     2109       98.4        3.1        0

 pos      U    U_ci    u'    u'_ci    V   V_ci    v'    v'_ci  uv/u'v'  u'/v'  u_sk   u_fl
55.31  454.83  0.17  3.585  0.068  0.00  0.00  0.000  0.000  0.000   0.00  0.033  2.87
55.31  453.91  0.08  3.622  0.080  0.00  0.00  0.000  0.000  0.000   0.00  0.041  2.96
55.42  454.34  0.11  3.555  0.048  0.00  0.00  0.000  0.000  0.000   0.00  0.010  2.88
55.53  453.55  0.12  3.573  0.027  0.00  0.00  0.000  0.000  0.000   0.00 -0.001  2.92
55.64  452.78  0.12  3.633  0.070  0.00  0.00  0.000  0.000  0.000   0.00 -0.020  2.90
55.75  451.99  0.11  3.740  0.043  0.00  0.00  0.000  0.000  0.000   0.00 -0.033  2.96
55.86  450.86  0.10  3.935  0.086  0.00  0.00  0.000  0.000  0.000   0.00 -0.021  2.85
55.97  449.42  0.07  4.063  0.063  0.00  0.00  0.000  0.000  0.000   0.00  0.005  2.83
56.08  448.31  0.12  4.053  0.060  0.00  0.00  0.000  0.000  0.000   0.00  0.015  2.84
56.19  447.92  0.11  4.097  0.072  0.00  0.00  0.000  0.000  0.000   0.00  0.053  2.77
56.30  446.93  0.12  4.222  0.070  0.00  0.00  0.000  0.000  0.000   0.00  0.101  2.76
56.41  446.18  0.06  4.038  0.054  0.00  0.00  0.000  0.000  0.000   0.00  0.125  2.79
56.51  446.20  0.09  3.984  0.046  0.00  0.00  0.000  0.000  0.000   0.00  0.113  2.87
56.62  446.92  0.12  3.929  0.060  0.00  0.00  0.000  0.000  0.000   0.00  0.076  2.86
56.73  446.81  0.12  3.963  0.029  0.00  0.00  0.000  0.000  0.000   0.00  0.163  2.82
56.84  445.74  0.11  4.319  0.074  0.00  0.00  0.000  0.000  0.000   0.00  0.070  2.82
56.95  443.22  0.13  4.673  0.092  0.00  0.00  0.000  0.000  0.000   0.00  0.155  2.94
57.06  442.00  0.10  4.644  0.089  0.00  0.00  0.000  0.000  0.000   0.00  0.209  3.00
57.17  442.27  0.13  4.544  0.072  0.00  0.00  0.000  0.000  0.000   0.00  0.313  3.02

 pos     U/Um     u'2/U2     integral     taylor     kolmog    diss rate  Re_tay
55.31   1.016  6.217e-005 -2.59e-004  0.00e+000  0.00e+000 -1.75e+005     0.0
55.31   1.014  6.377e-005 -2.59e-004  0.00e+000  0.00e+000 -1.74e+005     0.0
55.42   1.014  6.124e-005 -2.63e-004  0.00e+000  0.00e+000 -1.80e+005     0.0
55.53   1.013  6.208e-005 -2.68e-004  0.00e+000  0.00e+000 -1.84e+005     0.0
55.64   1.011  6.444e-005 -2.73e-004  0.00e+000  0.00e+000 -1.89e+005     0.0
55.75   1.009  6.849e-005 -2.78e-004  0.00e+000  0.00e+000 -1.93e+005     0.0
55.86   1.007  7.629e-005 -2.83e-004  0.00e+000  0.00e+000 -1.98e+005     0.0
55.97   1.004  8.179e-005 -2.88e-004  0.00e+000  0.00e+000 -2.02e+005     0.0
56.08   1.001  8.176e-005 -2.93e-004  0.00e+000  0.00e+000 -2.06e+005     0.0
56.19   1.000  8.374e-005 -2.98e-004  0.00e+000  0.00e+000 -2.12e+005     0.0
56.30   0.998  8.932e-005 -3.04e-004  0.00e+000  0.00e+000 -2.17e+005     0.0
56.41   0.996  8.195e-005 -3.09e-004  0.00e+000  0.00e+000 -2.22e+005     0.0
56.51   0.996  7.973e-005 -3.15e-004  0.00e+000  0.00e+000 -2.29e+005     0.0
56.62   0.998  7.734e-005 -3.20e-004  0.00e+000  0.00e+000 -2.37e+005     0.0
56.73   0.998  7.868e-005 -3.26e-004  0.00e+000  0.00e+000 -2.44e+005     0.0
56.84   0.995  9.398e-005 -3.32e-004  0.00e+000  0.00e+000 -2.49e+005     0.0
56.95   0.990  1.113e-004 -3.37e-004  0.00e+000  0.00e+000 -2.52e+005     0.0
57.06   0.987  1.105e-004 -3.43e-004  0.00e+000  0.00e+000 -2.58e+005     0.0
57.17   0.988  1.056e-004 -3.49e-004  0.00e+000  0.00e+000 -2.66e+005     0.0
```

---------- Comments ----------
- DT = 4.9 (98%); CJ = 5.6, PO = 24.0 psi
- 243 mm lens; -40 MHz frequency shift
- y = -0.45 cm (looked best to get clean wave crossing)
- 1/16" traverse
- Thesis label: SP1d

---------- Input Parameters ----------

Input filename	= j125z3		
Number of positions	= 12	Number of records	= 15
Starting position	= 747.0 mm	Increment	= 25.4000 mm
Mesh length	= 18.40 mm	Normalizing velocity	= -1.0 m/s
Static pressure	= 5.37 psi	Total pressure	= 21.28 psi
Traverse direction	= z	Total temperature	= 534.00 R
Transform method	= 1	Weighting method	= 2
x0/m	= 0.00		

Outliers removed: Sample st. dev. = 3.00; Record st. dev. = 2.50

---------- Global Information ----------

nu = 2.064e-005 kg/(m s) ; rho = 6.443e-001 kg/m3
Mach-p = 1.552; Mach-u = 1.573; U-mean = 446.015; Re_m = 397676
U-coef = 0.01371; U-exp = 1.2910; U-exp-ci = 0.6184; U-cor = -0.4161
V-coef = 0.00000; V-exp = 0.0000; V-exp-ci = 0.0000; V-cor = 0.0000

---------- Ensemble Information ----------

pos	Order	nsam	Rate(avg)	%Val(avg)	nrej(avg)	Rec_rej
40.60	1	1000	1106	99.9	3.2	1
41.98	6	1000	1788	99.5	1.2	1
43.36	2	1000	1562	98.7	4.7	0
44.74	7	1000	1884	99.1	4.3	0
46.12	3	1000	1570	99.5	4.5	0
47.50	8	1000	1456	99.8	3.7	0
48.88	4	1000	1176	99.7	4.1	0
50.26	9	1000	2181	98.6	5.5	0
51.64	0	1000	1396	98.8	4.6	1
51.64	5	1000	1677	98.5	4.9	0
51.64	11	1000	2244	98.7	5.0	0
53.02	10	1000	423	98.0	5.9	0

pos	U	U_ci	u'	u'_ci	V	V_ci	v'	v'_ci	uv/u'v'	u'/v'	u_sk	u_fl
40.60	458.75	0.05	4.436	0.034	0.00	0.00	0.000	0.000	0.000	0.00	-0.269	2.82
41.98	446.62	0.09	5.840	0.070	0.00	0.00	0.000	0.000	0.000	0.00	0.011	2.63
43.36	440.98	0.11	5.107	0.077	0.00	0.00	0.000	0.000	0.000	0.00	0.241	3.16
44.74	444.32	0.06	3.902	0.047	0.00	0.00	0.000	0.000	0.000	0.00	-0.011	2.91
46.12	447.82	0.07	3.838	0.041	0.00	0.00	0.000	0.000	0.000	0.00	-0.092	2.89
47.50	452.37	0.05	3.996	0.052	0.00	0.00	0.000	0.000	0.000	0.00	-0.123	2.94
48.88	451.63	0.07	4.097	0.037	0.00	0.00	0.000	0.000	0.000	0.00	-0.138	2.95
50.26	437.21	0.09	4.707	0.065	0.00	0.00	0.000	0.000	0.000	0.00	0.153	3.15
51.64	440.87	0.06	4.149	0.047	0.00	0.00	0.000	0.000	0.000	0.00	-0.078	3.02
51.64	439.88	0.07	4.165	0.042	0.00	0.00	0.000	0.000	0.000	0.00	-0.141	3.04
51.64	440.11	0.08	3.972	0.039	0.00	0.00	0.000	0.000	0.000	0.00	-0.125	3.05
53.02	440.57	0.09	3.988	0.052	0.00	0.00	0.000	0.000	0.000	0.00	-0.049	3.06

pos	U/Um	u'2/U2	integral	taylor	kolmog	diss rate	Re_tay
40.60	1.029	9.352e-005	4.13e-003	5.10e-004	2.35e-005	2.88e+004	121.6
41.98	1.001	1.711e-004	4.18e-003	5.26e-004	2.45e-005	2.46e+004	119.4
43.36	0.989	1.343e-004	4.23e-003	5.38e-004	2.51e-005	2.20e+004	118.1
44.74	0.996	7.719e-005	4.28e-003	5.44e-004	2.55e-005	2.09e+004	118.0
46.12	1.004	7.349e-005	4.33e-003	5.50e-004	2.58e-005	2.00e+004	117.9
47.50	1.014	7.811e-005	4.37e-003	5.56e-004	2.60e-005	1.92e+004	118.0
48.88	1.013	8.231e-005	4.42e-003	5.64e-004	2.65e-005	1.79e+004	117.4
50.26	0.980	1.160e-004	4.46e-003	5.81e-004	2.75e-005	1.53e+004	115.0
51.64	0.988	8.863e-005	4.50e-003	5.87e-004	2.78e-005	1.47e+004	115.1
51.64	0.986	8.967e-005	4.50e-003	5.88e-004	2.79e-005	1.46e+004	114.9
51.64	0.987	8.149e-005	4.50e-003	5.87e-004	2.78e-005	1.46e+004	115.0
53.02	0.988	8.201e-005	4.55e-003	5.95e-004	2.82e-005	1.38e+004	114.6

---------- Comments ----------
- DT = 5.0 (100%); CJ = 5.6; PO = 25.5 psi
- 243 mm lens; -40 MHz frequency shift
- Large-hole plate
- Thesis label: SP2a

---------- Input Parameters ----------

Input filename	= j125z4		
Number of positions	= 16	Number of records	= 10
Starting position	= 743.0 mm	Increment	= 6.3500 mm
Mesh length	= 18.40 mm	Normalizing velocity	= 445.0 m/s
Static pressure	= 5.37 psi	Total pressure	= 21.51 psi
Traverse direction	= z	Total temperature	= 533.00 R
Transform method	= 1	Weighting method	= 2
z0/m	= 0.00		

Outliers removed: Sample st. dev. = 3.00, Record st. dev. = 2.50

---------- Global Information ----------

nu = 2.045e-005 kg/(m s) ; rho = 6.475e-001 kg/m3

Mach-p = 1.560; Mach-u = 1.582; U-mean = 447.462; Re_m = 402648

U-coef = 9.39064; U-exp = 3.0754; U-exp-ci = 0.5844; U-cor = -0.5681

V-coef = 0.00000; V-exp = 0.0000; V-exp-ci = 0.0000; V-cor = 0.0000

---------- Ensemble Information ----------

pos	Order	nsam	Rate(avg)	%Val(avg)	nrej(avg)	Rec_rej
40.38	0	1000	1966	99.8	2.4	0
40.38	15	1000	1488	99.6	2.7	1
40.73	1	1000	1737	99.7	2.9	0
41.07	2	1000	1836	99.8	3.3	0
41.42	3	1000	2118	99.8	2.9	0
41.76	4	1000	2678	99.6	3.2	0
42.11	5	1000	3237	99.1	2.8	0
42.45	6	1000	2901	99.1	2.3	0
42.80	7	1000	2993	99.1	5.3	0
43.14	8	1000	2205	98.3	3.5	0
43.49	9	1000	2955	98.8	6.0	0
43.83	10	1000	2661	98.3	5.5	0
44.18	11	1000	2794	98.5	5.1	0
44.52	12	1000	2786	98.5	3.8	0
44.87	13	1000	2697	98.6	4.5	0
45.21	14	1000	2415	98.5	4.4	0

pos	U	U_ci	u'	u'_ci	V	V_ci	v'	v'_ci	uv/u'v'	u'/v'	u_sk	u_fl
40.38	457.67	0.05	4.270	0.057	0.00	0.00	0.000	0.000	0.000	0.00	-0.225	2.79
40.38	456.56	0.04	4.427	0.052	0.00	0.00	0.000	0.000	0.000	0.00	-0.146	2.81
40.73	458.86	0.08	4.343	0.043	0.00	0.00	0.000	0.000	0.000	0.00	-0.255	2.75
41.07	459.95	0.10	4.407	0.068	0.00	0.00	0.000	0.000	0.000	0.00	-0.286	2.79
41.42	454.51	0.09	4.769	0.034	0.00	0.00	0.000	0.000	0.000	0.00	-0.107	2.79
41.76	449.11	0.15	4.841	0.054	0.00	0.00	0.000	0.000	0.000	0.00	-0.048	2.74
42.11	444.01	0.13	4.858	0.066	0.00	0.00	0.000	0.000	0.000	0.00	0.377	3.00
42.45	445.97	0.08	4.129	0.067	0.00	0.00	0.000	0.000	0.000	0.00	0.179	2.89
42.80	444.04	0.13	4.300	0.053	0.00	0.00	0.000	0.000	0.000	0.00	0.165	2.95
43.14	440.94	0.13	4.947	0.084	0.00	0.00	0.000	0.000	0.000	0.00	0.426	3.16
43.49	441.64	0.08	4.106	0.052	0.00	0.00	0.000	0.000	0.000	0.00	0.204	3.09
43.83	440.66	0.11	4.146	0.092	0.00	0.00	0.000	0.000	0.000	0.00	0.140	3.14
44.18	442.23	0.05	3.869	0.098	0.00	0.00	0.000	0.000	0.000	0.00	0.110	3.00
44.52	444.74	0.08	3.769	0.068	0.00	0.00	0.000	0.000	0.000	0.00	0.051	2.93
44.87	443.15	0.11	3.723	0.038	0.00	0.00	0.000	0.000	0.000	0.00	0.075	2.94
45.21	444.47	0.08	3.626	0.048	0.00	0.00	0.000	0.000	0.000	0.00	0.056	2.92

pos	U/Um	u'2/U2	integral	taylor	kolmog	diss rate	Re_tay
40.38	1.028	8.710e-005	1.67e-003	3.29e-004	1.91e-005	6.42e+004	76.4
40.38	1.026	9.406e-005	1.67e-003	3.29e-004	1.91e-005	6.38e+004	76.3
40.73	1.031	8.961e-005	1.67e-003	3.30e-004	1.92e-005	6.25e+004	75.8
41.07	1.034	9.186e-005	1.66e-003	3.31e-004	1.94e-005	6.08e+004	75.2
41.42	1.021	1.101e-004	1.65e-003	3.34e-004	1.97e-005	5.67e+004	74.2
41.76	1.009	1.162e-004	1.64e-003	3.37e-004	2.00e-005	5.29e+004	73.1
42.11	0.998	1.197e-004	1.64e-003	3.41e-004	2.04e-005	4.95e+004	72.0
42.45	1.002	8.577e-005	1.63e-003	3.41e-004	2.05e-005	4.85e+004	71.6
42.80	0.998	9.382e-005	1.62e-003	3.43e-004	2.07e-005	4.63e+004	70.8
43.14	0.991	1.259e-004	1.61e-003	3.46e-004	2.10e-005	4.39e+004	70.0
43.49	0.992	8.647e-005	1.61e-003	3.47e-004	2.12e-005	4.27e+004	69.5
43.83	0.990	8.865e-005	1.60e-003	3.49e-004	2.14e-005	4.10e+004	68.8
44.18	0.994	7.669e-005	1.59e-003	3.50e-004	2.15e-005	4.02e+004	68.4
44.52	0.999	7.189e-005	1.59e-003	3.50e-004	2.16e-005	3.96e+004	68.1
44.87	0.996	7.061e-005	1.58e-003	3.52e-004	2.18e-005	3.80e+004	67.4
45.21	0.999	6.658e-005	1.57e-003	3.53e-004	2.19e-005	3.71e+004	67.0

---------- Comments ----------

- DT = 5.0 (100%); CJ = 5.6; PO = 25.5 psi
- 243 mm lens; -40 KHz frequency shift
- Large-hole plate
- y = -0.4 cm by accident
- 1/4" traverse

---------- Input Parameters ----------

Input filename	= j126x1		
Number of positions	= 26	Number of records	= 10
Starting position	= 756.0 mm	Increment	= 1.5875 mm
Mesh length	= 18.40 mm	Normalizing velocity	= 446.0 m/s
Static pressure	= 5.39 psi	Total pressure	= 21.30 psi
Traverse direction	= x	Total temperature	= 540.00 R
Transform method	= 1	Weighting method	= 2
x0/m	= 0.00		

Outliers removed: Sample st. dev. = 3.00; Record st. dev. = 2.50

---------- Global Information ----------

nu = 2.102e-005 kg/(m s) ; rho = 6.390e-001 kg/m3

Mach-p = 1.551; Mach-u = 1.563; U-mean = 445.904; Re_m = 390295

U-coef = 0.1116D; U-exp = 1.8634; U-exp-ci = 0.0000; U-cor = -0.1177

V-coef = 0.00000; V-exp = 0.0000; V-exp-ci = 0.0000; V-cor = 0.0000

---------- Ensemble Information ----------

pos	Order	nsam	Rate(avg)	%Val(avg)	nrej(avg)	Rec_rej
41.09	0	1000	2305	99.9	3.4	0
41.09	25	1000	2138	99.7	4.3	0
41.17	1	1000	2405	99.9	2.7	0
41.26	2	1000	2710	99.9	3.1	0
41.35	3	1000	2787	99.9	1.7	0
41.43	4	1000	2743	99.8	1.3	0
41.52	5	1000	2737	99.8	1.4	0
41.60	6	1000	3359	99.6	2.3	0
41.69	7	1000	3220	99.7	1.2	0
41.78	8	1000	3282	99.3	2.2	0
41.86	9	1000	3729	99.5	2.5	0
41.95	10	1000	4101	99.3	4.7	0
42.04	11	1000	4178	99.3	5.6	0
42.12	12	1000	4460	99.4	7.1	0
42.21	13	1000	3917	99.4	7.1	0
42.29	14	1000	3991	99.5	6.7	0
42.38	15	1000	4299	99.4	5.5	0
42.47	16	1000	3751	99.6	4.8	0
42.55	17	1000	1272	99.1	4.3	0
42.64	18	1000	2174	99.4	4.7	0
42.73	19	1000	3408	99.4	4.8	0
42.81	20	1000	4173	99.4	6.7	0
42.90	21	1000	4157	99.1	6.2	0
42.99	22	1000	4500	99.2	8.6	0
43.07	23	1000	4872	99.1	8.5	0
43.16	24	1000	3778	99.1	8.6	0

pos	U	U_ci	u'	u'_ci	V	V_ci	v'	v'_ci	uv/u'v'	u'/v'	u_sk	u_fl
41.09	455.84	0.16	3.900	0.045	0.00	0.00	0.000	0.000	0.000	0.00	-0.029	2.90
41.09	461.69	0.12	4.075	0.094	0.00	0.00	0.000	0.000	0.000	0.00	-0.333	2.91
41.17	455.57	0.07	3.970	0.048	0.00	0.00	0.000	0.000	0.000	0.00	0.005	2.86
41.26	455.26	0.17	4.094	0.068	0.00	0.00	0.000	0.000	0.000	0.00	-0.008	2.88
41.35	453.96	0.08	4.460	0.047	0.00	0.00	0.000	0.000	0.000	0.00	-0.025	2.78
41.43	452.66	0.12	4.858	0.101	0.00	0.00	0.000	0.000	0.000	0.00	-0.021	2.73
41.52	451.10	0.11	4.983	0.066	0.00	0.00	0.000	0.000	0.000	0.00	0.044	2.65
41.60	449.37	0.09	5.064	0.063	0.00	0.00	0.000	0.000	0.000	0.00	0.112	2.72
41.69	446.61	0.18	5.557	0.067	0.00	0.00	0.000	0.000	0.000	0.00	0.149	2.63
41.78	444.13	0.13	5.868	0.100	0.00	0.00	0.000	0.000	0.000	0.00	0.307	2.76
41.86	442.74	0.14	5.621	0.139	0.00	0.00	0.000	0.000	0.000	0.00	0.436	2.99
41.95	442.75	0.18	5.396	0.108	0.00	0.00	0.000	0.000	0.000	0.00	0.524	3.31
42.04	442.74	0.10	4.955	0.118	0.00	0.00	0.000	0.000	0.000	0.00	0.550	3.37
42.12	442.57	0.13	4.686	0.128	0.00	0.00	0.000	0.000	0.000	0.00	0.484	3.45
42.21	443.00	0.14	4.334	0.085	0.00	0.00	0.000	0.000	0.000	0.00	0.461	3.37
42.29	443.70	0.11	4.205	0.055	0.00	0.00	0.000	0.000	0.000	0.00	0.431	3.31
42.38	444.53	0.10	4.086	0.090	0.00	0.00	0.000	0.000	0.000	0.00	0.292	3.12
42.47	444.93	0.08	3.960	0.057	0.00	0.00	0.000	0.000	0.000	0.00	0.279	3.05
42.55	445.09	0.12	4.660	0.067	0.00	0.00	0.000	0.000	0.000	0.00	0.302	2.97
42.64	444.70	0.07	4.253	0.073	0.00	0.00	0.000	0.000	0.000	0.00	0.271	3.01
42.73	443.44	0.05	4.123	0.074	0.00	0.00	0.000	0.000	0.000	0.00	0.335	3.20
42.81	442.26	0.13	4.258	0.089	0.00	0.00	0.000	0.000	0.000	0.00	0.246	3.16
42.90	440.89	0.10	4.423	0.074	0.00	0.00	0.000	0.000	0.000	0.00	0.286	3.36
42.99	439.57	0.09	4.399	0.130	0.00	0.00	0.000	0.000	0.000	0.00	0.255	3.34
43.07	438.18	0.11	4.250	0.062	0.00	0.00	0.000	0.000	0.000	0.00	0.267	3.37
43.16	442.01	0.10	4.506	0.064	0.00	0.00	0.000	0.000	0.000	0.00	0.351	3.33

pos	U/Um	u'2/U2	integral	tayler	kolmog	diss rate	Re_tay
41.09	1.022	7.322e-005	2.83e-003	4.33e-004	2.22e-005	3.85e+004	98.3
41.09	1.035	7.803e-005	2.83e-003	4.30e-004	2.20e-005	4.00e+004	98.9
41.17	1.021	7.596e-005	2.83e-003	4.33e-004	2.22e-005	3.82e+004	98.2
41.26	1.021	8.093e-005	2.84e-003	4.34e-004	2.23e-005	3.79e+004	98.1
41.35	1.018	9.654e-005	2.84e-003	4.35e-004	2.23e-005	3.73e+004	97.8
41.43	1.015	1.153e-004	2.84e-003	4.36e-004	2.24e-005	3.68e+004	97.6

41.52	1.011	1.221e-004	2.84e-003	4.37e-004	2.25e-005	3.62e+004	97.3
41.60	1.008	1.270e-004	2.84e-003	4.38e-004	2.26e-005	3.55e+004	97.1
41.69	1.001	1.549e-004	2.84e-003	4.40e-004	2.27e-005	3.47e+004	96.7
41.78	0.996	1.747e-004	2.84e-003	4.42e-004	2.29e-005	3.39e+004	96.3
41.86	0.993	1.614e-004	2.84e-003	4.43e-004	2.30e-005	3.34e+004	96.1
41.95	0.993	1.487e-004	2.84e-003	4.43e-004	2.30e-005	3.32e+004	96.0
42.04	0.993	1.255e-004	2.84e-003	4.44e-004	2.30e-005	3.30e+004	95.9
42.12	0.992	1.123e-004	2.84e-003	4.44e-004	2.31e-005	3.28e+004	95.8
42.21	0.993	9.583e-005	2.84e-003	4.45e-004	2.31e-005	3.27e+004	95.8
42.29	0.995	8.986e-005	2.84e-003	4.45e-004	2.31e-005	3.26e+004	95.8
42.38	0.997	8.460e-005	2.84e-003	4.45e-004	2.31e-005	3.26e+004	95.8
42.47	0.998	7.926e-005	2.84e-003	4.45e-004	2.31e-005	3.25e+004	95.7
42.55	0.998	1.097e-004	2.84e-003	4.45e-004	2.31e-005	3.24e+004	95.7
42.64	0.997	9.155e-005	2.84e-003	4.46e-004	2.32e-005	3.21e+004	95.5
42.73	0.994	8.653e-005	2.84e-003	4.47e-004	2.33e-005	3.17e+004	95.3
42.81	0.992	9.282e-005	2.84e-003	4.48e-004	2.34e-005	3.12e+004	95.1
42.90	0.989	1.007e-004	2.84e-003	4.49e-004	2.34e-005	3.08e+004	94.9
42.99	0.986	1.004e-004	2.84e-003	4.51e-004	2.35e-005	3.03e+004	94.7
43.07	0.982	9.413e-005	2.84e-003	4.52e-004	2.36e-005	2.98e+004	94.4
43.16	0.991	1.040e-004	2.84e-003	4.50e-004	2.35e-005	3.05e+004	94.8

---------- Comments ----------
- DT = 5.0 (1001); CJ = 5.6; PO = 25.5 psi
- 243 mm lens; -40 MHz frequency shift
- Large-hole plate
- y = -0.65 cm (to get clean wave crossing)
- 1/16" traverse
- Thesis label: SP2c

---------- Input Parameters ----------

Input filename	= j126x2		
Number of positions	= 16	Number of records	= 10
Starting position	= 743.0 mm	Increment	= 6.3500 mm
Mesh length	= 18.40 mm	Normalizing velocity	= 446.0 m/s
Static pressure	= 5.38 psi	Total pressure	= 21.22 psi
Traverse direction	= x	Total temperature	= 537.00 R
Transform method	= 1	Weighting method	= 2
x0/m	= 0.00		

Outliers removed: Sample st. dev. = 3.00; Record st. dev. = 2.50

---------- Global Information ----------

nu = 2.087e-005 kg/(m s) ; rho = 6.410e-001 kg/m3

Mach-p = 1.549; Mach-u = 1.576; U-mean = 446.454; Re_m = 395468

U-coef = 2.23205; U-exp = 2.7083; U-exp-ci = 0.8795; U-cor = -0.3746

V-coef = 0.00000; V-exp = 0.0000; V-exp-ci = 0.0000; V-cor = 0.0000

---------- Ensemble Information ----------

pos	Order	nsam	Rate(avg)	%Val(avg)	nrej(avg)	Rec_rej
40.38	0	1000	2274	100.0	3.4	0
40.38	15	1000	2637	99.9	4.3	0
40.73	1	1000	2283	100.0	3.5	0
41.07	2	1000	2132	99.9	2.7	0
41.42	3	1000	2518	99.9	3.4	0
41.76	4	1000	3142	99.7	1.0	1
42.11	5	1000	3490	99.3	4.9	0
42.45	6	1000	3656	99.8	4.9	0
42.80	7	1000	2872	99.6	6.4	0
43.14	8	1000	3436	99.2	8.2	0
43.49	9	1000	3445	99.2	8.5	0
43.83	10	1000	4268	99.5	5.7	0
44.18	11	1000	3516	99.6	4.0	0
44.52	12	1000	3925	99.7	4.7	0
44.87	13	1000	3681	99.6	5.2	0
45.21	14	1000	3325	99.7	4.7	0

pos	U	U_ci	u'	u'_ci	V	V_ci	v'	v'_ci	uv/u'v'	u'/v'	u_sk	u_fl
40.38	459.72	0.11	4.154	0.077	0.00	0.00	0.000	0.000	0.000	0.00	-0.249	2.83
40.38	459.62	0.08	4.147	0.035	0.00	0.00	0.000	0.000	0.000	0.00	-0.294	2.85
40.73	462.06	0.08	4.118	0.072	0.00	0.00	0.000	0.000	0.000	0.00	-0.363	2.92
41.07	460.62	0.12	4.036	0.036	0.00	0.00	0.000	0.000	0.000	0.00	-0.210	2.73
41.42	457.07	0.07	3.954	0.041	0.00	0.00	0.000	0.000	0.000	0.00	-0.052	2.89
41.76	448.18	0.18	5.918	0.092	0.00	0.00	0.000	0.000	0.000	0.00	0.053	2.56
42.11	443.46	0.09	4.936	0.078	0.00	0.00	0.000	0.000	0.000	0.00	0.399	3.24
42.45	446.08	0.11	4.107	0.062	0.00	0.00	0.000	0.000	0.000	0.00	0.176	2.97
42.80	442.86	0.10	4.343	0.112	0.00	0.00	0.000	0.000	0.000	0.00	0.278	3.24
43.14	440.42	0.15	4.415	0.096	0.00	0.00	0.000	0.000	0.000	0.00	0.235	3.41
43.49	440.48	0.08	4.124	0.085	0.00	0.00	0.000	0.000	0.000	0.00	0.176	3.30
43.83	443.03	0.08	3.737	0.054	0.00	0.00	0.000	0.000	0.000	0.00	0.111	3.07
44.18	445.07	0.11	3.780	0.065	0.00	0.00	0.000	0.000	0.000	0.00	-0.016	2.92
44.52	445.30	0.05	3.637	0.053	0.00	0.00	0.000	0.000	0.000	0.00	0.010	2.86
44.87	445.28	0.08	3.644	0.056	0.00	0.00	0.000	0.000	0.000	0.00	-0.010	2.89
45.21	447.17	0.07	3.719	0.053	0.00	0.00	0.000	0.000	0.000	0.00	-0.074	2.89

pos	U/Um	u'2/U2	integral	taylor	kolmog	diss rate	Re_tay
40.38	1.031	8.171e-005	1.83e-003	3.53e-004	2.03e-005	5.30e+004	77.6
40.38	1.031	8.143e-005	1.83e-003	3.53e-004	2.04e-005	5.29e+004	77.6
40.73	1.036	7.950e-005	1.82e-003	3.53e-004	2.04e-005	5.21e+004	77.3
41.07	1.033	7.679e-005	1.82e-003	3.55e-004	2.06e-005	5.00e+004	76.6
41.42	1.025	7.487e-005	1.81e-003	3.58e-004	2.09e-005	4.74e+004	75.8
41.76	1.005	1.744e-004	1.80e-003	3.63e-004	2.14e-005	4.33e+004	74.5
42.11	0.994	1.240e-004	1.80e-003	3.67e-004	2.17e-005	4.07e+004	73.6
42.45	1.000	8.482e-005	1.79e-003	3.67e-004	2.18e-005	4.02e+004	73.3
42.80	0.993	9.633e-005	1.79e-003	3.70e-004	2.21e-005	3.82e+004	72.5
43.14	0.987	1.006e-004	1.78e-003	3.73e-004	2.23e-005	3.64e+004	71.8
43.49	0.988	8.774e-005	1.78e-003	3.74e-004	2.25e-005	3.54e+004	71.3
43.83	0.993	7.119e-005	1.77e-003	3.74e-004	2.26e-005	3.50e+004	71.1
44.18	0.998	7.220e-005	1.77e-003	3.75e-004	2.27e-005	3.44e+004	70.7
44.52	0.998	6.675e-005	1.76e-003	3.76e-004	2.28e-005	3.35e+004	70.3
44.87	0.998	6.700e-005	1.76e-003	3.78e-004	2.30e-005	3.26e+004	69.8
45.21	1.003	6.920e-005	1.75e-003	3.79e-004	2.31e-005	3.21e+004	69.5

---------- Comments ----------

- DT = 5.0 (100%); CJ = 5.6; PO = 25.5 psi
- 243 mm lens; -40 KHz frequency shift
- Large-hole plate
- same conditions as j125x4, but y=0
- 1/4" traverse
- Thesis label: SP2b

```
------------------------------ Input Parameters ------------------------------
  Input filename        = j126z3
  Number of positions   = 16              Number of records     = 10
  Starting position     = 787.0 mm        Increment             = 6.3500 mm
  Mesh length           = 14.50 mm        Normalizing velocity = 447.8 m/s
  Static pressure       =  5.43 psi       Total pressure        =  22.31 psi
  Traverse direction    = z               Total temperature     = 537.00 R
  Transform method      = 1               Weighting method      = 2
  z0/m                  =  0.00
  Outliers removed:  Sample st. dev. =   3.00;  Record st. dev. =   2.50

------------------------------ Global Information ----------------------------
  nu =  2.023e-005 kg/(m s)        ; rho =  6.546e-001 kg/m3
  Mach-p =   1.577; Mach-u =  1.584; U-mean    = 448.157; Re_m  =  321218
  U-coef = 0.01252; U-exp =  .2920; U-exp-ci =  0.6758; U-cor = -0.2433
  V-coef = 0.00000; V-exp =  0.0000; V-exp-ci =  0.0000; V-cor =  0.0000

---------------------------- Ensemble Information ----------------------------
 pos  Order  nsam  Rate(avg)  %Val(avg)  nrej(avg)  Rec_rej
54.28    0  1000       1107       99.6        3.1        0
54.28   15  1000       1392       99.4        5.0        0
54.71    1  1000       1252       99.5        4.4        0
55.15    2  1000       1308       99.5        5.0        0
55.59    3  1000       1487       99.7        4.2        0
56.03    4  1000       2241       99.4        3.7        0
56.47    5  1000       2807       99.6        4.8        0
56.90    6  1000       2684       99.4        3.1        0
57.34    7  1000       2836       98.6        7.2        0
57.78    8  1000       2842       99.3        5.1        0
58.22    9  1000       2451       99.2        5.2        0
58.66   10  1000       2361       99.5        1.8        0
59.09   11  1000       1951       99.5        3.4        0
59.53   12  1000       1863       99.3        3.5        0
59.97   13  1000       2270       99.1        3.7        0
60.41   14  1000       2385       99.5        3.6        0

 pos      U    U_ci     u'    u'_ci     V    V_ci     v'    v'_ci uv/u'v' u'/v' u_sk   u_fl
54.28  455.47  0.21  3.835  0.060  0.00  0.00  0.000  0.000  0.000  0.00 -0.054  2.87
54.28  454.89  0.11  3.707  0.074  0.00  0.00  0.000  0.000  0.000  0.00 -0.049  2.99
54.71  455.77  0.12  3.652  0.056  0.00  0.00  0.000  0.000  0.000  0.00 -0.039  2.95
55.15  455.81  0.10  3.677  0.091  0.00  0.00  0.000  0.000  0.000  0.00 -0.037  2.94
55.59  451.77  0.10  3.711  0.070  0.00  0.00  0.000  0.000  0.000  0.00 -0.052  2.92
56.03  450.89  0.21  3.616  0.127  0.00  0.00  0.000  0.000  0.000  0.00 -0.027  2.93
56.47  449.61  0.08  3.439  0.053  0.00  0.00  0.000  0.000  0.000  0.00 -0.041  2.91
56.90  445.59  0.13  4.156  0.055  0.00  0.00  0.000  0.000  0.000  0.00  0.088  2.83
57.34  439.44  0.13  4.691  0.103  0.00  0.00  0.000  0.000  0.000  0.00  0.481  3.44
57.78  443.17  0.08  3.601  0.049  0.00  0.00  0.000  0.000  0.000  0.00  0.158  3.00
58.22  444.20  0.09  3.486  0.059  0.00  0.00  0.000  0.000  0.000  0.00  0.112  2.95
58.66  446.93  0.11  3.539  0.080  0.00  0.00  0.000  0.000  0.000  0.00  0.029  2.85
59.09  448.04  0.07  3.354  0.084  0.00  0.00  0.000  0.000  0.000  0.00 -0.015  2.91
59.53  446.13  0.07  3.497  0.086  0.00  0.00  0.000  0.000  0.000  0.00  0.048  2.84
59.97  443.91  0.09  3.601  0.097  0.00  0.00  0.000  0.000  0.000  0.00  0.053  2.94
60.41  445.65  0.08  3.324  0.054  0.00  0.00  0.000  0.000  0.000  0.00  0.027  2.82

 pos    U/Um     u'2/U2     integral     taylor     kolmog   diss rate  Re_tay
54.28  1.017  7.095e-005  3.44e-003  5.20e-004  2.85e-005  1.67e+004    99.3
54.28  1.016  6.647e-005  3.44e-003  5.20e-004  2.86e-005  1.67e+004    99.2
54.71  1.018  6.425e-005  3.45e-003  5.22e-004  2.86e-005  1.64e+004    99.2
55.15  1.018  6.519e-005  3.46e-003  5.24e-004  2.88e-005  1.62e+004    99.1
55.59  1.009  6.753e-005  3.47e-003  5.29e-004  2.71e-005  1.54e+004    98.5
56.03  1.007  6.455e-005  3.48e-003  5.31e-004  2.72e-005  1.51e+004    98.3
56.47  1.004  5.854e-005  3.49e-003  5.34e-004  2.74e-005  1.47e+004    98.1
56.90  0.995  8.705e-005  3.50e-003  5.38e-004  2.77e-005  1.40e+004    97.5
57.34  0.981  1.141e-004  3.51e-003  5.44e-004  2.81e-005  1.32e+004    96.7
57.78  0.990  6.608e-005  3.52e-003  5.44e-004  2.81e-005  1.33e+004    97.0
58.22  0.992  6.163e-005  3.53e-003  5.45e-004  2.81e-005  1.32e+004    97.0
58.66  0.998  6.278e-005  3.54e-003  5.46e-004  2.81e-005  1.32e+004    97.2
59.09  1.000  5.813e-005  3.55e-003  5.47e-004  2.82e-005  1.31e+004    97.2
59.53  0.996  6.156e-005  3.56e-003  5.50e-004  2.84e-005  1.27e+004    96.9
59.97  0.991  6.594e-005  3.57e-003  5.54e-004  2.86e-005  1.23e+004    96.6
60.41  0.995  5.569e-005  3.57e-003  5.55e-004  2.87e-005  1.23e+004    96.7

------------------------------- Comments -------------------------------
- DT = 5.0 (100%); CJ = 5.6; PO = 25.5 psi
- 243 mm lens; -40 MHz frequency shift
- meant to be correction of j125z2, with y=0, but PO and DT slightly
  different.  These should have a negligible effect on results.
- 1/4" traverse
- Thesis label: SPic
```

```
------------------------------ Input Parameters ------------------------------
  Input filename       = j126i4
  Number of positions  =  7            Number of records    = 5
  Starting position    = 747.0 mm      Increment            = 25.4000 mm
  Mesh length          = 14.50 mm      Normalizing velocity =  1.0 m/s
  Static pressure      =  5.43 psi     Total pressure       = 18.20 psi
  Traverse direction   = (             Total temperature    = 537.00 R
  Transform method     = 1             Weighting method     = 2
  x0/m                 = 0.00
  Outliers removed:  Sample st. dev. =  3.00;  Record st. dev. =  2.50

------------------------------ Global Information ----------------------------
  nu =  2.253e-005 kg/(m s)       ; rho =  6.176e-001 kg/m3
  Mach-p =   1.437; Mach-u =  0.775; U-mean   = 225.651; Re_m  =  145223
  U-coef = 0.00000; U-exp =  0.0000; U-exp-ci =  0.0000; U-cor =  0.0000
  V-coef = 0.00000; V-exp =  0.0000; V-exp-ci =  0.0000; V-cor =  0.0000

---------------------------- Ensemble Information ----------------------------
 pos  Order  nsam  Rate(avg)  %Val(avg)  nrej(avg)  Rec_rej
20.00   0    1000    6281       100.0       2.6        0
21.00   1    1000    8817       100.0       3.2        0
22.00   2    1000    7525       100.0       2.8        0
23.00   3    1000    6171       100.0      11.0        0
24.00   4    1000    4354       100.0      10.0        0
25.00   5    1000    7344       100.0       6.2        0
26.00   6    1000    8495       100.0       5.0        0

 pos      U    U_ci    u'    u'_ci    V    V_ci    v'    v'_ci uv/u'v' u'/v' u_sk   u_fl
20.00  196.87  0.25  2.657  0.037  0.00  0.00  0.000  0.000  0.000  0.00  0.136  2.94
21.00  207.23  0.12  2.752  0.071  0.00  0.00  0.000  0.000  0.000  0.00  0.161  2.84
22.00  222.39  0.16  3.271  0.093  0.00  0.00  0.000  0.000  0.000  0.00  0.111  2.63
23.00  224.86  0.45  5.179  0.469  0.00  0.00  0.000  0.000  0.000  0.00  0.164  2.85
24.00  231.82  3.80  8.254  1.168  0.00  0.00  0.000  0.000  0.000  0.00  0.217  3.27
25.00  239.83  0.50  8.789  0.539  0.00  0.00  0.000  0.000  0.000  0.00  0.296  2.96
26.00  256.56  0.35 11.077  0.479  0.00  0.00  0.000  0.000  0.000  0.00 -0.335  2.94

 pos     U/Um     u'2/U2     integral     taylor     kolmog    diss rate  Re_tay
20.00  196.866  1.821e-004  0.00e+000  0.00e+000  0.00e+000  0.00e+000     0.0
21.00  207.228  1.765e-004  0.00e+000  0.00e+000  0.00e+000  0.00e+000     0.0
22.00  222.390  2.165e-004  0.00e+000  0.00e+000  0.00e+000  0.00e+000     0.0
23.00  224.860  5.340e-004  0.00e+000  0.00e+000  0.00e+000  0.00e+000     0.0
24.00  231.820  1.299e-003  0.00e+000  0.00e+000  0.00e+000  0.00e+000     0.0
25.00  239.834  1.347e-003  0.00e+000  0.00e+000  0.00e+000  0.00e+000     0.0
26.00  256.560  1.867e-003  0.00e+000  0.00e+000  0.00e+000  0.00e+000     0.0

---------------------------------- Comments ----------------------------------
- DI = 4.6 (92%); CI = 6.2; PO = 20-26 psi
- 243 mm lens; 0 KHz frequency shift
- Pressure traverse (tunnel calibration)
```

```
------------------------------ Input Parameters ------------------------------
  Input filename        = j126z5
  Number of positions   = 12              Number of records     = 15
  Starting position     = 747.0 mm        Increment             = 25.4000 mm
  Mesh length           = 14.60 mm        Normalizing velocity  = -1.0 m/s
  Static pressure       =  11.73 psi      Total pressure        =  16.16 psi
  Traverse direction    = z               Total temperature     = 535.00 R
  Transform method      = 1               Weighting method      = 2
  z0/m                  =  0.00
  Outliers removed:  Sample st. dev. =   3.00;  Record st. dev. =   2.50

------------------------------ Global Information ----------------------------
  nu =  1.644e-005 kg/(m s)        ; rho =  1.039e+000 kg/m3
  Mach-p =   0.692; Mach-u =  0.673; U-mean   = 222.284; Re_m  =  196105
  U-coef = 0.01202; U-exp =  1.0039; U-exp-ci =  0.0498; U-cor = -0.9753
  V-coef = 0.00000; V-exp =  0.0000; V-exp-ci =  0.0000; V-cor =  0.0000

------------------------------ Ensemble Information --------------------------
 pos  Order  nsam  Rate(avg)  %Val(avg)  nrej(avg)  Rec_rej
51.52   1    1000     7254        98.7        1.5        0
53.27   6    1000     7126        98.8        2.6        0
55.02   2    1000     7919        99.2        1.7        0
56.77   7    1000     4139        99.0        2.1        1
58.52   3    1000     5664        99.3        2.7        0
60.28   8    1000     6930        99.6        1.5        0
62.03   4    1000     7844        99.8        0.9        0
63.78   9    1000     7057        99.9        1.8        0
65.53   0    1000     6120        99.9        1.5        0
65.53   5    1000     5648        99.9        2.4        0
65.53  11    1000     5540        99.9        1.4        0
67.28  10    1000      742        99.9        2.1        0

 pos      U    U_ci    u'    u'_ci    V    V_ci    v'   v'_ci uv/u'v' u'/v' u_sk   u_fl
51.52 220.02 0.09 3.318 0.040 0.00 0.00 0.000 0.000 0.000 0.00 0.160 2.85
53.27 220.13 0.06 3.262 0.034 0.00 0.00 0.000 0.000 0.000 0.00 0.135 2.87
55.02 220.93 0.08 3.227 0.055 0.00 0.00 0.000 0.000 0.000 0.00 0.151 2.69
56.77 221.35 0.12 3.229 0.051 0.00 0.00 0.000 0.000 0.000 0.00 0.106 2.73
58.52 221.65 0.13 3.145 0.048 0.00 0.00 0.000 0.000 0.000 0.00 0.124 2.69
60.28 222.24 0.09 3.131 0.033 0.00 0.00 0.000 0.000 0.000 0.00 0.107 2.69
62.03 223.16 0.08 3.086 0.027 0.00 0.00 0.000 0.000 0.000 0.00 0.060 2.51
63.78 223.89 0.10 3.110 0.043 0.00 0.00 0.000 0.000 0.000 0.00 -0.032 2.63
65.53 224.26 0.06 2.955 0.039 0.00 0.00 0.000 0.000 0.000 0.00 -0.029 2.59
65.53 224.38 0.09 2.985 0.045 0.00 0.00 0.000 0.000 0.000 0.00 -0.085 2.55
65.53 224.07 0.12 3.006 0.039 0.00 0.00 0.000 0.000 0.000 0.00 -0.011 2.56
67.28 225.09 0.07 2.940 0.040 0.00 0.00 0.000 0.000 0.000 0.00 -0.114 2.71

 pos    U/Um     u'2/U2     integral     taylor      kolmog   diss rate  Re_tay
51.52  0.990  2.276e-004  7.52e-003  7.46e-004  3.08e-005  4.93e+003   151.3
53.27  0.990  2.197e-004  7.65e-003  7.58e-004  3.13e-005  4.62e+003   151.3
55.02  0.994  2.136e-004  7.77e-003  7.69e-004  3.17e-005  4.38e+003   151.6
56.77  0.996  2.130e-004  7.89e-003  7.80e-004  3.22e-005  4.13e+003   151.7
58.52  0.997  2.015e-004  8.01e-003  7.92e-004  3.27e-005  3.91e+003   151.8
60.28  1.000  1.985e-004  8.13e-003  8.02e-004  3.31e-005  3.71e+003   152.0
62.03  1.004  1.913e-004  8.25e-003  8.12e-004  3.34e-005  3.55e+003   152.3
63.78  1.007  1.931e-004  8.36e-003  8.22e-004  3.38e-005  3.39e+003   152.5
65.53  1.009  1.737e-004  8.48e-003  8.33e-004  3.43e-005  3.23e+003   152.7
65.53  1.009  1.772e-004  8.48e-003  8.33e-004  3.42e-005  3.23e+003   152.7
65.53  1.008  1.801e-004  8.48e-003  8.33e-004  3.43e-005  3.22e+003   152.6
67.28  1.013  1.708e-004  8.59e-003  8.42e-004  3.46e-005  3.09e+003   152.9

---------------------------------- Comments ----------------------------------
- DT = 4.6 (92%); CJ = 6.2; P0 = 22 psi
- 243 mm lens; 0 KHz frequency shift
- calibration (j126z4) shows it is in subsonic regime, but no plateau
  reached before transition to transonic regime
- decay law parameters very sensitive to data rejection criteria
- Thesis label: M59a
```

```
------------------------------ Input Parameters ------------------------------
  Input filename       = j126z6
  Number of positions  = 7              Number of records    = 10
  Starting position    = 747.0 mm       Increment            = 25.4000 mm
  Mesh length          = 14.50 mm       Normalizing velocity = 221.8 m/s
  Static pressure      =  11.73 psi     Total pressure       =  16.16 psi
  Traverse direction   = y              Total temperature    = 535.00 R
  Transform method     = 1              Weighting method     = 2
  z0/m                 =  0.00
  Outliers removed:  Sample st. dev. =   3.00;  Record st. dev. =   2.50

------------------------------ Global Information ----------------------------
  nu =  1.644e-005 kg/(m s)        ; rho =  1.039e+000 kg/m3
  Mach-p =   0.692; Mach-u =  0.675; U-mean   = 222.737; Re_m  =  196505
  U-coef = 0.00000; U-exp =  0.0000; U-exp-ci =  0.0000; U-cor =  0.0000
  V-coef = 0.00000; V-exp =  0.0000; V-exp-ci =  0.0000; V-cor =  0.0000

---------------------------- Ensemble Information ----------------------------
 pos  Order  nsam  Rate(avg)  %Val(avg)  nrej(avg)  Rec_rej
-0.47   0    1000    1414        99.6        4.3        0
-0.31   1    1000    4182        99.8        3.0        0
-0.16   2    1000    6838        99.6        3.0        0
 0.00   3    1000    7263        99.5        2.7        0
 0.16   4    1000    6353        99.8        2.4        0
 0.31   5    1000    3734        99.6        3.7        0
 0.47   6    1000    1230        99.6        4.0        0

 pos      U    U_ci    u'    u'_ci    V    V_ci     v'    v'_ci uv/u'v' u'/v' u_sk   u_fl
-0.47  224.11  0.15  3.577  0.074  0.00  0.00  0.000  0.000  0.000  0.00  0.010  2.69
-0.31  223.09  0.12  3.382  0.043  0.00  0.00  0.000  0.000  0.000  0.00  0.065  2.66
-0.16  221.78  0.07  3.193  0.048  0.00  0.00  0.000  0.000  0.000  0.00  0.126  2.78
 0.00  221.82  0.12  3.202  0.043  0.00  0.00  0.000  0.000  0.000  0.00  0.092  2.65
 0.16  222.00  0.11  3.223  0.071  0.00  0.00  0.000  0.000  0.000  0.00  0.102  2.65
 0.31  222.80  0.09  3.367  0.063  0.00  0.00  0.000  0.000  0.000  0.00  0.075  2.68
 0.47  223.55  0.11  3.670  0.058  0.00  0.00  0.000  0.000  0.000  0.00  0.047  2.75

 pos     U/Um     u'2/U2     integral     taylor      kolmog    diss rate  Re_tay
-0.47   1.010  2.530e-004  0.00e+000  0.00e+000  0.00e+000  0.00e+000     0.0
-0.31   1.006  2.299e-004  0.00e+000  0.00e+000  0.00e+000  0.00e+000     0.0
-0.16   1.000  2.074e-004  0.00e+000  0.00e+000  0.00e+000  0.00e+000     0.0
 0.00   1.000  2.085e-004  0.00e+000  0.00e+000  0.00e+000  0.00e+000     0.0
 0.16   1.001  2.110e-004  0.00e+000  0.00e+000  0.00e+000  0.00e+000     0.0
 0.31   1.004  2.286e-004  0.00e+000  0.00e+000  0.00e+000  0.00e+000     0.0
 0.47   1.008  2.698e-004  0.00e+000  0.00e+000  0.00e+000  0.00e+000     0.0

---------------------------------- Comments ----------------------------------
- same run as j126z5
- y-traverse
```

```
------------------------------ Input Parameters ------------------------------
  Input filename        = j12617
  Number of positions   =  7            Number of records     = 10
  Starting position     = 747 0 mm      Increment             = 25 4000 mm
  Mesh length           = 14 50 mm      Normalizing velocity = 222 1 m/s
  Static pressure       =  11 73 psi    Total pressure        =  16.16 psi
  Traverse direction    = x             Total temperature     = 535 00 R
  Transform method      = 1             Weighting method      = 2
  x0/m                  =  0 00
  Outliers removed   Sample st. dev  =   3 00,  Record st. dev  =   2.50

------------------------------ Global Information ----------------------------
  nu =  1.644e-005 kg/(m s)        , rho =  1.039e+000 kg/m3
  Mach-p =   0 692, Mach-u =  0 673, U-mean    = 222.317, Re_m  =  196134
  U-coef = 0.00000, U-exp =  0.0000, U-exp-ci =  0.0000; U-cor =  0.0000
  V-coef = 0 00000, V-exp =  0.0000, V-exp-ci =  0.0000; V-cor =  0.0000

------------------------------ Ensemble Information --------------------------
 pos  Order  nsam  Rate(avg)  %Val(avg)  nrej(avg)  Rec_rej
-0 24    0    152        18       99.1        0.3        0
-0 16    1   1000       206       99.0        3.6        0
-0 09    2   1000      1247       99.4        2.9        0
 0 00    3   1000      3010       99.2        2 7        0
 0 08    4   1000      3182       99.4        3.5        0
 0 16    5   1000      2417       99.7        3.8        0
 0 24    6   1000      2001       99.5        5.9        0

 pos      U    U_ci    u'    u'_ci    V   V_ci     v'    v'_ci uv/u'v' u'/v' u_sk   u_fl
-0 24  221.29  0 52  3.921  0.115  0.00  0.00  0.000  0.000  0.000  0.00  0.070  2.73
-0 16  221 66  0.20  3.470  0.043  0.00  0.00  0.000  0.000  0.000  0.00  0.148  2.75
-0 08  221 92  0.16  3.374  0.108  0.00  0 00  0.000  0.000  0.000  0.00  0.094  2.71
 0 00  222.09  0.21  3.429  0.102  0.00  0.00  0.000  0.000  0.000  0.00  0.062  2.72
 0 08  222.50  0.10  3.446  0.094  0.00  0.00  0.000  0.000  0.000  0.00  0.091  2.66
 0 16  222.83  0.22  3.623  0.087  0.00  0.00  0.000  0.000  0.000  0.00  0.010  2 70
 0 24  223.93  0.19  4.003  0.159  0.00  0.00  0.000  0.000  0.000  0.00  0.043  2.82

 pos     U/Um     u'2/U2     integral     taylor     helmeg     diss rate  Re_tay
-0 24  0 996  3.146e-004  0.00e+000  0.00e+000  0.00e+000  0.00e+000     0.0
-0 16  0.998  2 451e-004  0.00e+000  0.00e+000  0.00e+000  0.00e+000     0.0
-0 08  0.999  2.317e-004  0.00e+000  0.00e+000  0.00e+000  0.00e+000     0.0
 0 00  1.000  2.389e-004  0.00e+000  0.00e+000  0.00e+000  0.00e+000     0.0
 0 08  1.002  2.403e-004  0.00e+000  0.00e+000  0.00e+000  0.00e+000     0.0
 0.16  1.003  2.647e-004  0.00e+000  0.00e+000  0.00e+000  0.00e+000     0.0
 0.24  1.008  3.209e-004  0.00e+000  0.00e+000  0.00e+000  0.00e+000     0.0

---------------------------------- Comments ----------------------------------
- same run as j12614
- x-traverse
```

---------- Input Parameters ----------

Input filename	= jl31x1		
Number of positions	= 12	Number of records	= 15
Starting position	= 747.0 mm	Increment	= 25.4000 mm
Mesh length	= 14.50 mm	Normalizing velocity	= -1.0 m/s
Static pressure	= 11.89 psi	Total pressure	= 16.12 psi
Traverse direction	= x	Total temperature	= 535.00 R
Transform method	= 1	Weighting method	= 2
x0/m	= 0.00		

Outliers removed. Sample st. dev. = 3.00; Record st. dev = 2.50

---------- Global Information ----------

nu = 1.635e-005 kg/(m s) ; rho = 1.048e+000 kg/m3
Mach-p = 0.674; Mach-u = 0.656; U-mean = 217.150; Re_m = 192604
U-coef = 0.00709; U-exp = 0.9213; U-exp-ci = 0.0275; U-cor = -0.9908
V-coef = 0.00000; V-exp = 0.0000; V-exp-ci = 0.0000; V-cor = 0.0000

---------- Ensemble Information ----------

pos	Order	nsam	Rate(avg)	%Val(avg)	nrej(avg)	Rec_rej
51.52	1	1000	5987	90.4	2.7	0
53.27	6	1000	5849	94.0	4.2	0
55.02	2	1000	5526	93.6	3.5	0
56.77	7	1000	6155	95.6	3.4	0
58.52	3	1000	5727	95.6	4.6	5
60.28	8	1000	5354	97.0	3.0	0
62.03	4	1000	5835	97.4	2.8	1
63.78	9	1000	5298	98.0	3.3	1
65.53	0	1000	4672	97.2	3.1	0
65.53	5	1000	5612	98.2	2.9	0
65.53	11	1000	4984	98.5	2.8	0
67.28	10	1000	773	99.1	2.1	0

pos	U	U_ci	u'	u'_ci	V	V_ci	v'	v'_ci	uv/u'v'	u'/v'	u_sk	u_fl
51.52	214.27	0.05	2.925	0.033	0.00	0.00	0.000	0.000	0.000	0.00	0.078	2.79
53.27	215.39	0.06	2.917	0.038	0.00	0.00	0.000	0.000	0.000	0.00	0.081	2.68
55.02	215.47	0.07	2.872	0.035	0.00	0.00	0.000	0.000	0.000	0.00	0.073	2.75
56.77	216.36	0.06	2.841	0.039	0.00	0.00	0.000	0.000	0.000	0.00	0.022	2.77
58.52	216.61	0.11	2.794	0.047	0.00	0.00	0.000	0.000	0.000	0.00	0.074	2.79
60.28	217.70	0.06	2.768	0.036	0.00	0.00	0.000	0.000	0.000	0.00	0.107	2.89
62.03	217.84	0.06	2.717	0.046	0.00	0.00	0.000	0.000	0.000	0.00	0.033	2.91
63.78	218.83	0.04	2.689	0.026	0.00	0.00	0.000	0.000	0.000	0.00	0.115	2.99
65.53	218.29	0.05	2.635	0.032	0.00	0.00	0.000	0.000	0.000	0.00	0.070	2.96
65.53	219.04	0.07	2.697	0.030	0.00	0.00	0.000	0.000	0.000	0.00	0.113	3.03
65.53	219.47	0.05	2.665	0.026	0.00	0.00	0.000	0.000	0.000	0.00	0.142	2.98
67.28	219.99	0.05	2.686	0.024	0.00	0.00	0.000	0.000	0.000	0.00	0.162	2.98

pos	U/Um	u'2/U2	integral	taylor	kolmog	diss rate	Re_tay
51.52	0.987	1.864e-004	7.40e-003	7.87e-004	3.36e-005	3.41e+003	141.2
53.27	0.992	1.836e-004	7.54e-003	7.98e-004	3.40e-005	3.25e+003	141.8
55.02	0.992	1.777e-004	7.67e-003	8.11e-004	3.46e-005	3.06e+003	142.0
56.77	0.996	1.726e-004	7.80e-003	8.22e-004	3.50e-005	2.92e+003	142.4
58.52	0.998	1.664e-004	7.93e-003	8.34e-004	3.55e-005	2.76e+003	142.7
60.28	1.003	1.618e-004	8.06e-003	8.44e-004	3.58e-005	2.65e+003	143.2
62.03	1.003	1.557e-004	8.18e-003	8.56e-004	3.63e-005	2.51e+003	143.4
63.78	1.008	1.510e-004	8.31e-003	8.66e-004	3.67e-005	2.41e+003	143.9
65.53	1.005	1.458e-004	8.43e-003	8.79e-004	3.72e-005	2.27e+003	143.9
65.53	1.009	1.517e-004	8.43e-003	8.77e-004	3.71e-005	2.30e+003	144.1
65.53	1.011	1.475e-004	8.43e-003	8.76e-004	3.71e-005	2.31e+003	144.3
67.28	1.013	1.491e-004	8.55e-003	8.87e-004	3.75e-005	2.21e+003	144.6

---------- Comments ----------

- DT = 4.6 (92%); CJ = 6.2; PO = 22 psi
- 243 mm lens; 0 KHz frequency shift
- repeat of jl26x5 to check for consistency
- decay law parameters still very sensitive to data rejection criteria
- Thesis label: RS9b

```
------------------------------ Input Parameters ------------------------------
  Input filename       = j131x3
  Number of positions  = 12              Number of records    = 15
  Starting position    = 747.0 mm        Increment            = 25.4000 mm
  Mesh length          = 14.50 mm        Normalizing velocity =  -1.0 m/s
  Static pressure      =  12.67 psi      Total pressure       =  17.67 psi
  Traverse direction   = z               Total temperature    = 542.00 R
  Transform method     = 1               Weighting method     = 2
  x0/m                 =  0.00
  Outliers removed:  Sample st. dev. =   3.00;  Record st. dev. =   2.50

------------------------------ Global Information ----------------------------
  nu =  1.548e-005 kg/(m s)        ; rho =  1.111e+000 kg/m3
  Mach-p =   0.706; Mach-u =  0.686; U-mean   = 227.395; Re_m  =  213037
  U-coef = 0.00211; U-exp =  0.2366; U-exp-ci =  0.2432; U-cor = -0.2086
  V-coef = 0.00000; V-exp =  0.0000; V-exp-ci =  0.0000; V-cor =  0.0000

---------------------------- Ensemble Information ----------------------------
 pos  Order  nsam  Rate(avg)  %Val(avg)  nrej(avg)  Rec_rej
51.52   1    1000    5768        98.7        9.9        1
53.27   6    1000    5573        98.8        9.8        0
55.02   2    1000    4872        98.9        8.7        0
56.77   7    1000    5340        99.4        9.3        0
58.52   3    1000    5516        99.5        9.9        0
60.28   8    1000    4707        99.6        9.3        1
62.03   4    1000    5082        99.4        8.7        0
63.78   9    1000    4823        99.7        7.7        0
65.53   0    1000    4212        99.6        8.4        0
65.53   5    1000    4594        99.6        8.1        0
65.53  11    1000    4472        99.7        8.8        1
67.28  10    1000     585        99.8        9.3        0

 pos      U    U_ci    u'    u'_ci    V    V_ci    v'    v'_ci uv/u'v' u'/v' u_sk   u_fl
51.52  224.30  0.10  6.311  0.115  0.00  0.00  0.000  0.000  0.000  0.00  0.332  3.02
53.27  226.16  0.19  6.893  0.137  0.00  0.00  0.000  0.000  0.000  0.00  0.331  3.13
55.02  225.37  0.17  6.305  0.182  0.00  0.00  0.000  0.000  0.000  0.00  0.281  3.04
56.77  226.16  0.39  6.094  0.306  0.00  0.00  0.000  0.000  0.000  0.00  0.272  3.07
58.52  227.47  0.38  6.642  0.284  0.00  0.00  0.000  0.000  0.000  0.00  0.374  3.26
60.28  227.41  0.19  6.149  0.119  0.00  0.00  0.000  0.000  0.000  0.00  0.297  3.15
62.03  229.08  0.17  7.018  0.096  0.00  0.00  0.000  0.000  0.000  0.00  0.378  3.20
63.78  228.61  0.21  6.187  0.156  0.00  0.00  0.000  0.000  0.000  0.00  0.285  3.15
65.53  228.99  0.19  6.264  0.219  0.00  0.00  0.000  0.000  0.000  0.00  0.351  3.20
65.53  229.72  0.42  6.714  0.313  0.00  0.00  0.000  0.000  0.000  0.00  0.376  3.23
65.53  229.19  0.30  6.225  0.276  0.00  0.00  0.000  0.000  0.000  0.00  0.335  3.21
67.28  229.66  0.29  6.140  0.224  0.00  0.00  0.000  0.000  0.000  0.00  0.324  3.18

 pos     U/Um      u'2/U2     integral     taylor      kolmog    diss rate  Re_tay
51.52   0.986  7.928e-004  6.07e-002  1.48e-003  3.02e-005  4.46e+003   616.9
53.27   0.995  9.302e-004  6.25e-002  1.49e-003  3.03e-005  4.39e+003   627.4
55.02   0.991  7.853e-004  6.43e-002  1.52e-003  3.07e-005  4.17e+003   634.0
56.77   0.995  7.337e-004  6.61e-002  1.54e-003  3.09e-005  4.05e+003   642.8
58.52   1.000  8.587e-004  6.79e-002  1.56e-003  3.11e-005  3.97e+003   652.2
60.28   1.000  7.323e-004  6.97e-002  1.59e-003  3.14e-005  3.83e+003   659.5
62.03   1.007  9.391e-004  7.15e-002  1.60e-003  3.15e-005  3.78e+003   669.2
63.78   1.005  7.343e-004  7.33e-002  1.63e-003  3.18e-005  3.63e+003   675.6
65.53   1.007  7.519e-004  7.50e-002  1.65e-003  3.20e-005  3.62e+003   683.2
65.53   1.010  8.616e-004  7.50e-002  1.64e-003  3.19e-005  3.56e+003   684.3
65.53   1.008  7.431e-004  7.50e-002  1.65e-003  3.20e-005  3.53e+003   683.5
67.28   1.010  7.186e-004  7.68e-002  1.67e-003  3.22e-005  3.44e+003   691.1

------------------------------- Comments -------------------------------
- DT = 4.6 (92%); CJ = 6.2; PO = 24 psi
- 243 mm lens; 0 KHz frequency shift
- the tunnel configuration is identical to the runs j27x1 through j15x1.
  However, this time the tunnel is in the transonic regime.
- Thesis label: MS1
```

---------- Input Parameters ----------

Input filename	= j131x4		
Number of positions	= 8	Number of records	= 5
Starting position	= 747.0 mm	Increment	= 25.4000 mm
Mesh length	= 14.50 mm	Normalizing velocity	= 1.0 m/s
Static pressure	= 12.67 psi	Total pressure	= 17.67 psi
Traverse direction	= (	Total temperature	= 542.00 R
Transform method	= 1	Weighting method	= 2
x0/m	= 0.00		

Outliers removed: Sample st. dev. = 3.00; Record st. dev. = 2.50

---------- Global Information ----------

nu = 1.548e-005 kg/(m s) ; rho = 1.111e+000 kg/m3

Mach-p = 0.706; Mach-u = 0.530; U-mean = 175.797; Re_m = 164697

U-coef = 0.00000; U-exp = 0.0000; U-exp-ci = 0.0000; U-cor = 0.0000

V-coef = 0.00000; V-exp = 0.0000; V-exp-ci = 0.0000; V-cor = 0.0000

---------- Ensemble Information ----------

pos	Order	nsam	Rate(avg)	%Val(avg)	nrej(avg)	Rec_rej
19.00	0	1000	2639	100.0	2.2	0
20.00	1	1000	2493	100.0	3.4	0
21.00	2	1000	2251	100.0	4.0	0
22.00	3	1000	2104	100.0	2.4	0
23.00	4	1000	1972	100.0	2.4	0
24.00	5	1000	1945	100.0	4.2	0
25.00	6	1000	1855	100.0	3.8	0
26.00	7	1000	1725	100.0	3.0	0

pos	U	U_ci	u'	u'_ci	V	V_ci	v'	v'_ci	uv/u'v'	u'/v'	u_sk	u_fl
19.00	174.29	0.09	2.944	0.112	0.00	0.00	0.000	0.000	0.000	0.00	0.006	2.89
20.00	174.64	0.05	2.992	0.030	0.00	0.00	0.000	0.000	0.000	0.00	0.051	2.97
21.00	175.27	0.10	2.990	0.099	0.00	0.00	0.000	0.000	0.000	0.00	0.054	2.94
22.00	176.00	0.15	3.027	0.103	0.00	0.00	0.000	0.000	0.000	0.00	0.074	2.90
23.00	176.21	0.10	3.145	0.081	0.00	0.00	0.000	0.000	0.000	0.00	0.062	2.87
24.00	176.44	0.18	3.094	0.063	0.00	0.00	0.000	0.000	0.000	0.00	0.071	2.88
25.00	176.69	0.08	3.076	0.071	0.00	0.00	0.000	0.000	0.000	0.00	0.010	2.83
26.00	176.82	0.09	3.136	0.092	0.00	0.00	0.000	0.000	0.000	0.00	0.047	2.85

pos	U/Um	u'2/U2	integral	taylor	kolmog	diss rate	Re_tay
19.00	174.295	2.856e-004	0.00e+000	0.00e+000	0.00e+000	0.00e+000	0.0
20.00	174.640	2.936e-004	0.00e+000	0.00e+000	0.00e+000	0.00e+000	0.0
21.00	175.274	2.914e-004	0.00e+000	0.00e+000	0.00e+000	0.00e+000	0.0
22.00	176.003	2.961e-004	0.00e+000	0.00e+000	0.00e+000	0.00e+000	0.0
23.00	176.207	3.188e-004	0.00e+000	0.00e+000	0.00e+000	0.00e+000	0.0
24.00	176.437	3.077e-004	0.00e+000	0.00e+000	0.00e+000	0.00e+000	0.0
25.00	176.693	3.032e-004	0.00e+000	0.00e+000	0.00e+000	0.00e+000	0.0
26.00	176.824	3.148e-004	0.00e+000	0.00e+000	0.00e+000	0.00e+000	0.0

---------- Comments ----------

- DT = 3.8 (76%); CJ = 5.0; PO = 19-26 psi
- 243 mm lens; 0 MHz frequency shift
- Pressure traverse (tunnel calibration)

```
------------------------------ Input Parameters ------------------------------
  Input filename        = j131z5
  Number of positions   = 12              Number of records     = 15
  Starting position     = 747.0 mm        Increment             = 25.4000 mm
  Mesh length           = 14.50 mm        Normalizing velocity  =  -1.0 m/s
  Static pressure       =  14.01 psi      Total pressure        =  16.96 psi
  Traverse direction    = z               Total temperature     = 541.00 R
  Transform method      = 1               Weighting method      = 2
  x0/m                  = 14.00
  Outliers removed:  Sample st. dev. =   3.00;  Record st. dev. =   2.50

------------------------------ Global Information ----------------------------
  nu =  1.499e-005 kg/(m s)        ; rho =  1.182e+000 kg/m3
  Mach-p =   0.530; Mach-u =  0.517, U-mean    = 174.810; Re_m  =  169041
  U-coef = 0.01322; U-exp =  1.0020; U-exp-ci =  0.0331; U-cer = -0.9888
  V-coef = 0.00000; V-exp =  0.0000; V-exp-ci =  0.0000; V-cer =  0.0000

---------------------------- Ensemble Information ----------------------------
 pos  Order  nsam  Rate(avg)  %Val(avg)  nrej(avg)  Rec_rej
51.52   1    1000     3778       100.0        2.4        0
53.27   6    1000     1884       100.0        3.6        0
55.02   2    1000     2947       100.0        2.4        0
56.77   7    1000     3946       100.0        2.6        0
58.52   3    1000     3999       100.0        3.0        0
60.28   8    1000     2640       100.0        3.1        0
62.03   4    1000     3813       100.0        3.1        0
63.78   9    1000     3352       100.0        2.7        0
65.53   0    1000     2779       100.0        3.3        0
65.53   5    1000     3122       100.0        2.9        1
65.53  11    1000     2434       100.0        3.0        0
67.28  10     992      488       100.0        2.9        0

 pos      U    U_ci     u'    u'_ci     V    V_ci     v'    v'_ci uv/u'v' u'/v' u_sk   u_fl
51.52 173.26  0.08  3.217  0.031  0.00  0.00  0.000  0.000  0.000  0.00  0.000  2.81
53.27 174.05  0.20  3.231  0.072  0.00  0.00  0.000  0.000  0.000  0.00  0.046  2.88
55.02 174.22  0.08  3.067  0.030  0.00  0.00  0.000  0.000  0.000  0.00  0.024  2.90
56.77 174.23  0.12  3.067  0.039  0.00  0.00  0.000  0.000  0.000  0.00 -0.001  2.91
58.52 174.71  0.09  2.985  0.037  0.00  0.00  0.000  0.000  0.000  0.00  0.002  2.90
60.28 174.70  0.17  2.958  0.035  0.00  0.00  0.000  0.000  0.000  0.00  0.012  2.90
62.03 175.10  0.09  2.908  0.040  0.00  0.00  0.000  0.000  0.000  0.00  0.040  2.94
63.78 175.44  0.16  2.832  0.035  0.00  0.00  0.000  0.000  0.000  0.00  0.067  2.90
65.53 175.69  0.06  2.814  0.039  0.00  0.00  0.000  0.000  0.000  0.00  0.070  2.92
65.53 176.15  0.05  2.817  0.036  0.00  0.00  0.000  0.000  0.000  0.00  0.067  2.89
65.53 175.76  0.13  2.809  0.027  0.00  0.00  0.000  0.000  0.000  0.00  0.068  2.92
67.28 176.24  0.10  2.754  0.035  0.00  0.00  0.000  0.000  0.000  0.00  0.055  2.85

 pos    U/Um     u'2/U2     integral     tayler      kolmog    diss rate  Re_tay
51.52  0.991  3.449e-004  6.77e-003  6.85e-004  2.86e-005  5.03e+003   148.1
53.27  0.996  3.453e-004  6.93e-003  7.00e-004  2.92e-005  4.65e+003   148.5
55.02  0.997  3.100e-004  7.08e-003  7.15e-004  2.98e-005  4.27e+003   148.5
56.77  0.997  3.101e-004  7.23e-003  7.30e-004  3.04e-005  3.93e+003   148.5
58.52  0.999  2.920e-004  7.37e-003  7.44e-004  3.10e-005  3.65e+003   148.7
60.28  0.999  2.868e-004  7.52e-003  7.58e-004  3.16e-005  3.39e+003   148.7
62.03  1.002  2.760e-004  7.66e-003  7.71e-004  3.21e-005  3.16e+003   148.9
63.78  1.004  2.608e-004  7.80e-003  7.85e-004  3.27e-005  2.96e+003   149.0
65.53  1.005  2.567e-004  7.93e-003  7.98e-004  3.32e-005  2.78e+003   149.1
65.53  1.008  2.558e-004  7.93e-003  7.97e-004  3.31e-005  2.80e+003   149.3
65.53  1.005  2.555e-004  7.93e-003  7.98e-004  3.32e-005  2.78e+003   149.1
67.28  1.008  2.444e-004  8.06e-003  8.10e-004  3.37e-005  2.62e+003   149.3

------------------------------- Comments -------------------------------
- DT = 3.8 (76%); CJ = 5.0; PO = 20 psi
- 243 mm lens; 0 KHz frequency shift
- Calibration (j131z4) showed plateau was reached
- Thesis label: N58a
```

---------- Input Parameters ----------

Input filename	= alt1		
Number of positions	= 12	Number of records	= 15
Starting position	= 747.0 mm	Increment	= 25.4000 mm
Mesh length	= 14.50 mm	Normalizing velocity	= -1.0 m/s
Static pressure	= 13.84 psi	Total pressure	= 17.63 psi
Traverse direction	= x	Total temperature	= 537.50 R
Transform method	= 1	Weighting method	= 2
x0/m	= 6.50		

Outliers removed: Sample st. dev. = 3.00; Record st. dev. = 2.50

---------- Global Information ----------

nu = 1.462e-005 kg/(m s) ; rho = 1.193e+000 kg/m3

Mach-p = 0.598; Mach-u = 0.582; U-mean = 194.591; Re_m = 192993

U-coef = 0.01133; U-exp = 1.0005; U-exp-ci = 0.0202; U-cor = -0.9958

V-coef = 0.00000; V-exp = 0.0000; V-exp-ci = 0.0000; V-cor = 0.0000

---------- Ensemble Information ----------

pos	Order	nsam	Rate(avg)	%Val(avg)	nrej(avg)	Rec_rej
51.52	1	1000	4985	100.0	2.9	0
53.27	6	1000	4553	100.0	2.6	1
55.02	2	1000	4163	100.0	2.5	0
56.77	7	1000	4772	100.0	2.8	0
58.52	3	1000	4351	100.0	2.7	0
60.28	8	1000	4489	100.0	3.1	0
62.03	4	1000	4313	100.0	2.1	0
63.78	9	1000	4445	100.0	2.1	0
65.53	0	1000	3945	100.0	2.4	1
65.53	5	1000	4070	100.0	2.1	0
65.53	11	1000	3956	100.0	2.4	0
67.28	10	1000	1002	100.0	3.0	0

pos	U	U_ci	u'	u'_ci	V	V_ci	v'	v'_ci	uv/u'v'	u'/v'	u_sk	u_fl
51.52	192.62	0.06	3.034	0.030	0.00	0.00	0.000	0.000	0.000	0.00	-0.011	2.82
53.27	193.29	0.04	3.024	0.038	0.00	0.00	0.000	0.000	0.000	0.00	0.028	2.82
55.02	193.40	0.05	2.948	0.029	0.00	0.00	0.000	0.000	0.000	0.00	-0.003	2.82
56.77	194.00	0.07	2.926	0.039	0.00	0.00	0.000	0.000	0.000	0.00	0.015	2.78
58.52	194.15	0.06	2.843	0.039	0.00	0.00	0.000	0.000	0.000	0.00	0.034	2.79
60.28	195.06	0.08	2.833	0.028	0.00	0.00	0.000	0.000	0.000	0.00	0.018	2.83
62.03	195.03	0.07	2.787	0.038	0.00	0.00	0.000	0.000	0.000	0.00	0.010	2.84
63.78	195.85	0.07	2.750	0.033	0.00	0.00	0.000	0.000	0.000	0.00	-0.030	2.78
65.53	195.59	0.04	2.645	0.038	0.00	0.00	0.000	0.000	0.000	0.00	-0.012	2.78
65.53	195.91	0.06	2.710	0.035	0.00	0.00	0.000	0.000	0.000	0.00	-0.011	2.77
65.53	196.30	0.07	2.745	0.032	0.00	0.00	0.000	0.000	0.000	0.00	-0.033	2.81
67.28	196.61	0.04	2.677	0.042	0.00	0.00	0.000	0.000	0.000	0.00	0.002	2.80

pos	U/Um	u'2/U2	integral	taylor	kolmog	diss rate	Re_tay
51.52	0.990	2.483e-004	6.89e-003	7.04e-004	2.95e-005	4.13e+003	147.0
53.27	0.993	2.449e-004	7.03e-003	7.16e-004	3.00e-005	3.87e+003	147.2
55.02	0.994	2.324e-004	7.16e-003	7.29e-004	3.05e-005	3.60e+003	147.3
56.77	0.997	2.278e-004	7.29e-003	7.41e-004	3.10e-005	3.38e+003	147.5
58.52	0.998	2.146e-004	7.41e-003	7.54e-004	3.15e-005	3.17e+003	147.5
60.28	1.002	2.111e-004	7.54e-003	7.64e-004	3.19e-005	3.00e+003	147.9
62.03	1.002	2.043e-004	7.66e-003	7.77e-004	3.25e-005	2.82e+003	147.9
63.78	1.006	1.973e-004	7.78e-003	7.87e-004	3.29e-005	2.68e+003	148.2
65.53	1.005	1.830e-004	7.89e-003	8.00e-004	3.34e-005	2.51e+003	148.1
65.53	1.007	1.915e-004	7.89e-003	7.99e-004	3.34e-005	2.53e+003	148.2
65.53	1.009	1.957e-004	7.89e-003	7.98e-004	3.33e-005	2.54e+003	148.4
67.28	1.010	1.856e-004	8.01e-003	8.09e-004	3.38e-005	2.41e+003	148.5

---------- Comments ----------

- DT = 4.2 (84%); CJ = 5.0; PO = 20 psi
- 243 mm lens; 0 KHz frequency shift
- Thesis label: H56

---------- Input Parameters ----------

Input filename	= a2x2		
Number of positions	= 12	Number of records	= 15
Starting position	= 747.0 mm	Increment	= 25.4000 mm
Mesh length	= 14.50 mm	Normalizing velocity	= -1.0 m/s
Static pressure	= 12.72 psi	Total pressure	= 17.02 psi
Traverse direction	= x	Total temperature	= 543.00 R
Transform method	= 1	Weighting method	= 2
x0/m	= 23.00		

Outliers removed: Sample st. dev. = 3.00; Record st. dev. = 2.50

---------- Global Information ----------

nu = 1.580e-005 kg/(m s) ; rho = 1.101e+000 kg/m3

Mach-p = 0.659; Mach-u = 0.639; U-mean = 213.534; Re_m = 195992

U-coef = 0.00570; U-exp = 0.9964; U-exp-ci = 0.0225; U-cor = -0.9947

V-coef = 0.00000; V-exp = 0.0000; V-exp-ci = 0.0000; V-cor = 0.0000

---------- Ensemble Information ----------

pos	Order	nsam	Rate(avg)	%Val(avg)	nrej(avg)	Rec_rej
51.52	1	1000	8878	99.9	2.6	0
53.27	6	1000	8175	100.0	2.6	0
55.02	2	1000	7190	100.0	3.3	0
56.77	7	1000	8071	99.9	3.1	0
58.52	3	1000	7848	100.0	3.3	0
60.28	8	1000	7921	100.0	2.5	0
62.03	4	1000	7234	99.9	2.9	1
63.78	9	1000	7959	99.9	3.1	0
65.53	0	1000	6480	99.9	2.9	0
65.53	5	1000	6602	100.0	2.9	0
65.53	11	1000	6489	100.0	3.5	0
67.28	10	1000	1374	100.0	3.4	0

pos	U	U_ci	u'	u'_ci	V	V_ci	v'	v'_ci	uv/u'v'	u'/v'	u_sk	u_fl
51.52	210.65	0.05	3.011	0.034	0.00	0.00	0.000	0.000	0.000	0.00	-0.058	2.91
53.27	211.76	0.06	2.915	0.047	0.00	0.00	0.000	0.000	0.000	0.00	0.036	2.85
55.02	212.13	0.06	2.847	0.026	0.00	0.00	0.000	0.000	0.000	0.00	-0.005	2.80
56.77	212.84	0.04	2.745	0.035	0.00	0.00	0.000	0.000	0.000	0.00	0.013	2.81
58.52	213.03	0.06	2.723	0.029	0.00	0.00	0.000	0.000	0.000	0.00	-0.003	2.83
60.28	213.94	0.06	2.668	0.040	0.00	0.00	0.000	0.000	0.000	0.00	0.024	2.89
62.03	214.18	0.03	2.612	0.023	0.00	0.00	0.000	0.000	0.000	0.00	0.039	2.88
63.78	215.02	0.05	2.547	0.034	0.00	0.00	0.000	0.000	0.000	0.00	-0.004	2.78
65.53	215.09	0.04	2.537	0.035	0.00	0.00	0.000	0.000	0.000	0.00	-0.016	2.83
65.53	215.75	0.04	2.548	0.023	0.00	0.00	0.000	0.000	0.000	0.00	-0.003	2.82
65.53	215.64	0.04	2.501	0.031	0.00	0.00	0.000	0.000	0.000	0.00	-0.010	2.81
67.28	216.04	0.03	2.443	0.034	0.00	0.00	0.000	0.000	0.000	0.00	-0.032	2.79

pos	U/Um	u'2/U2	integral	taylor	kolmog	diss rate	Re_tay
51.52	0.986	2.045e-004	3.93e-003	5.58e-004	2.76e-005	6.83e+003	105.8
53.27	0.992	1.897e-004	4.05e-003	5.73e-004	2.83e-005	6.16e+003	106.1
55.02	0.993	1.802e-004	4.17e-003	5.89e-004	2.91e-005	5.54e+003	106.2
56.77	0.997	1.666e-004	4.28e-003	6.04e-004	2.98e-005	5.03e+003	106.4
58.52	0.998	1.634e-004	4.39e-003	6.19e-004	3.05e-005	4.66e+003	106.4
60.28	1.002	1.557e-004	4.50e-003	6.33e-004	3.11e-005	4.19e+003	106.6
62.03	1.003	1.487e-004	4.60e-003	6.47e-004	3.18e-005	3.84e+003	106.7
63.78	1.007	1.404e-004	4.71e-003	6.60e-004	3.24e-005	3.56e+003	106.9
65.53	1.007	1.393e-004	4.81e-003	6.74e-004	3.31e-005	3.27e+003	107.0
65.53	1.010	1.395e-004	4.81e-003	6.73e-004	3.30e-005	3.30e+003	107.1
65.53	1.010	1.346e-004	4.81e-003	6.73e-004	3.31e-005	3.30e+003	107.1
67.28	1.012	1.280e-004	4.91e-003	6.86e-004	3.37e-005	3.06e+003	107.2

---------- Comments ----------

- DT = 4.5 (90%); CJ = 5.6; PO = 23 psi
- 243 mm lens; 0 MHz frequency shift
- labelled a2x2 instead of a1x2 by accident
- Thesis label: HS7a

---------- Input Parameters ----------

Input filename	= aix4		
Number of positions	= 12	Number of records	= 15
Starting position	= 747.0 mm	Increment	= 25.4000 mm
Mesh length	= 14.50 mm	Normalizing velocity	= -1.0 m/s
Static pressure	= 12.71 psi	Total pressure	= 17.03 psi
Traverse direction	= x	Total temperature	= 547.50 R
Transform method	= 1	Weighting method	= 2
x0/m	= 20.00		

Outliers removed: Sample st. dev. = 3.00; Record st. dev. = 2.50

---------- Global Information ----------

nu = 1.603e-005 kg/(m s) ; rho = 1.091e+000 kg/m3

Mach-p = 0.660; Mach-u = 0.640; U-mean = 214.539; Re_m = 194018

U-coef = 0.00318; U-exp = 1.0077; U-exp-ci = 0.0260; U-cor = -0.9932

V-coef = 0.00000; V-exp = 0.0000; V-exp-ci = 0.0000; V-cor = 0.0000

---------- Ensemble Information ----------

pos	Order	nsam	Rate(avg)	%Val(avg)	nrej(avg)	Rec_rej
51.52	1	1000	6217	100.0	3.7	0
53.27	6	1000	5002	100.0	3.7	0
55.02	2	1000	5264	99.9	2.8	1
56.77	7	1000	5401	100.0	2.5	0
58.52	3	1000	5298	100.0	2.2	1
60.28	8	1000	5480	100.0	2.5	0
62.03	4	1000	5360	100.0	2.6	0
63.78	9	1000	5335	100.0	4.0	1
65.53	0	1000	5123	100.0	3.6	0
65.53	5	1000	5255	100.0	3.9	1
65.53	11	1000	5080	100.0	4.2	0
67.28	10	1000	746	100.0	4.5	0

pos	U	U_ci	u'	u'_ci	V	V_ci	v'	v'_ci	uv/u'v'	u'/v'	u_sk	u_fl
51.52	211.94	0.04	2.916	0.035	0.00	0.00	0.000	0.000	0.000	0.00	0.005	2.79
53.27	212.78	0.03	2.832	0.042	0.00	0.00	0.000	0.000	0.000	0.00	0.003	2.77
55.02	213.23	0.04	2.813	0.034	0.00	0.00	0.000	0.000	0.000	0.00	0.049	2.77
56.77	213.67	0.04	2.737	0.029	0.00	0.00	0.000	0.000	0.000	0.00	0.005	2.81
58.52	214.29	0.04	2.701	0.035	0.00	0.00	0.000	0.000	0.000	0.00	0.018	2.81
60.28	214.84	0.05	2.646	0.035	0.00	0.00	0.000	0.000	0.000	0.00	-0.049	2.84
62.03	215.38	0.03	2.577	0.029	0.00	0.00	0.000	0.000	0.000	0.00	0.005	2.81
63.78	215.93	0.03	2.516	0.027	0.00	0.00	0.000	0.000	0.000	0.00	0.006	2.73
65.53	216.20	0.03	2.472	0.037	0.00	0.00	0.000	0.000	0.000	0.00	-0.028	2.81
65.53	216.45	0.02	2.450	0.033	0.00	0.00	0.000	0.000	0.000	0.00	0.010	2.86
65.53	216.39	0.06	2.488	0.029	0.00	0.00	0.000	0.000	0.000	0.00	-0.021	2.80
67.28	216.89	0.04	2.453	0.040	0.00	0.00	0.000	0.000	0.000	0.00	0.013	2.86

pos	U/Um	u'2/U2	integral	taylor	kolmog	diss rate	Re_tay
51.52	0.988	1.894e-004	4.18e-003	5.86e-004	2.88e-005	6.01e+003	107.0
53.27	0.992	1.774e-004	4.29e-003	6.01e-004	2.95e-005	5.46e+003	107.2
55.02	0.994	1.741e-004	4.40e-003	6.16e-004	3.02e-005	4.96e+003	107.3
56.77	0.996	1.642e-004	4.51e-003	6.30e-004	3.09e-005	4.52e+003	107.4
58.52	0.999	1.590e-004	4.62e-003	6.44e-004	3.16e-005	4.15e+003	107.5
60.28	1.001	1.518e-004	4.72e-003	6.58e-004	3.22e-005	3.83e+003	107.6
62.03	1.004	1.432e-004	4.82e-003	6.71e-004	3.28e-005	3.54e+003	107.7
63.78	1.006	1.358e-004	4.92e-003	6.84e-004	3.35e-005	3.29e+003	107.9
65.53	1.008	1.308e-004	5.01e-003	6.97e-004	3.41e-005	3.05e+003	107.9
65.53	1.009	1.282e-004	5.01e-003	6.97e-004	3.41e-005	3.06e+003	108.0
65.53	1.009	1.323e-004	5.01e-003	6.97e-004	3.41e-005	3.06e+003	108.0
67.28	1.011	1.281e-004	5.11e-003	7.09e-004	3.47e-005	2.86e+003	108.1

---------- Comments ----------

- DT = 4.5 (90%); CJ = 5.6; PO = 23 psi
- 243 mm lens; 0 MHz frequency shift
- same conditions as aix2 (to check for repeatability)
- Thesis label: HS7b

```
------------------------------ Input Parameters ------------------------------
  Input filename       = a1x5
  Number of positions  = 12            Number of records    = 15
  Starting position    = 747.0 mm      Increment            = 25.4000 mm
  Mesh length          = 14.50 mm      Normalizing velocity =  -1.0 m/s
  Static pressure      =  14.01 psi    Total pressure       =  16.98 psi
  Traverse direction   = x             Total temperature    = 544.50 R
  Transform method     = 1             Weighting method     = 2
  x0/m                 = 10.00
  Outliers removed:  Sample st. dev. =   3.00;  Record st. dev. =   2.50

------------------------------ Global Information ----------------------------
  nu =  1.516e-005 kg/(m s)        ; rho =  1.175e+000 kg/m3
  Mach-p =   0.531; Mach-u =  0.517; U-mean   = 175.324; Re_m  =  167703
  U-coef = 0.01462; U-exp =  0.9969; U-exp-ci =  0.0326; U-cor = -0.9891
  V-coef = 0.00000; V-exp =  0.0000; V-exp-ci =  0.0000; V-cor =  0.0000

------------------------------ Ensemble Information --------------------------
 pos  Order  nsam  Rate(avg)  %Val(avg)  nrej(avg)  Rec_rej
51.52   1    1000     3273       100.0       2.0        0
53.27   6    1000     2219       100.0       2.7        0
55.02   2    1000     2458       100.0       2.7        0
56.77   7    1000     2349       100.0       3.5        0
58.52   3    1000     2385       100.0       3.6        0
60.28   8    1000     2181       100.0       3.8        0
62.03   4    1000     2316       100.0       3.3        0
63.78   9    1000     1833       100.0       3.2        0
65.53   0    1000     2472       100.0       2.2        0
65.53   5    1000     2714       100.0       2.5        0
65.53  11    1000     1632       100.0       2.3        1
67.28  10     998      400       100.0       2.6        0

 pos      U    U_ci    u'    u'_ci    V    V_ci    v'    v'_ci  uv/u'v'  u'/v'  u_sk   u_fl
51.52  174.01  0.05  3.311  0.047  0.00  0.00  0.000  0.000  0.000  0.00  0.094  2.93
53.27  174.78  0.06  3.218  0.039  0.00  0.00  0.000  0.000  0.000  0.00  0.091  2.86
55.02  174.89  0.08  3.154  0.041  0.00  0.00  0.000  0.000  0.000  0.00  0.066  2.80
56.77  175.04  0.14  3.096  0.043  0.00  0.00  0.000  0.000  0.000  0.00  0.101  2.78
58.52  175.22  0.05  3.069  0.040  0.00  0.00  0.000  0.000  0.000  0.00  0.086  2.81
60.28  175.24  0.13  2.993  0.041  0.00  0.00  0.000  0.000  0.000  0.00  0.073  2.83
62.03  176.20  0.17  2.961  0.018  0.00  0.00  0.000  0.000  0.000  0.00  0.073  2.72
63.78  175.71  0.11  2.939  0.038  0.00  0.00  0.000  0.000  0.000  0.00  0.086  2.72
65.53  176.73  0.04  2.918  0.030  0.00  0.00  0.000  0.000  0.000  0.00  0.075  2.74
65.53  176.54  0.08  2.920  0.037  0.00  0.00  0.000  0.000  0.000  0.00  0.036  2.66
65.53  175.84  0.08  2.907  0.033  0.00  0.00  0.000  0.000  0.000  0.00  0.080  2.72
67.28  175.59  0.08  2.789  0.018  0.00  0.00  0.000  0.000  0.000  0.00  0.109  2.73

 pos    U/Um     u'2/U2     integral     taylor      kolmog    diss rate  Re_tay
51.52  0.993  3.623e-004  7.60e-003  7.25e-004  2.94e-005  4.66e+003   157.2
53.27  0.997  3.392e-004  7.76e-003  7.39e-004  2.99e-005  4.35e+003   157.5
55.02  0.998  3.255e-004  7.91e-003  7.53e-004  3.05e-005  4.03e+003   157.6
56.77  0.998  3.130e-004  8.07e-003  7.68e-004  3.11e-005  3.74e+003   157.6
58.52  0.999  3.070e-004  8.22e-003  7.81e-004  3.16e-005  3.49e+003   157.7
60.28  1.000  2.919e-004  8.36e-003  7.95e-004  3.22e-005  3.25e+003   157.7
62.03  1.005  2.824e-004  8.51e-003  8.07e-004  3.26e-005  3.09e+003   158.2
63.78  1.002  2.800e-004  8.65e-003  8.21e-004  3.32e-005  2.86e+003   158.0
65.53  1.008  2.728e-004  8.79e-003  8.32e-004  3.36e-005  2.73e+003   158.4
65.53  1.007  2.738e-004  8.79e-003  8.33e-004  3.36e-005  2.72e+003   158.4
65.53  1.003  2.735e-004  8.79e-003  8.34e-004  3.37e-005  2.69e+003   158.0
67.28  1.002  2.524e-004  8.93e-003  8.48e-004  3.43e-005  2.52e+003   157.9

------------------------------------ Comments ------------------------------
- DT = 3.8 (76%); CJ = 5.0; PO = 20 psi
- 243 mm lens; 0 MHz frequency shift
- same conditions as j131x5 (to check for repeatability)
- Thesis label: HS5b
```

```
------------------------------ Input Parameters ------------------------------
  Input filename       = a1x6
  Number of positions  = 12            Number of records    = 15
  Starting position    = 747.0 mm      Increment            = 25.4000 mm
  Mesh length          = 14.50 mm      Normalizing velocity =  -1.0 m/s
  Static pressure      =  14.01 psi    Total pressure       =  16.99 psi
  Traverse direction   = x             Total temperature    = 545.00 R
  Transform method     = 1             Weighting method     = 2
  x0/m                 =  5.00
  Outliers removed:  Sample st. dev. =   3.00;  Record st. dev. =   2.50

------------------------------ Global Information ----------------------------
  nu =  1.518e-005 kg/(m s)       ; rho =  1.174e+000 kg/m3
  Mach-p =   0.532; Mach-u =  0.525; U-mean   = 177.973; Re_m  =  170010
  U-coef = 0.02013; U-exp =  1.0004; U-exp-ci =  0.0319; U-cor = -0.9895
  V-coef = 0.00000; V-exp =  0.0000; V-exp-ci =  0.0000; V-cor =  0.0000

---------------------------- Ensemble Information ---------------------------
 pos  Order  nsam  Rate(avg)  %Val(avg)  nrej(avg)  Rec_rej
51.52   1    1000     2959       99.9        1.7        0
53.27   6    1000     2782      100.0        2.0        0
55.02   2    1000     2830      100.0        2.2        0
56.77   7    1000     2746      100.0        1.3        0
58.52   3    1000     2010      100.0        2.1        1
60.28   8    1000     1999      100.0        2.0        0
62.03   4    1000     2193      100.0        1.7        0
63.78   9    1000     1699      100.0        2.5        0
65.53   0    1000     2207      100.0        2.3        0
65.53   5    1000     2382      100.0        1.9        0
65.53  11    1000     1403      100.0        2.3        0
67.28  10    1000      642      100.0        2.3        0

 pos      U    U_ci    u'    u'_ci    V    V_ci    v'    v'_ci uv/u'v' u'/v' u_sk   u_fl
51.52  176.20  0.05  3.637  0.040  0.00  0.00  0.000  0.000  0.000  0.00  0.073  2.79
53.27  176.96  0.10  3.589  0.055  0.00  0.00  0.000  0.000  0.000  0.00  0.033  2.73
55.02  176.89  0.05  3.575  0.041  0.00  0.00  0.000  0.000  0.000  0.00  0.045  2.75
56.77  177.75  0.11  3.510  0.037  0.00  0.00  0.000  0.000  0.000  0.00  0.050  2.72
58.52  177.87  0.05  3.456  0.050  0.00  0.00  0.000  0.000  0.000  0.00  0.028  2.73
60.28  178.31  0.08  3.404  0.043  0.00  0.00  0.000  0.000  0.000  0.00  0.029  2.77
62.03  178.31  0.14  3.360  0.035  0.00  0.00  0.000  0.000  0.000  0.00  0.024  2.73
63.78  178.91  0.14  3.294  0.053  0.00  0.00  0.000  0.000  0.000  0.00 -0.007  2.76
65.53  178.57  0.06  3.241  0.029  0.00  0.00  0.000  0.000  0.000  0.00  0.042  2.70
65.53  179.26  0.07  3.294  0.055  0.00  0.00  0.000  0.000  0.000  0.00  0.009  2.71
65.53  178.94  0.12  3.178  0.044  0.00  0.00  0.000  0.000  0.000  0.00 -0.023  2.70
67.28  179.26  0.11  3.177  0.051  0.00  0.00  0.000  0.000  0.000  0.00 -0.032  2.71

 pos    U/Um     u'2/U2     integral     taylor      kolmog   diss rate  Re_tay
51.52  0.990  4.263e-004  9.34e-003  7.62e-004  2.86e-005  5.26e+003   183.9
53.27  0.994  4.117e-004  9.52e-003  7.75e-004  2.90e-005  4.95e+003   184.3
55.02  0.994  4.088e-004  9.69e-003  7.89e-004  2.95e-005  4.60e+003   184.2
56.77  0.999  3.901e-004  9.86e-003  8.01e-004  2.99e-005  4.36e+003   184.7
58.52  0.999  3.778e-004  1.00e-002  8.14e-004  3.04e-005  4.09e+003   184.8
60.28  1.002  3.647e-004  1.02e-002  8.26e-004  3.09e-005  3.86e+003   185.0
62.03  1.002  3.552e-004  1.03e-002  8.39e-004  3.13e-005  3.63e+003   185.0
63.78  1.005  3.393e-004  1.05e-002  8.50e-004  3.17e-005  3.45e+003   185.3
65.53  1.003  3.296e-004  1.07e-002  8.64e-004  3.23e-005  3.23e+003   185.1
65.53  1.007  3.381e-004  1.07e-002  8.62e-004  3.22e-005  3.27e+003   185.5
65.53  1.005  3.158e-004  1.07e-002  8.63e-004  3.22e-005  3.25e+003   185.3
67.28  1.007  3.145e-004  1.08e-002  8.74e-004  3.26e-005  3.09e+003   185.5

------------------------------- Comments -------------------------------
- DT = 3.8 (76%); CJ = 5.0; PO = 20 psi
- 160 mm lens; 0 KHz frequency shift
- same conditions as j131x5 and a1x5, but different lens (to check for lens effect)
- Thesis label: H55c
```

---------- Input Parameters ----------

Input filename	= a1x7		
Number of positions	= 12	Number of records	= 15
Starting position	= 747.0 mm	Increment	= 25.4000 mm
Mesh length	= 14.50 mm	Normalizing velocity	= -1.0 m/s
Static pressure	= 14.02 psi	Total pressure	= 17.01 psi
Traverse direction	= x	Total temperature	= 543.00 R
Transform method	= 1	Weighting method	= 2
x0/m	= 6.00		

Outliers removed: Sample st. dev. = 3.00; Record st. dev. = 2.50

---------- Global Information ----------

nu = 1.507e-005 kg/(m s) ; rho = 1.180e+000 kg/m3

Mach-p = 0.533; Mach-u = 0.525; U-mean = 177.715; Re_m = 171041

U-coef = 0.01942; U-exp = 0.9991; U-exp-ci = 0.0467; U-cor = -0.9780

V-coef = 0.00000; V-exp = 0.0000; V-exp-ci = 0.0000; V-cor = 0.0000

---------- Ensemble Information ----------

pos	Order	nsam	Rate(avg)	%Val(avg)	nrej(avg)	Rec_rej
51.52	1	1000	3156	100.0	2.1	0
53.27	6	1000	2873	100.0	2.0	0
55.02	2	1000	2644	100.0	1.4	0
56.77	7	1000	2856	100.0	1.8	0
58.52	3	1000	2104	100.0	1.7	0
60.28	8	1000	2664	100.0	2.4	0
62.03	4	1000	2231	100.0	2.2	0
63.78	9	1000	925	100.0	3.1	0
65.53	0	1000	2529	100.0	2.1	0
65.53	5	1000	1344	100.0	2.3	0
65.53	11	1000	1336	100.0	1.5	0
67.28	10	1000	460	100.0	2.1	0

pos	U	U_ci	u'	u'_ci	V	V_ci	v'	v'_ci	uv/u'v'	u'/v'	u_sk	u_fl
51.52	176.78	0.07	3.651	0.045	0.00	0.00	0.000	0.000	0.000	0.00	0.053	2.80
53.27	176.64	0.06	3.562	0.029	0.00	0.00	0.000	0.000	0.000	0.00	0.050	2.73
55.02	176.61	0.05	3.482	0.041	0.00	0.00	0.000	0.000	0.000	0.00	0.026	2.78
56.77	177.29	0.13	3.466	0.033	0.00	0.00	0.000	0.000	0.000	0.00	0.047	2.75
58.52	177.58	0.06	3.450	0.049	0.00	0.00	0.000	0.000	0.000	0.00	0.049	2.78
60.28	177.91	0.13	3.391	0.036	0.00	0.00	0.000	0.000	0.000	0.00	0.032	2.78
62.03	178.09	0.16	3.386	0.040	0.00	0.00	0.000	0.000	0.000	0.00	0.019	2.72
63.78	178.92	0.12	3.253	0.039	0.00	0.00	0.000	0.000	0.000	0.00	0.035	2.75
65.53	178.28	0.06	3.217	0.023	0.00	0.00	0.000	0.000	0.000	0.00	0.000	2.74
65.53	179.00	0.13	3.259	0.040	0.00	0.00	0.000	0.000	0.000	0.00	0.014	2.67
65.53	179.27	0.11	3.266	0.029	0.00	0.00	0.000	0.000	0.000	0.00	-0.011	2.74
67.28	179.34	0.14	3.150	0.049	0.00	0.00	0.000	0.000	0.000	0.00	-0.015	2.73

pos	U/Um	u'2/U2	integral	taylor	kolmog	diss rate	Re_tay
51.52	0.989	4.318e-004	9.11e-003	7.52e-004	2.84e-005	5.28e+003	181.7
53.27	0.994	4.068e-004	9.29e-003	7.65e-004	2.88e-005	4.97e+003	182.1
55.02	0.994	3.888e-004	9.46e-003	7.79e-004	2.93e-005	4.62e+003	182.1
56.77	0.998	3.824e-004	9.63e-003	7.91e-004	2.98e-005	4.36e+003	182.5
58.52	0.999	3.779e-004	9.79e-003	8.04e-004	3.02e-005	4.09e+003	182.6
60.28	1.001	3.634e-004	9.95e-003	8.17e-004	3.07e-005	3.85e+003	182.8
62.03	1.002	3.617e-004	1.01e-002	8.29e-004	3.12e-005	3.63e+003	182.9
63.78	1.007	3.308e-004	1.03e-002	8.40e-004	3.15e-005	3.46e+003	183.3
65.53	1.003	3.257e-004	1.04e-002	8.54e-004	3.21e-005	3.22e+003	183.0
65.53	1.007	3.318e-004	1.04e-002	8.53e-004	3.20e-005	3.26e+003	183.4
65.53	1.009	3.320e-004	1.04e-002	8.52e-004	3.20e-005	3.28e+003	183.5
67.28	1.009	3.089e-004	1.06e-002	8.64e-004	3.24e-005	3.09e+003	183.5

---------- Comments ----------

- DT = 3.8 (76%); CJ = 5.0; PO = 20 psi
- 160 mm lens; 0 MHz frequency shift
- same conditions as a1x6
- Thesis label: M55d

```
------------------------------ Input Parameters ------------------------------
  Input filename        = ali8
  Number of positions   = 12              Number of records     = 15
  Starting position     = 747.0 mm        Increment             = 25.4000 mm
  Mesh length           = 14.50 mm        Normalizing velocity  = -1.0 m/s
  Static pressure       =  15.13 psi      Total pressure        =  17.58 psi
  Traverse direction    = x               Total temperature     = 540.00 R
  Transform method      = 1               Weighting method      = 2
  x0/m                  =  0.00
  Outliers removed:  Sample st. dev. =   3.00;  Record st. dev. =   2.50

---------------------------- Global Information ----------------------------
  nu =  1.413e-005 kg/(m s)        ; rho =  1.264e+000 kg/m3
  Mach-p =   0.468; Mach-u =  0.462; U-mean   = 156.838; Re_m  =  160936
  U-coef = 0.02072; U-exp =  1.0184; U-exp-ci =  0.0399; U-cor = -0.9844
  V-coef = 0.00000; V-exp =  0.0000; V-exp-ci =  0.0000; V-cor =  0.0000

---------------------------- Ensemble Information ----------------------------
 pos  Order  nsam  Rate(avg)  %Val(avg)  nrej(avg)  Rec_rej
51.52   1    1000     3742       100.0        3.2        1
53.27   6    1000     3377       100.0        2.9        0
55.02   2    1000     3365       100.0        2.1        1
56.77   7    1000     3672       100.0        2.5        0
58.52   3    1000     3187       100.0        2.6        0
60.28   8    1000     3397       100.0        2.4        0
62.03   4    1000     3361       100.0        1.8        0
63.78   9    1000     2999       100.0        2.7        0
65.53   0    1000     3855       100.0        2.1        0
65.53   5    1000     3530       100.0        2.7        0
65.53  11    1000     2604       100.0        2.5        0
67.28  10    1000     1290       100.0        1.9        0

 pos      U    U_ci    u'    u'_ci    V    V_ci    v'    v'_ci  uv/u'v'  u'/v'  u_sk   u_fl
51.52  155.94  0.04  3.029  0.045  0.00  0.00  0.000  0.000  0.000  0.00  0.066  2.70
53.27  155.82  0.08  2.954  0.026  0.00  0.00  0.000  0.000  0.000  0.00  0.049  2.66
55.02  156.50  0.04  2.917  0.026  0.00  0.00  0.000  0.000  0.000  0.00  0.060  2.69
56.77  156.44  0.07  2.832  0.042  0.00  0.00  0.000  0.000  0.000  0.00  0.057  2.72
58.52  156.73  0.06  2.869  0.033  0.00  0.00  0.000  0.000  0.000  0.00  0.044  2.73
60.28  156.83  0.06  2.819  0.021  0.00  0.00  0.000  0.000  0.000  0.00  0.040  2.74
62.03  157.06  0.05  2.783  0.025  0.00  0.00  0.000  0.000  0.000  0.00  0.007  2.73
63.78  157.44  0.04  2.741  0.022  0.00  0.00  0.000  0.000  0.000  0.00  0.000  2.73
65.53  158.14  0.05  2.678  0.018  0.00  0.00  0.000  0.000  0.000  0.00  0.000  2.82
65.53  157.56  0.05  2.675  0.026  0.00  0.00  0.000  0.000  0.000  0.00  0.003  2.73
65.53  157.40  0.05  2.719  0.035  0.00  0.00  0.000  0.000  0.000  0.00 -0.007  2.76
67.28  158.05  0.04  2.658  0.033  0.00  0.00  0.000  0.000  0.000  0.00 -0.007  2.82

 pos     U/Um     u'2/U2     integral     tayler     kolmog   diss rate  Re_tay
51.52  0.994  3.775e-004  9.46e-003  8.15e-004  3.14e-005  2.90e+003   174.0
53.27  0.994  3.595e-004  9.61e-003  8.29e-004  3.20e-005  2.70e+003   173.9
55.02  0.998  3.475e-004  9.77e-003  8.41e-004  3.24e-005  2.57e+003   174.2
56.77  0.997  3.280e-004  9.92e-003  8.54e-004  3.29e-005  2.41e+003   174.1
58.52  0.999  3.352e-004  1.01e-002  8.67e-004  3.34e-005  2.28e+003   174.2
60.28  1.000  3.232e-004  1.02e-002  8.79e-004  3.39e-005  2.15e+003   174.2
62.03  1.001  3.141e-004  1.04e-002  8.91e-004  3.43e-005  2.04e+003   174.3
63.78  1.004  3.032e-004  1.05e-002  9.03e-004  3.47e-005  1.94e+003   174.5
65.53  1.008  2.869e-004  1.06e-002  9.13e-004  3.51e-005  1.86e+003   174.8
65.53  1.005  2.883e-004  1.06e-002  9.15e-004  3.52e-005  1.84e+003   174.5
65.53  1.004  2.987e-004  1.06e-002  9.15e-004  3.52e-005  1.83e+003   174.4
67.28  1.008  2.831e-004  1.08e-002  9.25e-004  3.56e-005  1.76e+003   174.7

------------------------------ Comments ------------------------------
- DT = 3.4 (68%); CJ = 5.0; PO = 20 psi
- 160 mm lens; 0 MHz frequency shift
- Thesis label: H54
```

```
------------------------------ Input Parameters ------------------------------
  Input filename       = s129
  Number of positions  = 12              Number of records    = 15
  Starting position    = 747.0 mm        Increment            = 25.4000 mm
  Mesh length          = 14.50 mm        Normalizing velocity =  -1.0 m/s
  Static pressure      =  16.96 psi      Total pressure       =  18.70 psi
  Traverse direction   = z               Total temperature    = 538.50 R
  Transform method     = 1               Weighting method     = 2
  z0/m                 = -8.00
  Outliers removed:  Sample st. dev. =   3.00;  Record st. dev. =   2.50

------------------------------ Global Information ----------------------------
  nu =  1.288e-005 kg/(m s)        ; rho =  1.400e+000 kg/m3
  Mach-p =   0.376; Mach-u =  0.369; U-mean   = 126.179; Re_m  =  142024
  U-coef = 0.01888; U-exp =  0.9945; U-exp-ci =  0.0779; U-cor = -0.9416
  V-coef = 0.00000; V-exp =  0.0000; V-exp-ci =  0.0000; V-cor =  0.0000

------------------------------ Ensemble Information --------------------------
 pos  Order  nsam  Rate(avg)  %Val(avg)  nrej(avg)  Rec_rej
51.52   1    1000    6277       100.0       2.5        0
53.27   6    1000    5784       100.0       2.7        0
55.02   2    1000    5909       100.0       2.9        0
56.77   7    1000    5919       100.0       3.6        0
58.52   3    1000    5840       100.0       3.6        0
60.28   8    1000    5336       100.0       4.2        0
62.03   4    1000    5623       100.0       3.4        0
63.78   9    1000    5516       100.0       4.1        0
65.53   0    1000    6363       100.0       3.4        0
65.53   5    1000    6038       100.0       3.3        0
65.53  11    1000    4932       100.0       4.4        1
67.28  10    1000    2669       100.0       2.5        0

 pos      U     U_ci    u'     u'_ci    V     V_ci    v'     v'_ci  uv/u'v' u'/v' u_sk   u_fl
51.52  125.45  0.04  2.280  0.026  0.00  0.00  0.000  0.000  0.000  0.00  0.031  2.79
53.27  125.58  0.05  2.261  0.029  0.00  0.00  0.000  0.000  0.000  0.00  0.011  2.80
55.02  125.88  0.04  2.177  0.023  0.00  0.00  0.000  0.000  0.000  0.00 -0.011  2.78
56.77  125.83  0.05  2.158  0.020  0.00  0.00  0.000  0.000  0.000  0.00  0.014  2.77
58.52  126.15  0.04  2.142  0.019  0.00  0.00  0.000  0.000  0.000  0.00  0.014  2.80
60.28  126.19  0.04  2.081  0.021  0.00  0.00  0.000  0.000  0.000  0.00 -0.009  2.77
62.03  126.50  0.04  2.081  0.021  0.00  0.00  0.000  0.000  0.000  0.00  0.030  2.80
63.78  126.56  0.05  2.088  0.027  0.00  0.00  0.000  0.000  0.000  0.00  0.030  2.84
65.53  126.93  0.04  2.083  0.034  0.00  0.00  0.000  0.000  0.000  0.00 -0.002  2.84
65.53  126.80  0.03  2.111  0.035  0.00  0.00  0.000  0.000  0.000  0.00  0.025  2.81
65.53  126.58  0.02  2.091  0.035  0.00  0.00  0.000  0.000  0.000  0.00  0.002  2.78
67.28  126.84  0.03  2.019  0.025  0.00  0.00  0.000  0.000  0.000  0.00  0.024  2.80

 pos     U/Um     u'2/U2     integral     taylor     kolmog    diss rate  Re_tay
51.52   0.994  3.306e-004  1.04e-002  9.44e-004  3.73e-005  1.11e+003   165.6
53.27   0.995  3.245e-004  1.06e-002  9.57e-004  3.78e-005  1.05e+003   165.7
55.02   0.998  2.991e-004  1.07e-002  9.70e-004  3.83e-005  9.98e+002   165.9
56.77   0.997  2.943e-004  1.09e-002  9.83e-004  3.88e-005  9.44e+002   165.9
58.52   1.000  2.883e-004  1.10e-002  9.95e-004  3.92e-005  9.02e+002   166.1
60.28   1.000  2.722e-004  1.12e-002  1.01e-003  3.97e-005  8.57e+002   166.1
62.03   1.003  2.708e-004  1.13e-002  1.02e-003  4.02e-005  8.21e+002   166.3
63.78   1.003  2.725e-004  1.14e-002  1.03e-003  4.07e-005  7.82e+002   166.4
65.53   1.006  2.697e-004  1.16e-002  1.04e-003  4.11e-005  7.52e+002   166.6
65.53   1.005  2.776e-004  1.16e-002  1.04e-003  4.11e-005  7.50e+002   166.5
65.53   1.003  2.732e-004  1.16e-002  1.04e-003  4.11e-005  7.46e+002   166.4
67.28   1.005  2.536e-004  1.17e-002  1.06e-003  4.16e-005  7.16e+002   166.6

---------------------------------- Comments ----------------------------------
- DT = 2.8 (56%); CJ = 5.0; PO = 20 psi
- 160 mm lens; 0 KHz frequency shift
- Thesis label: RS3
```